Dry Foams in Pharmaceutical Formulation

Inaugural-Dissertation

zur Erlangung des Doktorgrades
der Mathematisch-Naturwissenschaftlichen Fakultät
der Heinrich-Heine-Universität Düsseldorf

vorgelegt von

Angela Sprunk

aus Schaffhausen

Düsseldorf, Oktober 2013

aus dem Institut für pharmazeutische Technologie und Biopharmazie
der Heinrich-Heine Universität Düsseldorf

Gedruckt mir der Genehmigung der
Mathematisch-Naturwissenschaftlichen Fakultät der
Heinrich-Heine Universität Düsseldorf

Referent: Prof. Dr. Peter Kleinebudde
Koreferent: Prof. Dr. Jörg Breitkreutz

Tag der mündlichen Prüfung: 25. November 2013

Abstract

Choosing the right formulation technology to ensure sufficient bioavailability and stability for new active pharmaceutical ingredients (APIs) becomes more and more important in pharmaceutical industry. The developability classification system established by Butler and Dressman (2010) is a good guiding principle, classifying active compounds according to their solubility in biorelevant medium and permeability, identifying either dissolution rate, solubility or permeability as absorption limiting factor. Formulating DCS IIa compounds, with dissolution rate as absorption limiting factor, granulation techniques including the use of a surfactant for wettability improvement are commonly employed. Dry foam granulation technology was developed as an approach to overcome poor oral bioavailability, by ensuring an optimal wetting of the active compound with the surfactant used. Briefly, first the API is suspended in a surfactant solution and thereby wetted thoroughly. Then, a filler is added embedding the API in its matrix. The resulting paste is exposed to reduced pressure at room temperature for foaming resulting in sponge-like structures. Residual water is removed at moderately accelerated temperatures. The resulting dry foam is downstream processed to granules and either filled into capsules or compressed to tablets. Dry foam formulation technology is expected to improve dissolution behavior and therefore bioavailability by wetting the API and inhibiting API agglomeration.

Investigating a new formulation technology it is important to learn about the key factors, such as process parameters and formulation aspects, influencing the performance and characteristics of the resulting product. Process parameters, such as pressure, temperature, paste water content, as well as equipment based parameters like heat transfer, air flow rate and speed of pressure reduction were investigated employing experimental design and different manufacturing equipments. Paste water content and process temperatures were identified as key parameters, influencing the morphology of the resulting dry foams as well as the drying kinetics. A model equation for the dimensionless water content of dry foams was derived, and could be transferred to the manufacturing equipment vacuum belt dryer for the foaming period after introducing correction factors. A basic understanding of the interplay between pressure, temperature, paste water content as well as the influence of heat transfer and air flow rate on resulting dry foam morphology and drying kinetic was established. It was found that the dissolution behavior of the resulting dry foam tablets was not affected by the process parameters changing within the explored ranges as well as manufacturing equipment used. Therefore, paste water content, process pressure and manufacturing equipment can be adapted to processability and desired batch size.

Investigating formulation aspects, the influence of different fillers and surfactants on the morphology, granule characteristics and dissolution behavior of dry foam tablets was exhibited. Distinct differences between dry foams prepared using spray dried glucose syrup, maltodextrin DE 21, and fast dissolving low molecular fillers, such as isomalt, or a mixture of mannitol and maltodextrin DE 21, were revealed. Using maltodextrin DE 21 resulted in foams with sponge like, porous structures with low specific surface area, due to surface smoothness, and slowly disintegrating tablets. The use of isomalt and mannitol resulted in more dense foams with less porous structures, high specific surface area and fast disintegrating tablets. Depending on the model compound the surfactant used for dry foam preparation exhibited a major effect on dissolution behavior of the resulting dry foam tablets.

Seeking for key characteristics identifying APIs benefiting from being formulated by dry foam granulation, a set of nine model compounds, with different physicochemical properties, was investigated by comparing granule and dissolution characteristics with fluid bed granules of the same model compound and surfactant. Interestingly, the very three model compounds with high lipophilicity in combination with a low melting point exhibited a superior dissolution behavior of dry foam compared to fluid bed granule tablets. Especially for the model compound orlistat, dry foam granulation technology showed beneficial dissolution behavior using all three filler systems, in comparison to fluid bed granules as well as to the market formulation ALLI®, in two different dissolution media. However, for the eight other model compounds either only selected dry foam surfactant-filler combinations showed beneficial dissolution behavior compared to fluid bed granulation, or most often similarity.

Therefore, dry foam granulation technology is an additional formulation method, which in some cases can lead to beneficial dissolution behavior due to improved wettability and inhibition of agglomeration tendencies. Additionally, the low process temperatures are an advantage for temperature sensitive active compounds.

Zusammenfassung

Eine der grössten Herausforderungen der pharmazeutischen Formulierungsentwicklung ist es, schwer lösliche Arzneistoffe für den Körper nach oraler Gabe ausreichend bioverfügbar zu machen. Trockenschäume stellen eine neue Formulierungsmethode dar, die entwickelt wurde, um die orale Verfügbarkeit von schwer löslichen und schlecht benetzbaren Arzneistoffen zu verbessern. Bei diesem Herstellungsverfahren wird der Arzneistoff zunächst in einer Tensidlösung suspendiert und dadurch benetzt. Durch Zugabe eines Füllstoffes zur Arzneistoffsuspension erhält man eine hochviskose Paste, die man unter reduziertem Druck bei Raumtemperatur aufschäumt, wobei eine schwammartige, poröse Struktur entsteht. Das restliche ungebundene Wasser wird bei leicht erhöhten Temperaturen, immer noch unter Vakuum, entfernt. Der entstandene Trockenschaum kann dann zu einem Granulat weiter verarbeitet, und schliesslich in Kapseln abgefüllt, oder zu Tabletten verpresst werden. Eine verbesserte Bioverfügbarkeit kann durch die gute Benetzung des Arzneistoffes im Herstellungsverfahren, sowie durch die Verhinderung der Agglomeration durch das Einbetten des Arzneistoffes in die Schaumstruktur erreicht werden.

Um ein vertieftes Verständnis für diese neue Formulierungstechnologie zu entwickeln, sollte der Einfluss verschiedener Prozess- und Formulierungsparameter auf die Produkqualität ermittelt werden. Prozessparameter, wie Druck, Temperatur und Wassergehalt der Paste, wurden unter Verwendung von statistischer Versuchsplanung und unterschiedlichen Herstellungsanlagen untersucht. Der Wassergehalt der Paste sowie die Prozesstemperatur beeinflussten sowohl die Morphologie der resultierenden Schäume, als auch ihre Trocknungskinetik. Mit Hilfe der gefundenen Modellgleichung kann der resultierenden dimensionslose Wassergehalt von Schäumen, bei der Herstellung, unter Verwendung des Vakuumbandtrockners, für die Aufschäumphase berechnet werden. Grundsätzliche Zusammenhänge zwischen Druck, Temperatur und Wassergehalt der Paste sowie dem Einfluss von Wärmeübertragung und Flussrate des trocknenden Luftstroms wurden hergestellt. Zusätzlich konnte gezeigt werden, dass das Auflösungsverhalten von Trockenschaumtabletten nicht durch die Variation der Prozessfaktoren innerhalb der untersuchten Grenzen beeinflusst wird. Folglich können Wassergehalt der Paste, Prozessdruck und die Herstellungsanlage an die gewünschte Ansatzgrösse und die Verarbeitbarkeit angepasst werden.

Bei der Untersuchung von Formulierungsparametern wurden Einflüsse von Füllstoffen und der Auswahl des Tensides auf die Morphologie der Schäume, die Eigenschaften des Schaumgranulates sowie auf das Auflösungsverhalten der Trockenschaumtabletten nachgewiesen. Ausgeprägte Unterschiede ergaben sich zwischen Trockenschäumen, die unter Verwendung von sprühgetrocknetem Glucosesirup als Füllstoff hergestellt wurden, und Schäumen, bei denen niedermolekulare, schnell

lösliche Füllstoffe, wie Isomalt und Mannitol, zur Herstellung eingesetzt wurden. Die Verwendung von sprühgetrocknetem Glucosesirup, Maltodextrin DE 21, führte zu porösen, schwammartigen Schaumstrukturen mit glatter Oberfläche, niedriger spezifischer Oberfläche und langen Zerfallszeiten der Tabletten. Unter Verwendung von Isomalt oder einer 1:1 Mischung von Mannitol mit Maltodextrin DE 21 entstanden kompaktere, weniger poröse Schaumstrukturen mit einer rauhen Oberfläche, einer grösseren spezifischen Oberfläche und schnelleren Zerfallseigenschaften der resultierenden Tabletten. In Abhängigkeit vom verwendetem Modellarzneistoff spielt die Auswahl des Tensides auf das resultierende Auflösungsverhalten der Trockenschaumtabletten eine mehr oder weniger grosse Rolle.

Auf der Suche nach charakteristischen Eigenschaften von Arzneistoffen, die von der Formulierung als Trockenschaum profitieren, wurden neun Modellarzneistoffe mit unterschiedlichen physikalisch-chemischen Eigenschaften herangezogen. Das Auflösungsverhalten von Trockenschaumtabletten wurde mit dem von Wirbelschichtgranulattabletten, bestehend aus dem gleichen Modelarzneistoff und dem gleichen Gehalt an Tensid, verglichen. Es stellte sich heraus, dass diejenigen Arzneistoffe mit einer hohen Lipophilie einhergehend mit einem niedrigen Schmelzpunkt, verbesserte Auflösungseigenschaften der Trockenschaumtabletten gegenüber den Wirbelschichtgranulattabletten zeigten. Besonders der Modellarzneistoff Orlistat profitierte von der Formulierung als Trockenschaum mit allen drei Füllstoffen. Die Tabletten zeigten ein verbessertes Auflösungsverhalten in zwei unterschiedlichen Freisetzungsmedien gegenüber den Wirbelschichtgranulattabletten, sowie der Marktformulierung ALLI® 60 mg Kapseln. Für alle anderen Arzneistoffe wurde überwiegend ein vergleichbares Auflösungsverhalten für die Wirbelschichtformulierungen und die Trockenschaumformulierungen beobachtet. Nur unter Verwendung bestimmter Füllstoff -Tensid - Kombinationen zeigte sich ein verbessertes Auflösungsverhalten für die Trockenschaumtabletten.

Zusammenfassend stellt die Trockenschaumformulierung eine interessante, alternative Formulierungstechnologie dar, die in einigen Fällen zu verbesserten Auflösungseigenschaften durch erhöhte Benetzbarkeit und die Verhinderung von Agglomeration führte.

Contents

List of Abbreviations

$\Phi_{DF(1)}$	dimensionless moisture content during foaming period
$\Phi_{DF(2)}$	dimensionless moisture content during drying period
$\Phi_{DF(VBT)}$	dimensionless moisture content after foaming period using VBT
Φ_{DF}	dimensionless moisture content of dry foam
Φ_{pred}	predicted dimensionless moisture content by established model
$k1$	drying rate foaming period
$k2$	drying rate drying period
50% MTL	1:1 mixture of maltodextrin DE 21 and mannitol
API	active pharmaceutical ingredient
AUC	area under the curve [mg/ml · min]
BCS	biopharmaceutics classification system
CETP	cholesteryl ester transfer protein
CP2	cholesteryl ester transfer protein-inhibitor (2)
CR	controlled rate
D50	particle diameter at 50% in the cumulative distribution
DAL	dalcetrapib
DCS	developability classification system
DDS	drug delivery system
DF	dry foam
DOSS	dodecyl succinate sodium
DRX	drug X
DSC	differential scanning calorimetry
DVS	dynamic vapor sorption

EVW	evaporated amount of water
FaSSIF-V2	fasted state simulated intenstinal fluid version 2
FBG	fluid bed granule
FDP	felodipine
FEN	fenofibrate
HBA	number of H-bond acceptors
HBD	number of H-bond donors
HLB	hydrophilic lypophilic balance
IDM	indomethacin
ISM	isomalt (galenIQ®721)
LOD	loss on drying [m/m %]
M21D	maltodextrin DE 21 (Glucidex 21D)
MAO	monoamine oxidase type B-inhibitor
MCC	microcrystalline cellulose
MP	melting point
MSB	magnetic suspension balance
MTL	mannitol (Parteck Delta M)
MW	molecular weight [g/mol]
Myrj	Myrj S40
NK1	Neurokinaserezeptor(1)-antagonist
p	process pressure
Ph.Eur.	European Pharmacopoeia
PLS	partial least square
PP103	Pluronic P103
PS80	polysorbate 80
PSA	polar surface area [$Å^2$/molecule]
PVP K30	povidone K30

PWC	paste water content calculated on wet mass [%]
PWC2	paste water content at the beginning of drying period
RF	reference formulation
SDS	sodium dodecyl sulfate
SEM	scanning electron microscopy
SF	solid fraction
SSA	specific surface area [m^2/g]
T1	temperature during foaming period
T2	temperature during drying period
THL	orlistat (tetrahydrolipstatin)
ToBo	torsional bonds
USP	United States Pharmacopoeia
VBT	vacuum belt dryer
VDC	vacuum drying cabinet
VitE	vitamin E TPGS
X-ray µ-CT	X-ray microcomputed tomography

1 Introduction

1.1 Oral bioavailability improvement of poorly soluble drugs

Major challenges for drug product developers are insufficient oral bioavailability and food effects of newly discovered active pharmaceutical ingredients (APIs). Therefore, they are seeking for early classification and prediction tools as guidance in formulation development. The biopharmaceutics classification system (BCS) (Amidon et al., 1995) categorizes drug substances based on their water solubility and intestinal permeability into one of four categories offering a better understanding of the physico-chemical and biopharmaceutical drug properties. Butler and Dressman introduced the developability classification system (DCS) as a revised concept addressing issues in formulation development rather than being a regulatory classification system (Butler and Dressman, 2010). The DCS distinguishes itself from the BCS by incorporating drug solubility in biorelevant media in more realistic volumes as a measure of in vivo solubility. Additionally, it divides the class of poorly soluble drugs with high permeability in a dissolution rate limited (IIa) and a solubility limited group (IIb) taking into account that permeability and solubility can be compensatory. In order to assess the development risks for drugs with dissolution rate limited adsorption, dissolution rate is expressed as a target drug particle size rather than a dose/solubility ratio. As a result of the compensatory influence of high permeability, compounds of class IIa can usually still be formulated as a standard oral dosage form from crystalline drug without using solubilization methods, whereas for class IIb compounds a solubilized form is inevitable for achieving complete absorption. Multiple approaches, like particle size reduction into submicron range, cyclodextrin complexation, amorphization and self-emulsifying drug delivery systems are studied to increase the apparent solubility of the compound (Kawabata et al., 2011).

Noyes and Whitney noticed that the rate of dissolution is proportional to the difference between the concentration C at a time t, and the saturation concentration C_s (Noyes and Whitney, 1897), resulting in Equation (1.1)

$$\frac{dC}{dt} = k(C_s - C)\,. \tag{1.1}$$

Nernst and Brunner further developed the Noyes-Whitney equation showing that the rate of dissolution depends amongst others on the exposed surface (Brunner, 1904), by Equation (1.2)

$$\frac{dC}{dt} = \frac{DS}{Vh}(C_s - C)\,, \tag{1.2}$$

where D is the diffusion coefficient, S the exposed surface area, h the thickness of the diffusion layer and V the volume of the dissolution.

For compounds of DCS class IIa, although offering the opportunity to use standard formulation approaches, factors such as particle size, surface area and wettability need to be controlled when complete absorption is targeted. Micronization is the most common method to increase available surface area of the drug and therefore its initial dissolution rate. Unfortunately, micronized drugs have the tendency to agglomerate diminishing the expected effect as the reduction in particle size often results in electrostatic attraction between particles (Spence et al., 2005; Khan and Zhu, 1998). Formulating these hydrophobic, poorly wettable and agglomerating drugs can be challenging.

Different granulation methods were studied in pharmaceutical formulation sciences in the past. Besides the most common wet granulation methods, like high shear and fluid bed spray granulation, dry granulation methods like roller compaction, and also melt granulation are of growing interest. The choice of granulation method is adapted to the physico-chemical properties of the API like hygroscopicity, water induced phase transitions, poor powder flow, cohesive properties, high compressibility and crystal morphology (Dalziel et al., 2013). Dry foam formulation technology reveals new opportunities facing the challenge of poor wettability and 'grease ball' characteristics of drug substances.

1.2 Granulation technologies in pharmaceutical formulation

Granulation in general is a particle agglomeration process extensively used in the pharmaceutical industry. Particle size enlargement is achieved either by dry granulation, e.g. roller compaction, or by the addition of a liquid to the powder formulation while mixing in a fluid bed, a high shear mixer or extruder. Particle agglomeration improves bulk properties of the formulation by increasing its density and enhancing flow properties, making it more suitable for tablet compression and final packaging. Wetting agents are added to improve the processability and dissolution characteristics of the active compound. The effectiveness of these additives is a result of their distribution and contact area with the API depending on the employed granulation method.

In dry granulation contact surfaces of API and wetting agent only evolve due to mixing and compaction forces. In high-shear granulation commonly the API is premixed with the surfactant and other powder components and the granulation liquid is added afterwards. An uniform distribution of the surfactant is promoted by the addition of the granulation liquid and the mixing of the material within the high-shear mixer. A surfactant dissolved in the granulation liquid is thought to contribute more to the wetting of the API. During fluid bed granulation the surfactant is usually added to the granulation liquid and finely sprayed onto the API powder mixture to provide a better distribution and wetting. Using a foamed surfactant solution the available surface area of the surfactant mixture is increased and therefore even

better distribution and wetting provided as shown by Thompson and coworkers. They introduced foam granulation as a new approach to continuous wet granulation using a twin-screw extruder. Here, the foamed binder solution provides improved spreading and distribution properties, resulting in a more uniformly wetted powder (Thompson et al., 2012; Thompson and Sheskey, 2013).

1.3 Foam and sponge-like structures in pharmaceutical formulation

Foam and sponge-like structures found their way into pharmaceutical formulation of poorly soluble drugs in the past. In general pharmaceutical foams can be divided in dispersive systems of gas and liquid and dispersive systems of gas and solid. The latter can be further divided in foams where the matrix is prepared together with the active pharmaceutical compound or systems where first the foam is prepared and the active pharmaceutical ingredient loaded onto the foam system afterwards.

Systems preparing the foam together with the API are most often prepared by freeze-drying or application of vacuum. Hajare and coworkers found vacuum foam drying of proteins to be a good alternative route to lyophilization using sugar-phosphate compositions and observed improvements with respect to storage stabilization (Hajare et al., 2010). Pisal and coworkers vacuum foam dried LaSota virus for preservation together with sucralose and povidone K30 (Pisal et al., 2006). Schoonman and coworkers developed solid foams consisting of maltodextrin DE12 and sodium caseinate via nitrogen injection (Schoonman et al., 2001). In extrusion foamed polymeric materials are prepared by using pressurized carbon dioxide as a temporary plasticizer and foaming agent (Verreck et al., 2006).

A variety of carrier systems is investigated for the latter class, where first the foam matrix is prepared and the API loaded onto the system afterwards. Inorganic materials are employed to form highly porous material with typically nanometer-sized pores. Especially mesoporous silica material is studied extensively as an efficient drug delivery carrier, as its structure, morphology, size, and surface properties have been found to be facilely tunable for the purposes of drug loading, controlled drug release and delivery, and multifuctionalization (He and Shi, 2011). Their large surface area and pore volume make them excellent candidates for efficient drug loading and rapid release (Vialpando et al., 2011; van Speybroeck et al., 2011). Zhang and coworkers investigated loading and the release of the poorly water-soluble drug telmisartan in correlation to the pore size distribution of mesoporous silica material (Zhang et al., 2010). Biodegradable porous starch foams were developed by solvent exchange method to improve the bioavailability by immersion/solvent evaporation loaded lovastatin (Wu et al., 2011). Such foam structures provide a large effective specific surface area and the possibility to embed microcrystalline or amorphous forms of drug molecules afterwards. Low density polymeric foams derived from lyophilization of biopolymers were investigated regarding controlled release of isoniazid loaded onto them by immersion into an aqueous solution (Hsu et al., 1997).

Large porous particles are developed for pulmonal delivery of macromolecules by gas foaming of PLGA matrices (Ungaro et al., 2010).

Dry foams as described in this thesis belong to the first mentioned class of sponge like dispersive systems of solid and gas phase, preparing the sponge like structure together with the incorporated API.

1.4 Dry foam formulation technology

Dry foam formulation technology was developed at F. Hoffmann-La Roche Ltd (Basel, Switzerland) (Busson and Schröder, 2006) as an alternative approach to overcome low oral bioavailability of poorly soluble APIs. It is intended to enable a faster and more efficient dissolution by avoiding agglomeration and floating of non-wetted API particles. Its inventors were inspired by food industry, where lipids of coffee whitener were incorporated in a maltodextrin matrix with a high solid content and dried under reduced pressure resulting in a foam or sponge like structure. The resulting granules reconstituted more quickly than the spray dried reference in coffee, despite the slower disintegration of the compressed foam material which was made up for by a faster dissolution of the incorporated lipid (Schröder, 1999).

In pharmaceutical dry foam preparation, the crystalline API is first wetted thoroughly with an aqueous surfactant solution, resulting in a suspension. Afterwards, a filler is added stepwise, embedding the suspended API in its matrix. The obtained viscous paste is exposed to reduced pressure at room temperature for foaming resulting in sponge-like structures. In order to remove the residual amount of water, moderately accelerated temperatures still under reduced pressure are applied. Finally, the dry foam can be downstream processed to granules and either filled into capsules or compressed to tablets. In this work only the preparation of dry foam tablets was investigated. The dry foam preparation process is schematically depicted in Figure 1.1. Dry foam formulation technology is expected to improve bioavailability by wetting the API and enhancing its dissolution rate. Additionally, agglomeration of the API particles is inhibited by the foam matrix.

Currently two manufacturing equipments are available for the foaming and drying of dry foams at F. Hoffmann-La Roche Ltd (Basel, Switzerland): a vacuum drying cabinet (VDC) for manufacturing of small scale batches and a vacuum belt dryer (VBT) for large scale and continuous processing. Using the VDC the paste is spread in single strands batchwise on a screen-like plate. Afterwards the plate is placed in

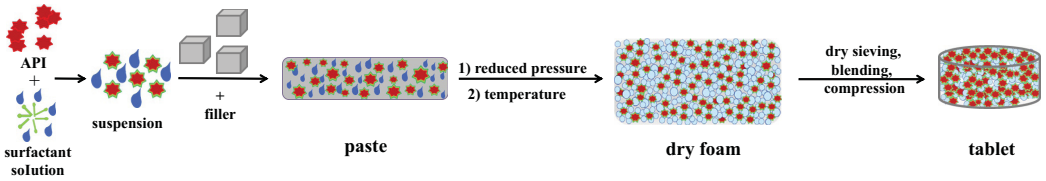

Figure 1.1: Scheme of the dry foam preparation process

the VDC and the pressure within the VDC adjusted using a vacuum pump. After foaming at room temperature, temperature within the VDC is increased and can be monitored by using resistance thermometers with radio transmission.

The vacuum belt dryer Drylab (0.6 m^2 of drying surface area, Bucher, Switzerland) is designed for the continuous drying of liquids, free flowing powders and heat sensitive products under vacuum. Its design is especially suitable for products passing a glutinous and highly viscous phase during the drying process. Liquid products are uniformly distributed on the belt with a swivel feeder or in parallel strands. The heating plates can be set to the desired temperature by independent heating and cooling water circuits to permit constant or variable drying rates. The last zone can be designed as a cooling zone if required. At the end of the belt the dried product is cut into smaller pieces by a guillotine type cutter.

The setup of the VBT as used for dry foam preparation in this study is illustrated in Figure 1.2. Paste for dry foam preparation is applied using an automatic cartridge pump connected via an inlet valve to a comb like syringe within the VBT resulting in parallel strands onto the moving PTFE (Teflon®) coated glass fabric belt. Up to four different temperature zones can be constituted by the independent heating and cooling of the four temperature plates. The different temperature zones are illustrated by blue and red bars in Figure 1.2. The grey structures illustrate paste and dry foam strands, exaggerating the volume gain during the foaming process. The different grey scales symbolize the drying state, the lighter the more water already evaporated. The moving belt is depicted in black. At the discharge side a cutter breaks down the foam strands in smaller pieces. Foam pieces leave the vacuum belt dryer via two outlet valves, which keep the pressure within the apparatus constant by opening alternately and adjusting the pressure in between to either ambient pressure or pressure within the VBT.

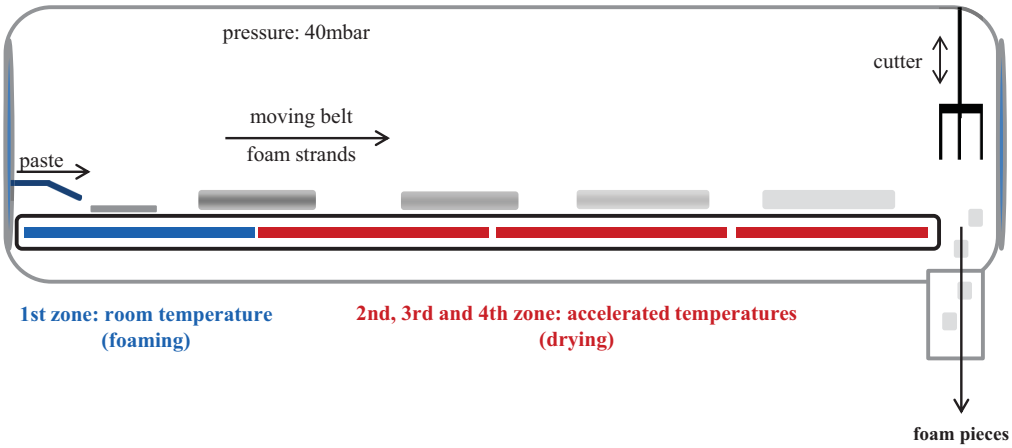

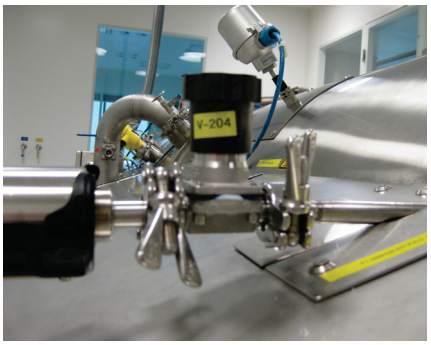

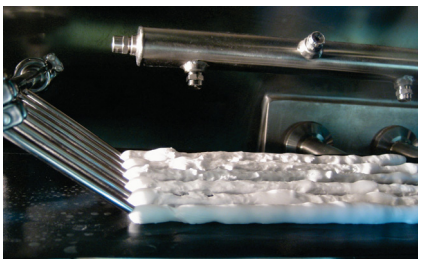

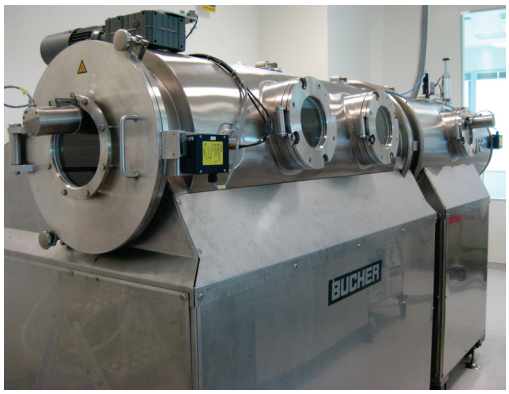

Figure 1.2: Scheme (top) and photographs of vacuum belt dryer (VBT) illustrating the inlet valve (top left), comb like syringe with paste strands (top right), feeding side (bottom left) and discharge side (bottom right).

1.5 Scope of this work

1.5.1 Investigating the dry foam process

When introducing a new formulation technology it is important to identify key process parameters and investigate their effect on the performance of the resulting product. The process step of transforming the paste into a dry foam is considered as most important for the resulting product properties and can be divided into two steps. First the paste is applied to reduced pressure and a wet foam structure develops due to expansion. This takes usually place at room temperature and below the boiling point of the liquid as described in the patent (Busson and Schröder, 2006). This step is referred to as foaming period in this work, even though already in this period drying of the paste takes place due to evaporation of water. In a second step accelerated temperatures are applied for complete drying of the product, here the boiling point of the liquid is reached. The second step will be referred to as the drying period.

A good reference describing mechanisms and kinetics of drying is the 'Handbook of Industrial Drying' (Mujumdar, 2006). Here, drying is described as a process of thermally removing volatile substances (moisture) to yield a solid product. The author proposes, that when a wet solid is subjected to thermal drying, multiple processes occur simultaneously: energy is transferred from the surrounding environment to the system, surface moisture evaporates and internal moisture is transferred to the surface. Each of these processes has its own kinetic and the decrease of liquid content within the product is the resulting sum of all single drying rates. Heat transfer can occur due to different mechanisms. In the case of convection, heat is supplied by heated air or gas flowing over the surface of the product. The evaporated moisture is carried away by the air or gas flow. In the case of conduction, heat for evaporation is supplied through heated surfaces. Drying can be made more efficient by removing the evaporated moisture by application of vacuum. This is especially recommended for heat sensitive products. Furthermore, heat transfer can occur by radiation and combinations of the mentioned mechanism. The rate of water removal as vapor from the product surface depends on the external conditions, such as temperature, air humidity and flow, exposed surface area and pressure. Especially during the initial stage of drying when unbound surface moisture is removed, these external conditions will be rate limiting. Whereas, the internal moisture movement is a function of the physical characteristics of the solid, its temperature and moisture content.

Mujumdar and coworkers (Mujumdar, 2006) described the surface evaporation as the diffusion of vapor from the surface of a solid to the surrounding atmosphere. It is controlled by its partial pressure (P_w) and its maximum value, the saturated vapor pressure (${P_w}^0$), whereas the partial pressure is given by Equation (1.3)

$$P_w \cdot V = \frac{m_w}{M_w} \cdot RT\,, \tag{1.3}$$

where m_w is the mass of vapor gas in the gaseous phase, V the volume, M_w the

molar mass, R the gas constant [J/(mol K)] and T the temperature.

The vapor-pressure curve is a result of plotting the vapor pressure of a liquid over the temperature, identifiying the region were liquid and vapor may coexist corresponding to the saturated vapor state. The Clausius-Clapeyron equation sets the slope of the vapor pressure-temperature curve (${dP_w}^0/dT$) into relation to the latent heat of vaporization at a constant pressure by Equation (1.4)

$$\frac{{dP_w}^0}{dT} = \frac{\Delta H_w}{T(V_w - V_L)}\,, \tag{1.4}$$

where V_w is the molar volume of the saturated vapor, V_L is the molar volume of the liquid and ΔH_w molar latent heat of vaporization (Mujumdar, 2006).

Consequently, the drying rate of process 1 is a function of partial pressure of the liquid in the drying gas, the latent heat of vaporization, temperature and pressure. The second process, the internal movement of moisture, is a result of temperature gradient and vapor-pressure gradient. A wet solid exposed to continuous supply of fresh gas continues to lose moisture until an equilibrium of the vapor pressure of the moisture in the solid and the partial pressure of the vapor in the gas is reached. The drying rate also depends on the physico-chemical habit of the solid, its capillarity, porosity and hygroscopicity. In the course of drying of macroporous and capillary materials, there will be a point in time when it can be divided into two parts, an already dried part and a still wet inner part. Afterwards, the vapor has to pass through the pores of the already dried part in order to leave the material. Furthermore, the required heat for drying has to pass through the already dried layer to cause evoparation (Mujumdar, 2006).

Investigating the drying rate of a paste as being a mixture of solid particles and dissolved solid in liquid, additional considerations such as solid content and viscosity have to be taken into account. Schoonman and coworkers found that in foamed maltodextrin/sodium caseinate powders prepared by nitrogen injection and freeze drying the amount of sodium caseinate and the amount of injected nitrogen are responsible for the pore size distribution and the porosity of the foams. A higher content of sodium caseinate resulted in smaller pores (Schoonman et al., 2001). Viscosity of a starch composition showed to have an effect on structure of foams prepared by microwave treatment. A higher viscosity caused by a higher rate of gelatinization resulted in smaller pores and slower loss of water (Sjøqvist and Gatenholm, 2005). Investigating the influence of process parameters on the dry foam process, particular attention should be given to parameters like paste water content and resulting viscosity.

Conventional gravimetric techniques are often employed to observe drying processes in literature. The main disadvantage of these methods is the mechanical and thermal influence of the sample room on the measuring cell of the balance. A magnetic suspension balance allows accurate weight change measurements under even severe conditions, by linking the sample to a permanent magnet, the so-called suspension magnet. The measuring device is thereby disconnected from the sample chamber allowing accurate measurements even under severe process conditions

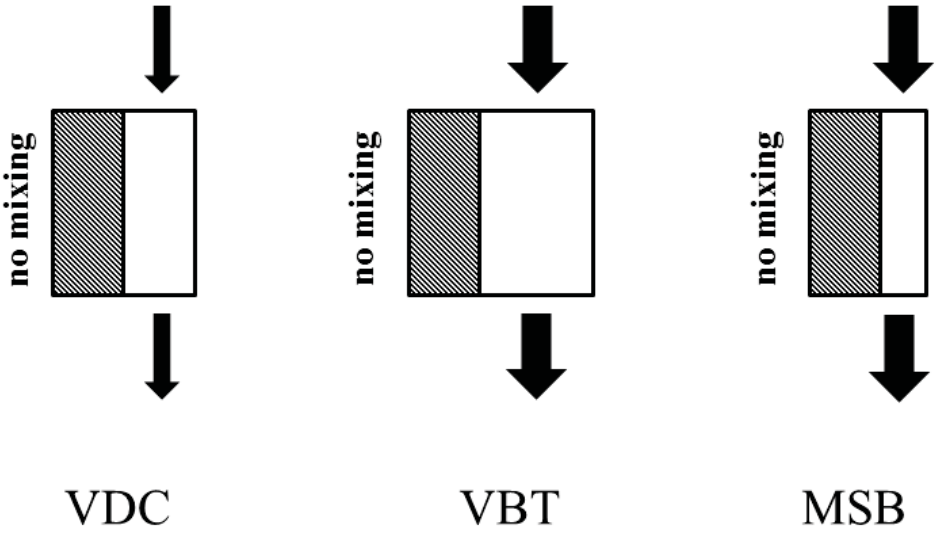

Figure 1.3: Schematic drying models for vacuum drying cabinet (VDC), vacuum belt dryer (VBT) and magnetic suspension balance (MSB). Shaded boxes symbolize wet mass, empty boxes symbolize the available air volume.

(Kwapinski and Tsotsas, 2004). Alternatively, thermogravimetric analysis (TGA) can be employed as described in literature for simulation of a spray drying process examining the evaporation profile of feed solutions (Wan et al., 2013). It was shown that exploring different aspects of a drying process can be advantageous for the understanding and development of a novel drying technique.

For basic simulations and calculations dryer models can be classified by their operation type, differentiating batch-wise, semibatch-wise or continuous process mode as well as mixing of the product and the gas flow type, cocurrent, countercurrent or cross-flow (Mujumdar, 2006). The schematic models of dryers used in this study, vacuum belt dryer (VBT), vacuum drying cabinet (VDC) and magnetic suspension balance (MSB), are depicted in Figure 1.3. The shaded boxes symbolize the wet paste, and are all of the same size. The empty boxes symbolize the available air volume within each dryer in relation to the batch size. Usually 100 g of paste are applied to the VDC or the VBT. Within the VDC an approximate volume of 1 m^3 is reached, whereas within the vacuum belt dryer over 3 m^3 are available. The average batch size within the MSB is about 0.2-0.4 g compared to a volume of approximately 45 cm^3. The gas flow transporting the humidity away from the product is also different in the three dryers. The arrows of different size illustrate the input and output drying gas flow. Whereas within the VDC and the VBT the equipment aerates the sample room only to the level it needs to balance the reduced pressure with the vacuum pump, the MSB setup needed a supply of 80 ml/min of nitrogen to keep the pressure of 20-80 mbar constant throughout the experiments.

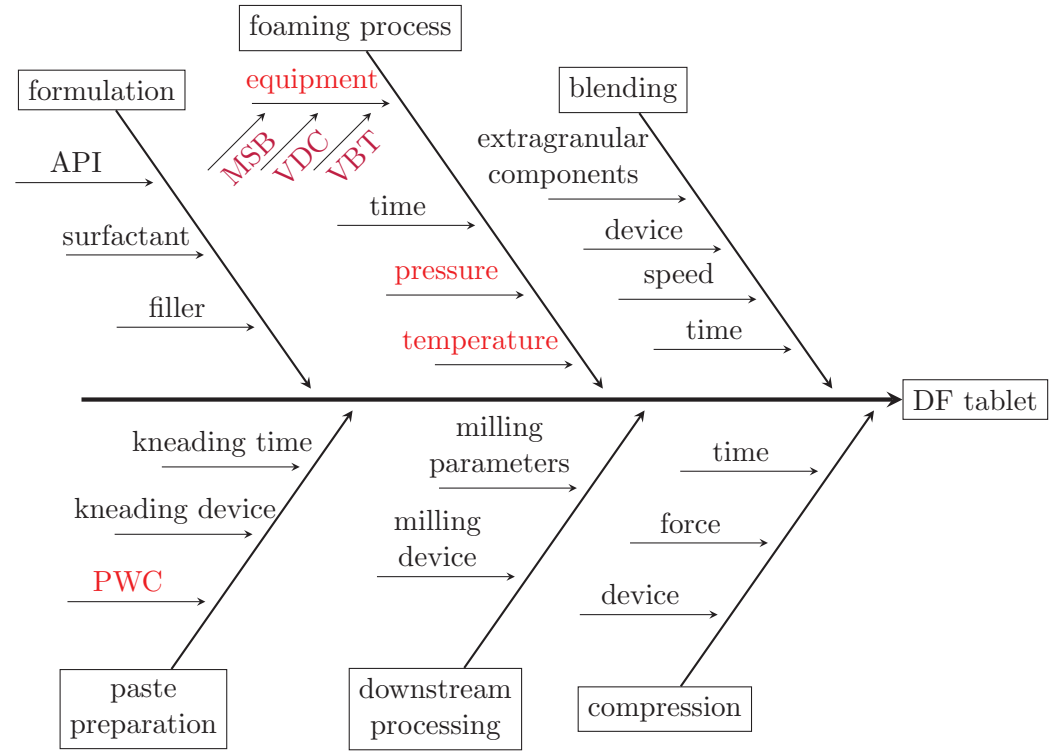

Figure 1.4: Process parameters having a potential influence on dry foam preparation process illustrated by a fishbone diagram. Investigated parameters are highlighted in red. PWC standing for paste water content.

As a first step the general effect of applying reduced pressure in the course of dry foam preparation, and whether this step is advantageous over drying at normal pressure and has substantial impact on the product characteristics is investigated.

Figure 1.4 illustrates the dry foam preparation process and identifies potential process parameters having an influence on the properties of the resulting dry foam tablet. The non-formulation process parameters investigated in this work are highlighted in red. The dry foam intermediate paste consists of API, surfactant, filler and water. Considering a fixed drug load, a fixed surfactant:API ratio and a target tablet weight, in other words a fixed dry formulation, the only variable in paste composition becomes the water content. Being responsible for the rheological behavior of the paste it is considered an important process variable for the resulting morphological dry foam characteristics. Paste water content can be considered as a process parameter instead of a formulation variable, as it is removed throughout the foaming and drying process, having no influence on the composition of the resulting dry foam or tablet. Furthermore, the foaming and drying period are investigated in terms of equipment used and process parameters, such as temperature and pressure.

Using the magnetic suspension balance the drying kinetic was investigated with regard to the process parameters paste water content, pressure and temperature of

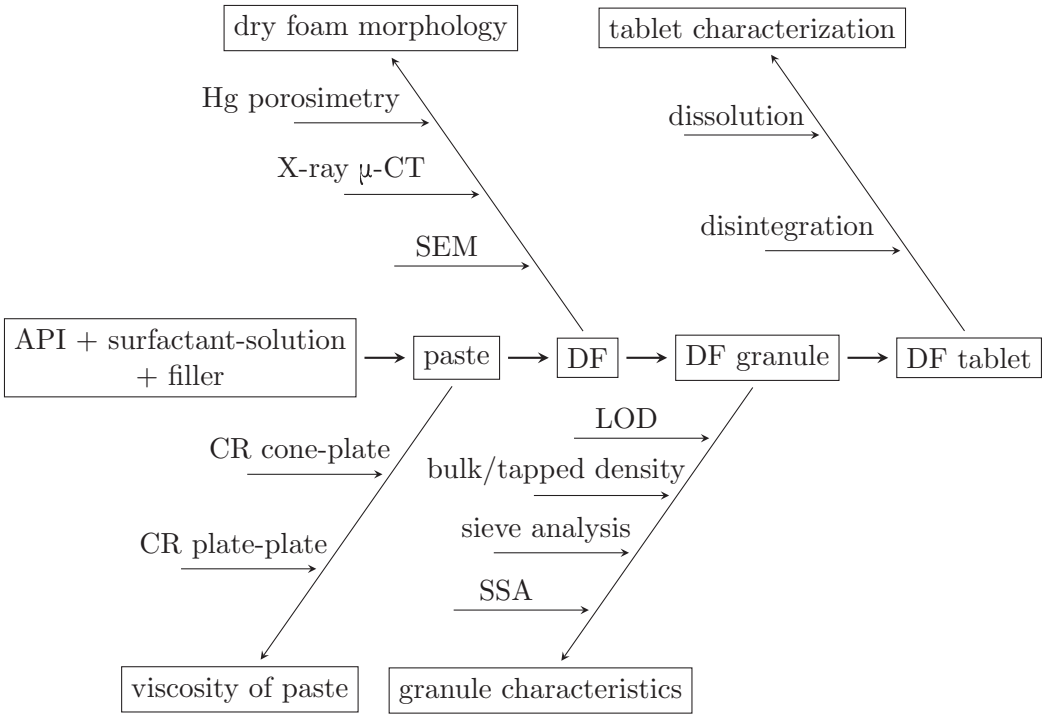

Figure 1.5: Characterization methods for dry foam intermediates and tablets. CR standing for controlled rate measurements.

the foaming and drying period. The obtained data were used for developing two models describing the foaming period and the drying period respectively. Afterwards the developed models were compared to results retrieved from the vacuum belt dryer. Therefore, experimental points of the foaming period were repeated on the vacuum belt dryer and the resulting drying kinetic compared to the developed model. As a last step, the influence of paste water content and type of equipment used on dry foam morphology, granule characteristics and dissolution behavior of the corresponding tablets was examined using indomethacin as model compound. Multiple analytical methods, namely scanning electron microscopy, X-ray micro-computed tomography, mercury porosimetry and specific surface area analysis were established for the characterization of dry foams and the resulting granules (Figure 1.5).

1.5.2 Investigating formulation aspects of dry foams

The early prediction of which formulation approach serves best for a sufficient bioavailability of a novel API in early formulation development bears high potential to save and better plan development resources. It was tried earlier to use the BCS as a basis for a decision tree in early formulation development (Ku, 2008), which was refined by dividing the BCS class II compounds with the help of the DCS into

IIa, primarily dissolution limited, and IIb, solubility limited. Kuentz and Imanidis made attempts to investigate the predictability of the solubility ratio of amorphous and crystalline form of a drug, in order to estimate the potential bioavailability improvement by an amorphous drug formulation (Kuentz and Imanidis, 2013). They found molecular weight, number of hydrogen bond acceptors, melting point, number of torsional bonds and polar surface area to be most important for the amorphous solubility ratio and suggested a refined decision tree, depicted in Figure 1.6. The development of DCS IIa compounds is herein described rather undifferentiated by 'solid dosage form of micronized API with optional addition of surfactant'. However, distinct differences in dissolution behavior and therefore oral bioavailability can be caused by employing different granulation methods. In literature each type of granulation process is described individually in detail, but cross comparison of different granulation technology is rarely discussed. Patel and coworkers found distinct influence on the dissolution behavior of the BCS I compound diclofenac by different granulation methods (Patel et al., 2010), and Mbah and coworkers revealed dramatic influence on the dissolution behavior of the BCS I compound metronidazol by employing different granulation methods and in between market products (Mbah et al., 2012). As the choice of surfactant as well as selected granulation method already have a considerable impact on the dissolution behavior of BCS I compounds, they are thought to influence the outcome of DCS class IIa formulations even more. Molecular characteristics like melting point, molecular weight, lipophilicity, polar surface area, hydrogen bond acceptors and donors might function as direction signs choosing the most appropriate granulation method for DCS IIa compounds.

In the second part of this work the focus was on the question for which group of APIs dry foam formulation can be advantageous over a conventional granulation formulation. Potential key characteristics of compounds benefiting from this formulation technology in regard to dissolution behavior and therfore oral bioavailability were sought after, making the decision which formulation route to take easier for formulators. Therefore a set of APIs with varying physico-chemical properties like melting point, lipophilicity and aqueous solubility was selected. Dry foam and fluid bed granule formulations were prepared using the same drug load and amount of surfactant. The characteristics and the dissolution behavior of the two granule types were compared with micronized API filled into a capsule.

The model compounds for this screening study were selected stepwise. First a set of four orally delivered BCS class II/IV APIs, of different melting point and lipophilicity was combined with six surfactants. The type of surfactant is thought to be crucial for improving the wettability of the API, and therefore the resulting dissolution behavior of the formulation. After investigation of the first API set high lipophilicity and low aqueous solubility were identified as potential key characteristics for APIs where the use of dry foam formulation technology can be advantageous over fluid bed granulation. The hypothesis that the melting point of an API can be an identifier for suitability for this formulation technology was further investigated by extending stepwise the set of selected APIs up to a total of nine compounds differing in melting point, lipophilicity and aqueous solubility. The prepared dry

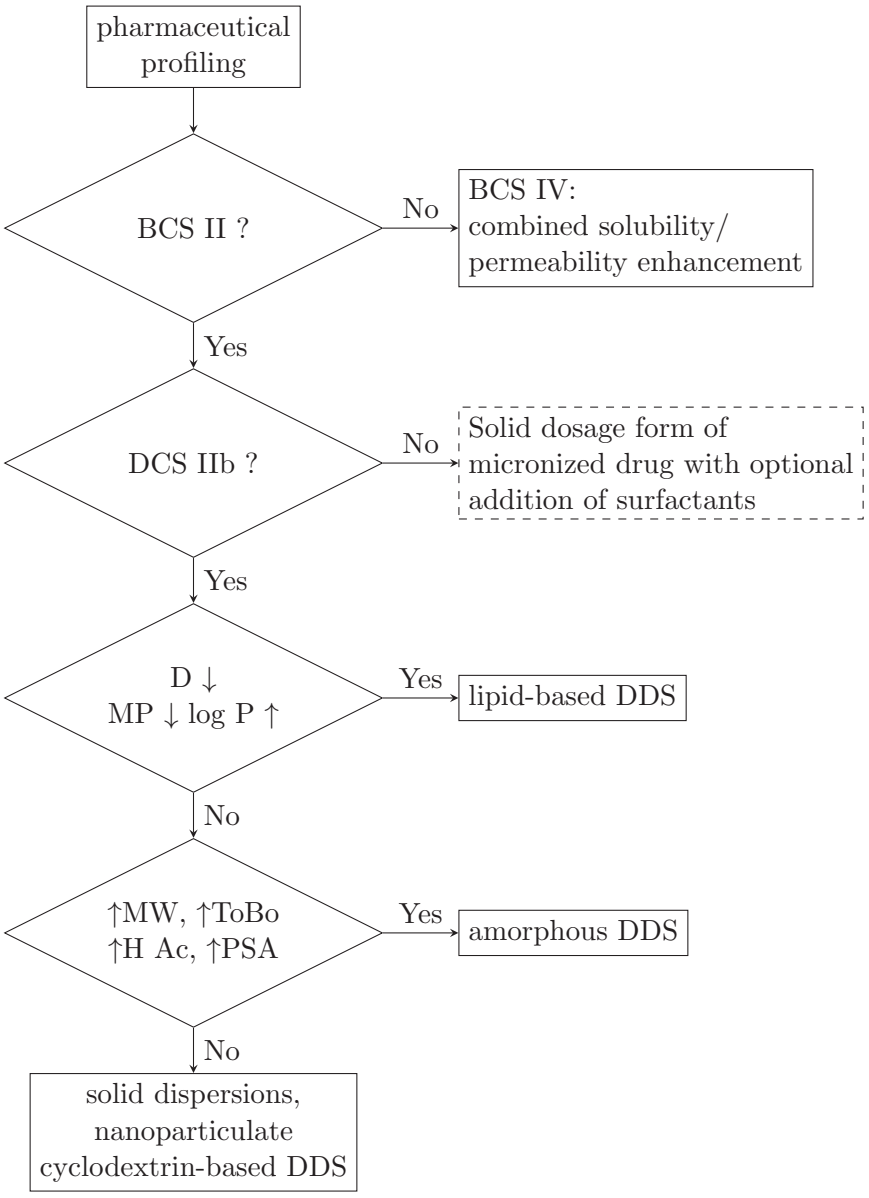

Figure 1.6: Flow chart modified according to Kuentz and Imanidis (2013) for the selection of formulation technologies using poorly soluble drugs. MP standing for melting point, log P for octanol-water partition coefficient, D for dose, MW for molecular weight, ToBo for the number of torsional bonds, H Ac for H-bond acceptor number, PSA for polar surface area and DDS for drug delivery system.

foams were investigated regarding granule characteristics and the dissolution behavior of their tablets compared to fluid bed granules. The potential correlation of molecular characteristics like molecular weight, polar surface area, hydrogen bond acceptors and donors and advantageousness of a dry foam granulation versus fluid bed granulation was investigated retrospectively.

In addition, the influence of type of filler on dry foam morphology, granule characteristics, disintegration and dissolution behavior was investigated. The filler represents the major component of dry foam formulations embedding the API and therefore is thought to affect the drug release crucially as well. Busson and Schröder described a variety of embedding materials, such as modified or substituted starch or cellulose derivatives, acacia gum or carrageenan (Busson and Schröder, 2006). The use of carrageenan for instance was found to be suitable for modified release formulations (Rauner, 2005). In recent studies the type of filler showed a distinct influence on dry foam morphology as well as dissolution characteristics (Lenz, 2012). The dissolution behavior of fenofibrate DF tablets using maltodextrines of different DE range, particle type and botanical origin as well as isomalt and a phosphatidylmaltodextrine complex as filler were compared. It was concluded that fast dissolving low molecular weight fillers like isomalt could improve the initial dissolution of the tested dry foam formulation tablets (Lenz et al., 2013).This hypothesis was further investigated by applying three different filler combinations to selected APIs. Maltodextrin DE21 (M21D) is a spray dried glucose syrup, consisting of a mixture of oligosaccharides with different chain length derived from hydrolyzed starch. The suffix DE21 stands for the dextrose equivalent, indicating the amount of reducing sugars representing, relative to dextrose, the average chain length of the mixture. The higher the dextrose equivalent, the shorter the chain length. In order to increase the dissolution rate of the drug embedded in the maltodextrin matrix, half of the maltodextrin was replaced by a fast dissolving delta-mannitol (Parteck Delta M, Merck Group). This was expected to improve the dissolution behavior while keeping the viscous character of the intermediate paste. The third filler tested was isomalt (ISM), which is a mixture of two disaccharides, each composed of one sugar and one sugar alcohol: glucose with mannitol, and glucose with sorbitol. A highly soluble grade, galenIQ®721, is commercialized by Beneo-Palatinit (Germany).

2 Investigating the dry foam process

2.1 The effect of vacuum in dry foam process

The dry foam preparation process is described in the patent by Busson and Schröder (2006) as the drying of a paste, consisting of API, surfactant, filler and liquid, under reduced pressure, whereas the boiling point of the liquid used is not reached. The boiling point of water at a pressure of 40 mbar is 29°C. Therefore, foaming at room temperature (20°C) is within the range specified in the patent. Foaming of the paste and therefore development of a sponge like dry foam structure is considered as key characteristic of dry foam formulation technology.

The general influence of applying reduced pressure in the course of dry foam preparation is investigated, and whether drying at reduced pressure is advantageous over drying at normal pressure. For this purpose, two batches of the same composition were prepared. For the first batch the vacuum belt dryer was used for foaming and drying of the paste at a reduced pressure of 40 mbar. For the second batch a drying oven at a temperature of 40°C at ambient pressure was used. Dalcetrapib (DAL) was used as a lipophilic, poorly soluble model compound, Vitamin E-TPGS (VitE) as surfactant and maltodextrin DE 21 as filler corresponding to the dry foam formulation composition listed in Table 5.6 at a paste water content of 19% based on the wet mass.

Complete drying of the batch manufactured in the drying oven at normal pressure took over 72 h, whereas foaming and drying within the vacuum belt dryer was completed after 135 min. Morphological differences of the resulting products are illustrated using X-ray μ-CT (Section 5.3.4.2) in Figure 2.1. Whereas the dry foam prepared at reduced pressure using the vacuum belt dryer exhibited a sponge like structure with connected pores, the product prepared at ambient pressure inherited a dense structure with only few, single pores. Gain in volume due to the reduced pressure turned out to be advantageous for a faster drying of the product. Due to the foaming step, connected pores develop and the inside as well as the surface of the product becomes more permeable for the evaporating water. Additionally, heat transfer in the inner part of the foam strands is accelerated by a porous structure with large pore diameters. The second batch, prepared at ambient pressure, developed a rigid smooth outer layer, making it difficult for the water from the inside of the paste strand to permeate through. After 24 h more and more cracks developed within the products surface, and the water slowly evaporated.

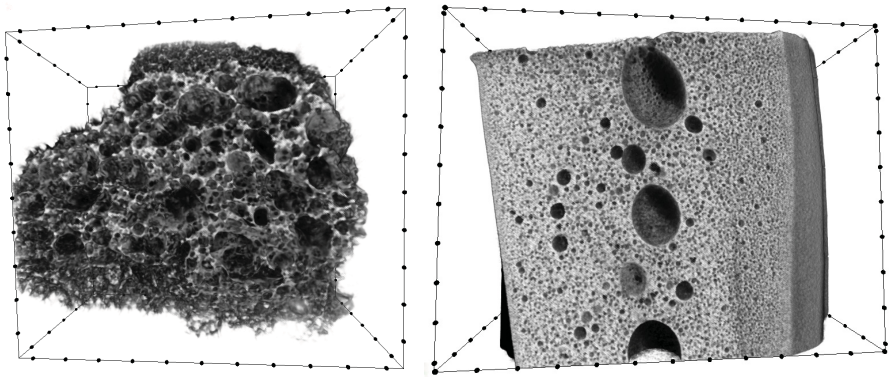

Figure 2.1: Morphological differences by drying of paste at 40 mbar (left) and at ambient pressure (right).

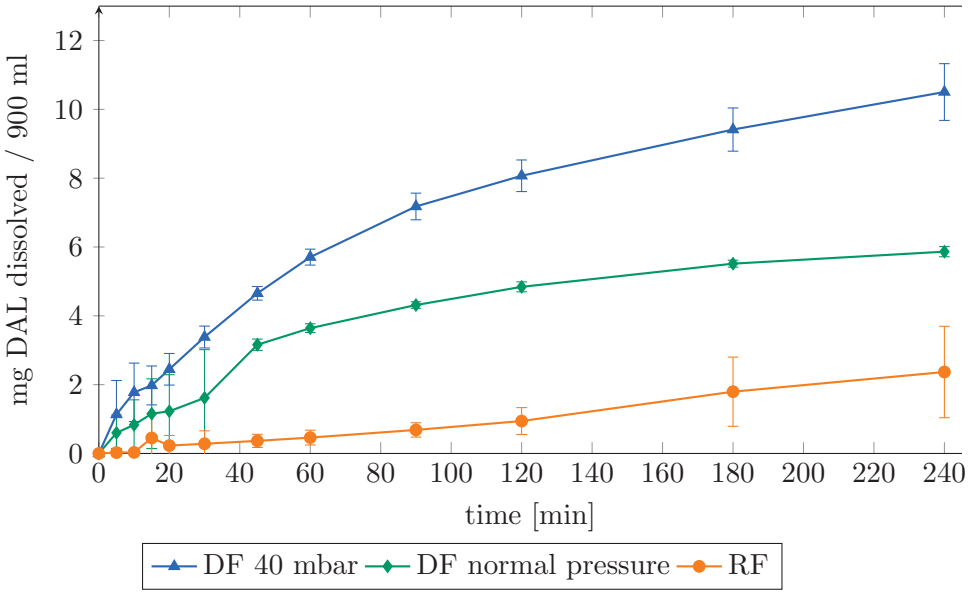

Figure 2.2: Dissolution behavior of DAL M21D VitE formulations prepared at a reduced pressure of 40 mbar using the VBT and at ambient pressure compared to RF (DAL in capsule) in FaSSIF-V2 (n=3, mean±sd).

The resulting dried products were supposed to be downstream processed in the same manner, using a Comil® for dry sieving (Section 5.2.2.6). The batch prepared at ambient pressure exhibited a denser and harder structure. DAL has a rather low melting point of 63°C. To prevent melting of the product within the Comil® due to the prolonged residence time it was crushed into smaller pieces using a glass pestle prior to dry sieving.

Specific surface area (SSA) of the resulting granules was analyzed using nitrogen absorption (Section 5.3.5.4). During dry sieving the foam pieces are broken down into smaller pieces, having approximately the size of the sieve openings. Inheriting a similar particle size distribution, differences in SSA are therefore thought to be caused by different surface structures or different foam pore sizes. The batch prepared at normal pressure exhibited only a marginally lower SSA ($0.373\,m^2/g$) than the dry foam prepared at a reduced pressure of 40 mbar ($0.398\,m^2/g$). Micronized DAL inherited a SSA of $1.15\,m^2/g$. The similar SSA of the two batches indicate a low contribution of pore surfaces as well as the micronized API to the specific surface area of the granules.

For preparation of tablets extragranular components were added to the granules and the resulting mixture compressed into tablets containing 50 mg DAL (drug load 15%) with a solid fraction of 85% (Section 5.2.2.6). Dissolution analysis of the resulting tablets was performed in triplicate using FaSSIF-V2 as dissolution medium and was compared to a reference formulation (RF) consisting of 50 mg micronized API filled into capsules (Section 5.3.7). The resulting dissolution curves are depicted in Figure 2.2. Initial dissolution rate as well as total amount of dissolved DAL increased due to the improved wettability of the API by preparation of a paste using VitE as a surfactant by both DF formulations. The foaming and drying process under vacuum seems to have an additional advantageous effect on the dissolution behavior of the resulting tablets, as the DF prepared at 40 mbar reduced pressure exceeds the DF prepared at normal pressure in both, initial dissolution rate and total amount of dissolved API.

In conclusion, dry foam preparation at reduced pressure showed to be advantageous compared to drying of paste at ambient pressure, as the drying time was reduced dramatically, downstream processing was less problematic and dissolution behavior of the resulting tablet was improved. This makes dry foam formulation technology an interesting novel technique, which is worth to be investigated further regarding process parameters as well formulation aspects.

2.2 Investigation of the foaming and drying process

2.2.1 General investigation of foaming and drying process

One of the most important process steps in dry foam preparation is the transformation of the paste to the dry foam under reduced pressure. This process step is divided in a foaming period at a lower temperature T1 and a drying period at a higher temperature T2. In order to evaluate the underlying drying kinetic during this transformation, experiments using a magnetic suspension balance were done. Using this equipment the loss in weight during foaming and drying can be recorded over the time.

The parameters paste water content (PWC [%]), process pressure (p), temperature during foaming period (T1) and temperature during drying period (T2) are thought to have an influence on the dry foam formation and were therefore varied within an experimental design as described in Section 5.2.2.2 and Table 5.7.

Table 2.1: Variable ranges of statistical design of experiments using MSB.

variable	unit	- 1	0	+ 1
PWC	%	17	21	25
p	mbar	20	50	80
T1	°C	20	30	40
T2	°C	40	50	60

The factors PWC and the time of foaming and drying period were set in a way that they mimic the typical process using the vacuum belt dryer for dry foam preparation (Section 5.2.2.5). Temperature and process pressure were varied to a higher extent. T1 for foaming was applied for 30 min and then increased to T2 for additional 105 min for further drying of the product in all experiments.

Evaporated amount of water (EVW [%]) is calculated according to Equation (2.1)

$$\mathrm{EVW}[\%] = \frac{\mathrm{X}[\%]}{\mathrm{PWC}[\%]} \cdot 100\%\,, \tag{2.1}$$

where X [%] is the loss of mass on drying [m/m] and PWC (paste water content) is calculated based on the wet mass of the paste.

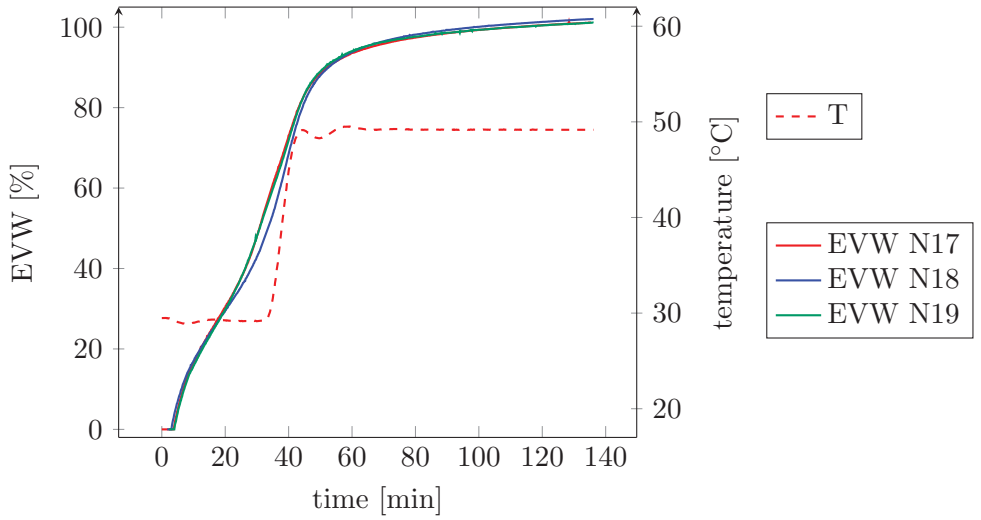

Figure 2.3: Drying curves of center point experiments (n=3) with 21% PWC at a p of 50 mbar. Experiment identification numbers Nx according to Table 5.7.

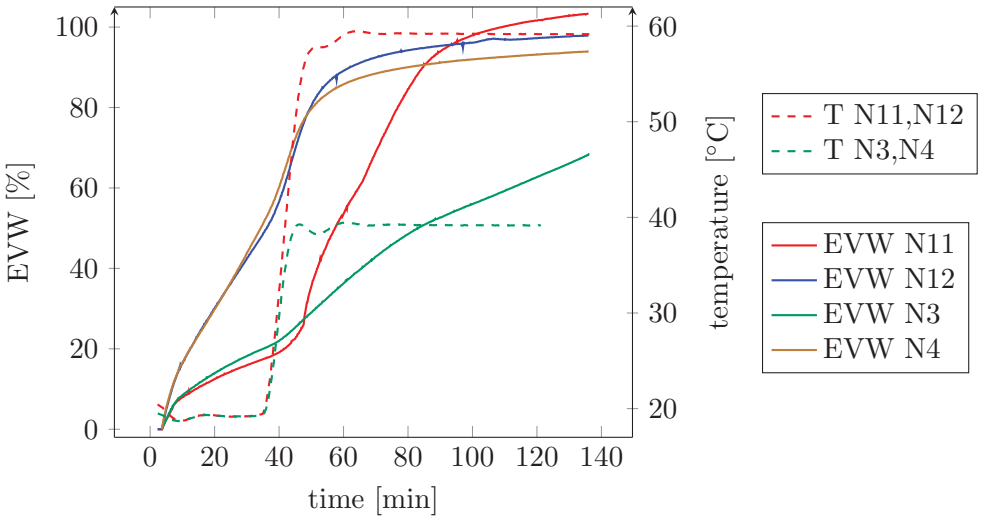

Figure 2.4: Drying curves exemplary for 17% (N3, N11) and 25% PWC (N4, N12) at a p of 80 mbar. Experiment identification numbers Nx according to Table 5.7.

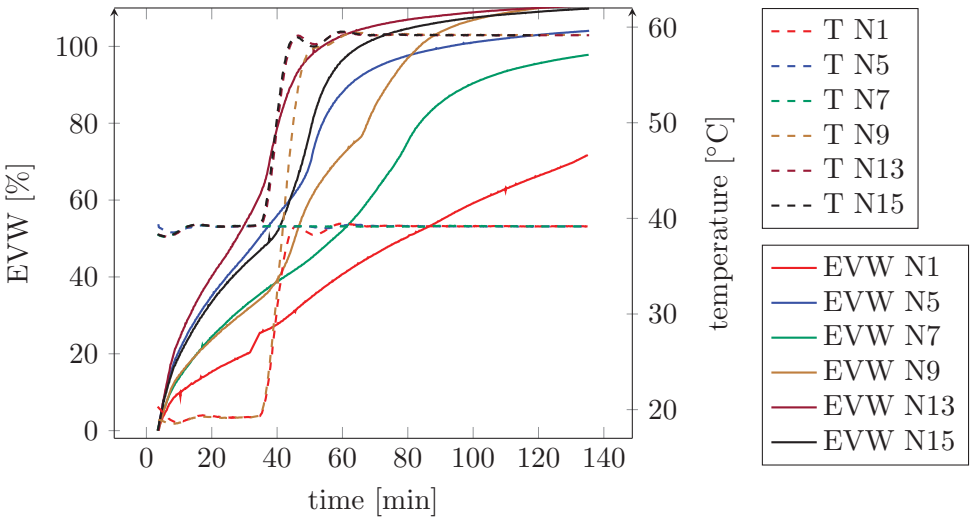

Figure 2.5: Drying curves for 17% PWC at a p of 20 mbar (N1, N5, N9, N13) and at 80 mbar (N7, N15). Experiment identification numbers Nx according to Table 5.7.

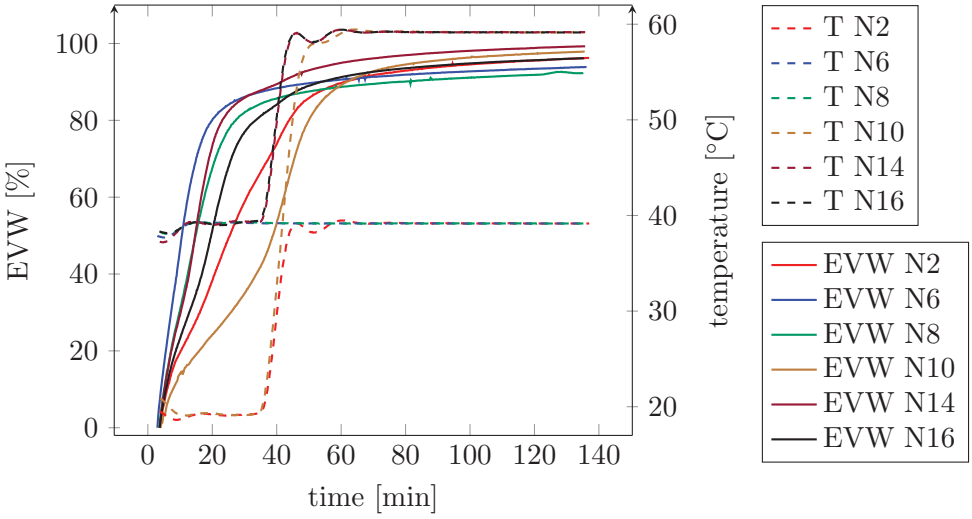

Figure 2.6: Drying curves for 25% PWC at a p of 20 mbar (N2, N6, N10, N14) and at 80 mbar (N8, N16). Experiment identification numbers Nx according to Table 5.7.

In Figure 2.3 EVW of the three center point experiments at a PWC of 21% and a p of 50 mbar is plotted over the time showing good repeatability. The temperature profile is plotted on the secondary y-axis. Loss in weight expressed by EVW exhibits an approximate sigmoidal-like behavior over time. The temperature increase after the first 30 min (T2) promotes an increasing drying speed. Afterwards, the drying rate is decreasing again at approximately 90% EVW ending in a plateau close to 100% EVW. The drying curve profile goes along with the theoretical reflections made by Mujumdar (2006). Evaporation of unbound surface moisture described as process 1 results in a fast drying during the first 10 min of the experiment, with a drying rate depending on the external conditions like temperature, pressure and air humidity. As soon as all unbound surface moisture is removed, the rate of further drying is dependent on the internal moisture movement, and in general slowed down.

In Figure 2.4 EVW is plotted over the time exemplary for 17% (N3, N11) and 25% PWC (N4, N12) at a p of 80 mbar for two different temperature profiles (T1 = 20°C, T2 = 40°C for N3 and N4, T1 = 20°C and T2 = 60°C for N11 and N12). The drying curves of the two 25% PWC samples (N4, N12) exhibit a very similar drying behavior. They exhibit a faster drying than the two samples containing 17% PWC, although being dried at the same experimental conditions like temperature and pressure. At 17% PWC the influence of temperature seems to have a higher effect on the drying speed. At a T2 of 40°C and 80 mbar pressure only 70% EVW were reached after in total 135 min of foaming and drying by sample N3.

For an complete overview the drying curves expressed by EVW of the remaining experiments are depicted in Figure 2.5 and 2.6 according to PWC. Overall, a faster drying seems to be promoted by a higher PWC (25% versus 17%) and higher drying temperatures.

Drying processes of wet solids are often described as first order kinetics, where the moisture content is a function of temperature, pressure, air humidity and time (Mujumdar, 2006). Assuming a first order kinetic for the evaporation process during foaming and drying period the dimensionless moisture content Φ_{DF} can be expressed by Equation (2.2)

$$\Phi_{\mathrm{DF}} = \frac{100 - \mathrm{EVW}}{100} = e^{-k \cdot t} \,. \tag{2.2}$$

Logarithmic transformation of Equation (2.2) results in a log of Φ_{DF} being a linear function of the time. Plotting the moisture content Φ_{DF} in a logarithmic scale over time (Figure 2.7) not a linear function, but approximately linear sections (beginning of drying periods) and the decrease in drying rate k (slope of function) are revealed (Figure 2.7). Therefore, foaming and drying of dry foam pastes can not be described as a first order kinetic. The drying rate k seems to be dependent on the time all over the drying process, resulting in Equation (2.3)

$$\Phi_{\mathrm{DF}} = e^{-k(t) \cdot t} \,. \tag{2.3}$$

Drying rate k can be calculated in every time point by the slope of the function ln Φ_{DF} over the time, according to Equation (2.4)

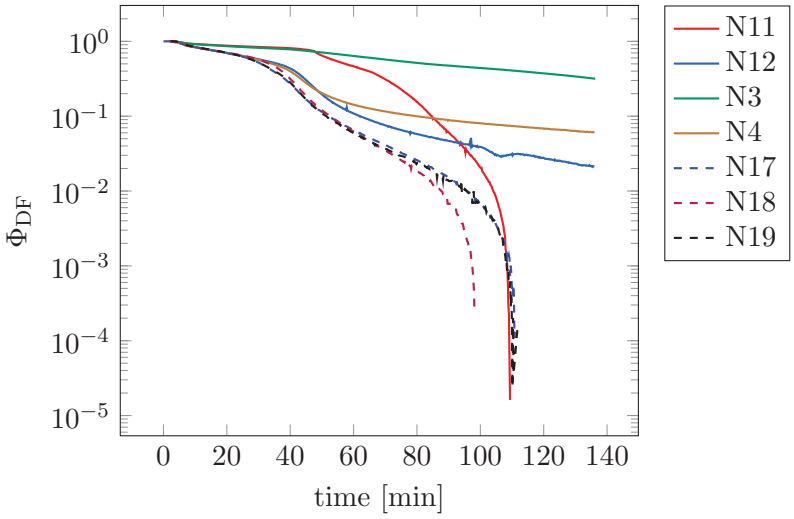

Figure 2.7: Logarithmic plot of the Φ_{DF} over time exemplary for 17% (N3, N11) and 25% PWC (N4, N12) at a p of 80 mbar and for the center point experiments at 21% PWC (N17, N18, N19).

$$k = -\frac{\Delta \ln \Phi_{DF}}{\Delta t} . \tag{2.4}$$

The change of drying rate k, calculated according to Equation (2.4), over the time during foaming period is further illustrated in Figure 2.8 and Figure 2.9. For most of the samples the drying rate is decreasing during the first 10 minutes of drying and rather constant for the last 20 minutes. This can be explained by a rapid drying of the surface moisture during the first 10 minutes, afterwards the moisture has to migrate through the developed foam and pore structure in order to reach the foam surface and evaporate. Interestingly a different drying behavior is revealed for samples containing 25% PWC at a temperature of 40°C and at 20°C at a pressure of 20 mbar. Here, the drying rate first decreases analog to the other samples, but increases after 10 to 15 minutes and afterwards decreases again. At a temperature of 40°C at 20 mbar pressure the boiling point of water is reached, whereas this is not the case at a temperature of 20°C and a pressure of 20 mbar. Therefore the difference of drying behavior can not be explained solely by samples being dried above or below the boiling point of water. It rather seems like during the first 10 minutes in these faster drying samples a porous structure is formed with an improved permeability for the evaporating water, causing an increase in drying rate.

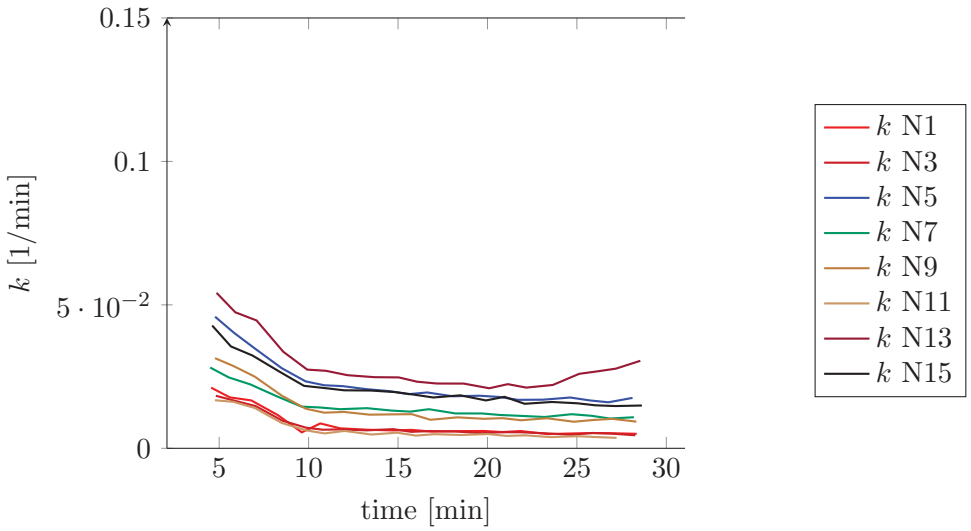

Figure 2.8: Drying rate k over the time of all MSB experiments with a PWC of 17%.

In general the drying rate depends on the external conditions (process 1) and on the characteristics of the drying solid (process 2, transfer of moisture). As the solid characteristics are changing on the course of the drying process, no specific kinetic order (zero or first order kinetic) can be fitted to the drying curves of dry foam pastes. The drying rate k is time-dependent.

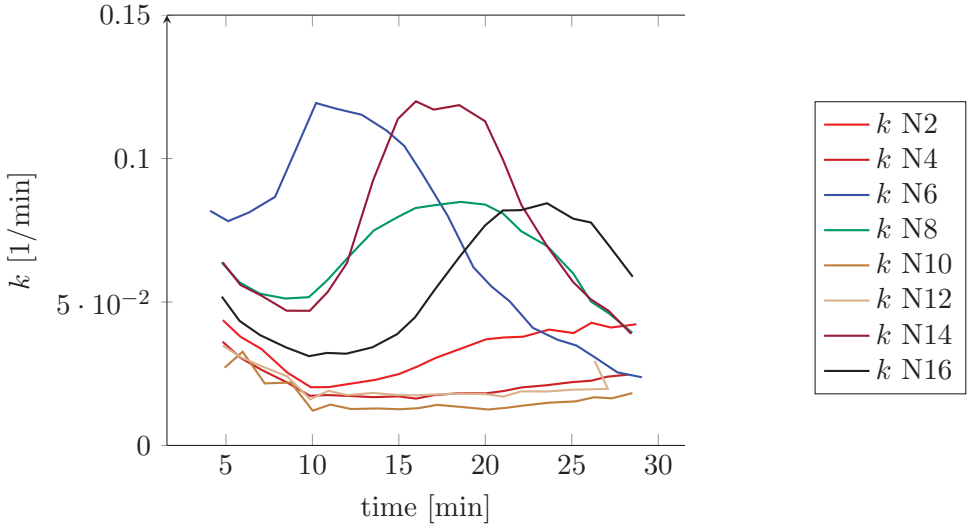

Figure 2.9: Drying rate k over the time of all MSB experiments with a PWC of 25%.

The MSB samples were subjected to X-ray microcomputed tomography (X-ray μ-CT) analysis (Section 5.3.4.2). Their pore structure could be linked to their paste water content, low paste water content samples (17%) revealed small pores, higher paste water content samples (25%) larger pores (Figure 2.10). Dry foam pores and sponge like structure are thought to develop due to the evaporation of water as a result of pressure reduction. Evaporating water forms spherical structures pressing against the surrounding paste which opposes their expansion with its viscosity and progressing drying. Depending on apparent paste viscosity, pressure and temperature different sizes of pores evolve until a dry and therefore stable structure is obtained. Theoretically, a low PWC and therefore high apparent viscosity results in small spherical slowly drying structures, whereas large, fast-drying pores are obtained at low apparent viscosities. This hypothesis was confirmed by the magnetic suspension balance experiments. The theory that the faster drying of the samples N4, N6, N8 and N16 is caused by the development of a very porous and therefore permeable structure is also confirmed by the X-ray μ-CT images. The sample N12 in Figure 2.10 exhibits a structure with smaller pores than the two other, faster drying samples at a PWC of 25%.

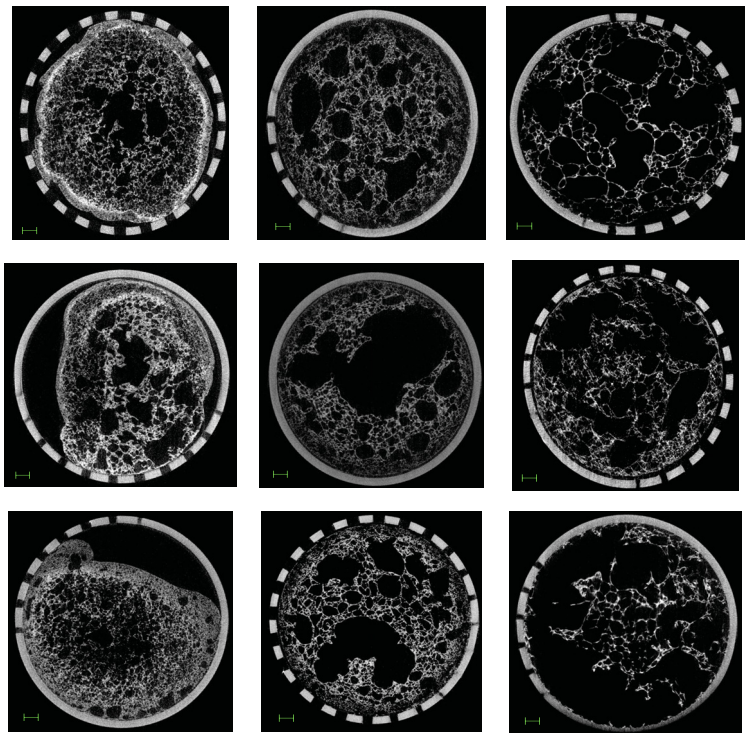

Figure 2.10: X-ray μ-CT images of DF with PWC 17% (left column, N3 (top), N11 (middle), N15 (bottom)), 21% (middle column, N17 (top), N18 (middle), N19 (bottom)) and 25% (right column, N4 (top), N12 (middle), N16 (bottom)). Scale indicated in green equals 1 mm.

2.2.2 Modelling the drying process of the foaming period

The drying kinetic of dry foam pastes is described by the drying rate k and the moisture content Φ_{DF}. In order to describe the influence of process parameters on the drying kinetic a statistical approach was used. In order to fit a model via Partial Least Square (PLS) analysis using Simca P+ 12.0.1 (Umetrics, Umeå, Sweden) to the measured data using the MSB, first the magnitude of data points was reduced by calculating average values for time and Φ_{DF} over 6 data points resulting in one data point approximately every minute. The drying rate k, the slope of $\ln\Phi_{\mathrm{DF}}$ over the time t, was calculated according to Equation (2.5) for all measurements

$$k_{(i)} = -\frac{\ln \Phi_{\mathrm{DF}_{(i-1)}} - \ln \Phi_{\mathrm{DF}_{(i+1)}}}{t_{(i-1)} - t_{(i+1)}} \,. \tag{2.5}$$

For the foaming period two independent models for $\Phi_{\mathrm{DF}(1)}$ and $k1$ were developed. $\Phi_{\mathrm{DF}(1)}$ and $k1$ were set as y variables and PWC, time, T1 and p as independent x variables without further transformation. By PLS analysis first a model without interaction terms of the x variables was developed, then interaction terms of all x variables were added, and in a third step the model refined by excluding insignificant coefficients (Tables 2.2 and 2.3).

Table 2.2: Summary table of MSB model simulating the foaming period for $\Phi_{\mathrm{DF}(1)}$.

model	interaction terms	components	R^2 $\Phi_{\mathrm{DF}(1)}$	Q^2 $\Phi_{\mathrm{DF}(1)}$
M1	without	1	0.819	0.816
M2	all	1	0.932	0.929
M3	refined	1	0.932	0.929

Table 2.3: Summary table of MSB model simulating the foaming period for $k1$.

model	interaction terms	components	R^2 $k1$	Q^2 $k1$
M1	without	1	0.619	0.618
M2	all	1	0.725	0.725
M3	refined	1	0.725	0.725

The coefficient plots of the two responses $k1$ and $\Phi_{\mathrm{DF}(1)}$ illustrate the influence of the different process parameters and the time on drying kinetic of dry foams during the foaming period (Figure 2.11). The drying rate $k1$ is decreasing over time. Increasing temperature T1 and increasing PWC promote a higher drying rate $k1$ and therefore a faster drying, whereas a high pressure decreases the drying rate k1. The product moisture content $\Phi_{\mathrm{DF}(1)}$ is decreased over time more rapidly with increasing temperature T1 and PWC. A higher pressure promotes a slower decrease in moisture content $\Phi_{\mathrm{DF}(1)}$.

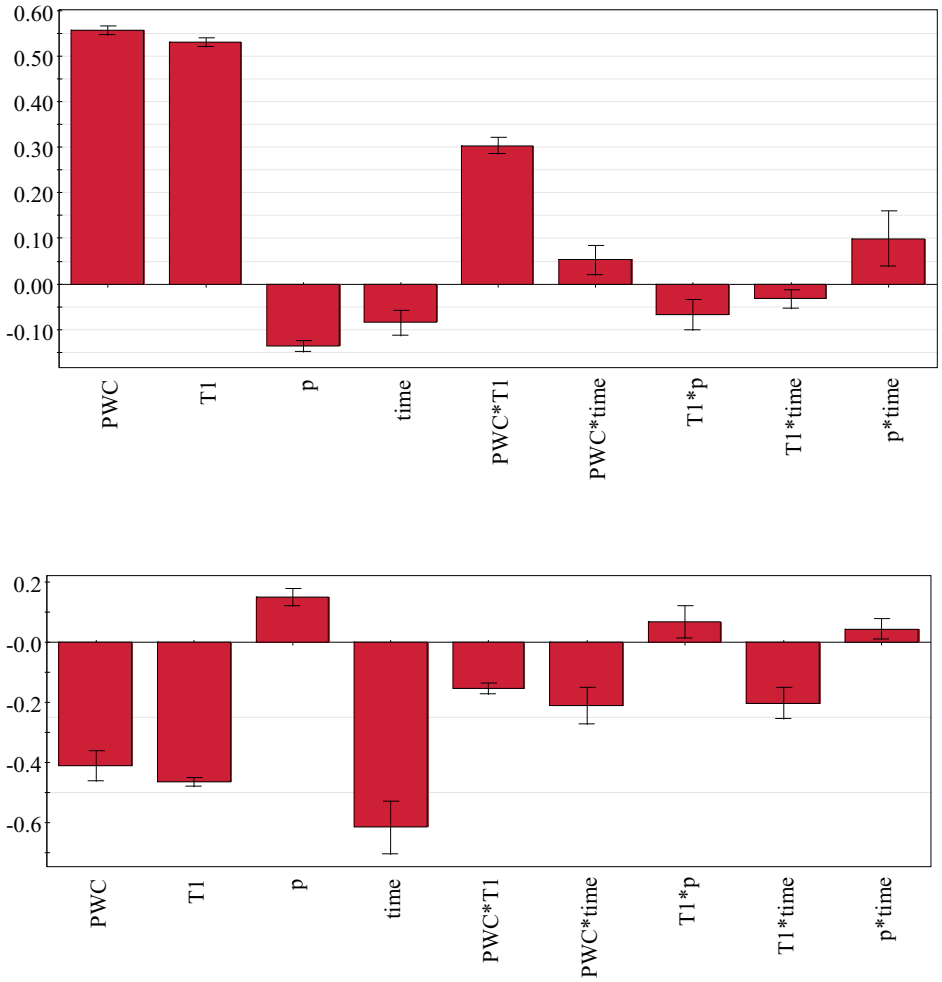

Figure 2.11: Scaled and centered coefficients of the responses drying rate $k1$ (top) and $\Phi_{\mathrm{DF}(1)}$ (bottom).

A model equation for $\Phi_{DF(1)}$ was established with the coefficients derived from the model, to predict $\Phi_{DF(1)}$ after a distinct time of foaming period under constant process conditions by Equation (2.6)

$$\begin{aligned}\Phi_{DF} = c + a_1 \cdot PWC + a_2 \cdot t + a_3 \cdot T1 + a_4 \cdot p + a_5 \cdot PWC \cdot t \\ + a_6 \cdot PWC \cdot T1 + a_7 \cdot t \cdot T1 + a_8 \cdot t \cdot p + a_9 \cdot T1 \cdot p\,,\end{aligned} \tag{2.6}$$

where a_1 etc. symbolize the coefficient values listed in Table 2.4.

Table 2.4: Unscaled coefficient values for predictive calculation of $\Phi_{DF(1)}$.

variable	symbol	coefficient	unit
constant	c	0.466302	-
PWC	a_1	0.027643	1/%
t	a_2	0.031239	1/min
T1	a_3	0.015198	1/°C
p	a_4	−0.001078	1/mbar
PWC · t	a_5	−0.001536	1/(% · min)
PWC · T1	a_6	−0.000861	1/(% · °C)
t · T1	a_7	−0.000603	1/(min · °C)
t · p	a_8	0.000043	1/(min · mbar)
T1 · p	a_9	0.000051	1/(°C· mbar)

In general, a R^2 close to 1 and a Q^2 higher than 0.5 are considered sufficient for a predictive model. The established model revealed for the y variable $k1$ a R^2 and Q^2 of 0.725. Figure 2.12 illustrates exemplary that especially the high drying rate values at the beginning of the foaming phase were not picked up on sufficiently. As no general behavior of drying rate $k1$ over the time was revealed (Figure 2.9), establishing different models for $k1$ for different time sections of the foaming period was not considered. Therefore, the model for $k1$ was not considered to fit appropiately to the measured data to establish a predictive equation for the drying rate of the foaming period.

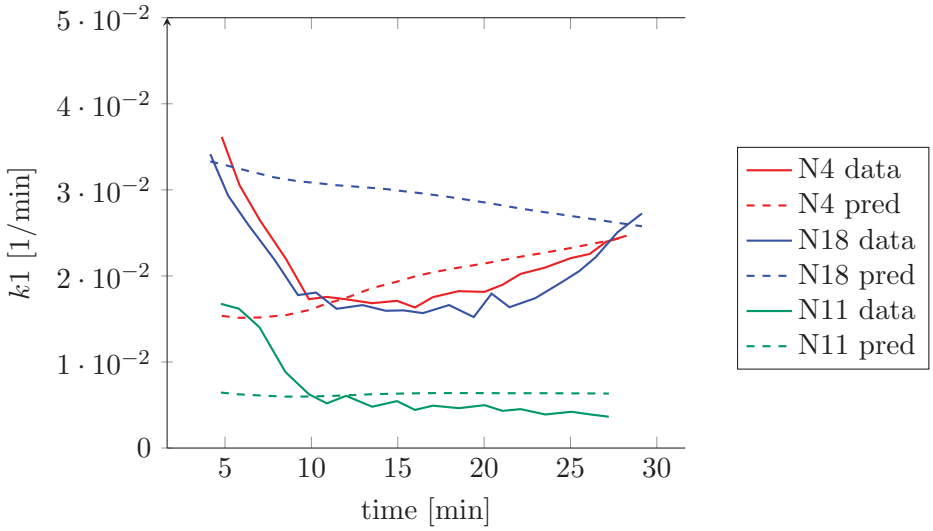

Figure 2.12: $k1$ deriving from measured data and predicted (pred) by the model.

2.2.3 Modeling the drying process of the drying period

For modeling the kinetics of the drying period upon dry foam preparation, the magnitude of data points was reduced in the same manner as described in Section 2.2.2. Independent models were established for $\Phi_{DF(2)}$ and $k2$, by setting them as y variables. PWC2, the paste water content at the beginning of the drying period was calculated according to Equation (2.7)

$$\mathrm{PWC2} = \frac{\mathrm{PWC} - \frac{\mathrm{EVW_{30min}}}{100} \cdot \mathrm{PWC}}{100 - \frac{\mathrm{EVW_{30min}}}{100} \cdot \mathrm{PWC}} \,. \tag{2.7}$$

PWC, T1, PWC2, time, T2 and p were set as x variables without further transformation. By PLS analysis first a model without interaction terms of the x variables was developed, then interaction terms of all x variables were added, and in a third step the model refined by excluding not significant coefficients (Tables 2.5 and 2.6).

Table 2.5: Summary table of MSB model simulating the drying period for $\Phi_{DF(2)}$.

model	interaction terms	components	R^2 $\Phi_{DF(2)}$	Q^2 $\Phi_{DF(2)}$
M1	without	4	0.727	0.727
M2	all	5	0.910	0.910
M3	refined	5	0.909	0.908

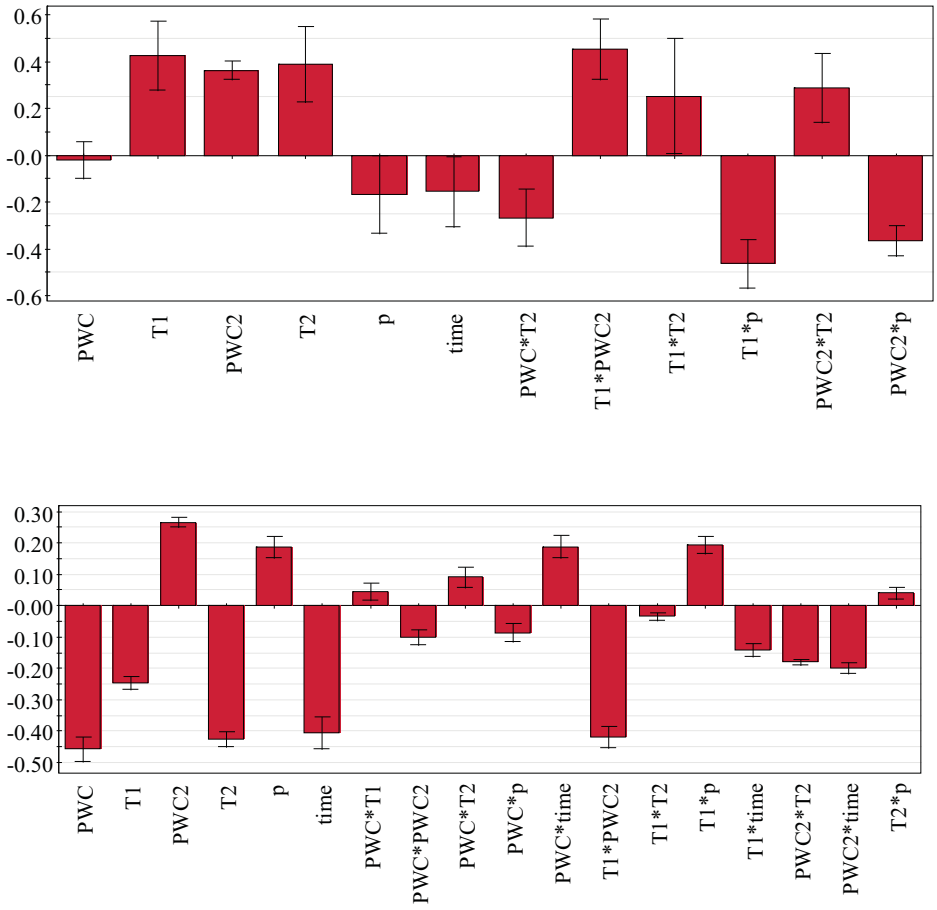

Figure 2.13: Scaled and centered coefficients of the responses drying rate $k2$ (top) and $\Phi_{\mathrm{DF}(2)}$ (bottom).

Table 2.6: Summary table of MSB model simulating the foaming period for $k2$.

model	interaction terms	components	R^2 $k2$	Q^2 $k2$
M1	without	4	0.258	0.255
M2	all	5	0.455	0.441
M3	refined	5	0.422	0.415

The coefficient plots of the two responses $k2$ and $\Phi_{DF(2)}$ illustrate the influence of the different process parameters and the time on the drying kinetic of dry foams during the drying period (Figure 2.13). Interpretation of the x variables influence on the drying kinetic during the drying period is more complex than in the foaming period, as the drying rate and moisture content of the products moisture content is influenced by the process conditions (T, p) as well as the dry foam structure predetermined by the PWC at the start of the foaming phase (PWC), the temperature during the foaming period (T1) and the moisture content of the product at the start of the drying phase (PWC2).

The terms PWC and T1 both have a decreasing effect on the moisture content of the DF during the drying period, as a high PWC and a high T1 during the foaming period will result in formation of large pores, and most of the water being vaporized. During the drying period the residual water slowly evaporates, as the gradient between moisture content and lowest possible moisture content is small. In case a high PWC is still present at the end of the foaming period (high PWC2) the moisture content $\Phi_{DF(2)}$ as well as the drying rate $k2$ are increased. The $\Phi_{DF(2)}$ is decreased and $k2$ increased by a high temperature T2, the pressure p has an opposite effect, as explained before.

The number of coefficients (18 versus 9) had to be doubled to establish a model describing the moisture content $\Phi_{DF(2)}$ during the drying period, with a good R^2 of 0.909. A model equation predicting the the moisture content Φ_{DF} during the drying period was established according to Equation (2.8) employing the coefficients listed in Table 2.7:

$$\begin{aligned}\Phi_{DF} = {} & c + a_1 \cdot PWC + a_2 \cdot T1 + a_3 \cdot PWC2 + a_4 \cdot T2 + a_5 \cdot p + a_6 \cdot t \\ & + a_7 \cdot PWC \cdot T1 + a_8 \cdot PWC \cdot PWC2 + a_9 \cdot PWC \cdot T2 + a_{10} \cdot PWC \cdot p \\ & + a_{11} \cdot PWC \cdot t + a_{12} \cdot T1 \cdot PWC2 + a_{13} \cdot T1 \cdot T2 + a_{14} \cdot T1 \cdot p \\ & + a_{15} \cdot T1 \cdot t + a_{16} \cdot PWC2 \cdot T2 + a_{17} \cdot PWC2 \cdot t + a_{18} \cdot T2 \cdot p\,.\end{aligned} \tag{2.8}$$

No predictive model equation was established for the drying rate $k2$, as with an R^2 and Q^2 of about 0.4 the model was not considered to be good enough.

Table 2.7: Unscaled coefficient values for predictive calculation of $\Phi_{DF(2)}$.

variable	symbol	coefficient	unit
constant	c	0.037999	-
PWC	a_1	−0.049752	1/%
T1	a_2	0.024794	1/°C
PWC2	a_3	0.196480	1/%
T2	a_4	−0.009028	1/°C
p	a_5	−0.000862	1/mbar
t	a_6	−0.003733	1/min
PWC*T1	a_7	0.000253	1/(% · °C)
PWC*PWC2	a_8	−0.001332	1/(% · %)
PWC*T2	a_9	0.000475	1/(% · °C)
PWC*p	a_{10}	−0.000173	1/(% · mbar)
PWC*t	a_{11}	0.000359	1/(% · min)
T1*PWC2	a_{12}	−0.003343	1/(°C · %)
T1*T2	a_{13}	−0.000071	1/(°C · °C)
T1*p	a_{14}	0.000156	1/(°C · mbar)
T1*t	a_{15}	−0.000107	1/(°C · min)
PWC2*T2	a_{16}	−0.000857	1/(% · °C)
PWC2*t	a_{17}	−0.000342	1/(% · min)
T2*p	a_{18}	0.000029	1/(°C · mbar)

In conclusion the experimental design and the derived model using the MSB for dry foam preparation identified paste water content and the temperature during foaming as well as drying period to be key process parameters. Not only the drying kinetic, but also the pore structure was influenced by the paste water content. The process pressure seemed to have a smaller influence on drying characteristics within the explored ranges. A predictive equation was established for $\Phi_{DF(1)}$ and $\Phi_{DF(2)}$. As a next step the comparability of the model developed on the MSB to the foaming process using the vacuum belt dryer was examined.

2.3 Comparing magnetic suspension balance with vacuum belt dryer

PWC and temperature during the foaming period exhibited a crucial influence on drying kinetic as well as morphology of dry foams in the MSB experiments. In order to investigate the comparability of the model developed on the MSB, the foaming period was investigated in more detail on the vacuum belt dryer (VBT). To allow a direct comparison of the measured values from the MSB and VBT the same set of parameters (PWC, p and T1) was used and the corresponding EVW-VBT [%] and $\Phi_{DF(VBT)}$ determined as described in Section 5.2.4.1.

In Figure 2.14 the measured EVW-MSB values of the MSB experiments and the measured EVW-VBT values are plotted next to each other for comparison. Interestingly, except for N2(N10), which exhibited a high standard deviation in the MSB experiments, and the center point experiments N17/N18/N19 (cP) the EVW-MSB values exceed the measured values of EVW-VBT.

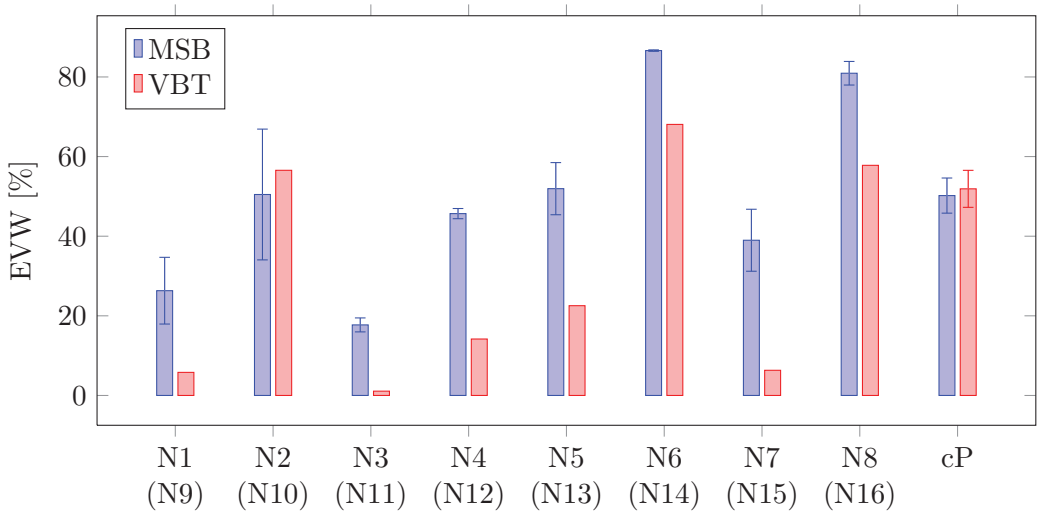

Figure 2.14: Measured EVW values of MSB (n=2, mean±sd) and VBT experiments. VBT values are single experiment values, except for the center point (cP) (n=3, mean±sd).

It becomes apparent that using the VBT a lower drying rate and therefore lower evaporated water values (EVW) are obtained under the same process conditions than using the MSB. One reason for this phenomenon can be the difference in heat transfer present in the VBT and the MSB. In the MSB the samples cell adapts quickly to the intended experimental temperature and heat is transfered faster and more efficient by convection to the drying sample. Whereas, in the VBT the temperature plates are heated to the desired temperature, and the heat is transfered by conduction first to the belt and then to the sample resulting in a less efficient drying.

Table 2.8: Measured $\Phi_{DF(VBT)}$ and predicted Φ_{pred} by the established model Equation (2.6) and the corresponding $(\Phi_{pred}- \Phi_{DF(VBT)})^2$ value as well as their sum.

exp.	PWC	p	T1	$\Phi_{DF(VBT)}$	Φ_{pred}	$(\Phi_{pred}- \Phi_{DF(VBT)})^2$
N1 (N9)	17	20	20	0.9420	0.7651	0.0313
N3 (N11)	17	80	20	0.9892	0.8303	0.0253
N2 (N10)	25	20	20	0.4345	0.4766	0.0018
N4 (N12)	25	80	20	0.8582	0.5480	0.0963
N6 (N14)	25	20	40	0.3192	0.0121	0.0943
N8 (N16)	25	80	40	0.4220	0.1450	0.0767
N5 (N13)	17	20	40	0.7745	0.4366	0.1142
N7 (N15)	17	80	40	0.9368	0.5634	0.1394
cP	21	50	30	0.4810	0.4721	0.0001
sum	-	-	-	-	-	0.5793

Another point to consider is the difference in nitrogen gas flow. Whereas for the MSB experiments a flow of 80 ml/min was necessary to maintain the predetermined reduced pressure throughout the experiment, the nitrogen flow in the VBT is much lower. A higher gas flow contributes to the transport of humidity away from the sample, and therefore promotes a faster drying.

$\Phi_{DF(VBT)}$ of the single experiments using the VBT and the predicted value $\Phi_{DF(pred)}$ by the established Equation (2.6), are listed in Table 2.8. Especially the $\Phi_{DF(VBT)}$ of experiments with a T1 of 40°C are higher than the predicted Φ_{pred} values and exhibit a higher $\sum(\Phi_{pred}- \Phi_{DF(VBT)})^2$ value.

Taking these considerations, that the influence of the gas flow and the temperature have a different influence on the drying kinetic using the VBT than the MSB, into account, attempts were made to adapt the Equation (2.6) by introducing corrective factors for the constant c (f_c) and the influence of the coefficients T1 (f_{T1}) resulting in Equation (2.9)

$$\begin{aligned}\Phi_{pred} = f_c \cdot c + a_1 \cdot PWC + a_2 \cdot t + f_{T1} \cdot a_3 \cdot T1 + a_4 \cdot p \\ +a_5 \cdot PWC \cdot t + f_{T1} \cdot a_6 \cdot PWC \cdot T1 + a_7 \cdot PWC \cdot p + \\ f_{T1} \cdot a_8 \cdot t \cdot T1 + a_9 \cdot t \cdot p + f_{T1} \cdot a_{10} \cdot T1 \cdot p\,.\end{aligned} \tag{2.9}$$

The values of f_{T1} and f_c were varied between 0 and 5 in 0.01 steps, and the corresponding sum $\sum(\Phi_{pred}- \Phi_{DF(VBT)})^2$ calculated. A minimum value of 0.151 was found for the combination of $f_{T1} = 0.74$ and $f_c= 1.14$. An overview plot of the resulting $\sum(\Phi_{pred}- \Phi_{DF(VBT)})^2$ values is depicted in Figure 2.15. A more detailed overview of the relevant section is given in Figure 2.16.

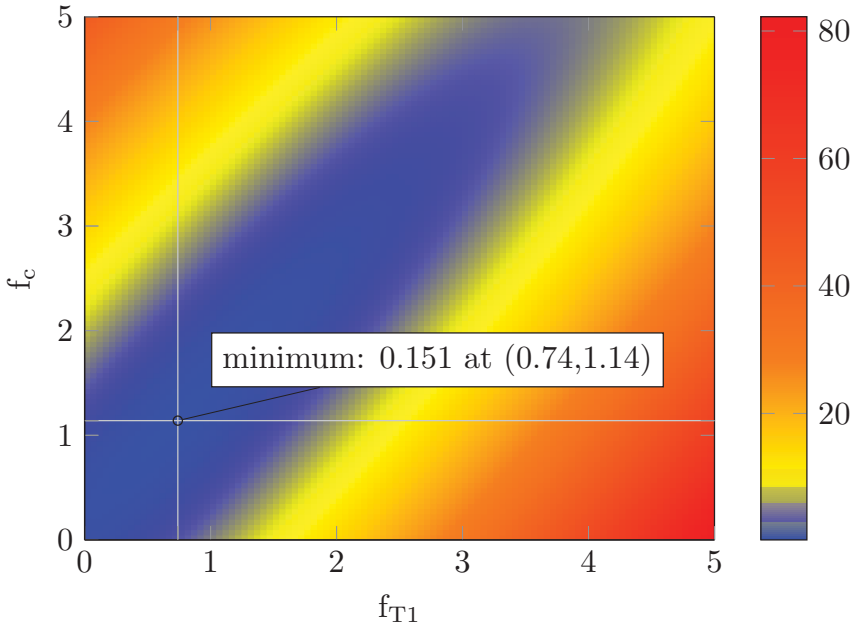

Figure 2.15: Overview plot illustrating the minimum area of $\sum(\Phi_{\text{pred}} - \Phi_{\text{DF(VBT)}})^2$ depending on the f_{T1} and f_c values.

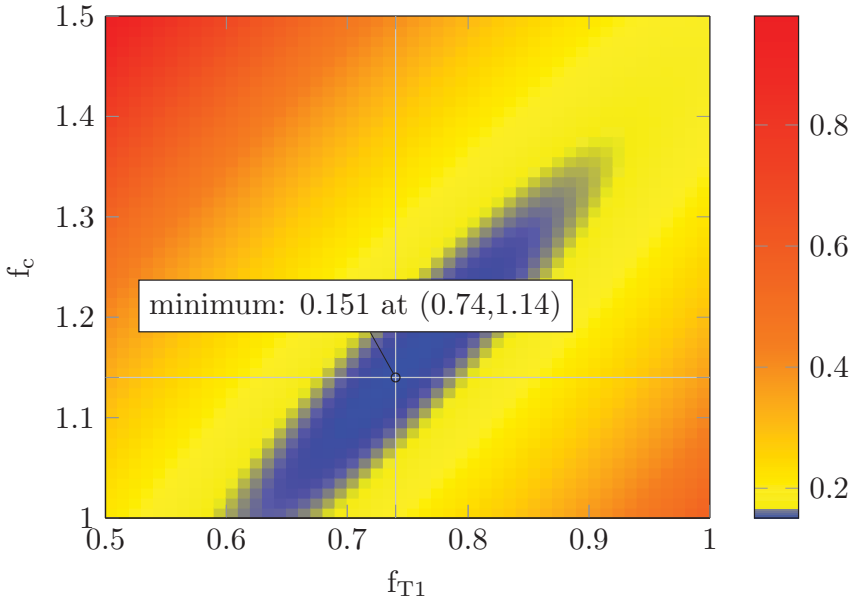

Figure 2.16: Detailed section illustrating the minimum area of $\sum(\Phi_{\text{pred}} - \Phi_{\text{DF(VBT)}})^2$ depending on the f_{T1} and f_c values.

Using X-ray µ-CT the pore structure of selected VBT samples was examined (Figure 2.17). Again, a relation between PWC and pore size development could be observed. The DF prepared with a low PWC of 17% exhibited pores of smaller diameter than the DF prepared at a higher PWC of 25%.

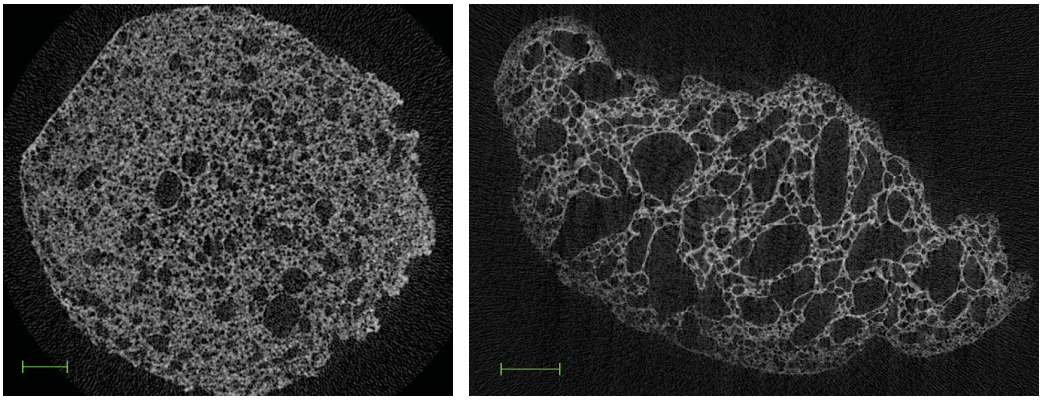

Figure 2.17: X-ray µ-CT images of DF with PWC 17% (N5 (N13)) (left) and 25% (N6 (N14)) (right) using the VBT. Scale indicated in green equals 1 mm.

Although the model derived from the MSB could not be transferred directly to the VBT as a simulation tool for dry foam preparation, it identified PWC, pressure and temperature of the two drying periods as crucial process parameters influencing dry foam morphology as well as drying kinetics. The established equation for Φ_{DF1} was adapted by introducing two corrective factors for the influence of temperature T1 and the constant c to a certain extent, and can be used for rough estimations of a resulting Φ_{DF} after the foaming period. The improvement of the model equation by introducing the correcting factors f_c and f_{T1} is illustrated in Figure 2.18. Additionally, the same correlations between paste water content and resulting dry foam morphology were observed using MSB and VBT. Pastes with a higher PWC resulted in larger pore sizes. Consequently, the questions arises whether PWC and dry foam morphology have an impact on dry foam granule characteristics as well as dissolution behavior of an incorporated API. This is examined in the following section by comparison of granule characteristics and dissolution behavior of dry foams prepared in parallel using two preparation equipments and varying paste water content.

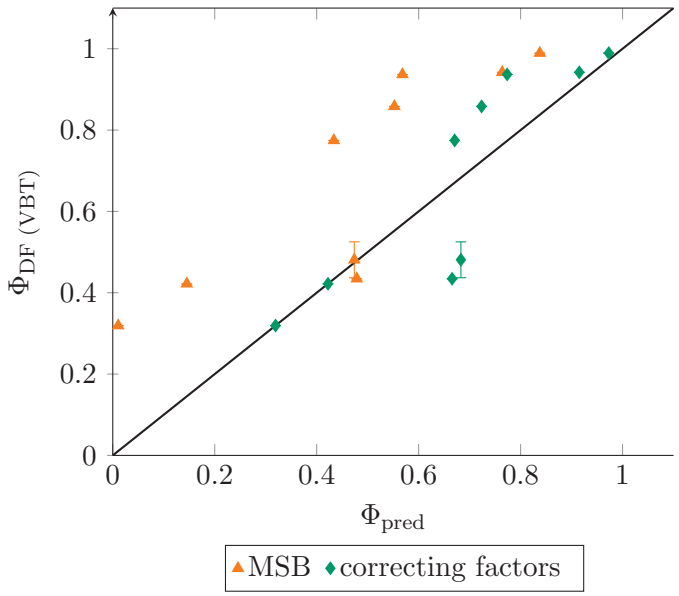

Figure 2.18: Observed $\Phi_{DF(VBT)}$ using the VBT values compared to predicted Φ_{pred} using the predictive equation derived directly from the MSB experiments (MSB) and after introducing the correcting factors f_c and f_{T1} (correcting factors). $\Phi_{DF(VBT)}$ are single experiment values, except for the center point (n=3, mean±sd).

2.4 Influence of process parameters and equipment

Currently two manufacturing equipments are available for the foaming and drying of dry foams at F. Hoffmann-La Roche Ltd. (Basel, Switzerland): a vacuum drying cabinet (VDC) for manufacturing of small scale batches and a vacuum belt dryer (VBT) for large scale and continuous processing. In the course of this section the influence of the paste water content (15 to 23%) and type of equipment used for manufacturing on the properties of dry foam granules and the corresponding tablets was investigated using indomethacin (IDM) as model compound. IDM was used as delivered (D50=33.5 µm analyzed by laser diffraction according to Section 5.3.1.1) (Section 5.1.1). Sodium laurylsufate was used as surfactant and maltodextrin DE 21 as filler. Each batch of paste was divided in two parts for parallel preparation of dry foams using the vacuum drying cabinet as described in Section 5.2.2.4 and the vacuum belt dryer as described in Section 5.2.2.5 at 40 mbar pressure. One additional batch of paste containing 17% water based on wet mass was used for preparation at 80 mbar. The final granule and tablet composition was always the same (Table 5.6).

Correlations of the examined paste water content and process pressure, apparent paste viscosity and dry foam granule characteristics are illustrated in Figure 2.19. By varying paste water content, apparent paste viscosity was changed in a non-linear logarithmic relationship. Avaltroni and coworkers found a similar correlation investigating maltodextrin concentration in solution and resulting viscosity for different types of maltodextrins and their mixtures (Avaltroni et al., 2004). Regarding processability pastes inheriting extreme apparent viscosities were difficult to handle and process as either their flow was hard to control (low viscosity) or they needed high exertion to be applied through the syringes. For the model composition the best range of apparent viscosity was 90 to 300 Pas (PWC 17% to 19%). Specific surface area (SSA) of dry foam granules represents the sum of surface area due to the pore structure, surface roughness and new surface areas originated by the sieving step of dry foam pieces. Due to the glassy nature of maltodextrin, dry foams inherit a smooth surface, which is illustrated by SEM pictures in Figure 2.21. The embedded API can contribute to the surface roughness depending on its location within the matrix. Fraction of fines (particles < 90 µm) determined by sieve analysis (Section 5.3.5.1) and SSA show no correlation in Figure 2.19. Therefore, differences in SSA are thought to be mainly originated by differences in pore size distribution. Illustrated in Figure 2.19, SSA seems to be related to PWC using VDC. 17 and 19% PWC provided the highest SSA, which was marginally influenced by the process pressure (p) used. A lower apparent paste viscosity resulted in lower SSA of the granules. However, the sample with 15% PWC prepared using the VDC inherited a lower SSA, which is thought to be due to tube formation as a result of the high apparent paste viscosity. For VBT batches no correlation between paste water content and SSA was observed, overall VBT batches inherited a lower SSA.

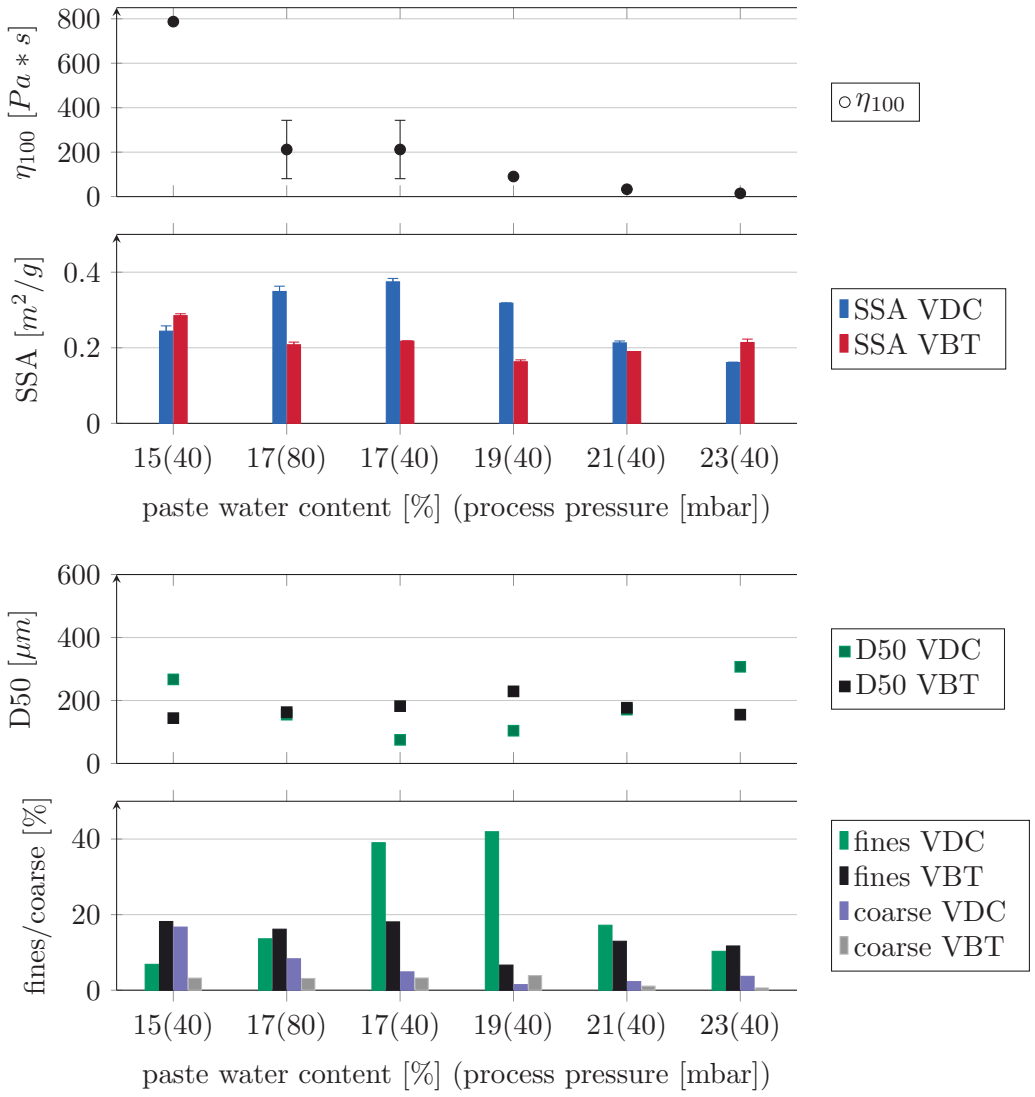

Figure 2.19: Relation of paste water content (process pressure), viscosity and granule characteristics. Viscosity of 17% PWC samples is depicted as average value with error bars indicating standard deviation. SSA measurements were performed in duplicates (mean±sd). Sieve analysis values are results of single measurements.

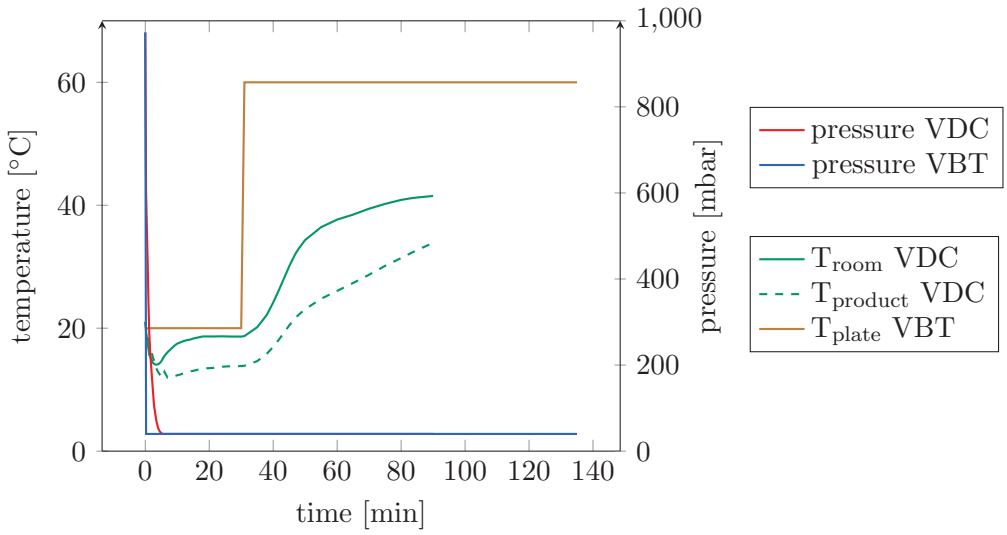

Figure 2.20: Temperature (T) and pressure profile of VDC and VBT process exemplary for a PWC of 19% and p of 40 mbar.

A comparison of the process parameters over time using VDC and VBT is depicted in Figure 2.20. Process pressure is reduced more slowly using the VDC. Hypothetically, due to slower pressure decrease a slower increase in pore size is promoted using the VDC. Therefore, smaller pores are developed until a dry and rigid foam structure is reached. Entering the VBT the paste is exposed to reduced pressure immediately, being the driving force for the growth of pores. Therefore pores grow faster during the VBT process and larger pores evolve until the dry and rigid stage of the paste is reached. This hypothesis is supported by the measured SSAs and the following X-ray µCT pictures (Figure 2.23). Variation of process pressure did not have a particular influence on SSA of the resulting granules using VDC and VBT.

Regarding sieve analysis, the fraction of fines was higher for the VDC batches with 17% and 19% water at 40 mbar process pressures, but lower at 17% water 80 mbar, whereas SSA was only marginally decreased for 17% water 80 mbar (Section 5.3.5.1). Considering the fact, that these experiments were only single measurements and not repeated, no distinct trend could be observed besides the fact that VDC batches showed a higher variability regarding fines and D50 value than VBT batches.

Another method employed to analyze pore size distribution in dry foam samples is mercury porosimetry (Section 5.3.4.1). Figure 2.22 illustrates the pore size and relative pore volume distribution of two IDM dry foams prepared with the same paste water content (19%) using VDC and VBT. The dry foam prepared using the VDC inherited a larger relative volume of pores with a diameter of 50-110 µm compared to the VBT batch. Pores larger than 120 µm, which are mainly present in the VBT sample as illustrated in Figure 2.21, are not detected by this analytical method, resulting in a smaller pore volume for the VBT sample.

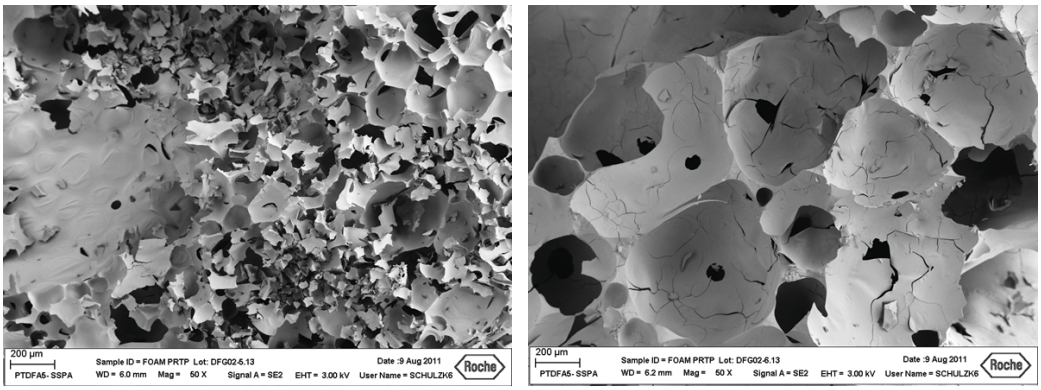

Figure 2.21: SEM images of DF prepared using VDC (left) and VBT (right) at 19% PWC and p of 40 mbar.

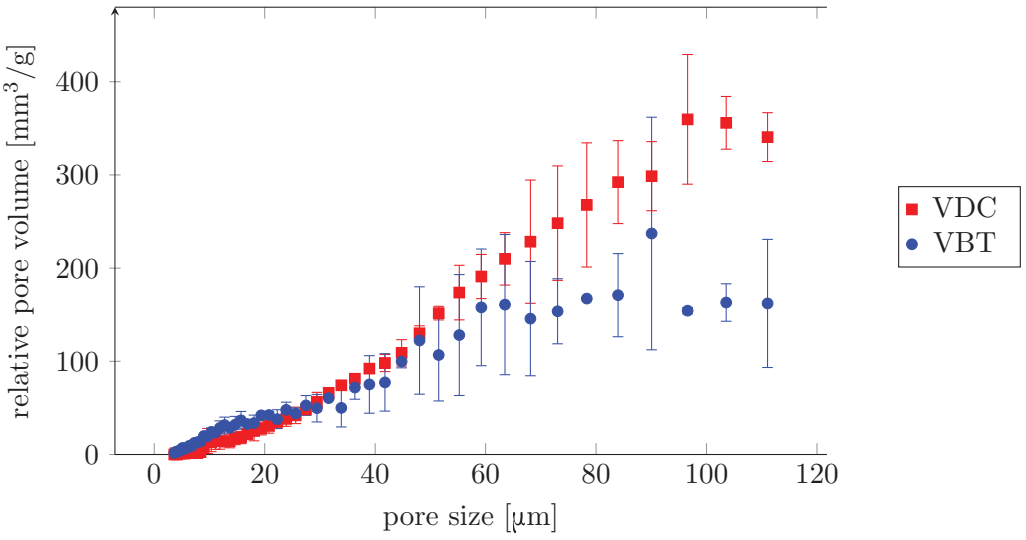

Figure 2.22: Relative pore volume of two IDM DFs prepared with 19% PWC using VDC and VBT at a p of 40 mbar analyzed by mercury porosimetry in duplicate, error bars indicating standard deviation from average value.

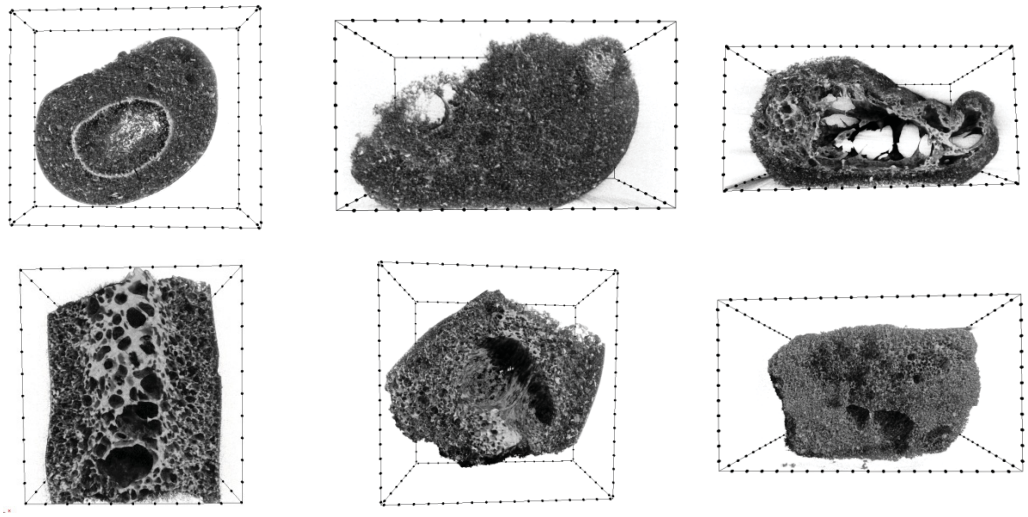

Figure 2.23: X-ray μ-CT images of DFs prepared using VDC (top) and VBT (bottom) with 17% PWC at 80 mbar (left), 19% PWC (middle) and 21% PWC (right) at 40 mbar.

Figure 2.23 illustrates the influence of paste viscosity on dry foam morphology on the basis of X-ray micro-computed tomography measurements (Section 5.3.4.2). Pore size distribution of dry foams prepared using the VDC interrelate with apparent paste viscosity, in the sense that high paste water content and therefore low viscosity resulted in larger pores. By decreasing the PWC the pore size was reduced as well, whereas also the formation of tube like structures in the inner part of the foam strand was promoted (17% water (80 mbar) VDC). During evaporation of samples with a PWC of 21% and 23% large pores tended to collapse, the difference in pore size from the inner part to the outer area of dry foam strands increased (Figure 2.23, 21% PWC). Using the VBT in general dry foams with larger pores were inherited. No distinct relation between paste water content and pore size distribution was observed. The difference in pore size between inner and outer part of the dry foam strands was more prominent for samples with paste water content of and below 19%.

In summary, using the VDC the hypothesis of small pores as result of high apparent paste viscosity was confirmed by different analytical methods. The smaller pores size of VDC dry foams in general indicate an influence of pressure reduction speed on the dry foam structure. Using the VBT for dry foam preparation paste water content and process pressure only marginally influenced dry foam morphology without revealing a distinct trend.

Loss on drying (LOD) of prepared dry foam batches using VDC and VBT was analyzed using a Moisture Analyzer (Mettler Toledo) at a temperature of 90°C. An overview of the results is given in Table 2.9. Batches with a low PWC exhibited a higher LOD [%] than batches with a higher PWC for both preparation equipments.

Table 2.9: LOD of the DF granules (LOD_{DF}) prepared using the VDC and VBT.

process	PWC [%]	p [mbar]	LOD_{DF} [%]
VBT	15	40	4.03
VBT	17	40	3.83
VBT	17	80	4.15
VBT	19	40	3.72
VBT	21	40	2.55
VBT	23	40	1.01
VDC	15	40	5.50
VDC	17	40	4.35
VDC	17	80	4.23
VDC	19	40	2.42
VDC	21	40	2.56
VDC	23	40	2.93

Overall, VDC batches exhibited higher LOD values than the corresponding VBT batches. PWC was found to influence drying kinetic of dry foams throughout the MSB and the corresponding VBT experiments in the sense, that a faster drying is achieved with a higher PWC, as larger pores are developed during the foaming period promoting a faster drying. This proposition was confirmed by the VBT and VDC experiments. The higher LOD values of the VDC samples can be explained by the shorter drying period and the lower gas flow within the VDC.

Dissolution behavior (Section 5.3.7) of DF formulations of IDM as delivered (D50=33.5 µm) prepared under different process conditions and of a reference formulation (RF) consisting of the same dose IDM as delivered filled in hard gelatin capsule were analyzed in FaSSIF-V2 (Jantratid et al., 2008) (Figure 2.24). RF exhibited a slow and variable dissolution behavior of IDM due to poor wettability and low dissolution rate characteristics. In contrast, all dry foam formulations resulted in complete dissolution of the applied dose IDM after 30 to 45 min respectively. The improved wettability of IDM by dry foam formulation technology resulted in a faster and more reproducible dissolution behavior. Considering the use of a non-micronized crystalline API for DF preparation rather than amorphous or monomolecular dispersed, good achievements were made in wettability and therefore dissolution behavior improvement. Process parameters and type of equipment used had no distinct influence on dissolution behavior. Small differences in total dissolved amount of API are understood as a result of non-uniformity of content. Although, dry foam morphologies and resulting granule characteristics are influenced by process parameters and equipment used the resulting formulations exhibit consistent dissolution characteristics. Similar results were obtained in an additional study using fenofibrate and felodipine as model compounds (Sprunk et al., 2012).

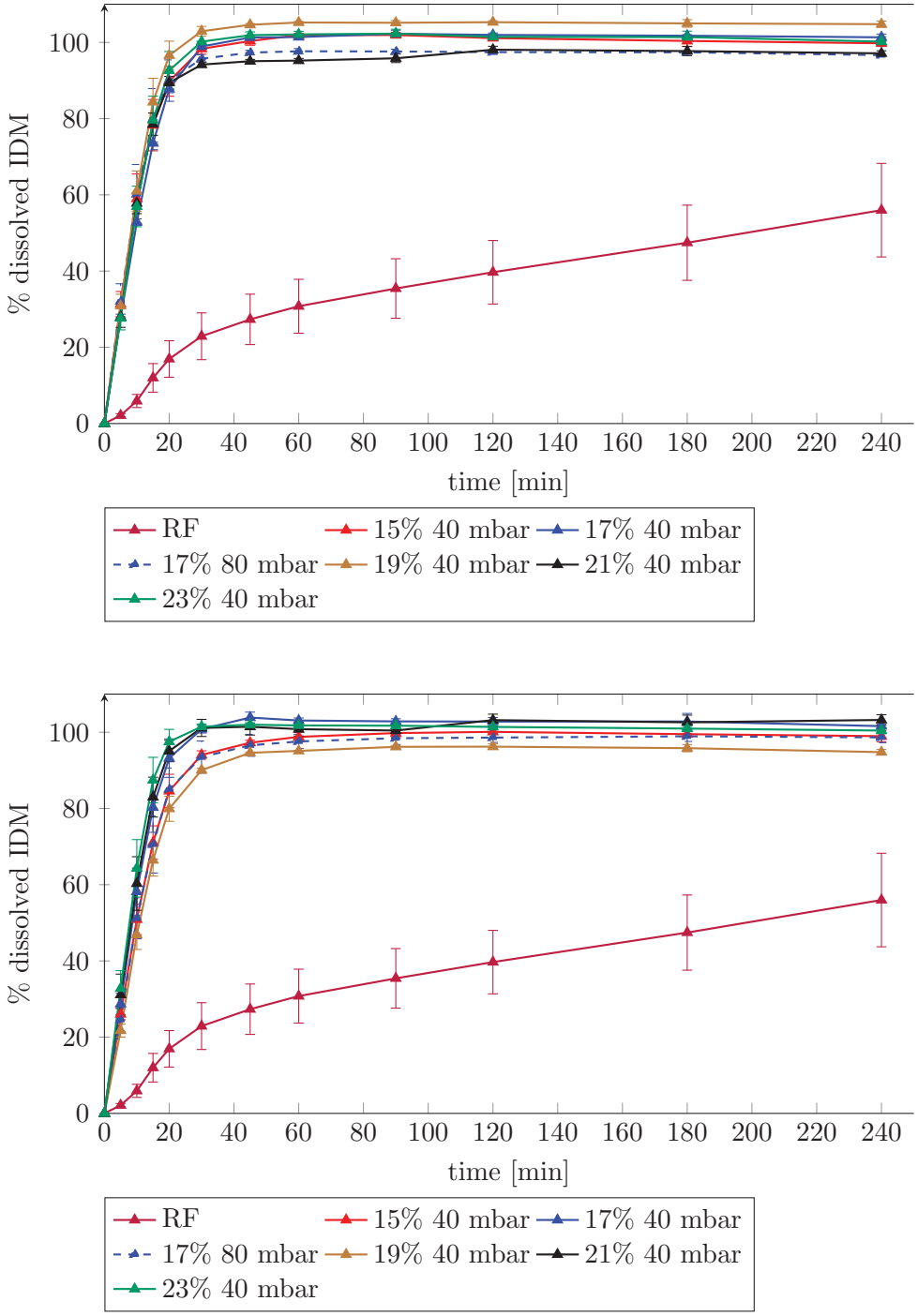

Figure 2.24: Dissolution behavior of 50 mg IDM (as delivered) formulations using VDC (top) and VBT (bottom) at different PWC [%] and process pressure [mbar] and RF (50 mg IDM as delivered in capsule) in FaSSIF-V2 (n=3, mean±sd).

2.5 Summary and Conclusion

The aim of this chapter was to further investigate the novel formulation process of dry foam granulation to identify its key process parameters and to assess useful analytical methods for formulation development. Drying of a paste under reduced pressure showed advantages over drying of a paste at normal pressure. Not only was drying time reduced and downstream processing improved, also the dissolution behavior of dry foam tablets was superior after vacuum foaming and drying.

Investigating drying kinetics of dry foam preparation by using the magnetic suspension balance, paste water content and process temperature were identified as main influence factors on the speed of drying. A higher paste water content and a higher temperature promoted faster drying of the samples. The process pressure used exhibited a less prominent influence on drying characteristics within the explored ranges. Drying kinetics showed to be also dependent on the process conditions used. As speed of pressure reduction, heat transfer as well as gas flow are different in the three explored preparation equipments MSB, VDC and VBT, different drying kinetics were exhibited. The model established by the MSB experiments could not be transfered directly to the VBT foaming period experiments, but was adapted introducing two correction factors, taking the difference in heat transfer and in gas flow into account.

Dry foam morphology was influenced mainly by paste water content. A low paste water content resulted in smaller pore diameters due to higher paste viscosity. The equipment used showed to influence dry foam morphology as well. In general larger pore diameters were achieved using the VBT compared to the VDC. Interrelations between dry foam morphology and drying kinetic were also observed. Samples developing pores of larger diameter during the foaming phase, dried faster during the drying period.

The influence of paste water content and type of equipment used on dry foam morphology, granule characteristics and dissolution behavior of the corresponding tablets was examined using indomethacin as model compound. Multiple analytical methods, namely scanning electron microscopy, X-ray micro-computed tomography and mercury porosimetry, specific surface area analysis and sieve analysis were employed. Dissolution of dry foam formulation tablets was compared to a reference formulation in biorelevant media. Relations between apparent paste viscosity and pore size distribution could be observed. Additionally, relationship between paste water content and final moisture content of the product (LOD) after drying was confirmed. The employed analytical methods allowed an insight into dry foam morphology and accomplished each other. Despite the morphological effects of paste water content and equipment used, the dissolution behavior of DF tablets was unaffected by changing process parameters used. In summary, small scale VDC experiments can give a good prospect on dissolution behavior after transfer to continuous manufacturing on the VBT but not on granule characteristics. Paste water content can be adjusted to required viscosity for processability reasons without diminishing the resulting formulations dissolution behavior.

3 Investigating formulation aspects of dry foams

3.1 Screening study on four poorly soluble APIs

Dry foam technology was developed to overcome low oral bioavailability of poorly soluble and wettable APIs. In order to further evaluate and examine the effect of granulation method on granule characteristics as well as dissolution behavior, dry foam technology is systematically compared to fluid bed granulation for a variety of APIs, with low aqueous solubility, and a range of different surfactants. As the physico-chemical properties of the API might have an effect on the granule characteristics and dissolution behavior, four different compounds should be investigated in the first study. In Figure 3.1 oral BCS class II compounds (Benet et al., 2011) are plotted according to their solubility, melting point and lipophilicity. Four compounds distinguishing themselves in melting point, lipophilicity (log P value), solubility in water and biorelevant media are highlighted in red and were selected for a screening study. The physico-chemical properties of the four poorly soluble, micronized model compounds, orlistat, fenofibrate, indomethacin and felodipine, are listed in Table 3.1. Particle size distribution was determined according to Section 5.3.1.1 by laser diffraction and specific surface area (SSA) according to Section 5.3.5.4 analog to the formulation granules.

For wetting of the model compounds six surfactants representing different chemical classes were selected. Docusate sodium (dodecyl succinate sodium) is an anionic surfactant and wetting agent with a hydrophilic lipophilic balance (HLB) value of 10. Sodium dodecyl sulfate (SDS) is an anionic surfactant and emulsifying agent with a HLB of approximately 40. Polyoxyethylene (20) sorbitan monooleate (polysorbate 80) is a nonionic surfactant and wetting agent with a HLB of 15, polyoxyethylene (40) monostearate (Myrj S40) (Myrj) is a solubilizing and wetting agent with a HLB of 17. Vitamin E TPGS (d-α-Tocopheryl Polyethyleneglycol 1000 Succinate) is a water soluble derivate of the natural vitamin E, prepared by esterification of the crystalline d-α tocopheryl succinate and polyethylene glycol 1000, with a HLB of approximately 13. It is widely used as solubilizing and wetting agent. Poloxamer 333 (Pluronic P103) (P103) is a pasty solubilizing and wetting agent consisting of 3250 g/mol polypropylene oxide and 30% polyethylene oxide [m/m] with a HLB of approximately 9.

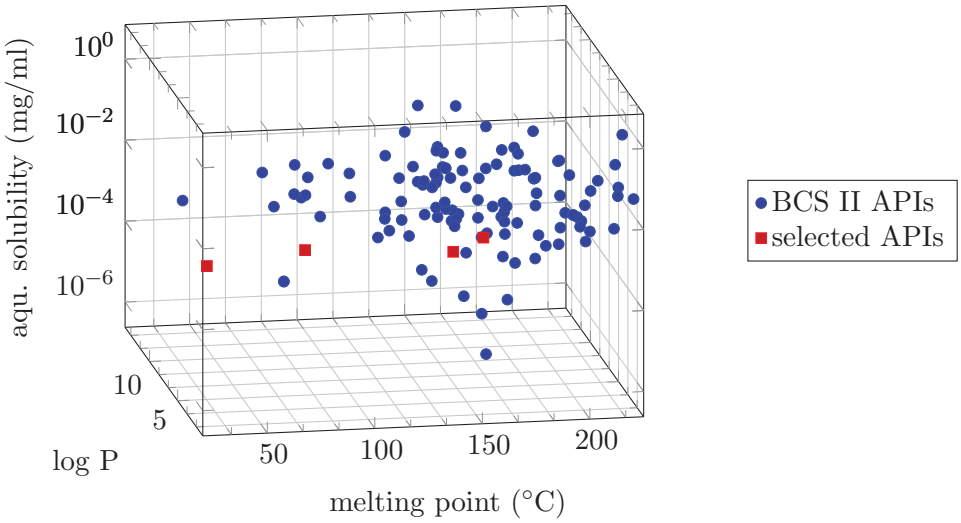

Figure 3.1: BCS II compounds deriving from Benet et al. (2011) for oral delivery and selected APIs.

Table 3.1: API characteristics including melting point (MP), log P and aqueous solubility according to Benet et al. (2011) and internal F.Hoffmann-La Roche data, FaSSIF-V2 solubility, D50 value, specific surface area (SSA) and their abbreviation (abbr.).

abbr.	API	MP [°C]	log P	aqueous solubility [µg/ml]	FaSSIF-V2 solubility [µg/ml]	D50 [µm]	SSA [m^2/g]
IDM	indomethacin	158	4.27	2.5	320.21	3.45	5.03
FDP	felodipine	145	3.86	1	10.15	5.89	3.07
FEN	fenofibrat	80	5.19	0.8	5.74	7.25	2.51
THL	orlistat	43	8.19	0.09	0.92	6.96	2.41

Solubility of indomethacin, a non-steroidal anti-inflammatory agent, in FaSSIF-V2 was determined as 0.32 mg/ml after 4 h at 37°C end-over-end rotation as described in Section 5.3.8. No increase in dissolved amount of API was found after 24 h. In comparison to the other model compounds, IDM has a rather good solubility in FaSSIF-V2, and a good permeability (BCS II) (Benet et al., 2011). Due to its poor wettability and therefore low initial dissolution rate, it can be categorized as DCS IIa compound at a dose of 50 mg. The initial dissolution rate in the gastrointestinal tract is considered as the rate limiting step for bioavailability. Solubility of felodipine (FDP) was determined as 10.15 µg/ml FaSSIF-V2, and is therefore identified as DCS class IIa (at a dose of 50 mg), anticipating its bioavailability to be dissolution rate limited. Solubility of fenofibrate (FEN) was determined as 5.74 µg/ml

in FaSSIF-V2 after 4 h end-over-end rotation, resulting in dose/solubility ratio of 8711 ml (=50 mg/ 0.00574 mg/ml) and therefore a DCS classification of class IIa (Butler and Dressman, 2010). THL solubility determination is rather difficult due to its poor wettability and floating tendency. End-over-end rotation at 37°C in FaSSIF-V2 resulted in a solubility of 0.9 µg/ml after 4 h and in 18.2 µg/ml after 24 h emphasizing the poor wettability and slow initial dissolution characteristics of the drug. Due to its poor permeability it is classified as BCS class IV (Benet et al., 2011). Orlistat (tetrahydrolipstatin, THL) is a potent gastrointestinal lipase inhibitor, and minimally absorbed in the systematic circulation. Its pharmaceutical point of activity is the lumen of the gastrointestinal tract (Harp, 1999). Improved initial dissolution behavior is thought to increase its local pharmacological activity.

The model compound THL was received from F. Hoffmann-La Roche in micronized quality, whereas IDM, FEN and FDP were subjected to air jet milling in order to reduce their particle size and enhance their initial dissolution rate and therefore bioavailability. Scanning electron microscopy (SEM) pictures, prepared as described in Section 5.3.10, illustrate their agglomeration tendency and morphology (Figure 3.2). Their specific surface area (SSA) and D50 values, determined by laser diffraction (Section 5.3.1.1), are listed in Table 3.1. Dry foams containing the four poorly soluble model compounds were prepared using the vacuum belt dryer, as described in Section 5.2.2.5. The paste water content was set to 19% calculated on the wet mass enabling a good processability of the paste. FBG were prepared according to Section 5.2.3. Dry foam pieces and fluid bed granules were downstream processed according to Section 5.2.2.6.

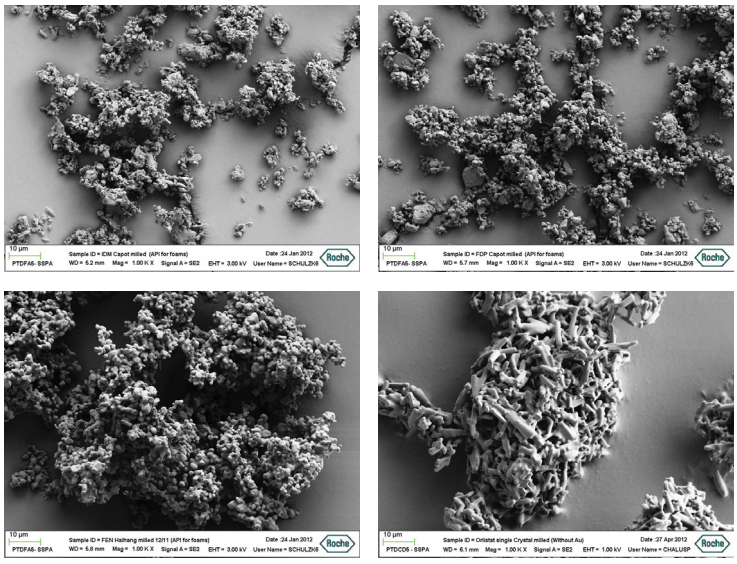

Figure 3.2: SEM pictures of micronized model compounds, IDM (top left), FDP (top right), FEN (bottom left) and THL (bottom right).

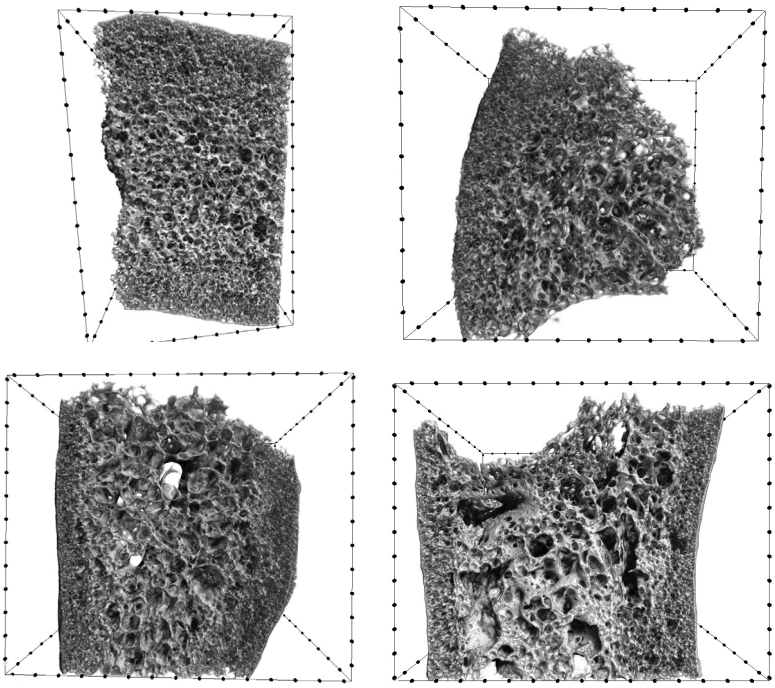

Figure 3.3: X-ray μ-CT pictures of DF IDM (top left), DF FDP (top right), DF FEN (bottom left) and DF THL (bottom right) using VitE as surfactant.

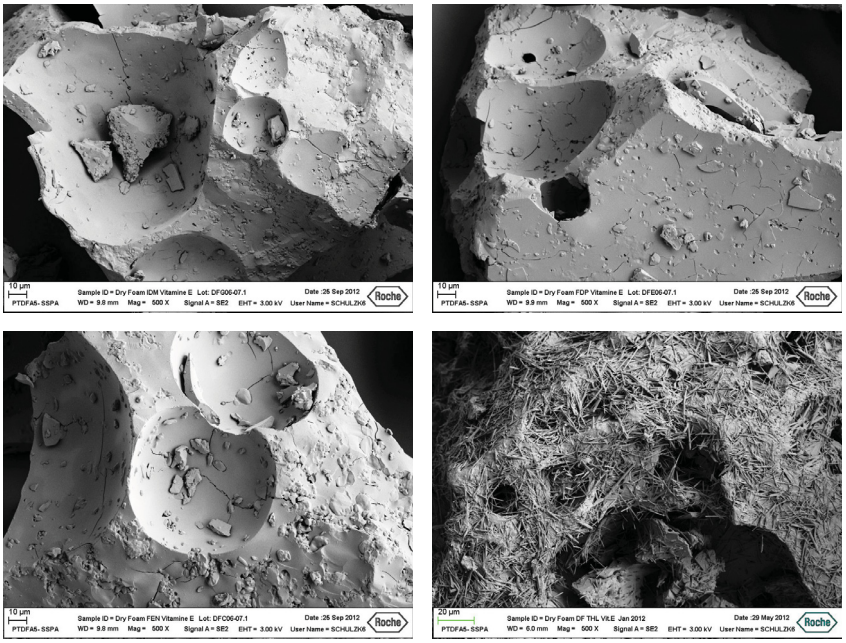

Figure 3.4: SEM pictures of DF IDM (top left), DF FDP (top right), DF FEN (bottom left) and DF THL (bottom right) using VitE as surfactant.

Dry foam morphology was analyzed using X-ray μ-CT (Section 5.3.4.2), exhibiting a similar morphology with small pores in the outer area and larger, sometimes tube-like structures in the inner part for all four APIs (Figure 3.3).

SEM pictures in Figure 3.4 illustrate the API distribution within the foam matrix and on the foam surface. Whereas IDM, FDP and FEN are mainly incorporated within the maltodextrin matrix, THL seems to accumulate on the dry foam surface in fine hair-like needles.

Specific surface area (SSA) (Section 5.3.5.4) of DF and FBG granules is illustrated in Figure 3.5. Interestingly, except for THL, FBG granules exceed DF granules by far in SSA. This difference can be explained by the difference in the manufacturing process and API distribution. Whereas by DF preparation the API is built in the fillers matrix resulting in a smooth surface area due to the glassy nature of maltodextrin DE 21, after fluid bed granulation the API can still contribute to the granules surface area. Higher specific surface area values for DFs containing THL can be explained by the accumulated THL needles on the dry foam surface contributing to the specific surface area.

D50 values derived from sieve analysis (Section 5.3.5.1) of DF and FBG granules are plotted in Figure 3.6. They do not correlate with SSA values in the way that a smaller D50 value and therefore smaller particle size results in a higher specific surface area. Therefore SSA differences are believed to derive from differences in surface structure and pore size distribution. DF granules prepared using SDS resulted in extremely low D50 values using IDM and FDP as model compounds, which goes along with the observed harder structure of the dry foam pieces prior to dry sieving. Due to the higher hardness of these dry foam pieces, they were abraded slowly rather than breaking down in smaller pieces, which resulted in a longer residence time within the milling cone as well as a higher fraction of fine particles.

The dissolution behavior of FBG and DF formulations inheriting the same drug load, tablet weight and API-surfactant ratio was compared to reference formulations (RFs) consisting of the micronized API filled into capsules according to Section 5.3.7. IDM is a frequently used model compound for testing the capability of formulation techniques to improve dissolution behavior. Besides amorphous strategies (Sun et al., 2012; Yano and Kleinebudde, 2010) crystalline formulation techniques like spheronization (Eerikäinen and Lindqvist, 1991) or non-aqueous liquisolid and compaction technique (Yadav and Yadav, 2009) are described in literature for solubility and dissolution improvement. Dissolution behavior is most often analyzed in phosphate buffer with or without adding surfactant (Eerikäinen and Lindqvist, 1991; Laakso and Eerikäinen, 1991; Yadav and Yadav, 2009). Van Speybroeck and coworkers emphasized the importance of biorelevant media in in-vitro dissolution analysis of poorly wettable APIs for predictive results in their work with ordered mesoporous silica SB-15 formulations. Here, the API is first dissolved in organic solvent and then loaded on the silica particles. It is thought to be monomolecular dispersed within the matrix. Complete dissolution of the IDM was accomplished after 20 min in FaSSIF (van Speybroeck et al., 2011).

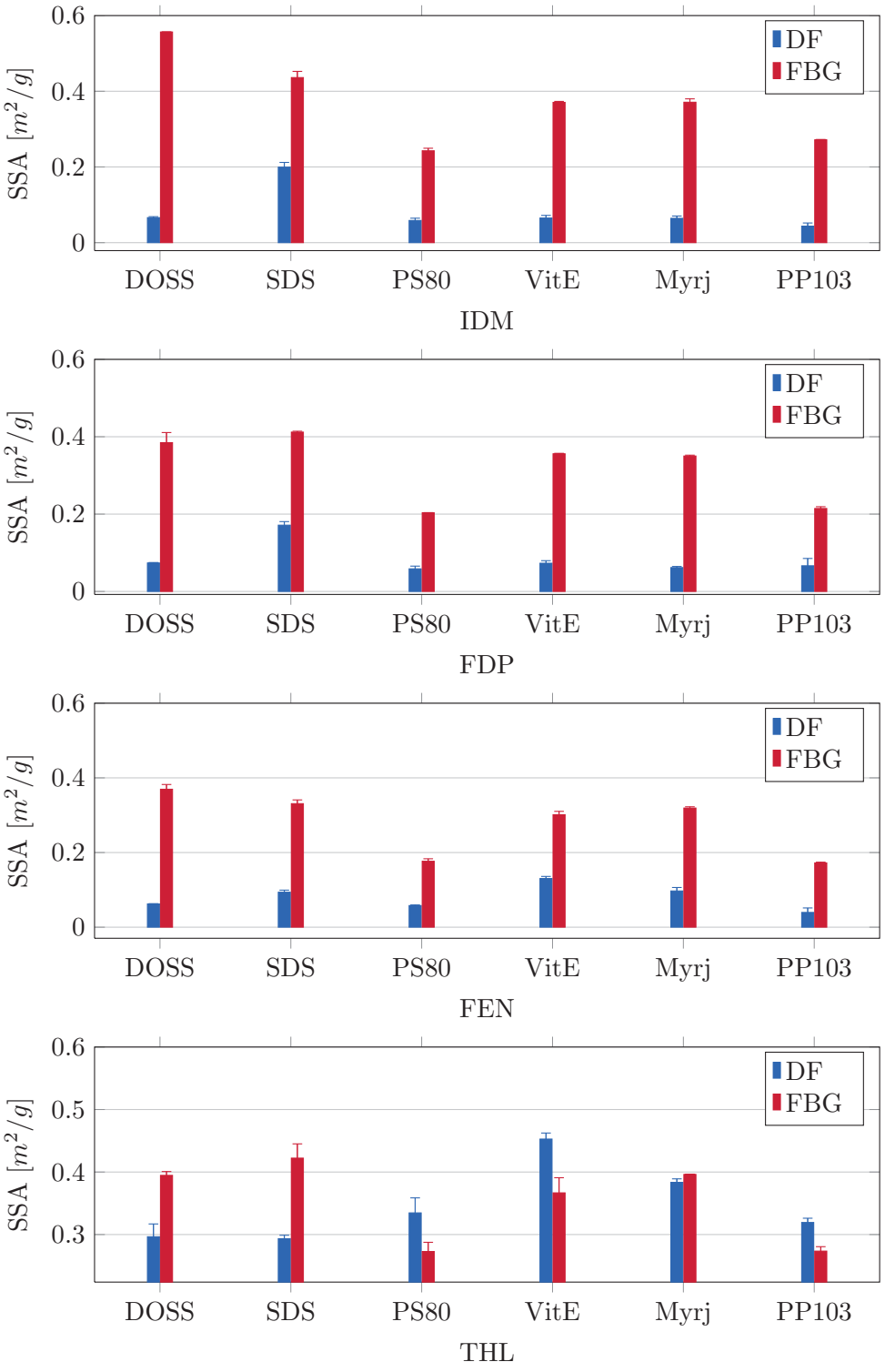

Figure 3.5: SSA of DF and FBG granules (n=2, mean±sd).

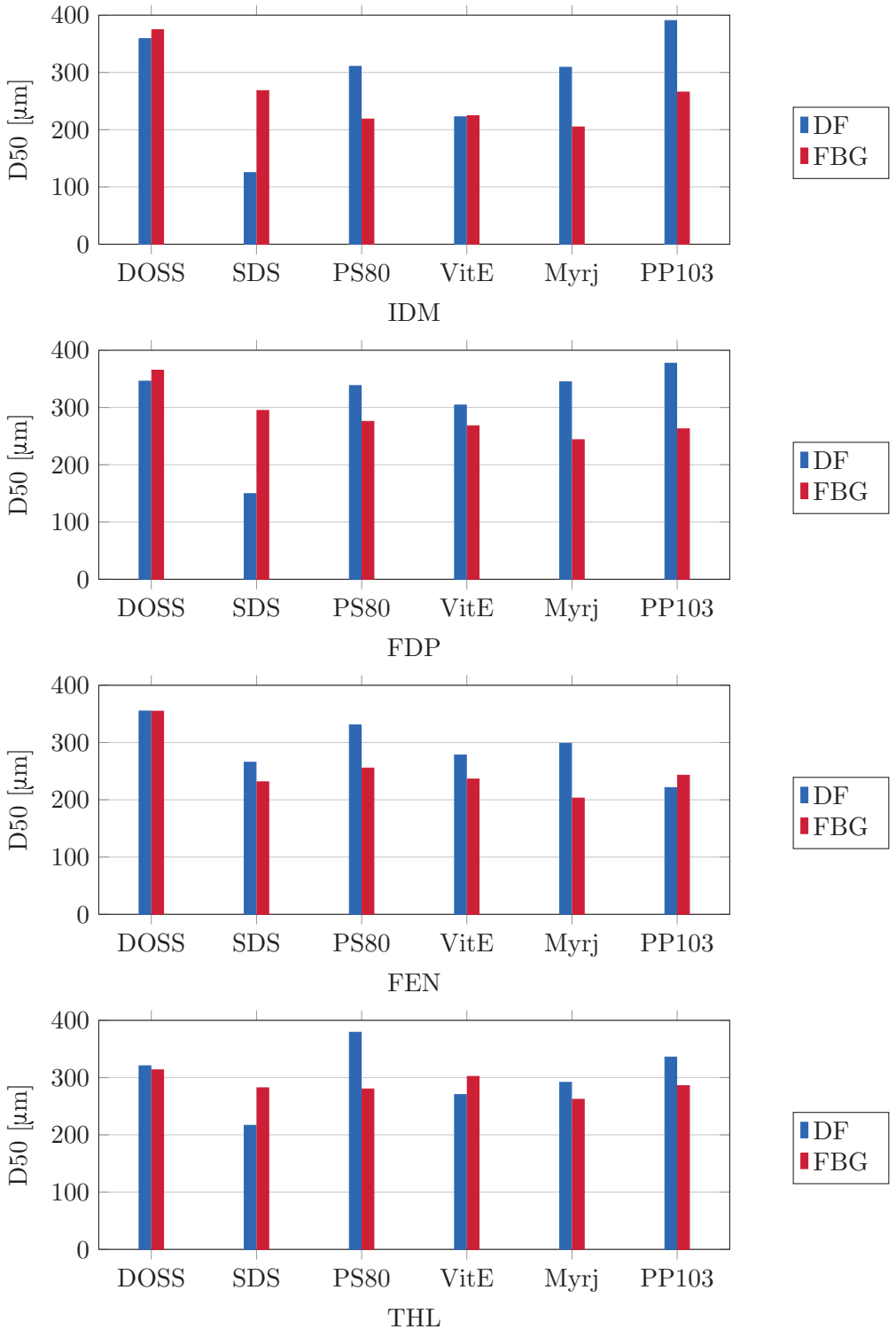

Figure 3.6: D50 value [µm] of DF and FBG granules (n=1).

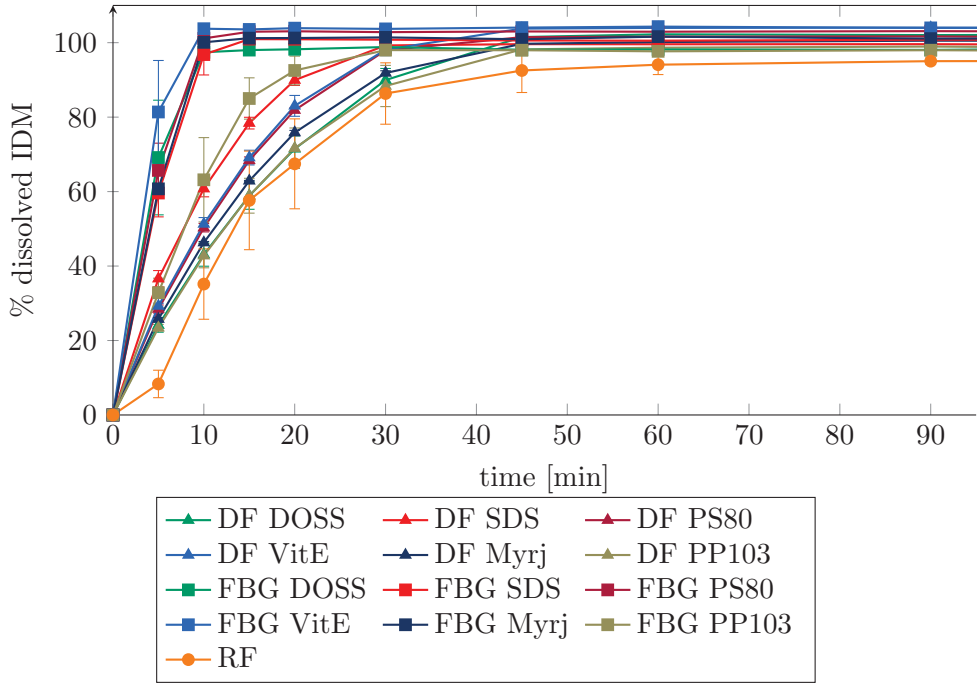

Figure 3.7: Dissolution behavior of IDM M21D DFs and FBGs in FaSSIF-V2 compared to RF IDM (n=3, mean±sd).

The dissolution behavior of IDM formulations in FaSSIF-V2 is depicted in Figure 3.7. Complete dissolution of the applied dose is obtained in all cases as the analysis was performed under sink conditions (factor 5.8). The slowest release was observed for RF followed by DFs. The hard gelatine capsules of RF disintegrated within the first 3 minutes causing only a marginal lag time of RF dissolution curves compared to the other formulations. Comparing the here shown dissolution curves with Figure 2.24, which were conducted with not micronized IDM, the effect of decreasing the APIs particle size by micronization on the initial dissolution rate of the reference formulation as well as the formulated tablets becomes apparent. The improved wettability of IDM can be seen in the first time points comparing RF and DF formulations. Differences in initial dissolution rate between FBG and DF seemed to occur due to the longer disintegration time of dry foam tablets caused by the high fraction of maltodextrin DE 21. The effect of granulation method and different fillers on the disintegration time of tablets is further elaborated in Section 3.2. The type of surfactant did not have remarkable influence on dissolution behavior of DF formulation tablets, except for PP103 which had a sustaining effect on the release of IDM for DF as well as the FBG formulation.

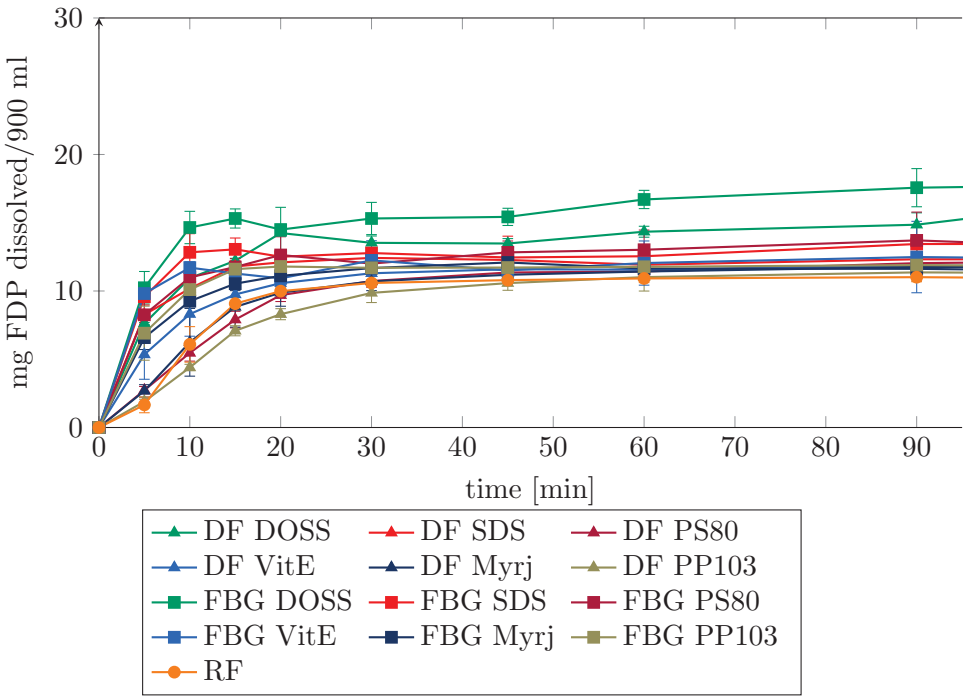

Figure 3.8: Dissolution behavior of FDP M21D DFs and FBGs in FaSSIF-V2 compared to RF FDP (n=3, mean±sd).

Felodipine, a calcium channel blocker, used for the indications hypertension and angina pectoris, is a widely used model compound for fast disintegrating tablets. Basalious and coworkers developed a rapidly absorbed orodispersible tablet for management of hypertensive crisis prepared with liquisolid compact technology (Basalious et al., 2013). The formulation was optimized employing experimental design and improved the initial dissolution rate of FDP in 0.5% SDS in water as dissolution medium compared to the conventional tablet. Nollenberger and coworkers developed a solid solution extrudate with amorphous FDP and improved the disolution behavior in simulated gastric fluid compared to the physical mixtures and crystalline FDP (Nollenberger et al., 2009). In this study dissolution of FDP in FaSSIF-V2 was performed under non-sink conditions (Figure 3.8). According to solubility analysis approximately 10 mg FDP are soluble in 900 ml FaSSIF-V2. Compared to dissolution of RF the DFs PS80, VitE, Myrj and PP103 exhibit a similar low initial dissolution rate. Particulary DF PS80 and PP103 showed an even slower initial dissolution than RF. In contrast DFs containing the anionic surfactants DOSS and SDS resulted in a faster dissolution and higher amount of dissolved FDP. FBG tablets in general exhibited a higher initial dissolution rate than the corresponding DF tablet using the same surfactant. The type of surfactant used has a remarkable influence on the dissolution behavior of the resulting FDP tablets. Anionic surfactants like DOSS and SDS promoted a faster initial dissolution of FDP.

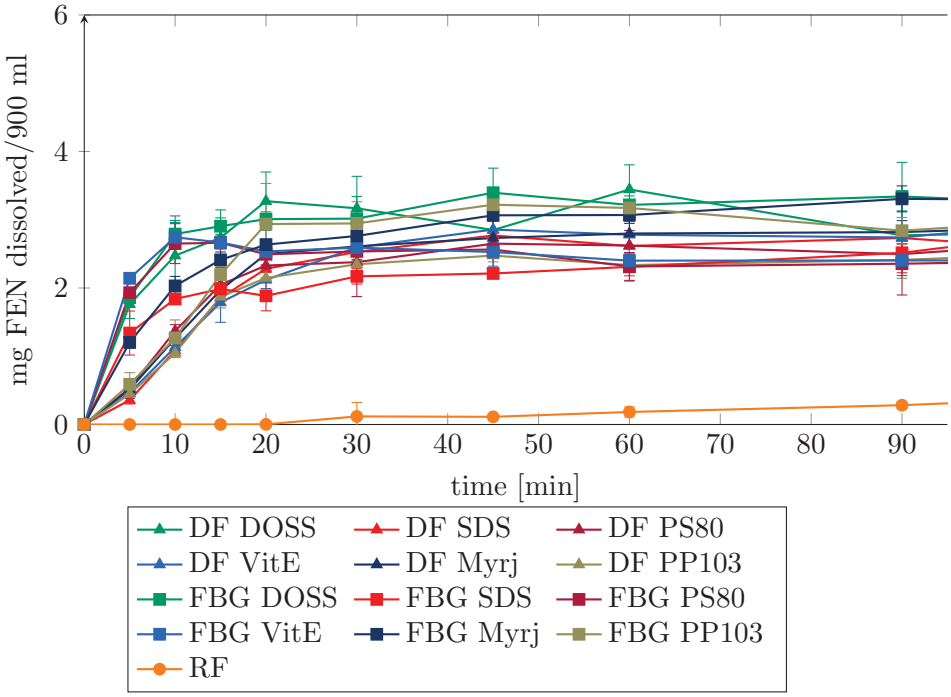

Figure 3.9: Dissolution behavior of FEN M21D DFs and FBGs in FaSSIF-V2 compared to RF FEN (n=3, mean±sd).

Fenofibrate is used for many years to lower cholesterol levels. As it is practically insoluble in water and has a high lipophilicity, its dissolution rate is expected to limit its absorption from the gastrointestinal tract. Therefore, multiple approaches have been tested to enhance its initial dissolution rate, e.g. by micronization or cogrinding, spray-drying or lipid formulations (Vogt et al., 2008; Fei et al., 2013). Naturally, the best achievements were made by amorphous spray dried, nanomilled formulations, as well as lipid formulations. In this study, dissolution of FEN was performed under non-sink conditions in FaSSIF-V2 (Figure 3.9). Dissolution behavior of FEN was improved by all DF and FBG formulations compared to RF. In general, DF tablets exhibited lower initial dissolution rate than the corresponding FBG tablets using the same surfactant, except for DF DOSS with a comparable initial dissolution rate to FBG DOSS. Using PP103 as surfactant the initial dissolution of FBG as well as DF tablets was sustained. After an initially slower dissolution (30 min) the DFs exhibited similar dissolution results to the FBGs. The type of surfactant used considerably influenced the initial dissolution behavior of FEN tablets. Whereas a general improvement of initial dissolution rate for DF as well as FBG tablet could be observed using DOSS as surfactant, the initial dissolution rates differed between DF and FBG tablets for the other surfactants probably due to differences in disintegration behavior due to the different fillers and granulation method used.

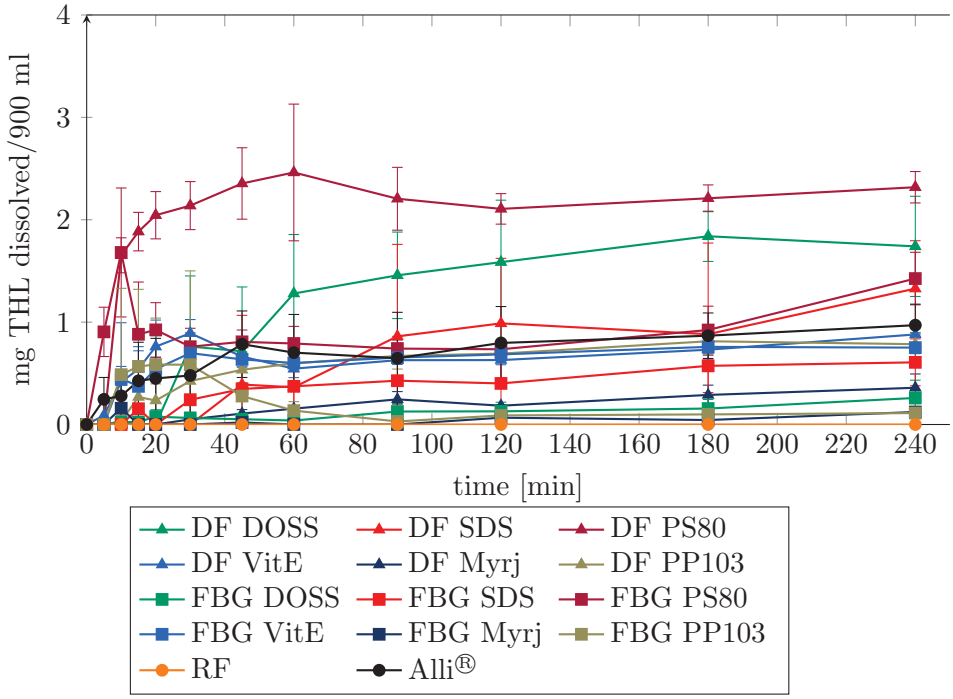

Figure 3.10: Dissolution behavior of THL M21D DFs and FBGs in FaSSIF-V2 compared to RF THL and Alli® 60 mg capsules (n=3, mean±sd).

Instead of USP 35 Orlistat (THL) monograph medium (3% SDS and 0.5% NaCl in water plus to 1-2 drops/10 L of n-octanol) biorelevant medium was chosen for better differentiation of formulations. THL is a highly lipophilic and in water practically insoluble compound, with a high floating tendency due to its poor wettability. Therefore, unfortunately dissolution tests of THL in FaSSIF-V2 revealed erratic results. The dissolution behavior of DF and FBG formulations was additionally compared to the marketed product Alli® containing 60 mg THL in a hard gelatine capsule. The amount of released THL was below the detection limit of 0.2 mg/900 ml FaSSIF-V2 during dissolution of RF. Therefore all formulations improved the dissolution of THL compared to the reference formulation. Type of surfactant used had a distinct influence on the dissolution behavior of the resulting tablets. The fastest initial dissolution was achieved by DF and FBG PS80. Whereas, the amount of dissolved THL dropped and no longer increased for the FBG, the DF exhibited the highest amount of dissolved THL throughout the whole experiment (4 h). After a slower initial dissolution compared to DF PS80 also DF DOSS exhibited a high amount of dissolved THL after 60 min, whereas the corresponding FBG DOSS revealed very low amounts. Interestingly, also the market formulation Alli® exhibited a slower initial dissolution than DF PS80, as well as a lower amount of dissolved THL than the DFs using PS80, DOSS and SDS as surfactants, and a similar amount to DF VitE. Using Myrj as well as PP103 as surfactant also THL DF tablets exhibited a

very slow dissolution THL throughout the dissolution experiment of 4 h indicating no improvement of solubility as well as wettability by these surfactants.

Additional to visual comparison of dissolution curves of both formulation methods, the ratio of the area under the curve (AUC) [mg/ml · min] (Section 5.3.7) of DF tablets compared to the corresponding fluid bed granule tablet, according to Equation (3.1)

$$\text{AUC ratio DF/FBG} = \frac{\text{AUC}_{\text{DF}}}{\text{AUC}_{\text{FBG}}}, \tag{3.1}$$

was calculated and the results listed in Table 3.2. According to regulations applicable in the European Economic Area two medicinal products are bioequivalent if they are pharmaceutically equivalent or pharmaceutical alternatives and if their bioavailabilities after administration in the same molar dose are similar to such a degree that their effects, with respect to both efficacy and safety, will be essentially the same. This is considered demonstrated if the 90% confidence intervals of the ratios for AUC and maximum concentration between the two preparations lie in the range 80-125% in in vivo exposure studies (European Medicines Agency, 2010). In analogy to these considerations, the dissolution behavior of the corresponding formulations (DF versus FBG) is compared by ranking them into three categories. DF formulations inheriting an AUC ratio below 80% (0.8) are considered as inferior, an AUC ratio between 80% and 125% (0.8-1.25) is considered as comparable and an AUC ratio above 125% (1.25) is considered as advantageous in in vitro dissolution behavior in this work.

Table 3.2: AUC ratio DF/FBG of IDM, FDP, FEN and THL formulations.

surfactant	IDM	FDP	FEN	THL
DOSS	0.99	0.86	0.83	**10.89**
SDS	0.97	0.93	0.94	**1.76**
PS80	0.95	0.90	1.08	**2.36**
VitE	0.96	0.97	1.15	1.02
MyrjS40	0.95	0.99	0.87	**4.76**
PP103	0.98	0.88	0.85	**4.01**

IDM DF and FBG tablets revealed very similar AUC values, despite the faster initial dissolution of FBG tablets, resulting in AUC ratios close to 1. Differences in AUC values between DF and FBG tablets can be observed using FDP as model compound. Here, the DF formulations using DOSS and PP103 as surfactant exhibited a 10% lower AUC value than the corresponding FBGs, caused by the faster initial dissolution of these FBG formulations. Interestingly, the two model compounds with a lower melting point and higher lipophilicity (log P value), FEN and THL, exhibited a higher variability within the AUC ratio values, indicating that the type of surfactant as well as granulation method used had an effect on the dissolution

behavior. Looking at the dissolution curves of FEN formulations the slight benefit of DF VitE over the FBG due to the higher amount of dissolved FEN after 30 min was not obvious but is discovered by calculating the AUC ratio. One might be surprised first by the AUC ratio close to one for THL VitE, which can be explained by a similar good dissolution behavior of the two different granule formulation caused by the use of VitE as surfactant. In difference, using especially DOSS, Myrj and PP103 as surfactant only preparation using dry foam technology showed to be beneficial regarding dissolution behavior over fluid bed granulation. The formulations using PS80 as surfactant revealed the highest amount of dissolved THL upon dissolution analysis, but here also fluid bed granulation could profit from the positive effect of the surfactant, resulting in a AUC ratio of 2.36.

In summary, THL was the only model compound out of the first screening set, where DF formulation showed to be advantageous with regard to dissolution behavior of the resulting tablets in biorelevant medium. FEN only showed slight improvement of dissolution behavior compared to FBG using VitE as surfactant. Differences in initial dissolution rate seemed to occur due to longer disintegration time of dry foam tablets caused by the high fraction of maltodextrin DE 21. Further investigations regarding influence of type of filler, are necessary to employ the full potential of this technique.

3.2 Impact of the filler

The filler represents the major component of dry foam formulations embedding the API and therefore is thought to have a crucial effect on the kinetic of drug release. The influence of different types of fillers on the characteristics of dry foam has been investigated before by Rauner (Rauner, 2005), who used carrageenan and thereby sustained the release of the model API. Lenz et al. investigated the influence of different maltodextrine types, isomalt and Soluthin MD, a maltodextrin phosphatidiylcholine complex, on dry foam characteristics. Using isomalt, in the combination with fenofibrate as model compound and Vitamin E-TPGS as surfactant, a faster initial dissolution of FEN was achieved. They concluded that by using fast dissolving low molecular weight fillers in dry foam preparation, the initial dissolution of dry foam tablets can be improved (Lenz et al., 2013). This hypothesis should be further investigated for fenofibrate and three additional APIs with different aqueous solubility (indomethacin, felodipine and orlistat) using a highly soluble grade of isomalt, galenIQ®721, commercialized by Beneo-Palatinit (Germany) and a 1:1 mixture of maltodextrin DE21 and a fast dissolving delta-mannitol (Parteck Delta M, Merck) and two different types of surfactant, the non ionic Vitamin E -TPGS (VitE) and the anionic docusate sodium (DOSS).

Dry foams were prepared according to Section 5.2.2.1 using the vacuum belt dryer (Section 5.2.2.5) and downstream processed to tablets according to Section 5.2.2.6. Paste water content using maltodextrin DE21 (M21D) and isomalt (ISM) as filler was kept at 19%, and was increased to 26% using the 1:1 mixture of maltodextrin DE21 and mannitol (50%MTL) for sufficient processability. Dry foam morphology was examined via X-Ray µ-CT (Section 5.3.4.2) and SEM analysis (Section 5.3.10). The dissolution behavior of dry foam tablets was investigated in FaSSIF-V2. THL tablets and capsules were analyzed additionally in the USP 35 THL monography medium (Section 5.3.7).

The influence of type of filler on dry foam morphology employing X-Ray µ-CT (Section 5.3.4.2) is depicted exemplary for the two APIs differing the most with regard to melting point, aqueous solubility and lipophilicity, in Figure 3.11 and SEM (Section 5.3.10) in Figure 3.12. The use of M21D as filler results in sponge like dry foams, with thin pore walls and a smooth surface in which the API particles are embedded (IDM) or finely distributed in fine hair like needles (THL) (Figures 3.3 and 3.4). With the substitution of 50% M21D by mannitol (50%MTL) the dry foam structure changes substantially. Less porous, denser structures with a rough surface, probably caused by mannitol needles, evolved. With the use of ISM still sponge like structures with thicker walls and a rough surface resulted. Dry foam pores and sponge like structure are thought to develop due to the evaporation of water as a result of pressure reduction. Evaporating water forms spherical bubbles pressing against the surrounding paste which opposes their expansion with its viscosity and advancing drying. Depending on the rheological properties of the paste, and therefore on the filler characteristics in aqueous suspension, either sponge-like or more compact structures evolve.

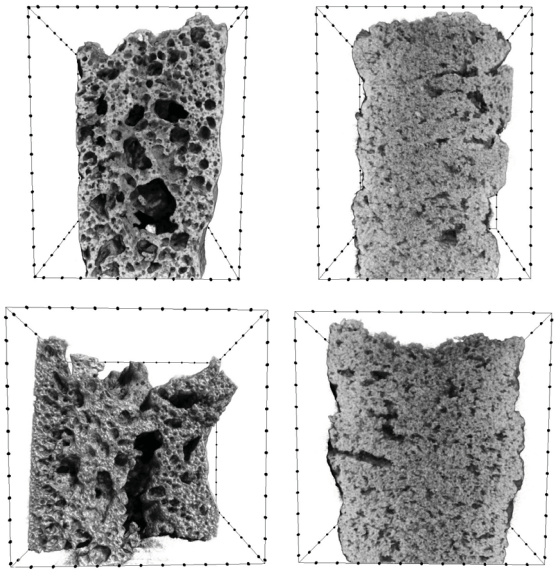

Figure 3.11: X-Ray µ-CT pictures of DF ISM IDM (top left), DF 50% MTL IDM (top right), DF ISM THL (bottom left) and DF 50% MTL THL (bottom right) using VitE as surfactant.

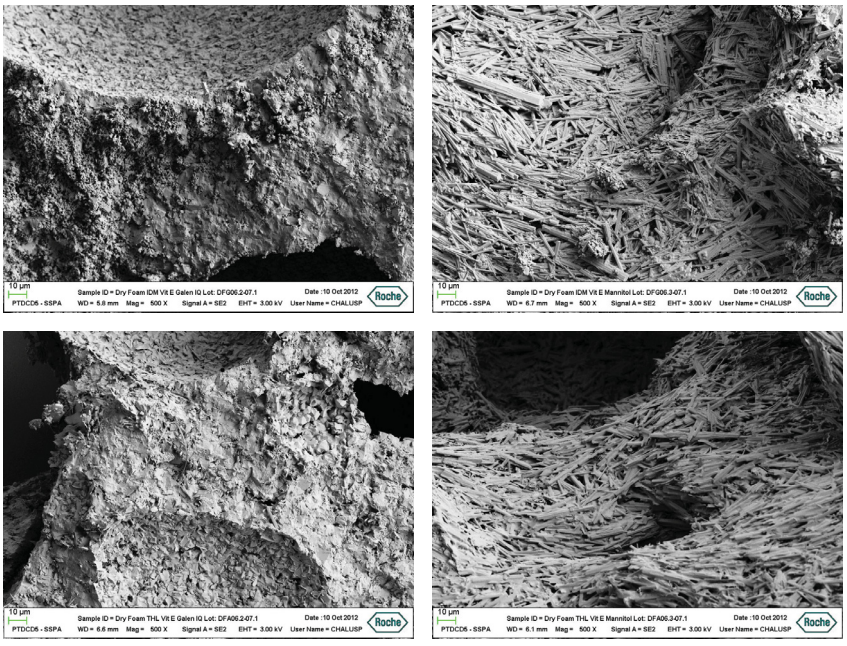

Figure 3.12: SEM pictures of DF ISM IDM (top left), DF 50% MTL IDM (top right), DF ISM THL (bottom left) and DF 50% MTL THL (bottom right) using VitE as surfactant.

Spray dried M21D is in its amorphous, glassy state. Its DF pastes show glutinous, ropey flow behavior. Characteristic sponge like structures evolve due to the slow evaporation of water and growing of pores until a dry state is reached, due to the pastes flexible characteristics. MTL and ISM are both in their crystalline state, their pastes show a cream-like flow behavior, without glutinous and ropey characteristics. During evaporation they don't behave as flexible, therefore dense and compact structures evolve. Exemplary rheological measurements curves of pastes with different fillers are depicted in Section 6.6.

Specific surface area (SSA) of dry foam granules, depicted in Figure 3.13, reflects the surface structure of the corresponding dry foam pieces as discussed before in Section 3.1. DF M21D samples inherit the lowest SSA for all APIs, caused by the smooth surface due to the glassy structure of dried glucose syrup. API particles located on the surface of the dry foam cavities contribute to the SSA of the granule. SSA of the micronized API is listed in Table 3.1. Although IDM exceeds THL in API SSA, DF M21D IDM inherited a lower SSA than DF M21D THL, due to the finely distributed THL needles on the DF surface. The rough surface of DF ISM and DF 50%MTL is reflected by the high SSA values of these batches. No considerable influence of API or surfactant on SSA of the granules could be observed after fluid bed granulation (FBG) or using mannitol for dry foam preparation (50%MTL). Using isomalt for dry foam preparation granules and DOSS as surfactant inherited a higher SSA than in the combination with VitE.

D50 values derived from sieve analysis (Section 5.3.5.1) are compared with each other in Figure 3.14. With only a few exceptions granules prepared with DOSS exhibited higher D50 values compared to the corresponding VitE granules, using M21D or the combination of 50%MTL as filler. For DF ISM granules it was just the other way around: higher D50 values were received with VitE as surfactant, except for THL granules. This goes along with the higher SSA for ISM DOSS granules observed in Figure 3.13. Hypothetically, lower D50 values and therefore finer granules are received out of DF pieces with a hard, dense structure, as they are rather abraded than falling apart, exhibiting a longer residence time within the Comil® and resulting in finer granules.

Bulk and tapped density (Section 5.3.5.3) of DF and FBG granules are compared with each other in Figure 3.15. Interestingly, for all four model compounds DF granules exhibited higher tapped densities and a higher difference between bulk and tapped density values than the corresponding FBGs. In general a high tapped density is achieved by small particles with low porosity. Comparing the D50 values DFs do not in general exhibit smaller particle size than FBGs. FBGs are thought to be shaped more regular and round, and to inherit a high porosity due to the preparation process. By dry sieving irregular shaped dry foam fragments are achieved. Dry foam pores are mainly destroyed to cavities, as the dry foam pieces theoretically break at their thinnest and therefore weakest points, the thin pore walls. The irregular shape can cause a high bulk density, by being the reason for a poor flow behavior of the granule. By tapping movements the irregular flat shapes become more closely packed, resulting in high tapped density values.

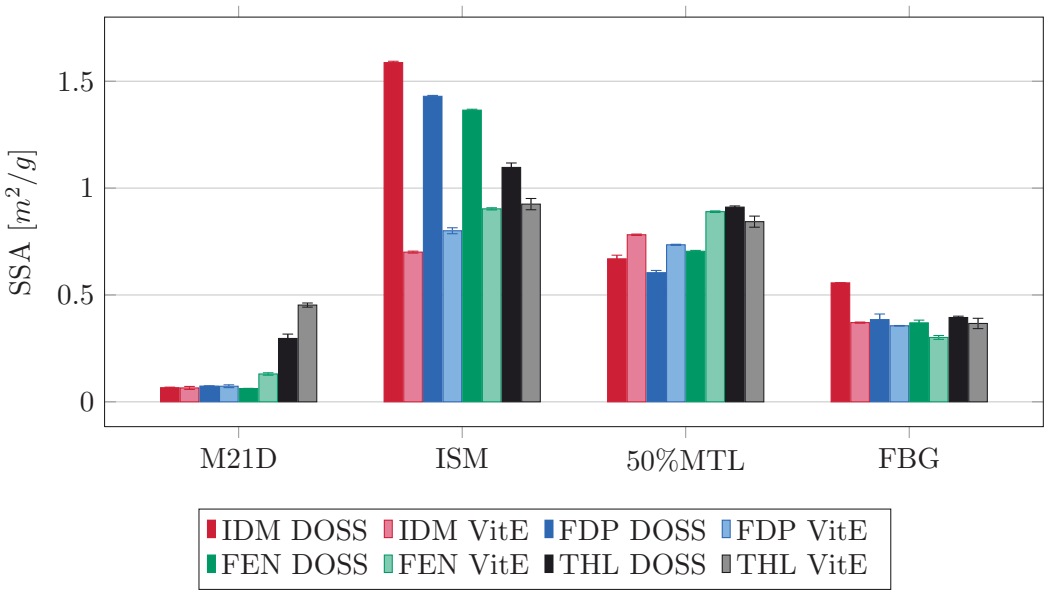

Figure 3.13: SSA of DF and FBG granules (n=2, mean±sd).

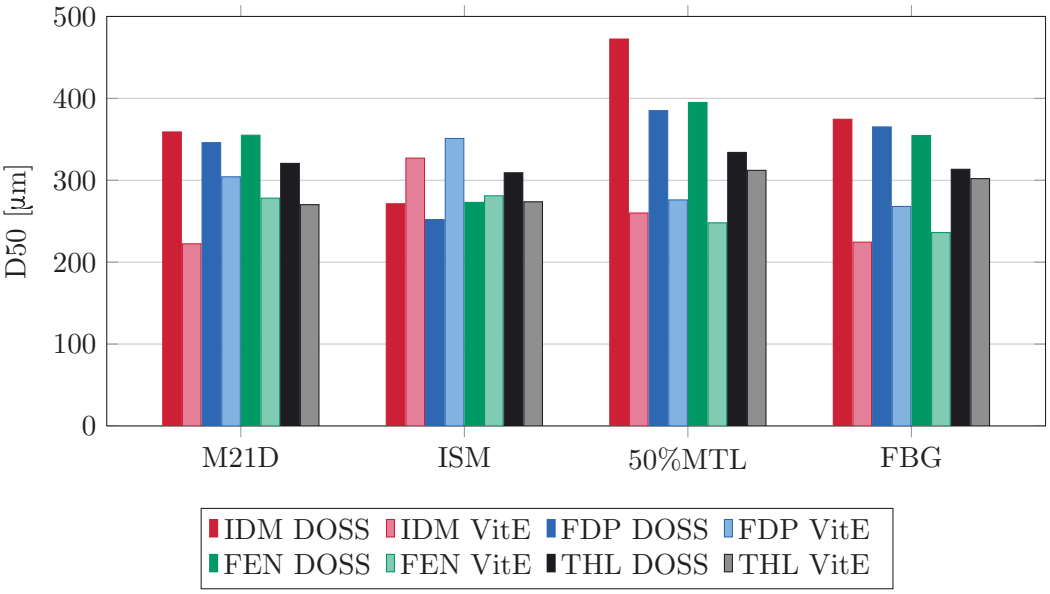

Figure 3.14: D50 of DF and FBG granules (n=1).

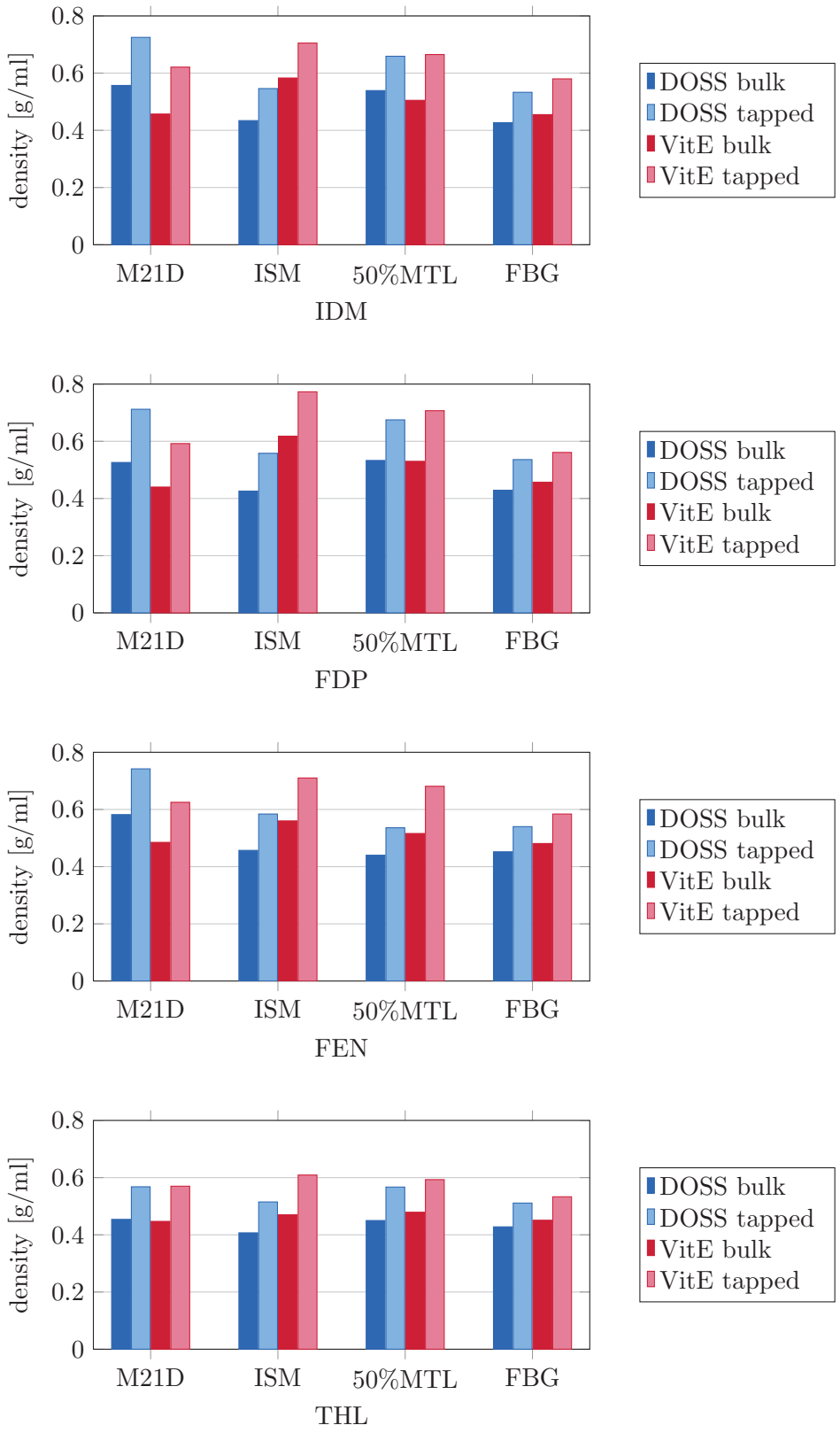

Figure 3.15: Bulk and tapped density of DF and FBG granules (n=1).

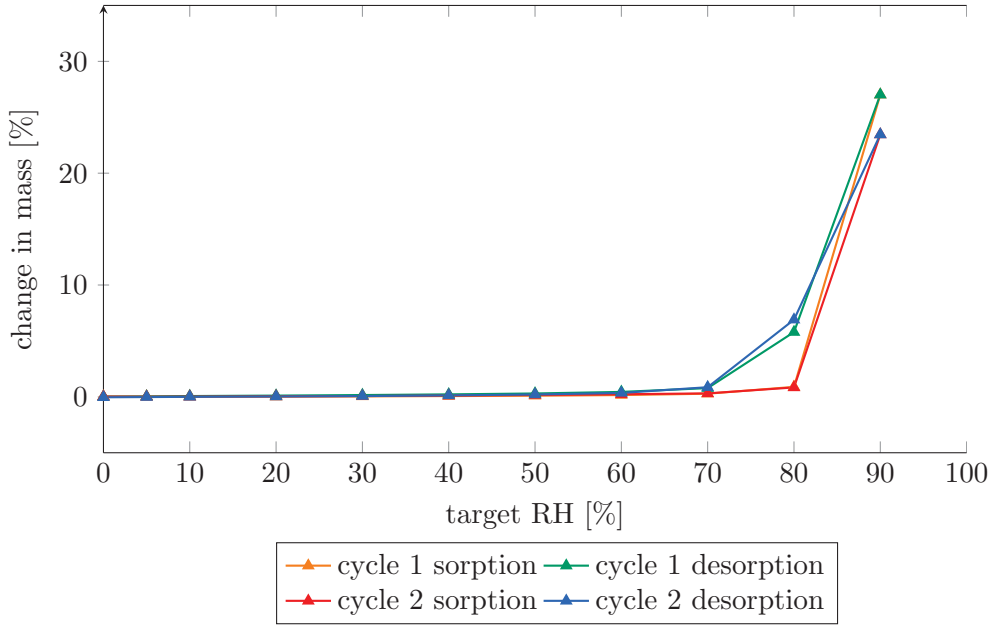

Figure 3.16: DVS diagram of isomalt (galenIQ® 721).

Dynamic vapor sorption (DVS) analysis was conducted for the three fillers maltodextrin DE 21, isomalt and mannitol (Section 5.3.2). The resulting diagrams of two cycle sorption and desorption measurements of the fillers are depicted in Figures 3.16, 3.17 and 3.18. Isomalt shows slightly hygroscopic behavior up to a relative humidity of 80%. From 80% relative humidity on a steep increase in weight gain was observed. A hysteresis exists between sorption and desorption curve, as desorption of the sample takes place at lower relative humidity values than sorption (70%). The second measurement cycle revealed reversibility of the process.

Mannitol DVS analysis (3.17) revealed desorption and sorption of water below 0.5% up to a relative humidity of 90% and is therefore not considered as hygroscopic.

Maltodextrin DE 21 DVS analysis (Figure 3.18) revealed hygroscopic behavior during the first sorption measurement cycle. Interestingly, desorption of the sample reached only a value of 5% weight gain. During the second measurement cycle the sorption of water was reversible, exhibiting a hysteresis between sorption and desorption curve over the complete relative humidity range.

An exemplary DVS measurement of a dry foam piece consisting of maltodextrin DE 21, orlistat and Myrj as surfactant is depicted in Figure 3.19. Similar sorption and desorption behavior was found to the filler sample of maltodextrin DE 21, indicating that no additional hygroscopic properties are caused by the sponge-like, porous structures of the dry foam.

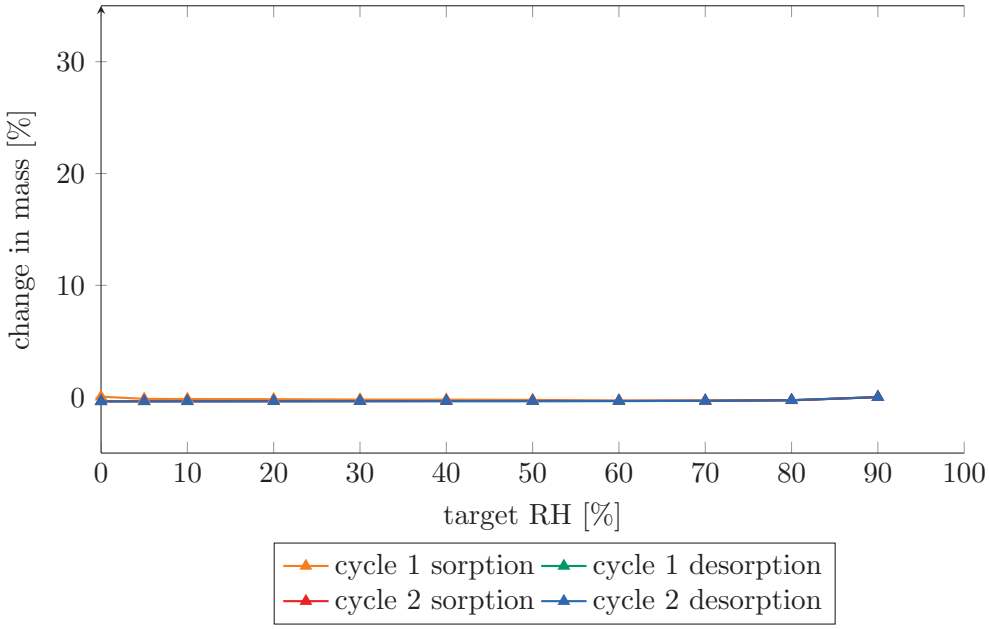

Figure 3.17: DVS diagram of mannitol (Parteck Delta M).

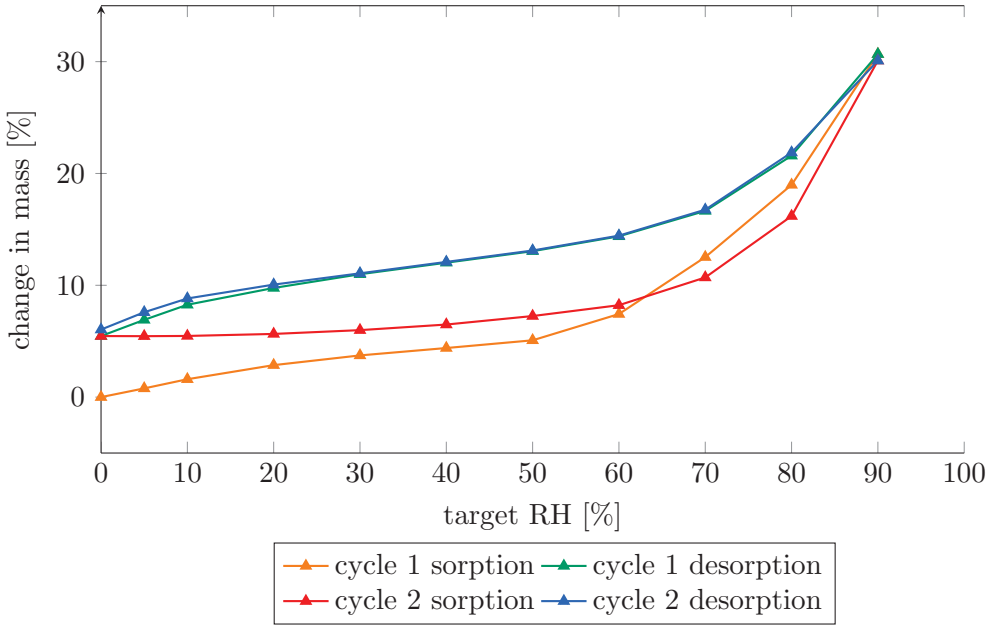

Figure 3.18: DVS diagram of maltodextrin DE 21 (Glucidex 21D).

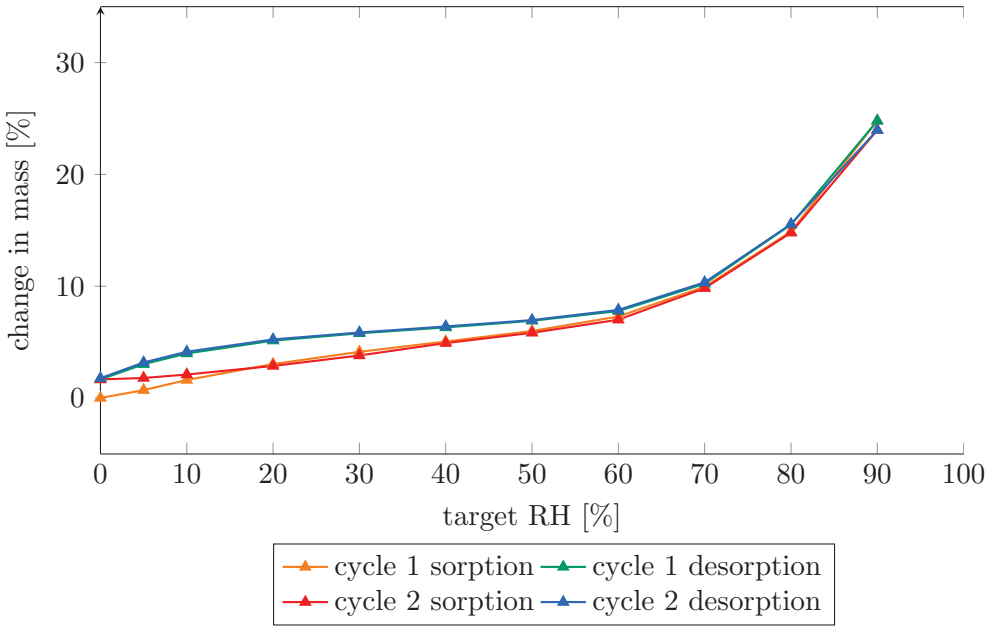

Figure 3.19: DVS diagram of DF specimen consisting of maltodextrin DE 21 as filler, THL as model compound and Myrj as surfactant.

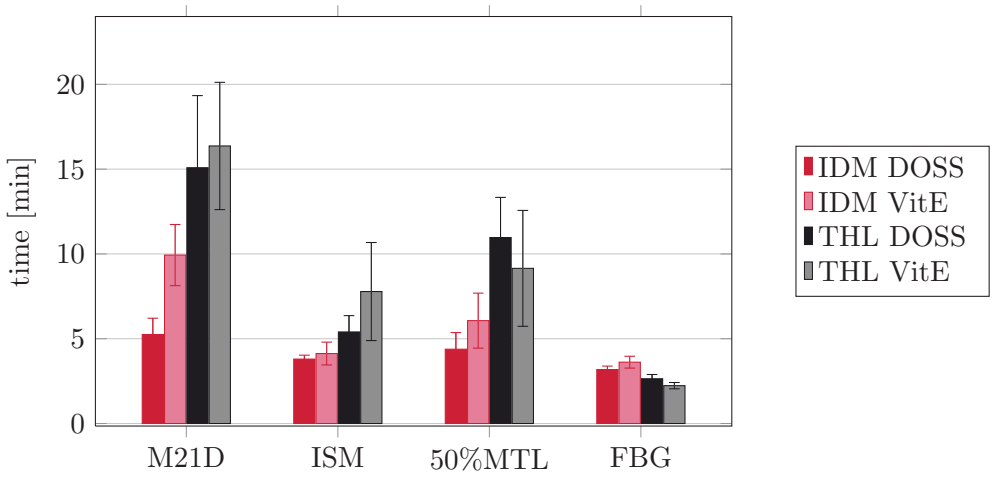

Figure 3.20: Disintegration time of IDM and THL formulations (n=6, mean±sd).

Disintegration times of DF and FBG tablets determined for THL and IDM DFs and FBG are depicted in Figure 3.20. DFs containing M21D show the slowest and most erratic disintegration behavior. Tablets tended to stick on the discs and erode slowly. Disintegration of DF tablets is improved by the use of low molecular fast dissolving fillers (ISM and 50%MTL) for IDM and THL formulations. FBG tablets show the fastest disintegration for both APIs. A general difference in disintegration behavior of DF and FBG tablets was observed. Whereas, DF tablets eroded from top and bottom getting thinner and thinner upon disintegration testing, FBG tablets actually fell apart into smaller pieces, resulting in a shorter disintegration time.

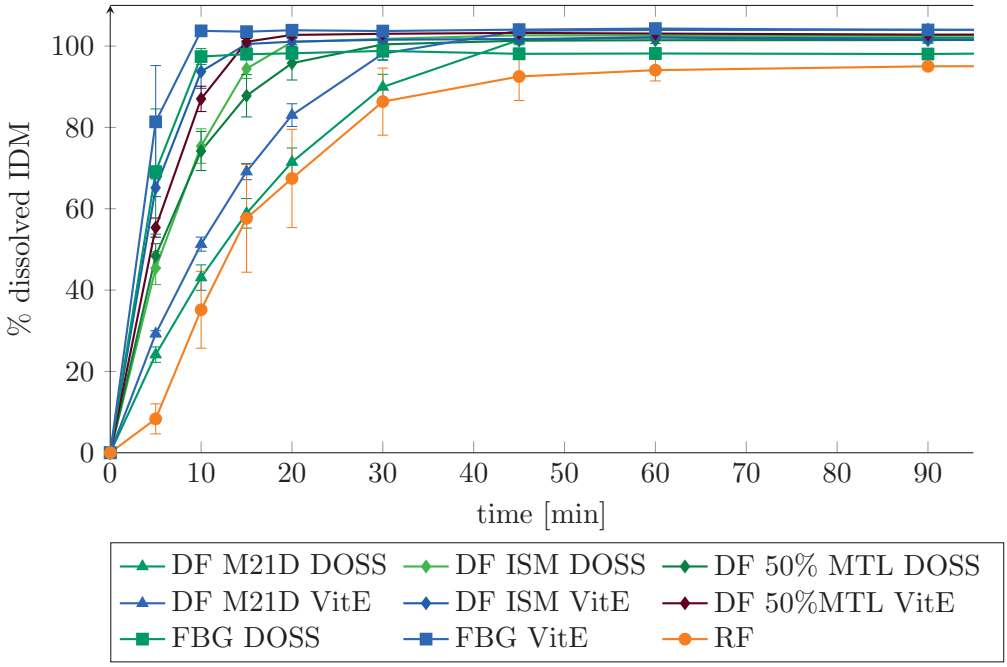

Figure 3.21: Dissolution behavior of IDM DFs and FBGs in FaSSIF-V2 (n=3, mean±sd).

Dissolution behavior of IDM formulations is depicted in Figure 3.21. DF M21D showed only marginally improved dissolution behavior compared to RF IDM, with the use of low molecular weight fillers (ISM, 50% MTL) initial dissolution rate was increased. DF ISM and 50%MTL formulations exceeded the corresponding DF M21D formulation with both surfactants (DOSS, VitE). FBG IDM still inherited the fastest initial dissolution behavior. Dissolution results of IDM formulation correlate well with their determined disintegration behavior. The fast initial dissolution seems to be caused by a fast disintegration of the tablets and a sufficiently wetted API within the formulation. As dissolution experiments were carried out under sink-conditions complete dissolution of the applied amount of IDM is reached for all formulations. Although a distinct improvement of initial dissolution rate by the use of ISM and 50%MTL as filler for IDM DF tablets can be observed in the dissolution curve diagram (Figure 3.21) the AUC ratio rose only marginally, (DF ISM DOSS 1.03, DF ISM VitE 0.97, DF 50%MTL DOSS 1.02, DF 50%MTL VitE 0.98), which can be explained by the already high AUC values.

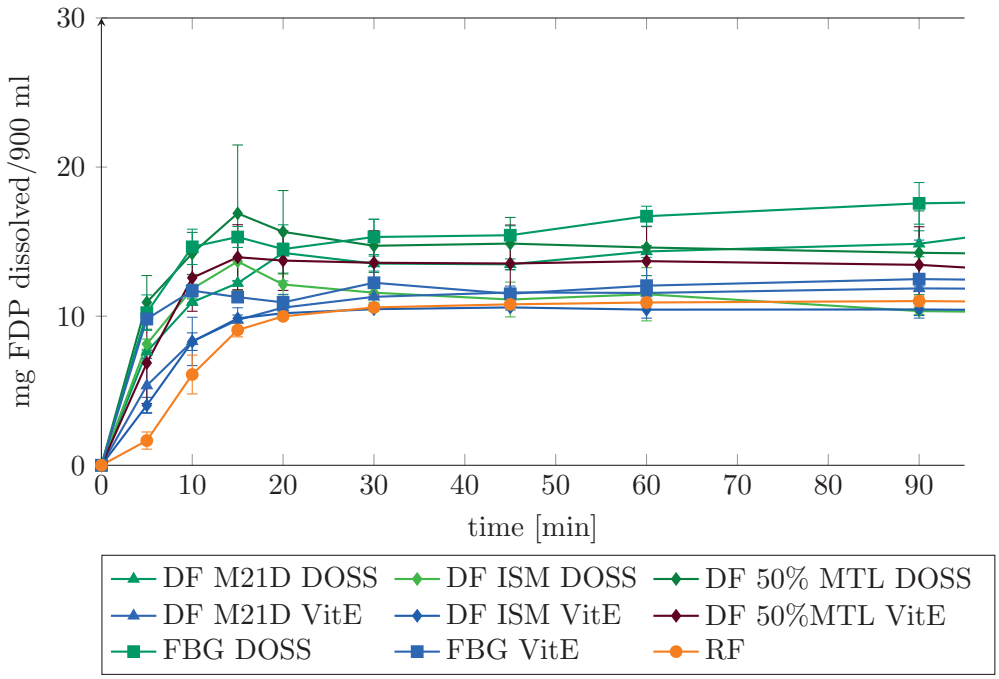

Figure 3.22: Dissolution behavior of FDP DFs and FBGs in FaSSIF-V2 (n=3, mean±sd).

Dissolution behavior of FDP formulations is depicted in Figure 3.22. Interestingly, the initial dissolution rate of FDP was not increased by the use of ISM in DF formulation, their dissolution behavior was similar to DF M21D. However, using 50% MTL as filler both DF formulations (DOSS and VitE) exhibited higher initial dissolution rates similar to the corresponding FBGs. The higher initial dissolution rate is not reflected by a higher SSA of the DF granules. In fact, the highest SSA of FDP granules is inherited by the combination of ISM and DOSS, with a medium initial dissolution rate compared to the other tablets. AUC ratio was decreased for ISM DOSS (0.60), ISM VitE (0.85) and 50%MTL DOSS (0.80) compared to M21D DOSS (0.86) and VitE (0.97). The only increase in AUC ratio could be observed for 50%MTL VitE with a value of 1.06. Therefore no advantage of dry foam formulation process, also in the combination with fast dissolving fillers, was found for the model compound felodipine.

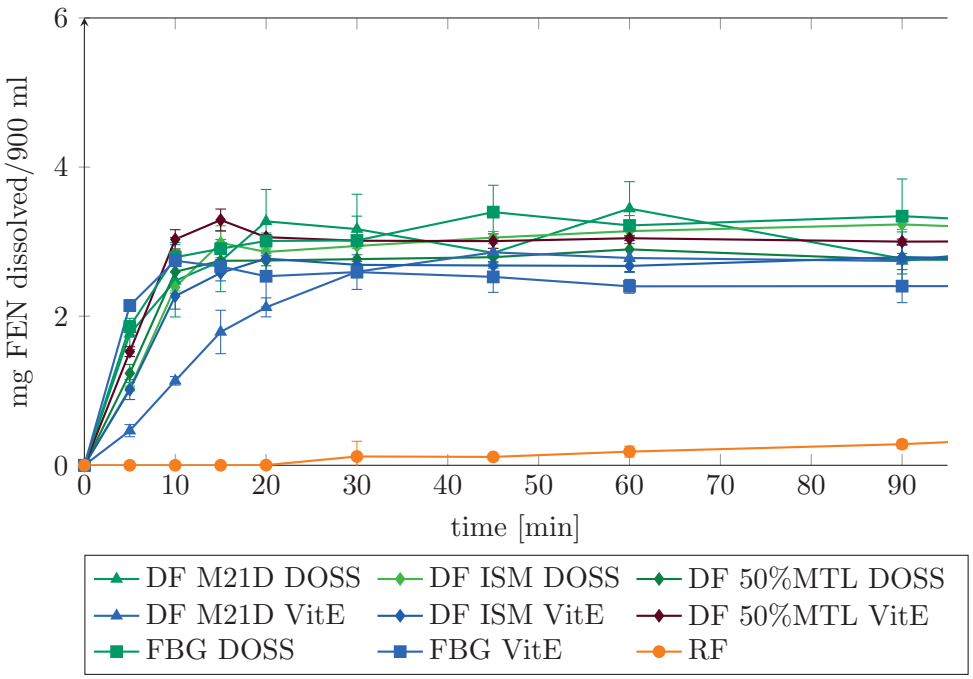

Figure 3.23: Dissolution behavior of FEN DFs and FBGs in FaSSIF-V2 (n=3, mean±sd).

Figure 3.23 illustrates the dissolution behavior of FEN DF and FBG formulations in biorelevant medium. After 5 min the highest dissolved amount of FEN is achieved by the two FBG formulations, followed closely by DF M21D DOSS and the fast dissolving filler formulations DF 50%MTL DOSS and VitE as well as DF ISM DOSS and VitE. Comparing the DF formulations containing VitE with each other, initial dissolution rate is substantially increased by the use of fast dissolving fillers in DF formulation. Using DOSS as surfactant, the difference is not as prominent. Interestingly, taken the complete dissolution analysis behavior into account by comparing the AUCs, only a minor effect is observed using DOSS as surfactant by the use of fast dissolving fillers (ISM DOSS = 0.95, 50%MTL DOSS = 0.85, compared to M21D DOSS = 0.83). The AUC ratio is increased by using ISM and VitE (1.09) and by the use of 50%MTL and VitE (1.19). This discrepancy between visual classification of initial dissolution rate and calculation of AUC ratio throughout the whole dissolution experiment can be explained by the high impact of higher total amount of dissolved FEN values during the later time points. In summary, no distinct advantage of DF formulation tablets over FBGs is revealed in dissolution behavior.

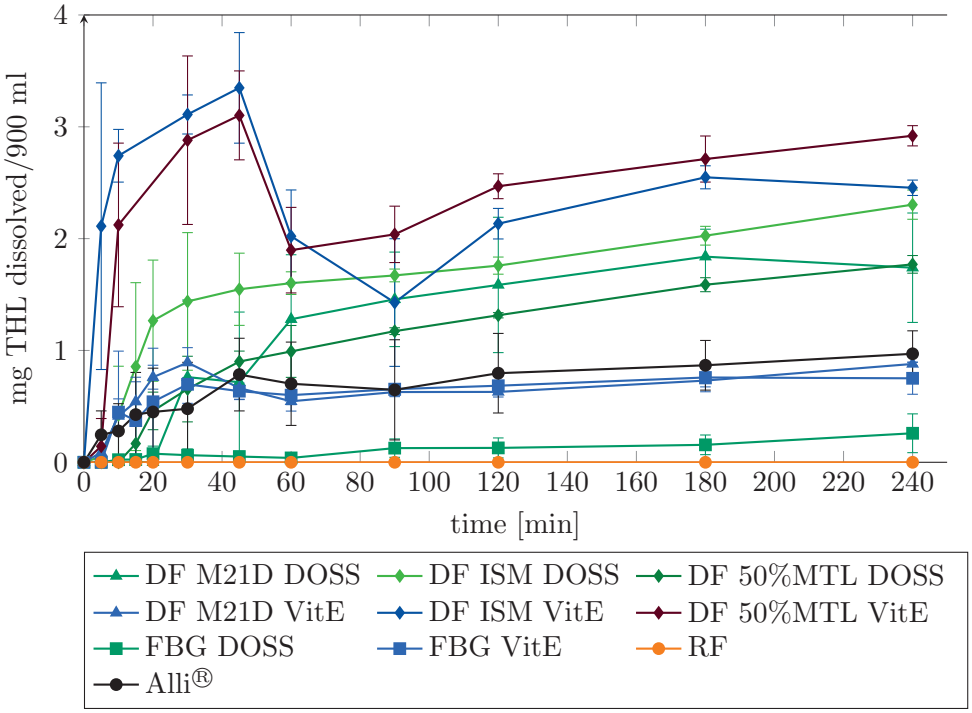

Figure 3.24: Dissolution behavior of THL DFs and FBGs in FaSSIF-V2 (n=3, mean±sd).

Dissolution behavior of THL formulations in FaSSIF-V2 is depicted in Figure 3.24. A further improvement regarding initial dissolution rate as well as total amount of dissolved THL was achieved with the use of low molecular weight fillers in combination with VitE (DF ISM VitE, DF 50% MTL VitE). The intermittent irregularity in DF ISM VitE and DF 50%MTL VitE dissolution curves after 60 min is supposed to occur due to slow redistribution of disintegrated THL within the FaSSIF-V2 micelles. The phenomenon is not considered as a supersaturation as the amount of dissolved THL is still below the solubility limit of THL in the medium after 24 h (16.4 mg/900 ml FaSSIF-V2). In case of THL the dissolution behavior does not reflect the determined disintegration characteristics of the tablets only, but also the improved wettability of the API by DF formulation technology. Although FBG THL tablets disintegrated faster than DF tablets, THL is dissolved faster by the use of low molecular weight fillers and sufficient wetting by a suitable surfactant. Comparison of AUC values reveals advantageous dissolution behavior of all THL DF tablets (ISM DOSS = 13.78, ISM VitE = 3.31, 50%MTL DOSS = 9.7, 50%MTL VitE = 3.53). The lower values of VitE DF formulations are caused by the higher AUC value of FBG VitE.

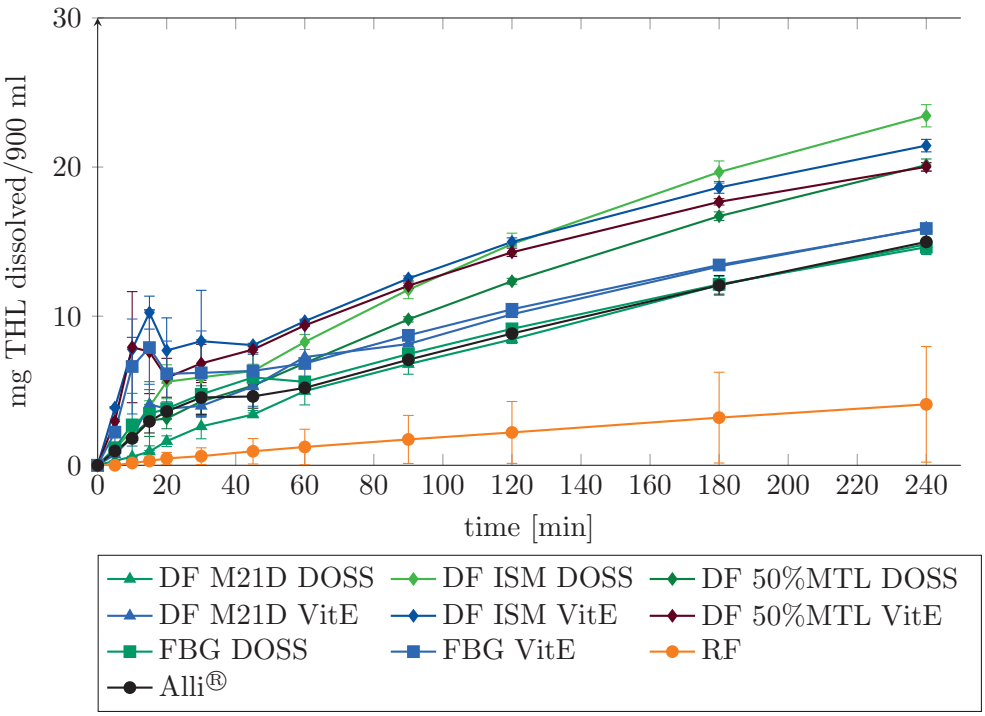

Figure 3.25: Dissolution behavior of THL DFs and FBGs in USP 35 THL monograph medium (n=3, mean±sd).

Overall, dissolution analysis of THL in FaSSIF-V2 revealed high standard deviations. Therefore additionally USP 35 THL monograph medium (3% SDS and 0.5% NaCl in water plus to 1-2 drops/10 L of n-octanol) was used for dissolution analysis (Figure 3.25). Here solubility analysis resulted in 12.20 mg THL dissolved in 900 ml USP 35 medium after 4 h and 37.45 mg dissolved THL in 900 ml after 24 h (Section 5.3.8). RF THL dissolution analysis resulted in detectable amounts of dissolved THL but still high standard deviations. In contrast to the RF, DF and FBG formulations showed a quite similar dissolution behavior. Nevertheless, two different groups can be distinguished: the slowly dissolving DF M21D, FBG DOSS and Alli® and the faster disintegrating DF ISM VitE and DF 50%MTL VitE. DF ISM and DF 50%MTL in combination with DOSS disintegrate more slowly, but still show higher dissolved amount of THL than the marketed formulation Alli® after 60 min.

In summary, the type of filler in DF formulation technology showed to have comprehensible impact on DF morphology as well as dissolution characteristics of the resulting tablets. DFs prepared with low molecular weight fillers (ISM, 50%MTL) revealed more compact and less porous structures compared to DF M21D. This can be explained by the rheological properties of the corresponding pastes. Specific surface area of DF ISM and DF 50%MTL was increased, reflecting their rough surface, compared to DFs using M21D as filler as well as FBGs. The initial dissolution rate of DF tablets was in general improved by the use of ISM and 50%MTL. Dissolution of fenofibrate and felodipine dry foam formulations was improved by the use of fast dissolving fillers depending on surfactant used. Still, no advantage of DF formulation compared to fluid bed granules could be shown for the model compounds indomethacin, felodipine and also fenofibrate. In case of Orlistat, the compound with the lowest aqueous solubility, the lowest melting point as well as the highest log P value, additional to the initial dissolution rate improvement also the total amount of dissolved API was further increased by the use of low molecular weight fillers. Superiority over fluid bed granulation as well as market formulation in in vitro analysis using two different dissolution media was be shown.

3.3 Impact of the model compound

In Section 3.1 dry foams prepared containing the poorly water soluble API orlistat with a low melting point and high lipophilicity (log P value) showed improved dissolution behavior compared to fluid bed granules and the marketed formulation Alli® 60 mg capsules. Seeking for key characteristics that identify compounds for whom the use of dry foam technology is advantageous over fluid bed granulation as formulation technology, two additional model compounds were added to the screening study. The model compound Neurokinaserezeptor(1)-antagonist (NK1) inherits a high log P value, situated between the model compounds orlistat and fenofibrate, a similar aqueous solubility to orlistat, but a higher melting point (Table 3.3). Monoamine oxidase type B-inhibitor (MAO) inherits a higher aqueous solubility than orlistat, but lower than fenofibrate, a higher melting point and a low log P value (Table 3.3). The two model compounds were received from F. Hoffmann-La Roche Ltd. (Basel, Switzerland) in micronized quality. Their physico-chemical characteristics, as well as solubility in dissolution medium FaSSIF-V2 after 4 h (Section 5.3.8), D50 value (determined according to Section 5.3.1.1) and specific surface area (SSA) (determined according to Section 5.3.5.4) are listed in Table 3.3 in comparison to the model compounds from the screening study. They are plotted together according to their melting point (Section 5.3.1.2), lipophilicity and solubility in FaSSIF-V2 (Section 5.3.8) in Figure 3.26.

Table 3.3: API characteristics including melting point (MP), log P and aqueous solubility according to Benet et al. (2011) and internal F.Hoffmann-La Roche data, FaSSIF-V2 solubility, D50 value, specific surface area (SSA) and their code.

code	API	MP [°C]	log P	aqueous solubility [µg/ml]	FaSSIF-V2 solubility [µg/ml]	D50 [µm]	SSA [m^2/g]
IDM	indomethacin	158	4.27	2.5	320.21	3.45	5.03
FDP	felodipine	145	3.86	1	10.15	5.89	3.07
FEN	fenofibrat	80	5.19	0.8	5.74	7.25	2.51
THL	orlistat	43	8.19	0.09	0.92	6.96	2.41
NK1	NK-rez.(1)-ant.	130	5.94	0.1	1.47	4.48	1.57
MAO	Mao-B-inh.	179	1.93	3	3.37	1.93	4.77

Scanning electron microscopy (SEM) analysis (Section 5.3.10) illustrates the morphology and agglomeration tendency of the two model compounds NK1 and MAO in Figure 3.27. Whereas, NK1 exhibits rather round and oblong particles, MAO particles are more needle like shaped.

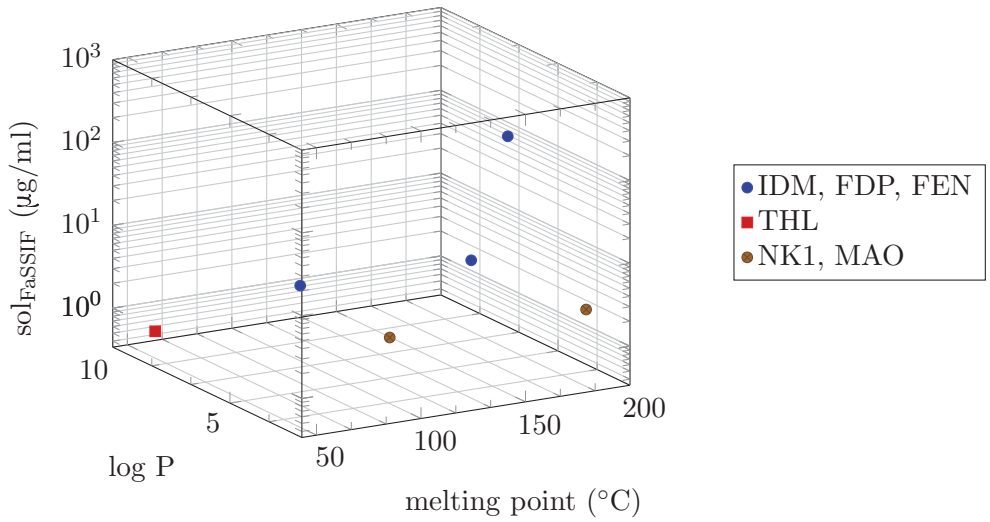

Figure 3.26: Investigated model compounds plotted according to their melting point, lipophilicity (log P value) and solubility in FaSSIF-V2 after 4 h at 37°C (sol_{FaSSIF}).

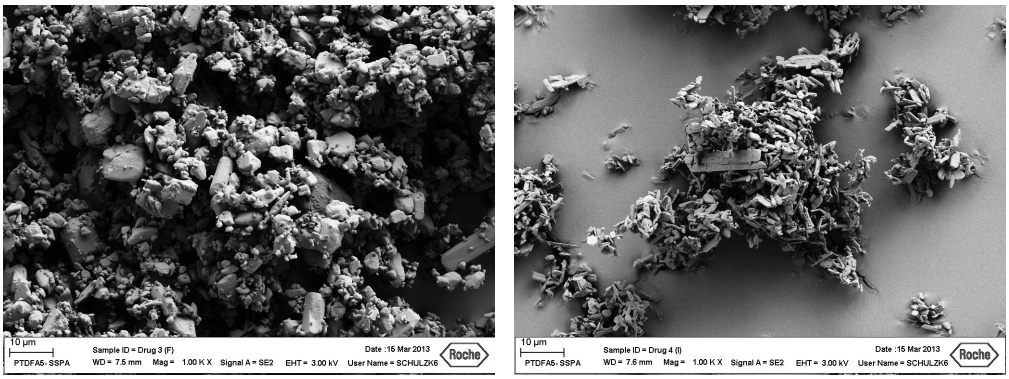

Figure 3.27: SEM pictures of the micronized model compounds NK1 (left) and MAO (right).

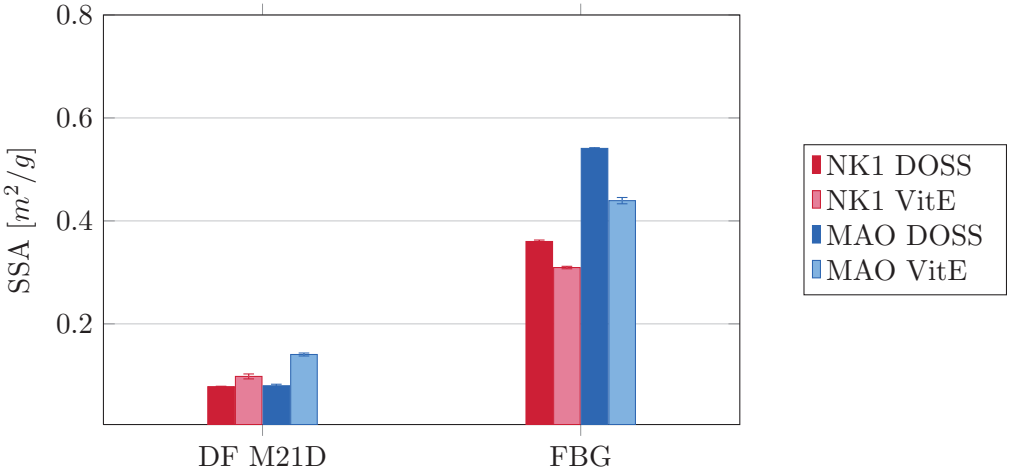

Figure 3.28: SSA of NK1 and MAO DF and FBG granules.

Dry foams and fluid bed granules of the two additional model compounds were prepared using maltodextrin DE 21 (M21D) for dry foam preparation, DOSS and VitE as surfactants at a paste water content of 19%, according to Section 5.2.2.1 using the vacuum belt dryer (Section 5.2.2.5). FBG were prepared according to Section 5.2.3. Dry foam pieces and fluid bed granules were downstream processed according to Section 5.2.2.6. The specific surface area (SSA) values of the resulting granules (Section 5.3.5.4) are depicted in Figure 3.28. All FBGs exceed the corresponding DF in SSA, in accordance with previously data (Figure 3.5), due to the difference in their surface structure.

Dissolution behavior of NK1 was analyzed in FaSSIF-V2 (Section 5.3.7). NK1 exhibited a solubility of 1.5 µg/ml in FaSSIF-V2 proposing a maximum soluble amount of 1.3 mg in 900 ml. The resulting dissolution curves are depicted in Figure 3.29. The amount of released NK1 was below the detection limit of 0.2 mg/900 ml FaSSIF-V2 during dissolution of RF. All four formulations improved dissolution behavior of NK1 compared to RF. Nevertheless, the two FBG prepared with DOSS and VitE as surfactant exceeded both DF formulations regarding initial dissolution rate. After 3 h of dissolution time all formulations reached a similar amount of total dissolved NK1 in 900 ml FaSSIF-V2 of approximately 1.3 mg going along with the determined solubility of NK1 after 4 h. The high standard deviation error bars are thought be caused by the low NK1 concentration in the dissolution media samples and redistribution processes of the API within the dissolution media micelles. Comparing AUC of the dissolution curves employing AUC ratio no advantage of DF formulation over fluid bed granulation could be observed using M21D and DOSS as surfactant (0.95) nor VitE (0.79).

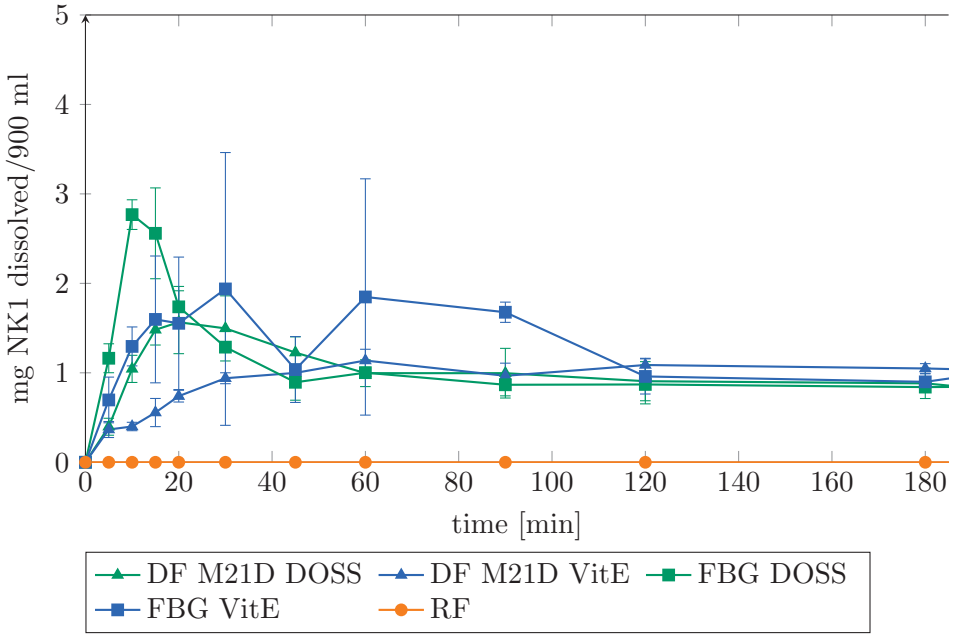

Figure 3.29: Dissolution behavior of NK1 DFs and FBGs in FaSSIF-V2 (n=3, mean±sd).

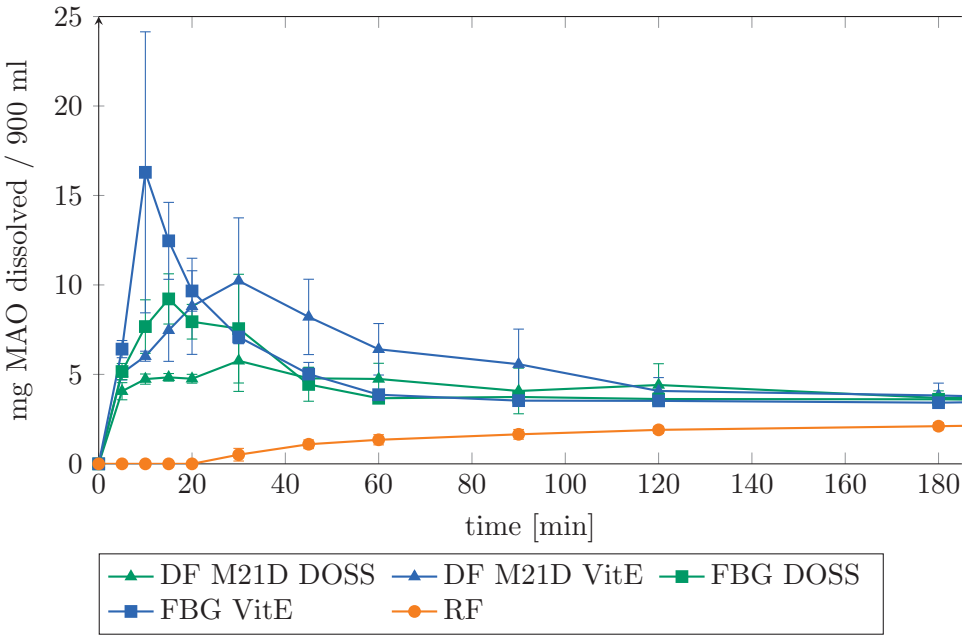

Figure 3.30: Dissolution behavior of MAO DFs and FBGs in FaSSIF-V2 (n=3, mean±sd).

Dissolution behavior of MAO formulations was analyzed in FaSSIF-V2 (Section 5.3.7) as well. In solubility analysis MAO exhibited a solubility of 3.37 µg/ml in FaSSIF-V2 proposing a total of 3 mg MAO to be soluble in 900 ml FaSSIF-V2. During the first 20 min of the dissolution test the amount of dissolved MAO by RF was below the detection limit. Afterwards, the amount of dissolved API slowly increased, emphasizing the poor wettability of the compound (Figure 3.30). Interestingly all four formulations exhibited a higher amount of dissolved MAO during the first 90 min of dissolution analysis to a different extent than at the end of the experiment. This could be either due to polymorphic changes of the API during dissolution analysis or similar to THL a temporary higher concentration of the API within the drawn samples due to slow redistribution of dissolved MAO within the FaSSIF-V2 micelles. Nevertheless, no improvement in initial dissolution rate and total amount of dissolved API could be observed by DF formulation compared to FBG, using the two surfactants DOSS and VitE for MAO. AUC ratios exhibit a slight improve by using dry foam formulation with M21D and VitE as surfactant with a value of 1.15, caused by the more slowly decreasing amount of dissolved API, and equality using DOSS as surfactant (AUC ratio = 1).

In conclusion, the two model compounds NK1 and MAO seem not to fit in the pattern of key characteristics of APIs profiting from dry foam formulation in regard to dissolution behavior. Although NK1 exhibits a high log P value, no benefit of dry foam formulation technology could be shown over fluid bed granulation. Therefore, high lipophilicity seems not to be the only necessary characteristic for superiority of dry foam formulation. As Orlistat, showing an advantage of DF formulation, inherits a low melting point of 43°C in difference to NK1, this API characteristic is further investigated. Three more model compounds of high lipophilicity, two with a low and one with a high melting point were added to the data set.

Table 3.4: API characteristics including melting point (MP), log P value and aqueous solubility according to Benet et al. (2011) and internal F.Hoffmann-La Roche data, FaSSIF-V2 solubility, D50 value, specific surface area (SSA) and their code.

code	API	MP [°C]	log P	aqueous solubility [µg/ml]	FaSSIF-V2 solubility [µg/ml]	D50 [µm]	SSA [m^2/g]
IDM	indomethacin	158	4.27	2.5	320.21	3.45	5.03
FDP	felodipine	145	3.86	1	10.15	5.89	3.07
FEN	fenofibrat	80	5.19	0.8	5.74	7.25	2.51
THL	orlistat	43	8.19	0.09	0.92	6.96	2.41
NK1	NK-rez.(1)-ant.	130	5.94	0.1	1.47	4.48	1.57
MAO	Mao-B-inh.	179	1.93	3	3.37	1.93	4.77
CP2	CETP-inh.(2)	143	8.86	<1	0.36	5.90	2.07
DRX	drug X	63	10.37	<1	3.01	6.91	2.14
DAL	dalcetrapib	64	7.15	<1	4.66	6.90	1.15

Three additional model compounds, namely dalcetrapib (DAL), cholesteryl ester transfer protein inhibitor (2) (CP2) and drug X (DRX) were received in micronized quality from F. Hoffmann-La Roche.

Their physico-chemical characteristics as well as solubility in FaSSIF-V2 (Section 5.3.8), D50 value (Section 5.3.1.1) and specific surface area (Section 5.3.5.4) are compared to the already investigated APIs in Table 3.4. Figure 3.31 illustrates the distribution of the model compounds regarding melting point, lipophilicity and solubility in FaSSIF-V2. DAL and DRX both exhibit a very low melting point as well as a high log P value, similar to Orlistat. CP2 exhibits a higher log P value than NK1, similar to THL, but a similar high melting point to NK1. This setup should give an indication whether compounds with high log P value, or high log P value in combination with low melting point, benefit from the dry foam formulation technology in comparison to fluid bed granulation.

The morphology of the three additional model compounds DAL, DRX and CP2 was analyzed by scanning electron microscopy (SEM) (Section 5.3.10) (Figure 3.32). Whereas DRX exhibited rather spherical particles, DAL and CP2 inherit oblong to needle like particle morphology. All of them seem to inherit a high agglomeration tendency.

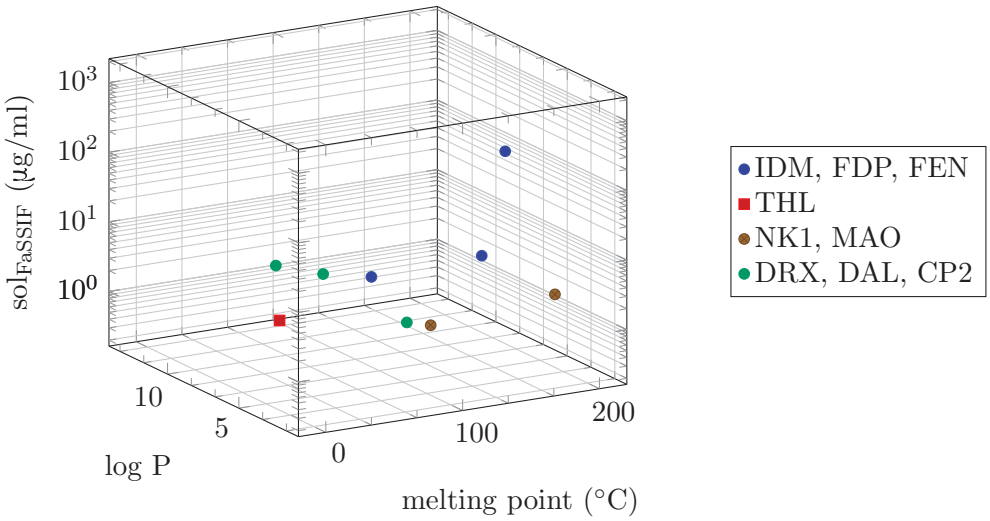

Figure 3.31: Investigated model compounds plotted according to their melting point, lipophilicity (log P value) and solubility in FaSSIF-V2 after 4 h at 37°C (sol_{FaSSIF}).

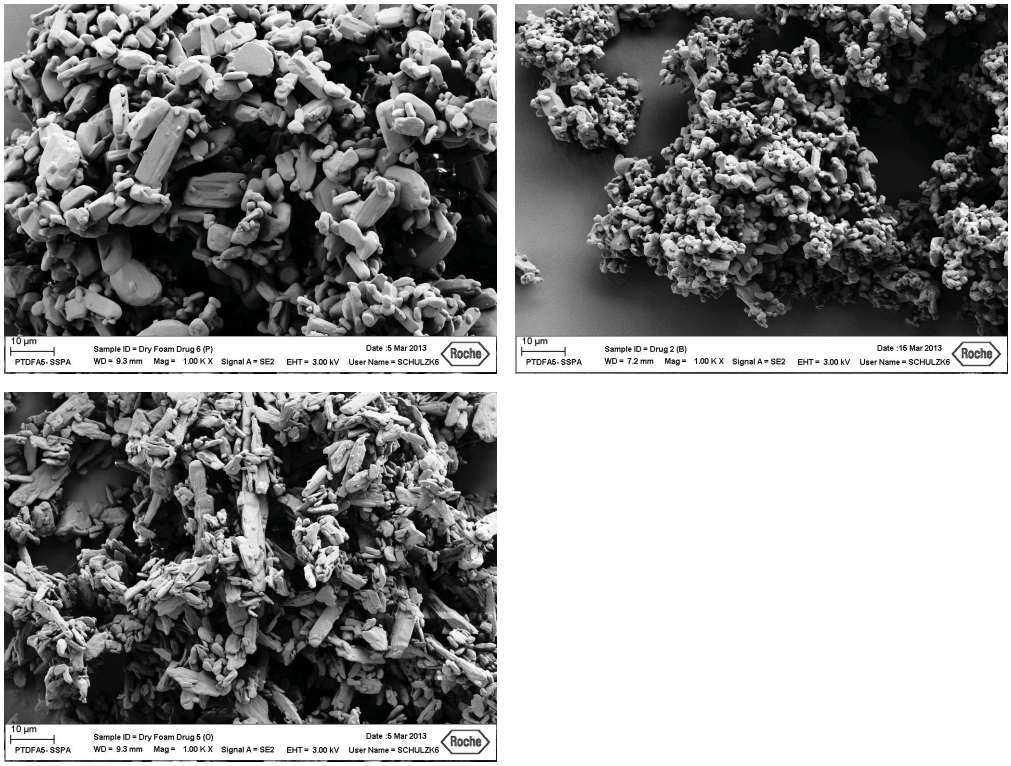

Figure 3.32: SEM pictures of micronized model compounds, DAL (top left) and DRX (top right) and CP2 (bottom).

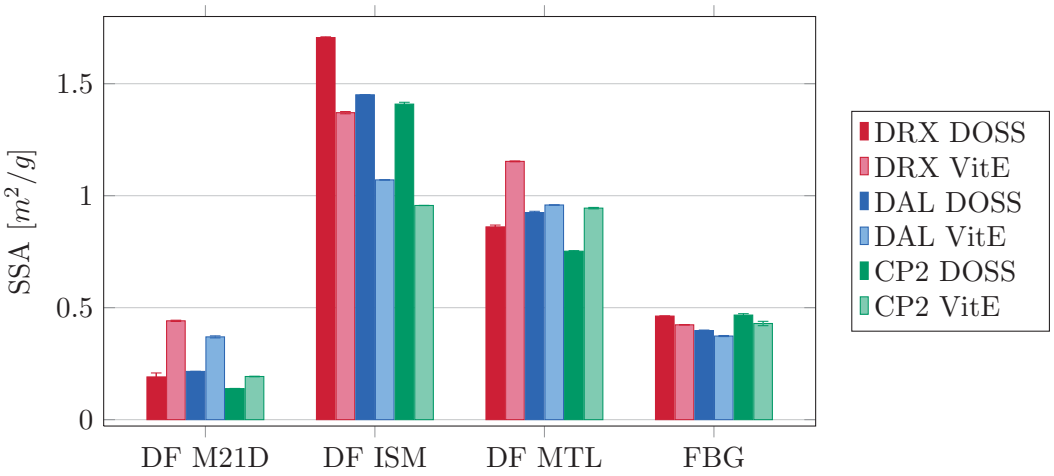

Figure 3.33: SSA of drug X (DRX), dalcetrapib (DAL) and CETP-inhibitor(2) (CP2) DF and FBG granules (n=2, mean±sd).

Dry foams as well as fluid bed granules (Section 5.2.3) of the three additional model compounds were prepared using DOSS and VitE as surfactants. For dry foam preparation the three different fillers maltodextrin DE 21 (M21D), isomalt (ISM) as well as the 1:1 mixture of maltodextrin DE 21 and mannitol (50% MTL) were used. Pastes were prepared according to Section 5.2.2.1, containing 19% paste water content using M21D and ISM, and 26% using 50%MTL respectively. For foaming and drying the vacuum belt dryer was used (Section 5.2.2.5). Dry foam pieces and fluid bed granules were downstream processed according to Section 5.2.2.6.

Specific surface area (SSA) of the resulting granules was analyzed as described in Section 5.3.5.4 and the results are compared with each other in Figure 3.33. Dry foam granules using fast dissolving low molecular fillers (ISM, 50% MTL) exhibit higher specific surface area than dry foams prepared using maltodextrin DE 21 (M21D) and the corresponding fluid bed granules which can be drawn back to their rough surface. These data are in accordance with results obtained earlier with IDM, FDP, FEN and THL (Figure 3.13). In general DF ISM granules using DOSS as surfactant exhibited the highest surface area. Additionally to their rough surface, the resulting foam strands had a very porous and fragile structure.

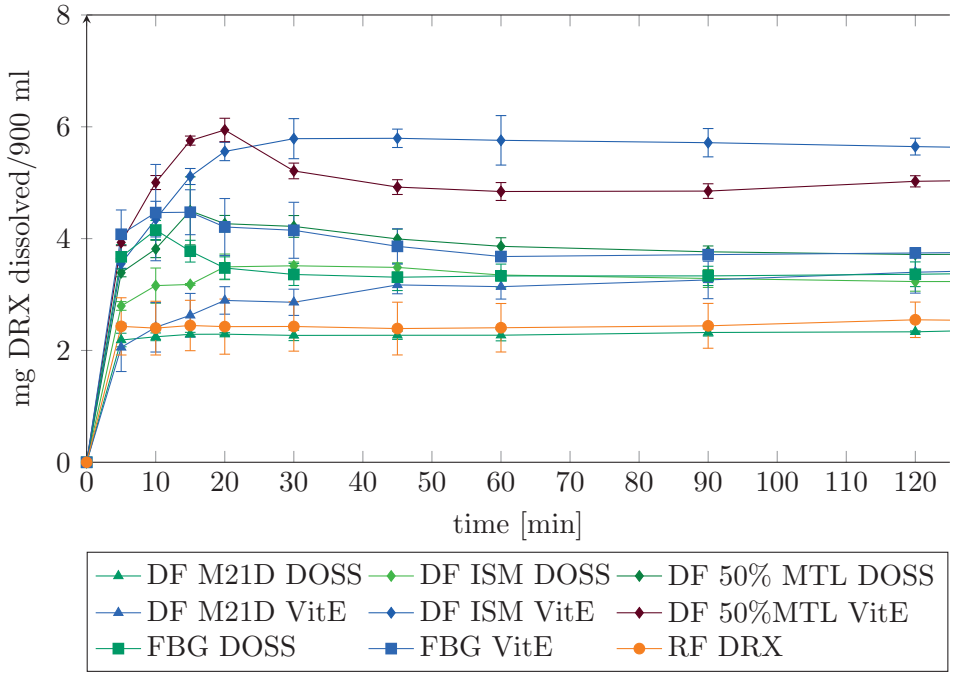

Figure 3.34: Dissolution behavior of drug X (DRX) DFs and FBGs in FaSSIF-V2 (n=3, mean±sd).

Dissolution behavior of the prepared dry foam and fluid bed granule tablets was compared to API filled into a capsule (RF) in FaSSIF-V2 (Section 5.3.7). Drug X is a lipophilic model compound with a determined solubility of 3 µg/ml in FaSSIF-V2. Considering a dose of 50 mg results in a dose solubility ratio of 16000 ml, which situates DRX on the borderline of DCS class IIa and IIb compounds according to Butler and Dressman (2010). In dissolution analysis (Figure 3.34) RF DRX exhibited a similar dissolution behavior to the dry foam tablet prepared using M21D and DOSS as surfactant. Using VitE as surfactant instead of DOSS the total amount of dissolved API was generally improved. Compared to DF M21D formulations the initial dissolution rate as well as dissolved amount of API were increased by using fast dissolving fillers, ISM and 50%MTL, in dry foam formulation. DF ISM and 50%MTL using VitE as surfactant exhibited the highest amount of dissolved API in dissolution analysis. FBG showed similar dissolution behavior to DF ISM DOSS. AUC ratios of DF ISM (1.44) and DF 50%MTL (1.32) using VitE as surfactant exceeded 1.25, and therefore are considered as advantageous compared to fluid bed granulation.

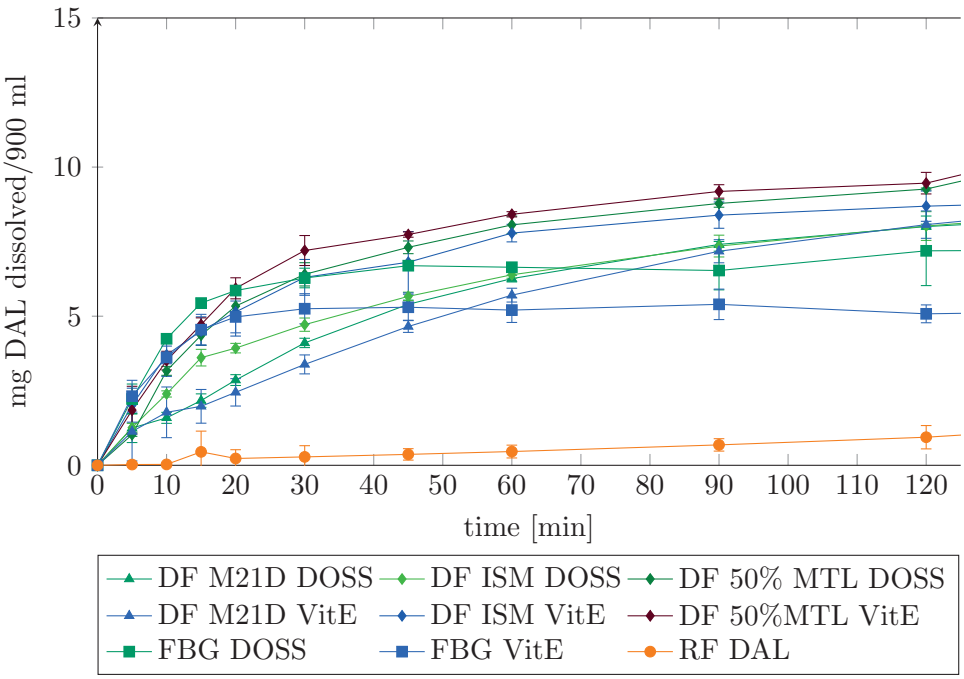

Figure 3.35: Dissolution behavior of dalcetrapib (DAL) DFs and FBGs in FaSSIF-V2 (n=3, mean±sd).

Dalcetrapib is a cholesteryl ester transfer protein modulator (Gross et al., 2012) for the prevention of dyslipidemia and cardiovascular disease. In solubility analysis it exhibited a soluble amount of 4.66 µg/ml in FaSSIF-V2, resulting in a dose/solubility ratio of 10700 ml, and therefore it classifies as a borderline DCS class IIa compound as well (Butler and Dressman, 2010). RF DAL exhibited a very low amount of dissolved API in dissolution analysis, emphasizing the poor wettability and agglomeration tendency of the model drug (Figure 3.35). Its dissolution behavior was improved by all formulations. Dry foams prepared using M21D as filler exhibited the slowest initial dissolution behavior. The initial dissolution rate was increased by using ISM as filler and DOSS as surfactant. A further improvement in dissolution behavior was observed for the two FBG formulations. A similar fast initial dissolution rate but a higher amount of dissolved API was observed for the for DF 50%MTL using DOSS as surfactant as well as DF ISM and 50%MTL using VitE as surfactant. AUC ratios exceed 1.25 for all DFs using VitE (M21D = 1.43, ISM = 1.57, 50%MTL = 1.92) as surfactant as well as DF 50%MTL using DOSS as surfactant (1.40). Therefore, superiority of dry foam formulation compared to fluid bed granulation could be shown for the model compound DAL.

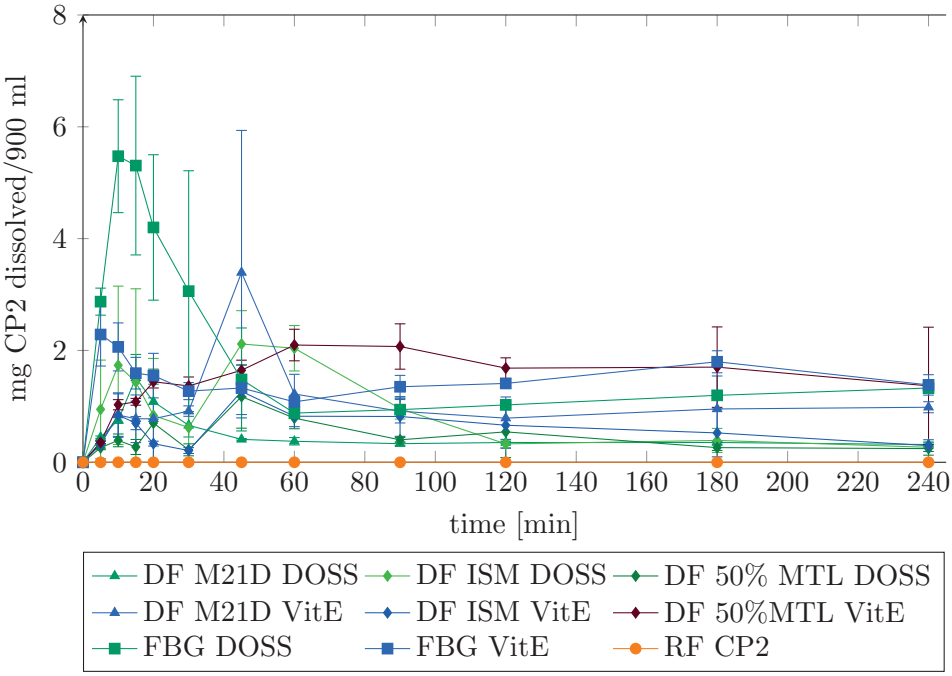

Figure 3.36: Dissolution behavior of CETP-inhibitor (2) (CP2) DFs and FBGs in FaSSIF-V2 (n=3, mean±sd).

Cholesteryl ester transfer protein inhibitor (2) (CP2) is a development compound of F. Hoffmann-La Roche Ltd. (Basel, Switzerland) for prevention of dyslipedimia and cardiovascular disease. Its solubility in FaSSIF-V2 was determined as 0.36 µg/ml and therefore it classifies itself as the compound with the lowest soluble amount in the used dissolution media in the course of this investigation (Table 3.4). Dissolution analysis of RF resulted in dissolved amount of CP2 below the detection limit of 0.17 µg/ml (Figure 3.36). FBG and DF tablets exhibited rather erratic dissolution results. Interestingly, again a higher amount of dissolved CP2 was detected during the first 30 min especially for FBG tablets, proposing a polymorphic change of the API or slower redistribution of the dissolved API in FaSSIF micelles. Nevertheless, no advantageous dissolution behavior of DF tablets was observed compared to FBGs. DF using 50%MTL and VitE as surfactant only reach similarity to FBG tablets with regard to dissolution behavior and AUC ratio (Table 3.5).

DAL and CP2 are under research development for the same target. DAL inherits a thioester structure in contrast to CP2, forming disulfide derivates via the thiol structure in vivo. In contrast CP2 exhibits a similar structure to DRX, both having either 5 or 6 halogen atoms (Figure 5.1).

In summary, it was possible to prepare dry foam formulation with all nine investigated model compounds, showing at least similar dissolution characteristics to the compared fluid bed granule formulations. Three out of the nine investigated model compounds revealed superiority of DF tablets in dissolution behavior compared to FBG tablets. Table 3.5 summarizes the calculated AUC ratios of all investigated dry foam formulations and highlights the ones where beneficial dissolution behavior of dry foam formulations was observed (AUC ratio above 1.25) by printing in bold. These three model compounds inherit poor aqueous solubility (although not the lowest solubility of all tested model compounds), high lipophilicity (log P value above 6) and low melting points (below 80°C). Taking a closer look, it appears that, the three model compounds with melting point below 80°C do not profit in general from being formulated as a dry foam. AUC of THL DF tablets exceeds AUC of FBG in all surfactant and filler combinations, except for M21D and VitE. AUC of DF VitE tablets is increased by the use of low molecular fillers, resulting in advantageous dissolution behavior of THL DF tablets over the corresponding FBG. DAL profits from dry foam formulation in general using VitE as surfactant regardless of the type of filler used, but not using DOSS as surfactant. DRX profits only from two out of the six investigated dry foam formulations in dissolution behavior. Dry foam formulation using low molecular fillers was not investigated using NK1 and MAO as model compounds. Therefore, an improvement of dissolution behavior by using ISM and 50%MTL as filler can not be precluded.

Table 3.5: AUC ratio DF/FBG.

API	filler	DOSS	SDS	PS80	VitE	MyrjS40	PP103
IDM	M21D	0.99	0.97	0.95	0.96	0.95	0.98
IDM	ISM	1.03			0.97		
IDM	50%MTL	1.02			0.98		
FDP	M21D	0.86	0.93	0.90	0.97	0.99	0.88
FDP	ISM	0.60			0.85		
FDP	50%MTL	0.80			1.06		
FEN	M21D	0.83	0.94	1.08	1.15	0.87	0.85
FEN	ISM	0.95			1.09		
FEN	50%MTL	0.85			1.19		
THL	M21D	**10.89**	**5.90**	**2.36**	1.02	**4.76**	**4.01**
THL	ISM	**13.78**			**3.31**		
THL	50%MTL	**9.70**			**3.53**		
NK1	M21D	0.95			0.79		
MAO	M21D	1.00			1.15		
CP2	M21D	0.28			0.72		
CP2	ISM	0.51			0.41		
CP2	50%MTL	0.29			1.11		
DRX	M21D	0.70			0.86		
DRX	ISM	0.96			**1.44**		
DRX	50%MTL	1.12			**1.32**		
DAL	M21D	1.07			**1.43**		
DAL	ISM	1.10			**1.57**		
DAL	50%MTL	**1.40**			**1.92**		

Table 3.6: Additional API characteristics including molecular weight (MW), polar surface area (PSA), number of hydrogen bond acceptors (HBA) and donors (HBD).

abbr.	API	PSA [Å^2]	HBD	HBA	MW [g/mol]
IDM	indomethacin	57.04	1	4	357.80
FDP	felodipine	48.83	1	3	384.26
FEN	fenofibrat	42.85	0	3	360.84
THL	orlistat	64.01	1	3	495.75
NK1	NK-rez.(1)-ant.	36.92	0	5	565.56
MAO	Mao-B-inh.	65.32	3	5	302.31
CP2	CETP-inh.(2)	32.04	1	3	531.00
DRX	drug X	17.10	0	2	554.00
DAL	dalcetrapib	30.93	1	3	389.60

In order to examine if other physico-chemical characteristics like polar surface area (PSA), molecular weight (MW), number of hydrogen bond acceptors (HBA) and donors (HBD) relate to the beneficial dissolution behavior of formulations prepared by dry foam granulation compared to fluid bed granulation for specific APIs, these characteristics are listed in Table 3.6 and plotted together with log P value in Figures 3.37, 3.38, 3.39 and 3.40. PSA values were calculated using internal F.Hoffmann-La Roche sources and software called COSAR, which is based on the calculation method established by Clark (1999).

Polar surface area, number of hydrogen acceptors and donors, as well as molecular weight of the model compounds showed no correlation with beneficial dissolution behavior of dry foam tablets compared to fluid bed granule tablets. Therefore, the only relevant characteristics indicating a possible superiority of dry foam granulation technology seem to be a low melting point in combination with high lipophilicity (log P value) of the model compound. Figure 3.41 summarizes this hypothesis and observed correlation, that key characteristics of model compounds for whom use of dry foam formulation technology can be advantageous with regard to dissolution behavior, are besides poor solubility, high lipophilicity and a melting point below 80°C.

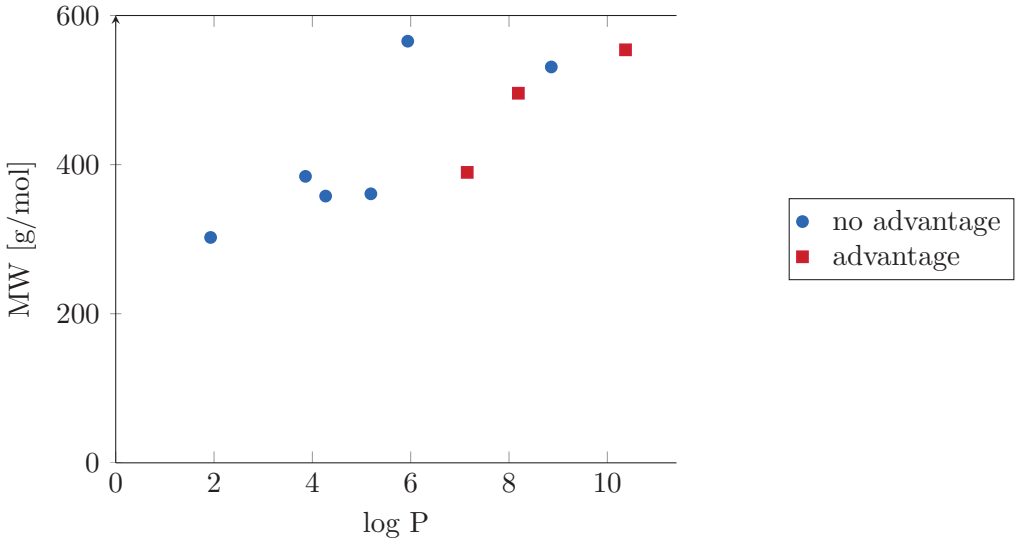

Figure 3.37: Investigated model compounds plotted according to their molecular weight (MW) and lipophilicity (log P value).

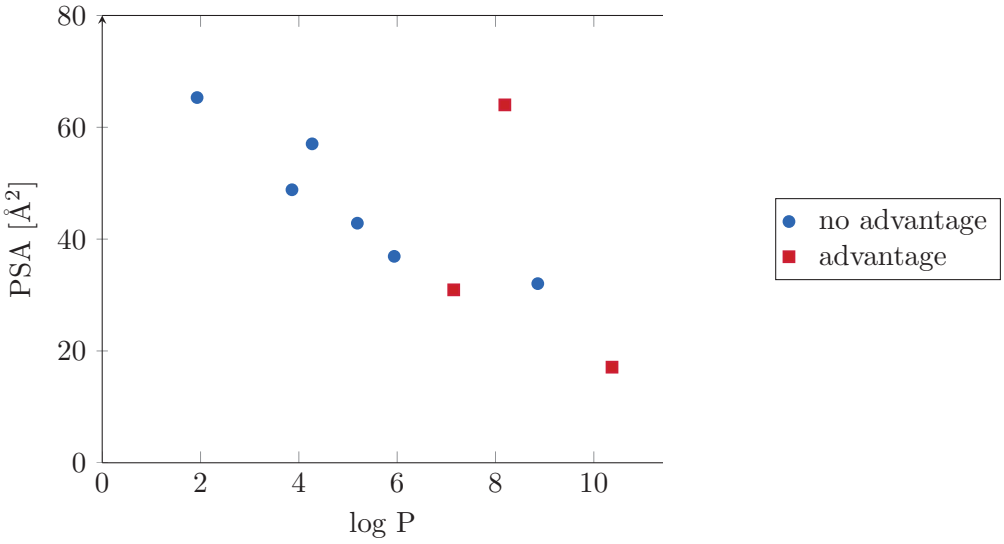

Figure 3.38: Investigated model compounds plotted according to their polar surface area (PSA) and lipophilicity (log P value).

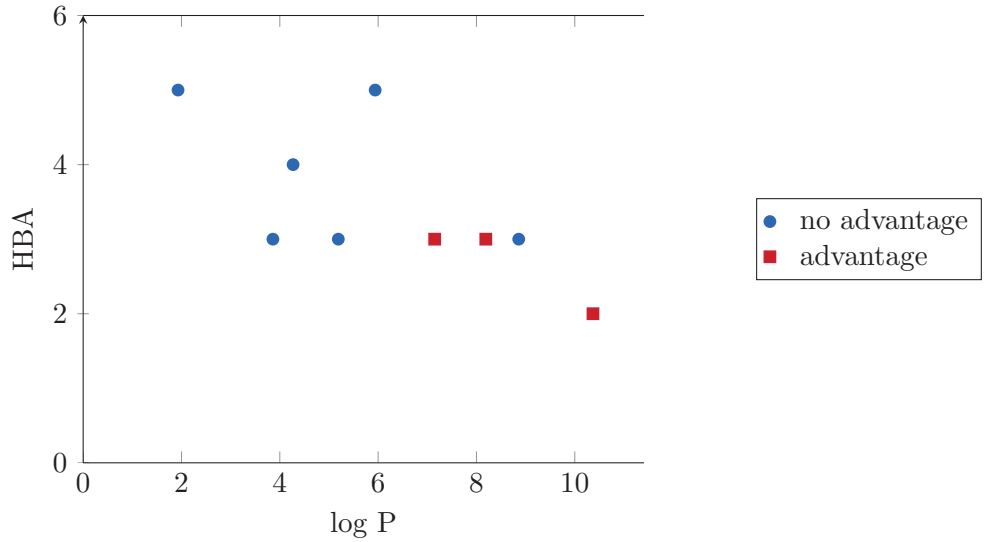

Figure 3.39: Investigated model compounds plotted according to their number of H-bond acceptors (HBA) and lipophilicity (log P value).

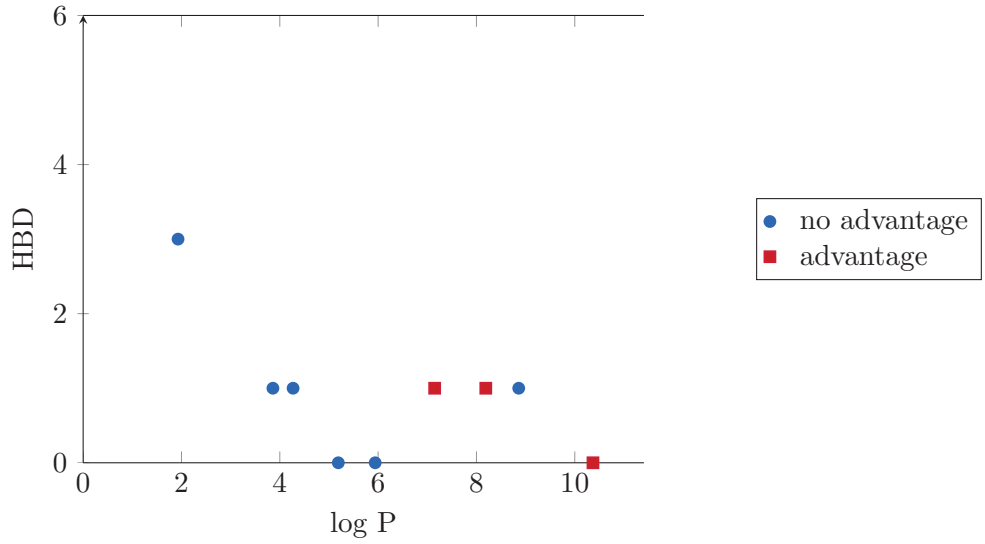

Figure 3.40: Investigated model compounds plotted according to their number of H-bond donors (HBD) and lipophilicity (log P value).

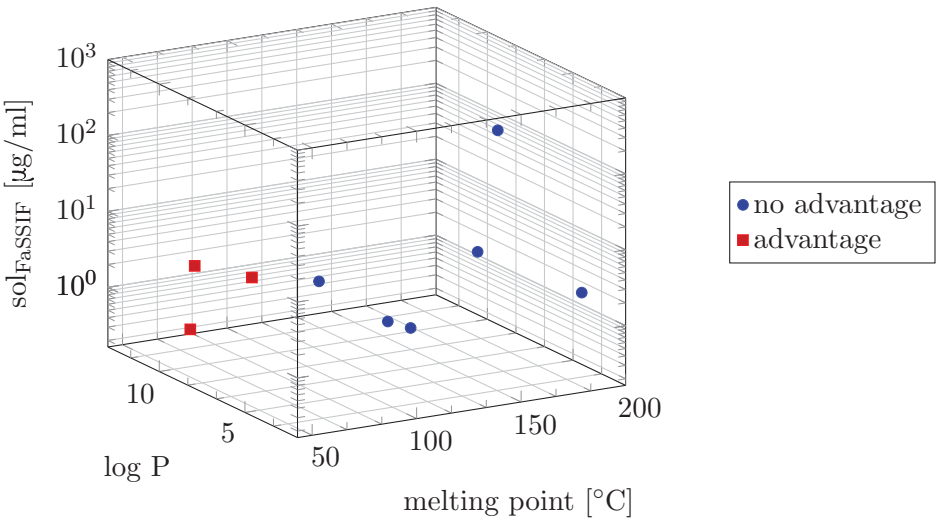

Figure 3.41: Investigated model compounds plotted according to their melting point, lipophilicity (log P value) and solubility in FaSSIF-V2 after 4 h at 37°C (sol_{FaSSIF}).

3.4 Summary and Conclusion

Dry foam formulation technology provided granules with suitable, comparable to fluid bed granule characteristics for all nine investigated model compounds. Depending on the model compound, the type of surfactant chosen for dry foam preparation had a high impact on the dissolution behavior of the resulting tablets. Whereas, indomethacin formulations showed very similar dissolution behavior in FaSSIF-V2, especially orlistat, but also felodipine and fenofibrate revealed a high influence of the surfactant used. Therefore, the surfactant used for both dry foam as well as fluid bed granulation should be selected carefully. The type of filler used for dry foam preparation showed to have a high influence on dry foam morphology, specific surface area of the resulting granules, disintegration as well as dissolution behavior of the tablets. Fast dissolving, low molecular weight fillers, namely isomalt and substitution of maltodextrin DE21 with 50% mannitol, led to more compact, less porous structures and granules with a higher specific surface area, due to surface roughness. The resulting tablets showed a faster disintegration behavior, as well as a higher initial dissolution rate.

Seeking for key characteristics classifying active pharmaceutical ingredients for which the use of dry foam granulation technology can be beneficial compared to fluid bed granulation, nine model compounds with different physico-chemical properties were investigated. Three model compounds, namely orlistat, dalcetrapib and drug X, showed improved dissolution behavior of dry foam compared to fluid bed granule tablets. Orlistat showed superiority with all three filler combinations, even in comparison to the market formulation ALLI®, whereas dalcetrapib and drug X only showed superior dissolution behavior using fast dissolving fillers. These three model compounds have in common a low melting point as well as a high log P value. In contrast CETP-inhibitor (2) inheriting a high log P value but also a melting point higher than 80°C, showed no beneficial dissolution behavior, in contrast, almost all dry foam tablets revealed an AUC ratio below 0.8, except for the combination of 50%MTL with VitE as surfactant. Investigation of additional physico-chemical characteristics, namely polar surface area, molecular weight, number of hydrogen bond acceptors and donors revealed no additional correlation with beneficial dissolution behavior of dry foam tablets compared to fluid bed granules. Therefore, a melting point below 80°C and a high lipophilicity (log P value above 6) are the only indicators of possible superiority of dry foam granulation technology over fluid bed granulation so far.

4 Conclusion

With the introduction of the dry foam granulation technology into the pharmaceutical area new opportunities for formulation of challenging molecules are available. When introducing a new technology it's important to learn about the factors, such as process parameters and formulation aspects, influencing the performance and characteristics of the resulting product.

During first fundamental experiments foaming and drying of wet pastes under reduced pressure showed to be advantageous over drying at normal pressure. Not only drying time was reduced and downstream processing improved, also the dissolution behavior of dry foam tablets was superior after vacuum foaming and drying.

Process temperature and paste water content were identified as important process parameters during foaming and drying of dry foam preparation process. By increasing the temperature during foaming and drying period a higher drying rate was observed. In the examined range the process pressure did not have a remarkable influence on drying kinetics. Paste water content and thereby paste viscosity, had a strong influence on drying kinetics during foaming and drying of dry foam preparation. Pastes with a low water content and therefore high viscosity exhibit a slower drying kinetic than pastes with higher water content. Furthermore, the morphology of the resulting dry foam pieces is affected by the paste viscosity and water content. Smaller pores evolve from paste with a low water content and therefore high viscosity, whereas a low viscosity causes larger pores. These correlations were confirmed using different preparation equipments. Magnetic suspension balance, vacuum drying cabinet and vacuum belt dryer, covering different batch scales, are known to differ with respect to heat transfer, air flow rate and speed of pressure reduction. Nevertheless, a model equation predicting the dimensionless moisture content of dry foams during foaming period was derived from using the magnetic suspension balance and transferred to the vacuum belt dryer process, after introducing two correction factors. Prediction and modeling of the drying rate during dry foam foaming and drying process appeared to be impossible, as drying rate changes over the time with different kinetic orders and is strongly influenced by the evolving dry foam morphology, which changes substantially during foaming and drying.

In spite of the substantial effect of paste water content and preparation equipment on dry foam morphology and drying kinetics, the dissolution behavior of resulting dry foam formulation tablets was not changed by the different process parameters used. This allows the formulator to adapt process parameters in distinct ranges without diminishing the dissolution performance of the resulting product. X-Ray μ-CT, mercury porosimetry, scanning electron microscopy and determination of specific surface area by nitrogen adsorption, were identified as useful, each other accom-

plishing analytical methods with regard to dry foam morphology. Batch wise small scale experiments using the vacuum drying cabinet can give a good prospect on dissolution behavior after transfer to continuous processing using the vacuum belt dryer, but not on granule characteristics.

Dry foam granulation technology showed to be a feasible formulation method for the nine investigated model compounds, in combination with different fillers and surfactants. The type of filler showed to have a remarkable influence on the resulting dry foam morphology, specific surface area of the resulting granules, as well as on the disintegration and dissolution behavior of the dry foam formulation tablets. Using fast dissolving, low molecular weight fillers, in general resulted in dry foams with a dense, less porous structure, granules with a higher specific surface area, and faster disintegrating as well as dissolving dry foam formulation tablets.

The type of surfactant used for dry foam preparation influenced the dissolution behavior of dry foam tablets remarkably, depending on the model compound, and therefore should be selected carefully. A screening system, predicting the wettability and solubility improving effect upon dry foam preparation would be a useful tool in dry foam formulation development.

Knowing for which group of active pharmaceutical ingredients dry foam granulation technology is suitable, or even superior compared to other formulation techniques, e.g. with regard to dissolution behavior and therefore possibly oral bioavailability, would be an achievement in formulation research and development. Therefore, the model compounds were chosen with respect to varying physico-chemical characteristics, potentially identifying key characteristics of compounds benefiting from dry foam formulation. In summary, model compounds with high lipophilicity in combination with a low melting point showed beneficial dissolution behavior compared to fluid bed granule tablets, using the same drug load and surfactant. Other physico-chemical characteristics like molecular weight, polar surface area, number of hydrogen bond acceptors and donors exhibited no correlation with beneficial dissolution behavior of dry foam tablets. Dry foam granulation technology showed to be especially beneficial for the model compound orlistat. Orlistat is a very lipophilic compound, with poor wettability as well as aqueous solubility, agglomeration tendency and a low melting point of 43°C. The prepared dry foam tablets showed superior dissolution behavior, with regard to initial dissolution rate as well as total amount of dissolved orlistat, compared to fluid bed granule tablets as well as the market formulation ALLI® in two different dissolution media tests. An additional advantage to improved dissolution behavior, especially for temperature sensitive compounds, is the low process temperature of dry foam preparation. Using e.g. fluid bed granulation or drying, the process temperature would have to be adapted for such compounds, causing difficulties like sticking of the granules to the granulator and longer process times. Dry foam granulation technology reveals new opportunities for formulation scientists seeking for an alternative formulation approach to fluid bed granulation, or even lipid and amorphous formulation approaches, e.g. in case of stability issues.

5 Experimental part

5.1 Materials

5.1.1 Active pharmaceutical ingredients

Active pharmaceutical ingredients (API) listed in Table 5.1 used for dry foam preparation and fluid bed granulation were purchased either from Haihang (China) and CAPOT Chemical (China) in not micronized quality, or received from F. Hoffmann-La Roche Ltd (Switzerland) in micronized quality. The APIs purchased in not micronized quality were further processed using an air jet mill Alpine 50 AS (Hosokawa Alpine, Germany) prior to use as described in Section 5.2.1 or used as delivered for the investigation of process parameters and equipment on dry foam properties in Section 2.4.

The chemical structures of the model compounds are depicted in Figure 5.1. Particle size distribution (Section 5.3.1.1) and specific surface area analysis (Section 5.3.5.4) results are listed in Section 6.1. Differential scanning calorimetry (DSC) diagrams for melting point determination can be found in Section 6.1.

Table 5.1: Model compounds used for dry foam and fluid bed granule preparation.

API	abbr.	source	quality	processing
indomethacin	IDM	CAPOT Chemical	not micronized	milling
felodipine	FDP	CAPOT Chemical	not micronized	milling
fenofibrate	FEN	Haihang	not micronized	milling
orlistat	THL	F. Hoffmann-La Roche	micronized	-
NK-rez.(1)-ant.	NK1	F. Hoffmann-La Roche	micronized	-
Mao-B-inh.	MAO	F. Hoffmann-La Roche	micronized	-
CETP-inh.(2)	CP2	F. Hoffmann-La Roche	micronized	-
drug X	DRX	F. Hoffmann-La Roche	micronized	-
dalcetrapib	DAL	F. Hoffmann-La Roche	micronized	-

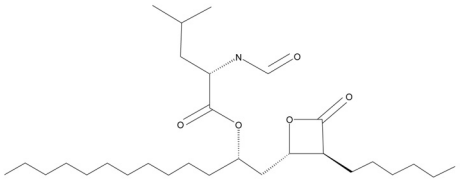

orlistat (THL)

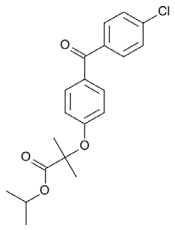

fenofibrate (FEN)

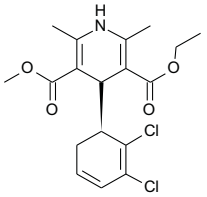

felodipine (FDP)

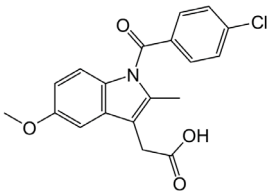

indomethacin (IDM)

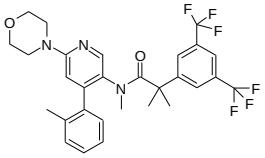

NK-rez.(1)-ant. (NK1)

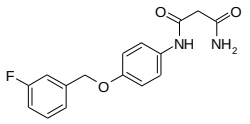

Mao-B-inh. (MAO)

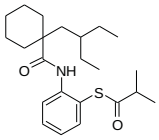

dalcetrapib (DAL)

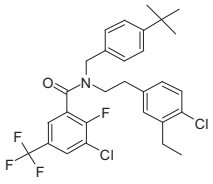

drug X (DRX)

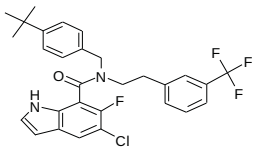

CETP-inh.(2) (CP2)

Figure 5.1: Chemical structures of model compounds.

Table 5.2: Fillers used for dry foam preparation.

filler	trade name	abbr.	source
maltodextrin DE21	Glucidex 21D	M21D	Roquette frères (France)
isomalt	galenIQ®721	ISM	Beneo Palatinit (Germany)
mannitol	Parteck Delta M	MTL	Merck (Germany)

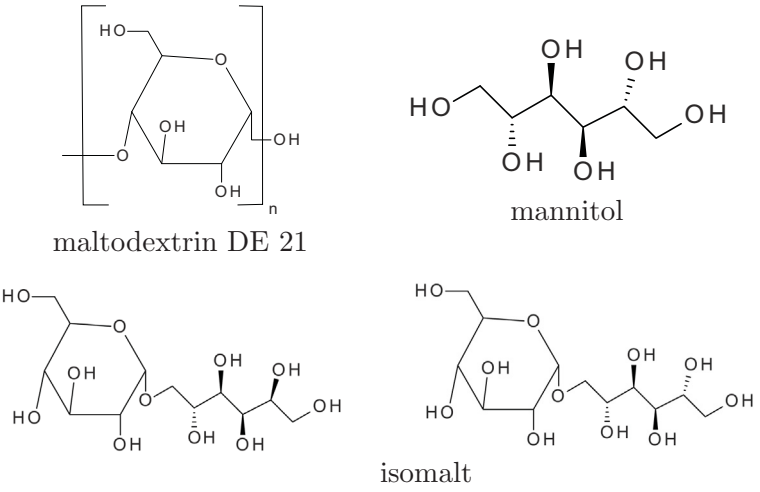

Figure 5.2: Chemical structures of fillers.

5.1.2 Fillers, surfactants and other excipients

Fillers used for dry foam preparation and their purchasing source are listed in Table 5.2. Maltodextrin 21D (M21D) is a spray dried glucose syrup, consisting of a mixture of oligosaccharides with different chain length derived from hydrolyzed corn starch. Parteck Delta M is a fast dissolving delta-mannitol. Isomalt (ISM) is a mixture of two disaccharides, each composed of a sugar and a sugar alcohol: glucose with mannitol, and glucose with sorbitol. A highly soluble grade, galenIQ®721, is commercialized by Beneo-Palatinit. The chemical structures of the three fillers are depicted in Figure 5.2.

Six different types of surfactants listed in Table 5.3 were used for preparation of dry foams and fluid bed granules. Their chemical structure is depicted in Figure 5.3.

For fluid bed granulation crystalline alpha-lactose monohydrate and microcrystalline cellulose (MCC) were used as fillers, and povidone K30 (PVP K30) as binder. As extragranular components, croscarmellose sodium was used as disintegrant and magnesium stearate as lubricant for preparation of tablets (Table 5.4).

Excipients listed in Table 5.5 were used for preparing the dissolution media, media for HPLC analysis as well as laser diffraction particle size analysis.

Table 5.3: Surfactants used for dry foam and fluid bed granule preparation.

surfactant	trade name	abbr.	source
docusate sodium		DOSS	Sigma Aldrich (USA)
sodium dodecylsulfate	Stepanol 100	SDS	Fluka Chemie (Switzerland)
polysorbate 80	Tween 80	PS80	Hänseler AG (Switzerland)
vitamin E TPGS		VitE	Eastman Ch. Company (UK)
PEG-40 Stearate	Myrj S40	Myrj	CRODA international (UK)
Poloxamer 333	Pluronic P103	PP103	BASF (Germany)

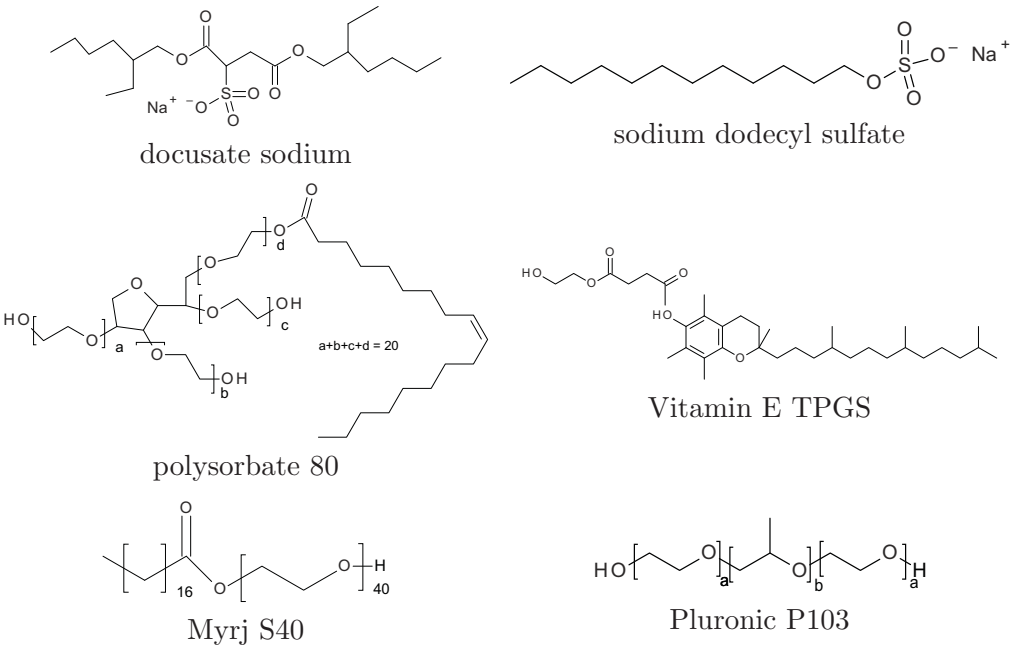

Figure 5.3: Chemical structures of surfactants used.

Table 5.4: Excipients used for fluid bed granule preparation and extragranular components of tablets.

excipient	trade name	source
alpha-lactose monohydrate	lactose cryst.	Friesland Foods (Netherlands)
microcrystalline cellulose	Avicel PH101	FMC Biopolymer (USA)
povidone K30	Kollidon 30	BASF (Germany)
croscarmellose sodium	Disolcel GF	Mingtai Chemical (Taiwan)
magnesium stearate		Peter Greven (Germany)

Table 5.5: Excipients for dissolution experiments, HPLC analysis and laser diffraction.

excipient	source
sodium taurocholate	PCA (Italy)
lecithine (Lipoid S100)	Lipoid (Germany)
maleic acid	Fluka Chemie (Switzerland)
sodium chloride	Fluka Chemie (Switzerland)
sodium hydroxid solution (Titrisol)	Merck (Germany)
acetonitrile	Merck (Germany)
trifluoroacetic acid	Merck (Germany)
phosphoric acid	Fluka Chemie (Switzerland)
2-propanol	Sigma Aldrich (USA)
n-octanol	Fluka Chemie (Switzerland)
sodium dodecylsulfate	Fluka Chemie (Switzerland)
sorbitane monooleate (Span 80)	Fluka Chemie (Switzerland)
n-heptan (technical quality)	F.Hoffmann - La Roche Ltd (Switzerland)

5.2 Manufacturing methods

5.2.1 Air jet milling of model compounds

The model compounds indomethacin, fenofibrate and felodipine were purchased in unmicronized quality. For particle size reduction 1 kg batches were subjected to air jet milling using a Alpine 50 AS (Hosokawa Alpine, Germany). Prior to milling APIs were sieved through an 0.8 mm screen. Nitrogen gas was used at an inlet pressure of approximately 7.2 bar and a milling pressure of 6.5 bar. Depending on the stickiness of the different model compounds the milling chamber had to be cleaned in between several times during one batch process.

5.2.2 Preparation of dry foam tablets

Dry foam tablets are prepared according to the process scheme depicted in Figure 5.4 and the composition listed in Table 5.6. After preparation of the paste in a kneading device it is exposed to reduced pressure at room temperature. In this period an expansion and partially drying of the paste takes place and the foam like structure is formed (foaming period). In order to remove the residual amount of water, moderately accelerated temperatures are applied afterwards (drying period). In the course of this investigation these two steps are conducted in different equipments:

- magnetic suspension balance (MSB)
- vacuum belt dryer (VBT)
- vacuum drying cabinet (VDC)

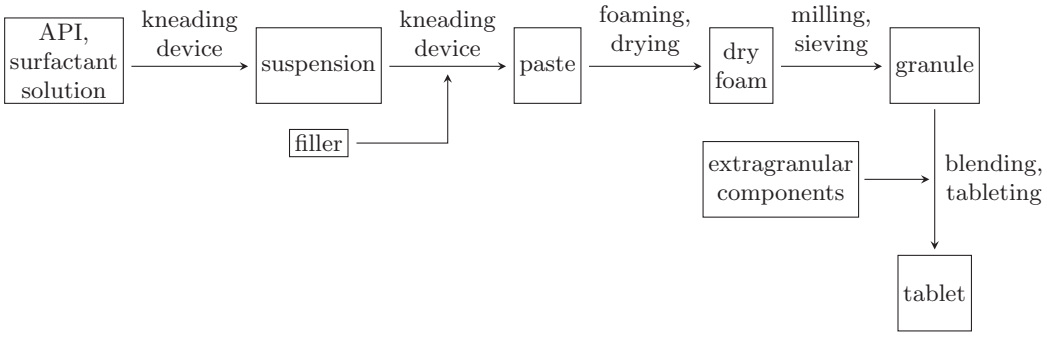

Figure 5.4: Dry foam preparation process scheme.

Table 5.6: Composition [%] of dry foam tablets exemplary for 19% paste water content based on wet mass.

component	DF paste	DF granule	DF tablet
API	12.60	15.54	15.00
surfactant	1.70	2.07	2.00
filler	66.70	82.39	79.50
water	19.00	-	-
magnesium stearate	-	-	0.50
croscarmellose sodium	-	-	3.00

The dry foams manufactured either using VBT or VDC are downstream processed by dry sieving and compressed to dry foam tablets (Section 5.2.2.6).

5.2.2.1 Preparation of paste

For dry foam paste preparation a surfactant solution was prepared using a magnetic stirrer. This solution contained already the necessary amount of water in order to obtain the declared paste water content based on the wet mass. For dry foam preparation using the VDC (Section 5.2.2.4) and the VBT (Section 5.2.2.5) 200 g paste was prepared and divided into 100 g batches for each preparation equipment. First, the API was suspended in the surfactant solution using a Planetron HKV1 Standard planetary kneader (IKA, Germany) at a mixing speed of 106 rpm of the outer and 23.5 rpm of the inner satellite arm respectively for 10 min. Maltodextrin DE 21 was added stepwise and processed to a homogeneous paste within 10 min at the same mixing speed. In case of isomalt and the 1:1 mixture of maltodextrin DE 21 and mannitol the mixing time was prolonged to 20 min in order to obtain a homogeneous paste.

For magnetic suspension balance experiments, a Roche planetary mixer at a mixing speed of 70 rpm was used and a batch size of 50 g paste prepared.

The resulting paste was filled in stainless steel cartridges for dry foam preparation

(Section 5.2.2.4, Section 5.2.2.5) and in sealed 5 ml syringes for characterization and magnetic suspension balance experiments (Section 5.2.2.2).

5.2.2.2 Dry foam preparation using a magnetic suspension balance

For simulation of the foaming and drying process during dry foam preparation process a magnetic suspension balance (MSB) (Rubotherm, Germany) was used. It allows determination of the drying curve as a function of pressure and temperature. The detailed experimental setup of the MSB is presented in Figure 5.5. The MSB measuring unit was equipped with a Mettler Toledo balance, with an accuracy of 1 µg, a pressure indicator PR4000B (MKS, USA), a vacuum pump (Vacubrand, USA) with a Julabo cooling unit (Germany) and a Huber Ministat heating bath (Germany). Nitrogen was used as inert 'Gas 1' at a flow of 80 ml/min in order to ensure the intended reduced pressure throughout the experiments. Air bath heating temperature was set to 30°C for all experiments. In Figure 5.5 the MSB setup provides the additional opportunity of using a second air flow 'Gas 2' with adjusted humidity, which was not used in performed experiments. Dry foam pastes consisting of micronized indomethacin (IDM) as model compound, sodium laurylsulfate as surfactant and maltodextrin DE 21 as filler according to the composition in Table 5.6 were prepared with the predetermined paste water content (PWC) using a Roche planetary mixer in a batch size of 50 g (Section 5.2.2.1). In order to determine the drying curve over time of different dry foam pastes, samples of approximately 0.2-0.4 g were placed in baskets. The cylindric baskets were perforated at the side and open at the top. Their weight with and without sample was noted before being transferred to the preconditioned MSB measuring unit and starting the experiment immediately. After each experiment using the MSB the dried samples were reweighed for verification of water content and loss on drying.

Design of experiments was used to investigate which process parameters have an effect on drying behavior of pastes forming the dry foams using the magnetic suspension balance (MSB). Paste water content (PWC), process pressure (p), temperature during foaming period (T1) and temperature during drying period (T2) were defined as factors. The factors were set in a way that they mimic the typical process using the vacuum belt dryer for dry foam preparation (Section 5.2.2.5).

The statistical design of experiments was generated and evaluated with MODDE v9.0 (Umetrics,Umeå, Sweden). A full factorial 2 levels orthogonal screening design with 16 experimental points and the center point in triplicate was chosen in order to examine main effects and interactions of the different factors. The experiments listed in Table 5.7 were conducted in randomized order.

Independent models were established for Φ_{DF} and drying rate k for the foaming and the drying period. The further way of proceeding is described in detail in Section 2.2.

Table 5.7: Design of experiments using magnetic suspension balance and vacuum belt dryer.

exp.	PWC [%]	p [mbar]	T1 [°C]	T2 [°C]	equipment
N1	17	20	20	40	MSB, VBT
N2	25	20	20	40	MSB, VBT
N3	17	80	20	40	MSB, VBT
N4	25	80	20	40	MSB, VBT
N5	17	20	40	40	MSB, VBT
N6	25	20	40	40	MSB, VBT
N7	17	80	40	40	MSB, VBT
N8	25	80	40	40	MSB, VBT
N9	17	20	20	60	MSB
N10	25	20	20	60	MSB
N11	17	80	20	60	MSB
N12	25	80	20	60	MSB
N13	17	20	40	60	MSB
N14	25	20	40	60	MSB
N15	17	80	40	60	MSB
N16	25	80	40	60	MSB
N17	21	50	30	50	MSB, VBT
N18	21	50	30	50	MSB, VBT
N19	21	50	30	50	MSB, VBT

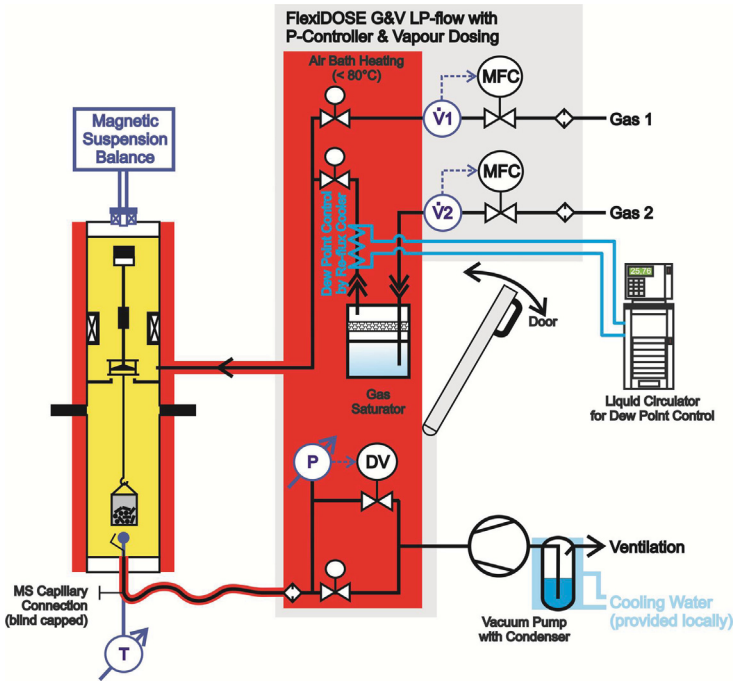

Figure 5.5: Detailed setup of the magnetic suspension balance measuring unit

5.2.2.3 Dry foam preparation using a drying cabinet without vacuum

For dry foam preparation in a drying cabinet without applying reduced pressure a drying oven with a high air change rate (Memmert, Germany) set to a temperature of 40°C was used. The paste was spread on a screen-like plate using an automatic cartridge pump Dewalt DC542 Type 1 (Dewalt Idstein, Germany) equipped with a nozzle orifice diameter of 5 mm. Afterwards the plate was placed in the drying oven for over 72 h. The resulting dry product was downstream processed according to Section 5.2.2.6 after crushing it down to smaller pieces using a glass pestle.

5.2.2.4 Dry foam preparation using the vacuum drying cabinet

For dry foam preparation in a vacuum drying cabinet (VDC) a Heraeus high vacuum drying cabinet (Thermo Fisher Scientific, USA) with a membrane vacuum pump (Vacuubrand, Germany) and a pressure sensor (Comat AG, Germany) were used. The paste (100 g) was spread on a screen-like plate using an automatic cartridge pump Dewalt DC542 Type 1 (Dewalt Idstein, Germany) equipped with a nozzle orifice diameter of 5 mm. Afterwards the plate was placed in the VDC and the pressure reduced to 40 mbar or 80 mbar respectively (± 3 mbar) within 5 min at room temperature. These process parameters were kept for 30 min, before the target cabinet temperature was increased to 45°C, resulting in a product temperature of approximately 40°C after 60 min. Product and cabinet temperatures were monitored using Jumo resistance thermometer (Jumo, Germany) with radio transmission.

5.2.2.5 Dry foam preparation using the vacuum belt dryer

For the preparation on the vacuum belt dryer (VBT) Drylab (0.6 m^2 of drying surface area, Bucher, Switzerland) the automatic cartridge pump Dewalt DC542 Type 1 (Dewalt Idstein, Germany) was connected via an inlet valve to a comb like syringe with 6 nozzle orifice diameters of 2 mm within the VBT. The paste (100 g for parallel experiments with VDC as described in Section 5.2.4.2, 200 g for other preparations) was applied in 6 parallel strands onto the moving PTFE (Teflon®) coated glass fabric belt at a speed of 2 cm/min. The moving belt passes four separately heated or cooled temperature zones. For the foaming period the plate temperature of zone 1 (60 cm length) is set to 20°C (30 min). For further drying the 3 following zones (each 70 cm length) are set to a plate temperature of 60°C plate temperature and are passed within additional 105 min. A final product temperature of approximately 40°C was targeted. Pressure within the vacuum belt dryer was controlled via a vacuum pump targeting 40 mbar or 80 mbar respectively (± 3 mbar). Product surface temperature was occasionally measured in zone 4 using an Raytek infrared sensor (Raytek GmbH, Germany). At the end of zone 4 a cutter broke down the foam strands into smaller pieces. Foam pieces left the vacuum belt dryer via two outlet valves, which kept the pressure within the apparatus constant by opening alternately and adjusting the pressure in between to either ambient pressure or pressure within the VBT.

5.2.2.6 Downstream processing and tablet preparation of dry foams and fluid bed granules

Dry sieving of dry foam pieces and fluid bed granules was conducted using a Comil® (Quadro, Canada) equipped with a screen with round openings of 2.108 mm diameter at a speed of 4000 rpm. For dry foams prepared with ISM and 50%MTL as filler sieving speed had to be reduced to 2200 rpm due to their harder structure.

For blending with extragranular components to tabletting mixtures approximately 20 g of the resulting dry foam granules or fluid bed granules were used, and mixed with croscarmellose sodium and magnesium stearate, according to Table 5.6 and 5.8 in 200 ml containers. Granules were mixed for 3 min in a Turbula® T2F mixer (Willy A. Bachofen AG, Switzerland) at a speed of 30 rpm with croscarmellose sodium first. 1/3 of the resulting mixture was premixed with the total amount of magnesium stearate under the same conditions. Afterwards the remaining granule mixture was added and blended for additional 3 min under the same conditions.

Circular flat-faced tablets of 10 mm diameter with a solid fraction (SF) of 85% ± 2% and a drug content of 50 mg were prepared using a hydraulic press (Perkin-Elmer). The target height of the tablets was calculated based on the helium density (ρ), determined by AccuPyc 1330 V3.03 (micromeritics, USA), tablet volume (V), and tablet mass (m) (Tye et al., 2005) according Equation (5.1)

$$\mathrm{SF} = \frac{m}{\rho \cdot V}\,. \tag{5.1}$$

Table 5.8: Composition [%] of fluid bed granule tablets

component	FBG granule	FBG tablet
API	15.54	15.00
surfactant	2.07	2.00
PVP K30	5.18	5.00
lactose	56.48	54.50
MCC	20.73	20.00
magnesium stearate	-	0.50
croscarmellose sodium	-	3.00

The required compression force was retained for a few seconds. Correct tablet volume was verified by measuring the actual tablet dimensions.

5.2.3 Preparation of fluid bed granules

Fluid bed granules (FBG) were prepared by spraying an aqueous solution (total weight of spraying solution 100 g) of binder (5 g/100 g water) and surfactant (2 g/100 g water) through a 0.5 mm air nozzle, at a spraying pressure of 0.5 bar, and a spray rate of 5.8 g/min on the API-filler mixture within a Mini-Glatt® fluid bed granulator (Glatt, Germany) with a batch size of 100 g. Their composition is listed in Table 5.8. Inlet air temperature was set to 60°C, and to 35°C respectively for THL FBG taking the low melting point of THL into account. After approximately 18 min of spray granulation, the granules were dried for approximately 5 min until an outlet air moisture of 25% relative humidity was reached. Fluid bed granules were downstream processed to tablets according to Section 5.2.2.6 and Table 5.8.

5.2.4 Investigating the dry foam preparation process

5.2.4.1 Comparing the foaming process on the magnetic suspension balance with the vacuum belt dryer

In order to investigate the applicability of the statistical model developed on the MSB, the foaming period was investigated in more detail on the vacuum belt dryer (VBT). To allow a direct comparison of the measured values from the MSB and VBT the same set of parameters (PWC, p and T1) was used and the experiments N1 to N8 singular and the center point experiments N17, N18, N19 in triplicate repeated on the VBT (Table 5.7). Micronized indomethacin (IDM) was used as model compound, sodium laurylsulfate as surfactant and maltodextrin DE 21 as filler according to the composition in Table 5.6. For each experiment approximately 100 g of paste were used. In order to be able to manually discharge the paste strands of the VBT after 30 min, the belt velocity of the VBT was set to 7 cm/min and all four temperature zones were set to the predefined temperature T1. After 30 min the vacuum belt dryer was opened and the still wet product placed immediately

into a Moisture Analyzer HR 83P (Mettler Toledo) at a temperature of 100°C for at least 90 min. For complete drying the samples were put for 72 h in a drying oven (Memmert, Germany) at 100°C and the total loss on weight (X [%]) noted.

The evaporated amount of water (EVW) value was calculated according to Equation (2.1). The dimensionless moisture content Φ_{DF}, using the magnetic suspension balance, and the dimensionless moisture content of dry foams prepared using the vacuum belt dryer, $\Phi_{DF(VBT)}$, were calculated according to Equation (2.2).

5.2.4.2 Influence of process parameters and equipment on dry foam properties

Paste for dry foam preparation was prepared as described in Section 5.2.2.1. Indomethacin (IDM) was used as model compound as delivered, sodium laurylsulfate as surfactant and maltodextrin DE 21 as filler according to the composition listed in Table 5.6. The paste water content was varied in 2% steps between 15-23% based on wet mass. Each batch of paste was divided in two parts for parallel preparation of dry foams using the vacuum drying cabinet as described in Section 5.2.2.4 and the vacuum belt dryer as described in Section 5.2.2.5 at 40 mbar reduced pressure. One additional batch of paste containing 17% water based on dry mass was used for preparation at 80 mbar. The final granule and tablet composition was always the same (Table 5.6).

5.3 Analytical methods

5.3.1 API characterization

5.3.1.1 Particle size distribution analysis by laser diffraction

Particle size distribution of model compounds as delivered and after air jet milling was analyzed in triplicate using a Malvern Mastersizer 2000 (Malvern Instruments, UK) with a Hydro 2000S wet dispersion unit or a Sympatec Helos KF (Sympatec GmbH, Germany) with sucell malvern wet dispersion unit (Malvern Instruments, UK) respectively. The dispersion medium was prepared by dissolving first the indicated amount of surfactant in purified water or n-heptan. An excess of model compound was added and a saturated solution prepared by stirring at least 4 h using a magnetic stirrer and allowing the compound to dissolve for at least 12 h. The suspension was filtered through 0.22 µm Millipore-filters (EMD Millipore, Merck, Germany) and used as dispersion medium as well as blank measurements. Samples were analyzed in triplicate after method development at a stirring rate of 3000 rpm and a measuring time of 30 s. The Fraunhofer model was used for deconvolution of the diffraction pattern by the software Mastersizer 2000 version 5.6.0 or Windox 5.7.0.0 for Sympatec Helos KF measurements respectively. The cumulative values D10, D50 and D90 of the volume-weighted particle size distributions were calculated. Sample preparation and measuring conditions are listed in detail in Table 5.9.

Table 5.9: Sample preparation and analytical conditions for particle size analysis of model compounds, after air jet milling or as delivered (ad). M indicates the use of Mastersizer 2000, S using Sympatec Helos KF for analytical measurements.

API	instr.	dispersion medium	stirring	ultra sonic
$\text{indomethacin}_{\text{ad}}$	M	0.2 % PS80 in water	60 s	
indomethacin	M	0.2 % PS80 in water	60 s	30 s 20%
$\text{felodipine}_{\text{ad}}$	M	0.2 % PS80 in water	60 s	30 s 80%
felodipine	M	0.2 % PS80 in water	60 s	30 s 20%
$\text{fenofibrate}_{\text{ad}}$	M	0.2 % PS80 in water	60 s	
fenofibrate	M	0.2 % PS80 in water	60 s	30 s 100%
orlistat	M	0.2 % PS80 in water	60 s	
NK-rez.(1)-ant.	S	0.3 % SDS in water	120 s	120 s 100%
Mao-B-inh.	S	0.1 % span80 in n-heptan	120 s	120 s 40%
CETP-inh.(2)	M	0.1 % PS80 in water	60 s	30 s 60%
drug X	S	0.3 % SDS in water	60 s	30 s 60%
dalcetrapib	M	0.5 % SDS in water	60 s	30 s 100%

5.3.1.2 Determination of melting point of APIs

Differential scanning calorimetry (DSC) measurements were performed in triplicate for verification and determination of model compound melting points. DSC samples were weighed using XP205 Delta Range analytical balance (Mettler Toledo, Switzerland) in 40 µl aluminium crucibles and closed with aluminium-piercing lids. DSC measurements were performed using Mettler Toledo DSC 1 STARe System and software version 9.20 (Mettler Toledo, Switzerland). Measurements were started at 20°C and the temperature was increased by 10 K per minute up to 200°C. The temperature range was selected to cover the melting points mentioned in literature for the APIs. Blind sample measurements were performed with empty crucibles and piercing lids.

5.3.2 Characterization of fillers

Dynamic vapor sorption analysis was performed as single experiments using a Dynamic Sorption Analyzer DVS1 (Surface Measurement Systems Ltd., UK) and approximately 10 mg of three different fillers, namely maltodextrin DE 21, isomalt and mannitol. Continuous gravimetric determination of adsorbed vapor was performed at a temperature of 25°C varying the relative humidity from 0 to 90% in two cycles.

5.3.3 Characterization of dry foam paste

Rheological measurements of the paste containing M21D as filler were performed in duplicate using a HAAKE MARS II (Thermo electron corporation) and RheoWin 3.30.05 software, a cone-plate geometry with a cone of 2° and 20 mm diameter, and a gap of 0.105 mm. A controlled shear rate from 0 to 101 1/s was applied within 120 s, after keeping a shear rate of approximately 100 1/s for 10 s it was reduced to 0 1/s in 120 s measuring the shear stress. Dry foam pastes containing maltodextrin 21D as filler showed nearly Newtonian flow behavior with a small hysteresis between the ascending and descending shearing curve at 15% paste water content based on wet mass. As the apparent viscosity of dry foam pastes depends on the shear rate, average values at a shear rate of 100 1/s for 10 s (η_{100}) were used for comparison. As pastes containing ISM or a 50%MTL as filler showed non Newtonian, shear-thinning behavior in the method established before, the rheological measurements were performed in duplicate using a plate-plate geometry with a diameter of 40 mm, and a gap of 0.500 mm. A controlled shear rate from 0 1/s to 10 1/s was applied, after keeping a shear rate of approximately 10 1/s for 10 s it was reduced to 0 1/s measuring the shear stress, collecting 200 data points in total. As the apparent viscosity depends on the shear rate, average values at a shear rate of 10 /s (η_{10}) for 10 s were used for comparison.

5.3.4 Characterization of dry foam morphology

5.3.4.1 Mercury porosimetry

A PASCAL 140 (Pressurization by Automatic Speed-up and Continuous Adjustment Logic) (Thermo Fisher, Italy) and SOLID software (Solver of Intrusion Data Software for PASCAL140/240/440 Series version 1.3.0) were used for mercury porosimetry of intact dry foam pieces in duplicate. At the beginning of each determination, the dilatometer was evacuated up to a pressure of 0.07 kPa. Then it was filled with mercury under increasing pressure up to 400 kPa at the recommended speed mode 5, where the PASCAL system automatically determines the correct pressurization speed according to the presence of pores and to the real penetration rate of mercury into the pores. The pore sizes corresponding to the intrusion pressures were calculated assuming cylindrical pores using the Washburn equation (Washburn, 1921) according to Equation (5.2)

$$R = -2\sigma \cdot \frac{cos(\Theta)}{P_c}\,, \tag{5.2}$$

where R is the pore radius, σ is the surface tension of pure mercury (0.48 N/m), Θ the contact angle of mercury with the sample (140°) and P_c the corrected pressure.

5.3.4.2 X-Ray microcomputed tomography

X-Ray micro-computed tomography measurements for visualization of dry foam morphology were performed on a Skyscan 1172 (Skyscan, Belgium) equipped with a 50 mm Hamamatsu Camera without any sample preparation (n=1). The source was tuned to 55 kV and 180 µA for the data acquisition. The resolution was set to 6.8 µm. The 2D images are displayed via the software CTView from Skyscan in full resolution. The 3D images are displayed with the Software CTVox from Skyscan with two fold resolution reduction.

5.3.5 Characterization of dry foam and fluid bed granules

5.3.5.1 Sieve analysis

After downstream processing to granules, DF and FBG granules were characterized by sieve analysis (AS 200 control, Retsch) (n=1) using the complete batch of approximately 70-100 g (Ph.Eur. 7.8). As most of the batches did not follow the RRSB distribution after Rosin, Rammler, Sperlin and Bennet, the D50 value (µm), the particle diameter at 50% in the cumulative distribution, calculated by easysieve software, fractions of fines (< 90 µm) and coarse particles (> 710 µm) were used for comparison.

5.3.5.2 Loss on drying

Loss on drying (LOD) of granules was analyzed using a Moisture Analyzer HR83P (Mettler Toledo) at a temperature of 90°C according to Ph.Eur. 7.8 (n=1).

5.3.5.3 Bulk and tapped density

Bulk and tapped density were analysed according to Ph.Eur. 7.8 using a Engelsmann STAV 2003 equipped with a measuring cylinder of 250 ml volume using the complete batch yield of approximately 70-100 g (n=1). First bulk volume (V_0) and thereby bulk density (ρ_{bulk}) [g/ml] was determined according to Equation (5.3)

$$\rho_{\text{bulk}} = \frac{m_{\text{sample}}}{V_0}\,. \tag{5.3}$$

The corresponding volume after 10, 500, 1250 und 2500 tappings was noted and the tapped density (ρ_{tapped}) [g/ml] calculated using the volume after 2500 tappings (V_{2500}) according to Equation (5.4)

$$\rho_{\text{tapped}} = \frac{m_{\text{sample}}}{V_{2500}}\,. \tag{5.4}$$

5.3.5.4 Specific surface area

Specific surface area (SSA) samples (granules as well as API substance) were evacuated for 12 h at room temperature and washed over with nitrogen right before

Table 5.10: Composition [%] of FaSSIF-V2 dissolution medium.

component	g/L	mM
sodium taurocholate	1.79	3.0
lecithin	0.16	0.2
maleic acid	2.24	19.1
sodium chloride	4.03	68.6
sodium hydroxide	-	35.8

analysis using a VacPrep (micromeritics, USA). The adsorbed amount of nitrogen was measured at 5 steps from 0.05-0.25 p/p_0 in duplicate using a Gemini 2375 V4.02 (micromeritics, USA) for samples in Section 2.4 and a Gemini VII 2390A V1.03 (micromeritics, USA) for all other measurements. This change of analytical equipment was due to technical reasons and no longer availability of the equipment used first. SSA was calculated according to BET (Brunauer, Emmet and Teller) equation (Brunauer et al., 1938).

5.3.6 Disintegration experiments

Disintegration time of tablets was analyzed in water using an automated Sotax® disintegration apparatus (Sotax, Switzerland) with discs at 37 ± 2°C (Ph.Eur. 7.0) (n=6).

5.3.7 Dissolution experiments

Dissolution of tablets was carried out in triplicate using a USP II apparatus (Sotax AT 7 smart, Sotax, Switzerland) and 900 ml FaSSIF-V2 (Jantratid et al., 2008) as dissolution medium. FaSSIF-V2 was prepared by dissolving sodium taurocholate in purified water and adding lecithin under stirring afterwards. After all lecithin was dissolved, a solution of sodium chloride and maleic acid in purified water was added. The mixture was set to a pH of 6.5 with sodium hydroxide solution and the volume adjusted to 10.0 L. Composition of FaSSIF-V2 medium is listed in Table 5.10.

For analysis of THL tablets and capsules USP 35 THL monograph medium, consisting of 3% SDS and 0.5% NaCl in water plus 1-2 drops/10 L of n-octanol was used. USP 35 THL monography medium was adjusted to a pH of 6.0 with phosphoric acid.

The paddle speed was set to 100 rpm and 1.5 ml samples were taken through glass fiber filters after 5, 10, 15, 20, 30, 60, 90, 120 and 240 min without replacement. HPLC analysis was carried out according to the specified methods in Section 5.3.9. For comparison 50 mg of each API were filled in hard gelatine capsules sizes 1 as reference formulation (RF) (Capsugel, France) and analyzed regarding dissolution behavior using a sinker in triplicates. Alli® 60 mg capsules marketed formulation was analyzed in triplicate using a sinker as well.

In addition to visual comparison of the dissolution curves of the tablets derived

from the two different formulation methods, the ratio of the area under the curve (AUC) [mg/ml · min] of DF tablets compared to the corresponding fluid bed granule tablets, according to Equation (5.5)

$$\text{AUC ratio DF/FBG} = \frac{\text{AUC}_{\text{DF}}}{\text{AUC}_{\text{FBG}}}\,, \tag{5.5}$$

was calculated.

The AUC was determined by applying the trapezoidal rule from 0 to 240 min, where the region under the graph of the function is approximated as a trapezoid and its area calculated, according to Equation (5.6)

$$\int_{\text{a}}^{b} f(x)dx \approx (\text{b} - \text{a})\frac{\text{f(a)} + \text{f(b)}}{2}\,, \tag{5.6}$$

where a and b are the x-values (time points) and f(a) and f(b) the corresponding y-values (dissolved amount of API / 900 ml dissolution medium).

5.3.8 Solubility of model compounds in dissolution medium

Solubility of model compounds was determined in triplicate by end-over-end rotation in FaSSIF-V2 at 37°C for 4 h and 24 h. THL solubility was additionally analyzed in USP 35 THL monograph medium. After filtration using 1 µm glass fiber filters, samples were diluted 1:1 with HPLC mobile phase and quantitative HPLC analysis was conducted immediately (Section 5.3.9).

5.3.9 HPLC analysis

API concentration in solubility and dissolution samples was analyzed using a Waters alliance separation module 2690 combined with Waters dual wavelength absorbance detector 2487 (Waters, USA). Two different columns, namely a Nova Pak C18 4 µm 3.9x150 mm for analysis of orlistat samples and a XTerraTMMS C18 3.5 µm 3.0x50 mm for all other APIs were used at a temperature of 40°C. Mobile phase, flow rate and detection wavelength are indicated in Table 5.11. KH_2PO_4 buffer is prepared by dissolving 1.35 g potassium dihydrogen phosphate in 500 ml MilliQ water and adding phosphoric acid up to a pH of 2.5.

Exemplary HPLC diagrams with retention time are depicted in Section 6.3. Linearity was verified over the investigated concentration range from 0.5 to 50 µg/ml (FEN, THL, NK1, MAO, CP2, DRX, DAL) or 500 µg/ml (IDM, FDP) respectively.

5.3.10 Scanning electron microscopy

Scanning electron microscopy (SEM) images of granules and APIs were prepared using a Sigma VP system from Zeiss (Zeiss, Germany) (n=1). The acquisition is performed under high vacuum with a secondary electron detector after sputtering gold on the sample. The extraction power of the electron from the cathode as well as the magnification are indicated on the images.

Table 5.11: Analytical conditions for HPLC analysis of dissolution and solubility samples. ACN is the abbreviation of acetonitrile, PHA of phosporic acid and TFA of trifluoroacetic acid.

API	mobile phase	flow rate	detection
indomethacin	ACN:H2O:TFA 60:40:0.05	1 ml/min	254 nm
felodipine	ACN:water 90:10	0.5 ml/min	362 nm
fenofibrate	ACN:water 60:40	1.7 ml/min	288 nm
orlistat	ACN:water:PHA 86:14:0.0025	2 ml/min	195 nm
NK-rez.(1)-ant.	ACN:H2O:TFA 60:40:0.1	1 ml/min	215 nm
Mao-B-inh.	ACN:water 50:50	0.5 ml/min	250 nm
CETP-inh.(2)	ACN:H2O:TFA 80:20:0.1	1 ml/min	220 nm
drug X	ACN:water:TFA 80:20:0.1	1 ml/min	220 nm
dalcetrapib	60:40 2-propanol: KH_2PO_4 buffer	0.4 ml/min	248 nm

6 Appendix

6.1 API characteristics

Table 6.1: API particle size distribution [µm] with corresponding standard deviation (stdev) of triplicate measurements analyzed according to Section 5.3.1.1 of compounds as delivered (ad) and after air jet milling.

API	abbr	D10	$D10_{stdev}$	D50	$D50_{stdev}$	D90	$D90_{stdev}$
$indomethacin_{ad}$	IDM_{ad}	9.00	0.20	33.50	0.90	73.80	5.10
indomethacin	IDM	0.85	0.01	3.45	0.09	7.58	0.34
$felodipine_{ad}$	FDP_{ad}	10.80	0.29	39.35	0.98	112.05	2.59
felodipine	FDP	1.13	0.09	5.89	0.32	12.29	0.77
$fenofibrate_{ad}$	FEN_{ad}	20.86	0.35	103.21	2.28	215.78	6.18
fenofibrate	FEN	1.41	0.04	7.25	0.10	16.44	0.20
orlistat	THL	1.81	0.04	6.96	0.42	18.63	1.45
NK-rez.(1)-ant.	NK1	1.07	0.01	4.48	0.12	12.33	0.09
Mao-B-inh.	MAO	0.79	0.02	1.93	0.04	4.58	0.08
CETP-inh.(2)	CP2	1.70	0.10	5.90	0.10	13.20	0.30
drug X	DRX	1.41	0.04	6.91	0.24	13.59	0.34
dalcetrapib	DAL	1.60	0.01	6.90	0.18	16.00	0.12

Table 6.2: Specific surface area (SSA) analyzed according to Section 5.3.5.4 in duplicate with corresponding standard deviation (stdev) of compounds as delivered (ad) and after air jet milling.

API	abbr	SSA	SSA_{stdev}
$indomethacin_{ad}$	IDM_{ad}	0.33	0.01
indomethacin	IDM	5.03	0.01
$felodipine_{ad}$	FDP_{ad}	0.32	0.07
felodipine	FDP	3.07	0.03
$fenofibrate_{ad}$	FEN_{ad}	0.07	0.00
fenofibrate	FEN	2.51	0.03
orlistat	THL	2.41	0.11
NK-rez.(1)-ant.	NK1	1.57	0.03
Mao-B-inh.	MAO	4.77	0.12
CETP-inh.(2)	CP2	2.07	0.03
drug X	DRX	2.14	0.04
dalcetrapib	DAL	1.15	0.09

6.2 Differential scanning calorimetry diagrams

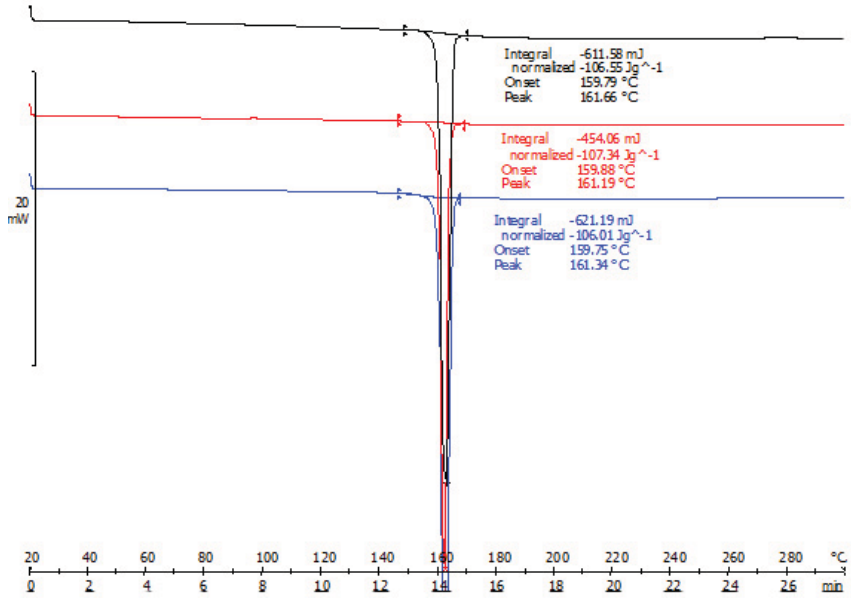

Figure 6.1: DSC diagram of IDM for melting point determination.

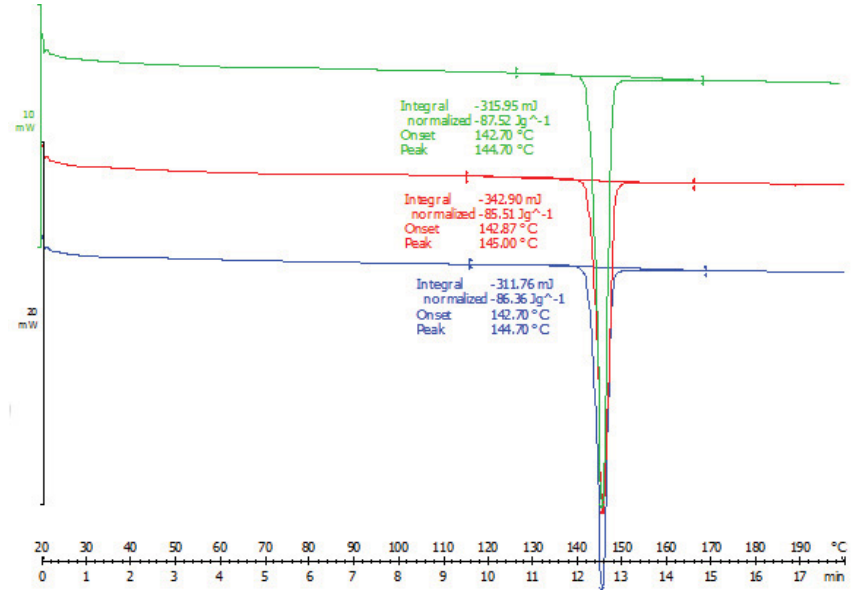

Figure 6.2: DSC diagram of FDP for melting point determination.

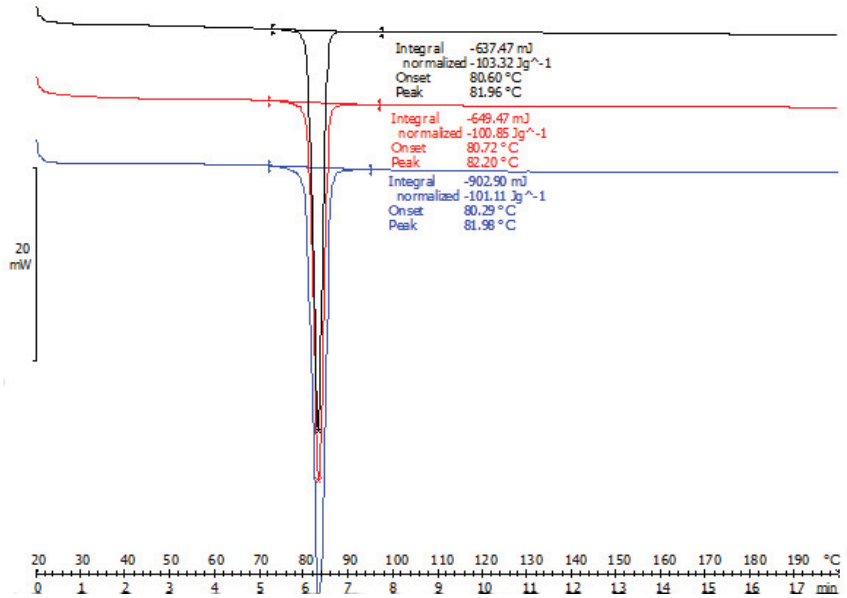

Figure 6.3: DSC diagram of FEN for melting point determination.

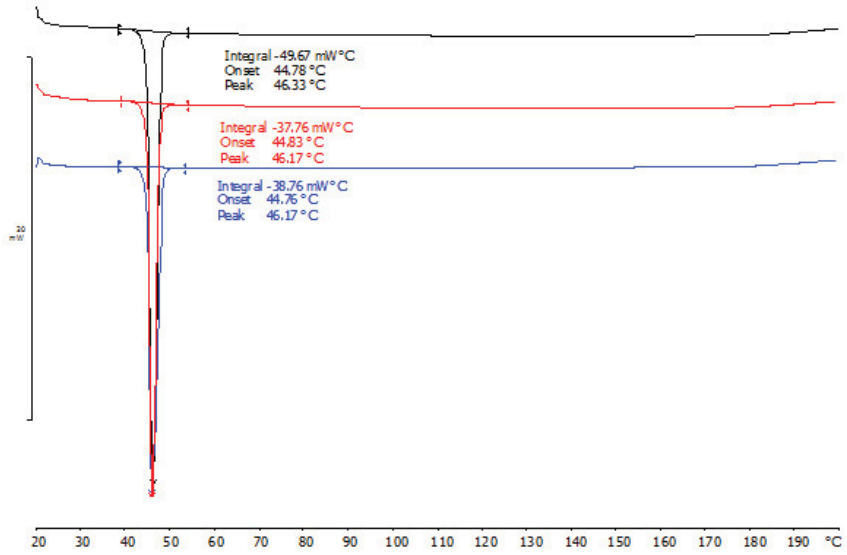

Figure 6.4: DSC diagram of THL for melting point determination.

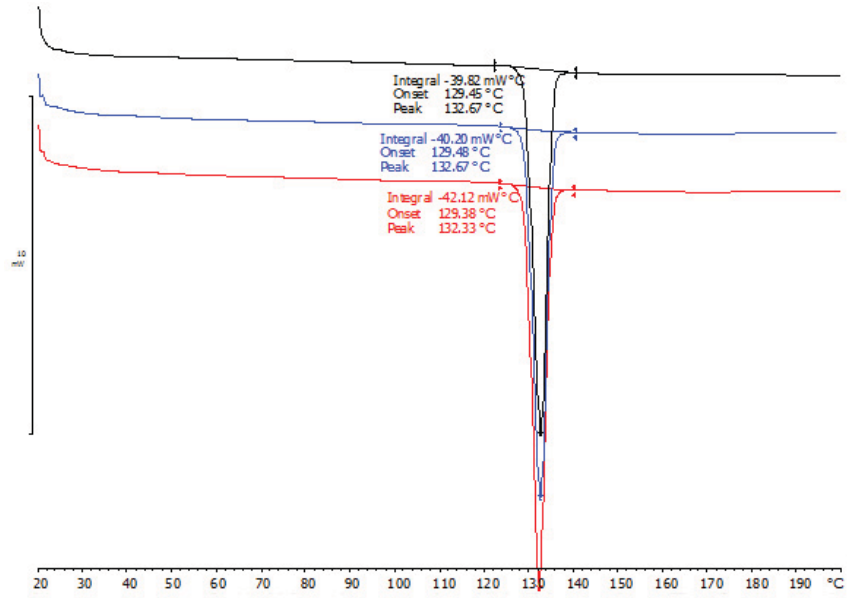

Figure 6.5: DSC diagram of NK1 for melting point determination.

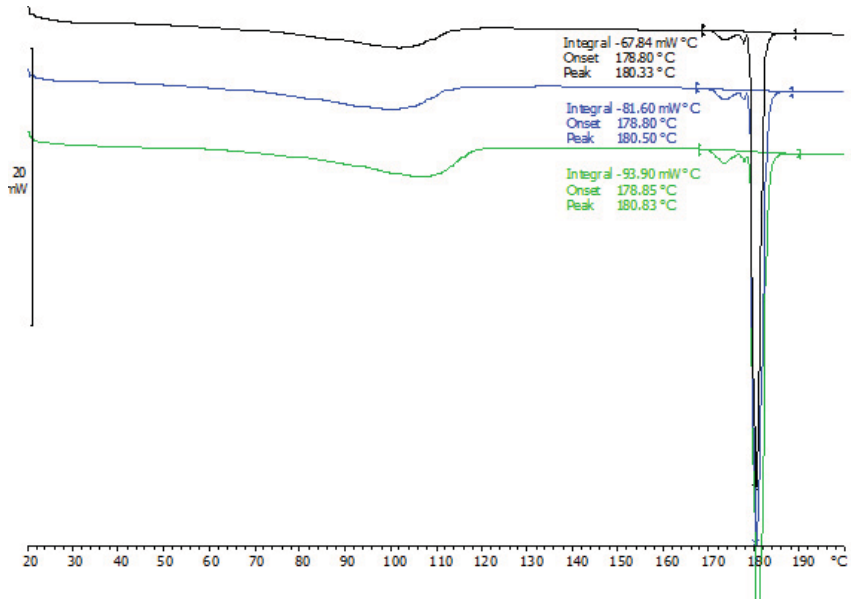

Figure 6.6: DSC diagram of MAO for melting point determination.

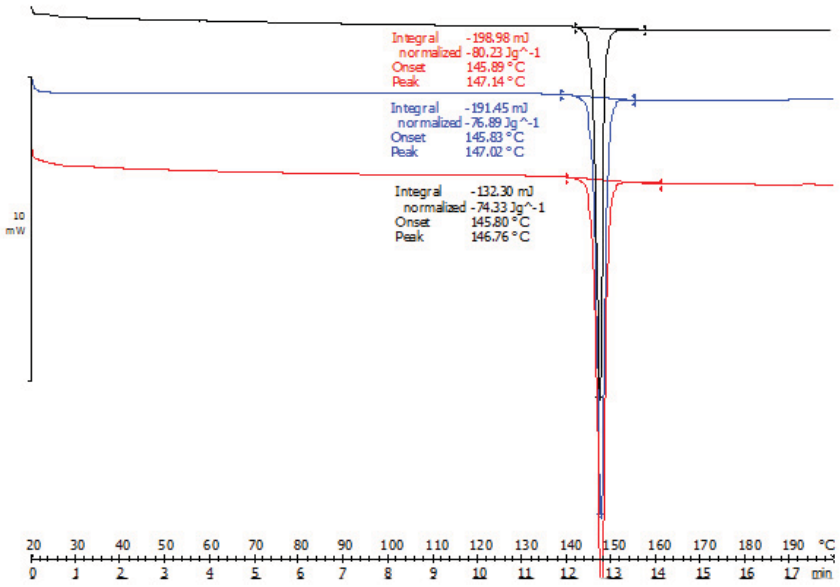

Figure 6.7: DSC diagram of CP2 for melting point determination.

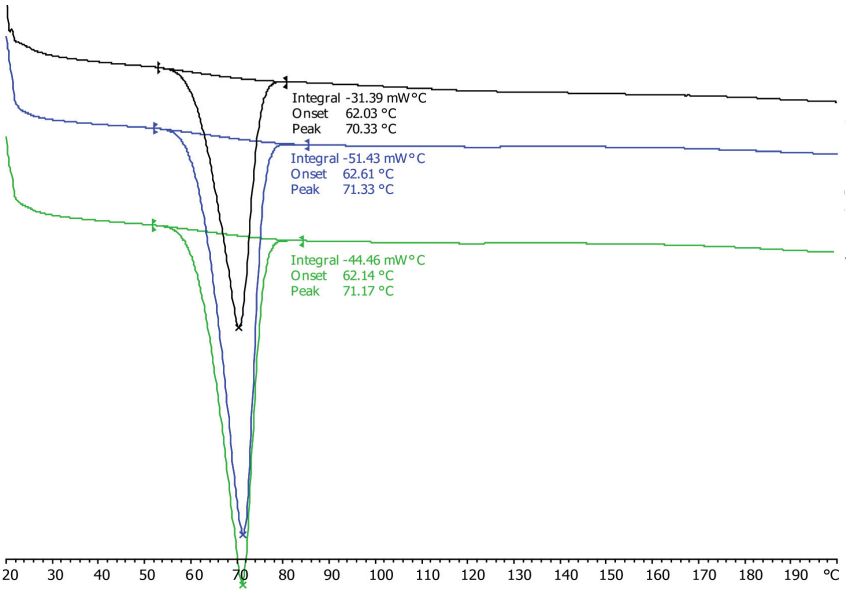

Figure 6.8: DSC diagram of DRX for melting point determination.

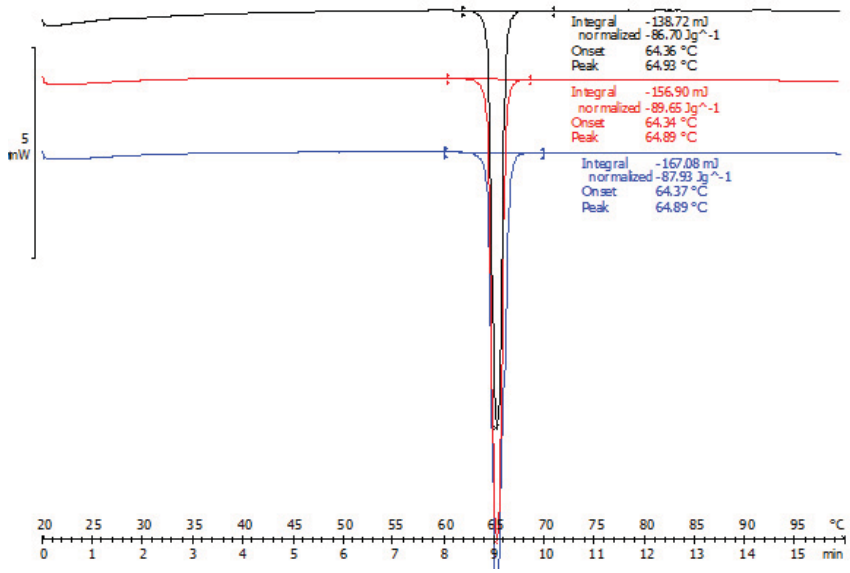

Figure 6.9: DSC diagram of DAL for melting point determination.

6.3 HPLC diagrams

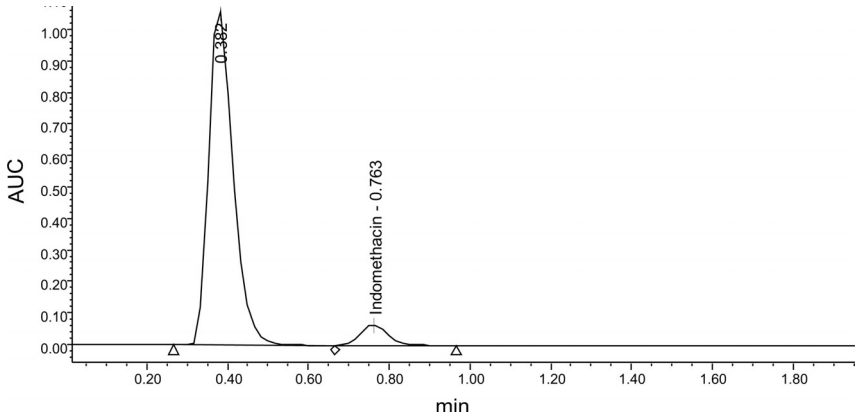

Figure 6.10: Exemplary HPLC diagram of IDM in mobile phase.

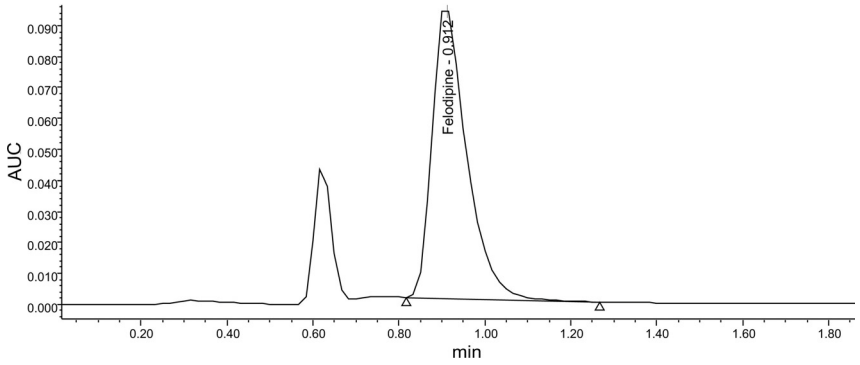

Figure 6.11: Exemplary HPLC diagram of FDP in mobile phase.

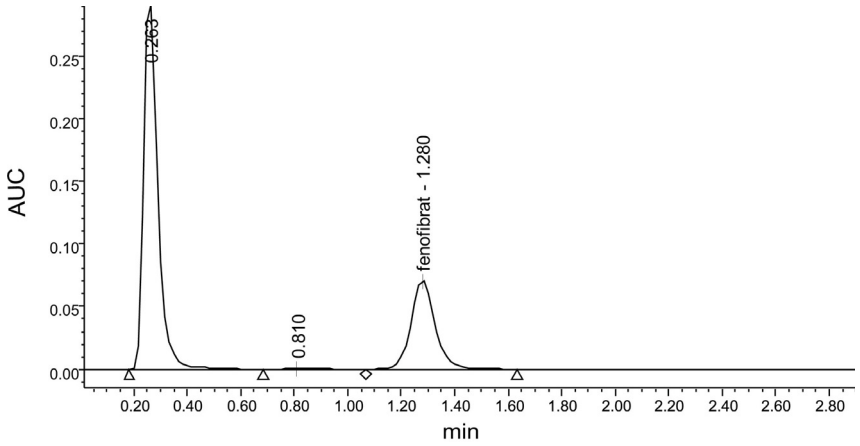

Figure 6.12: Exemplary HPLC diagram of FEN in mobile phase.

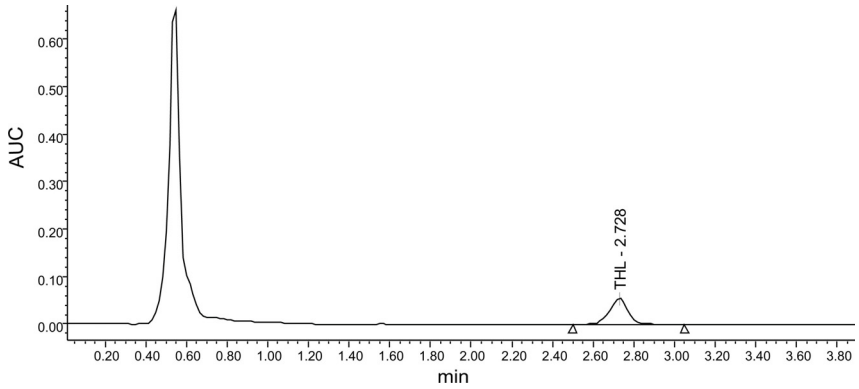

Figure 6.13: Exemplary HPLC diagram of THL in mobile phase.

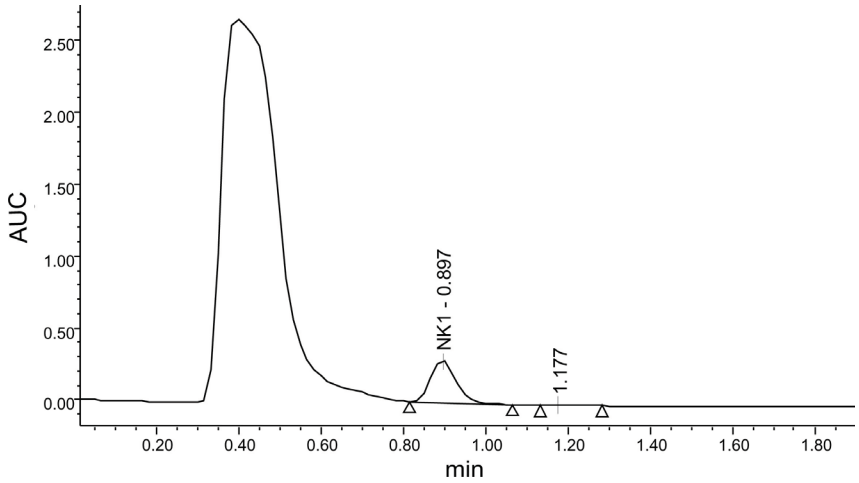

Figure 6.14: Exemplary HPLC diagram of NK1 in FaSSIF-V2.

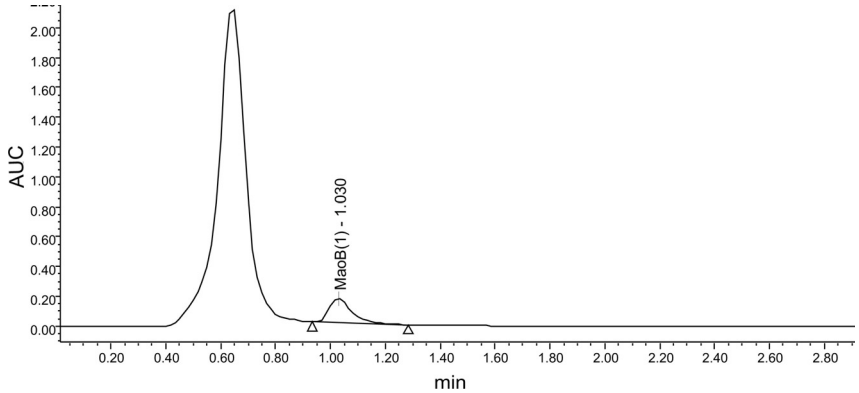

Figure 6.15: Exemplary HPLC diagram of MAO in FaSSIF-V2.

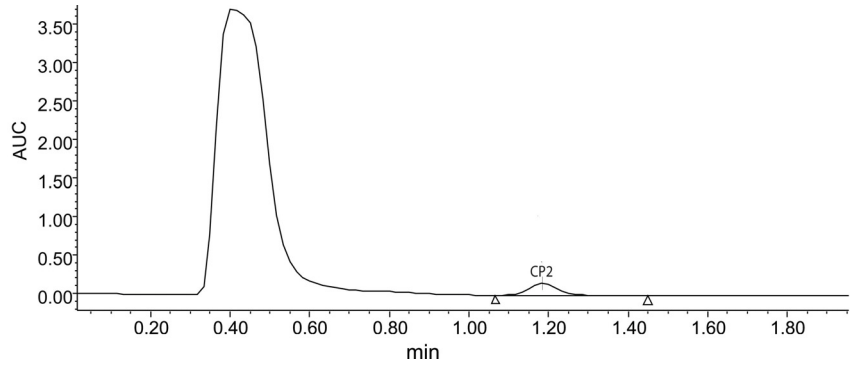

Figure 6.16: Exemplary HPLC diagram of CP2 in FaSSIF-V2.

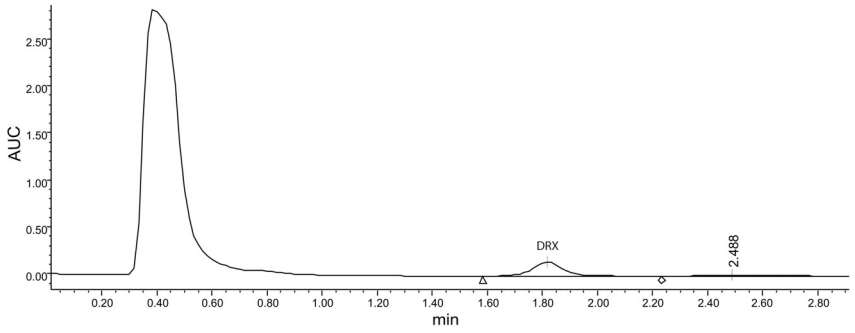

Figure 6.17: Exemplary HPLC diagram of DRX in FaSSIF-V2.

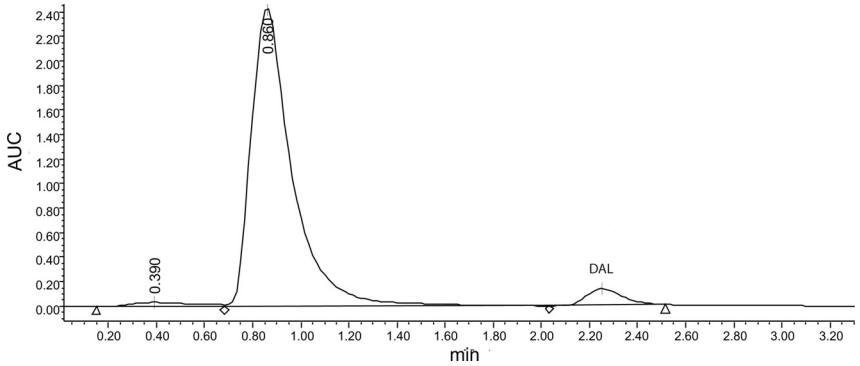

Figure 6.18: Exemplary HPLC diagram of DAL in FaSSIF-V2.

6.4 X-ray µ-CT images of MSB samples

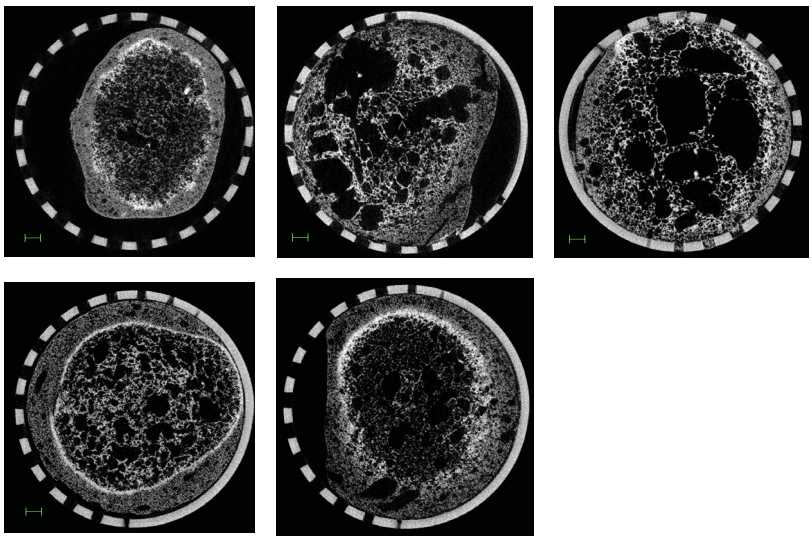

Figure 6.19: X-ray µ-CT images of DF with PWC 17% (N1 (top left), N5 (top middle), N7 (right), N9 (bottom left) and N13 (bottom middle). Scale indicated in green equals 1 mm.

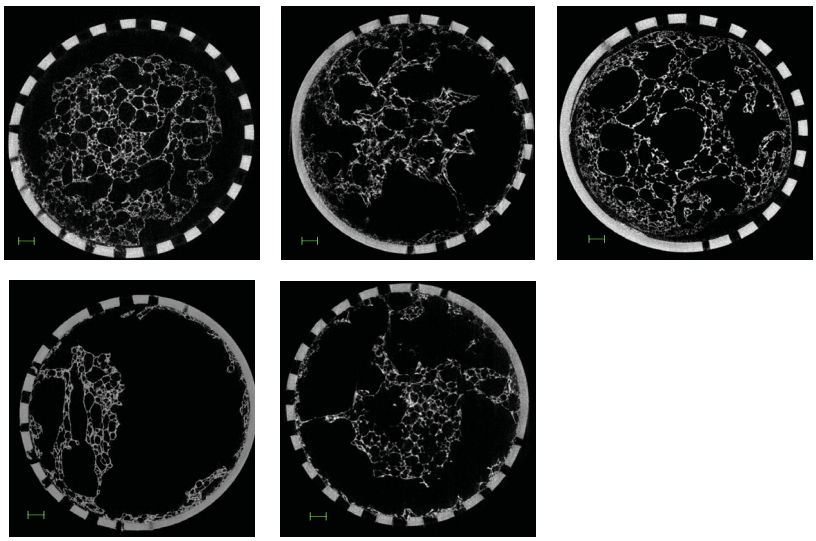

Figure 6.20: X-ray µ-CT images of DF with PWC 25% (N2 (top left), N6 (top middle), N8 (top right), N10 (bottom left) and N14 (bottom middle). Scale indicated in green equals 1 mm.

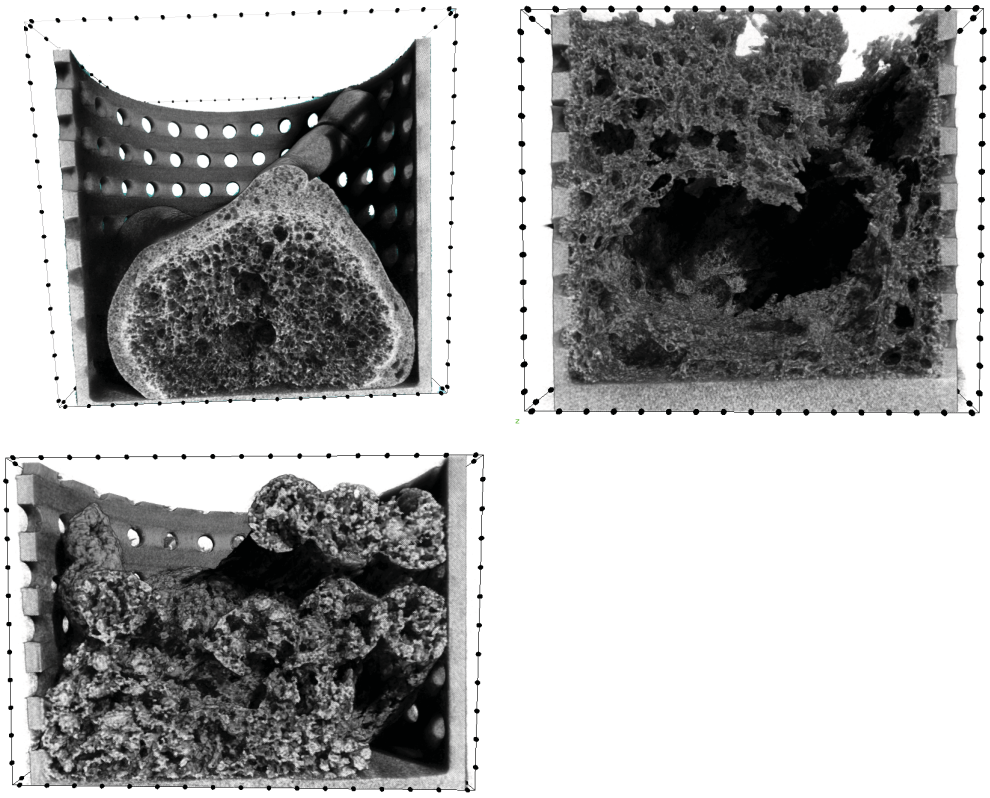

Figure 6.21: X-ray μ-CT images of DF prepared using MSB with M21D (top left), ISM (top right) and 50%MTL (bottom left) as filler.

6.5 Scanning electron microscopy images of dry foams

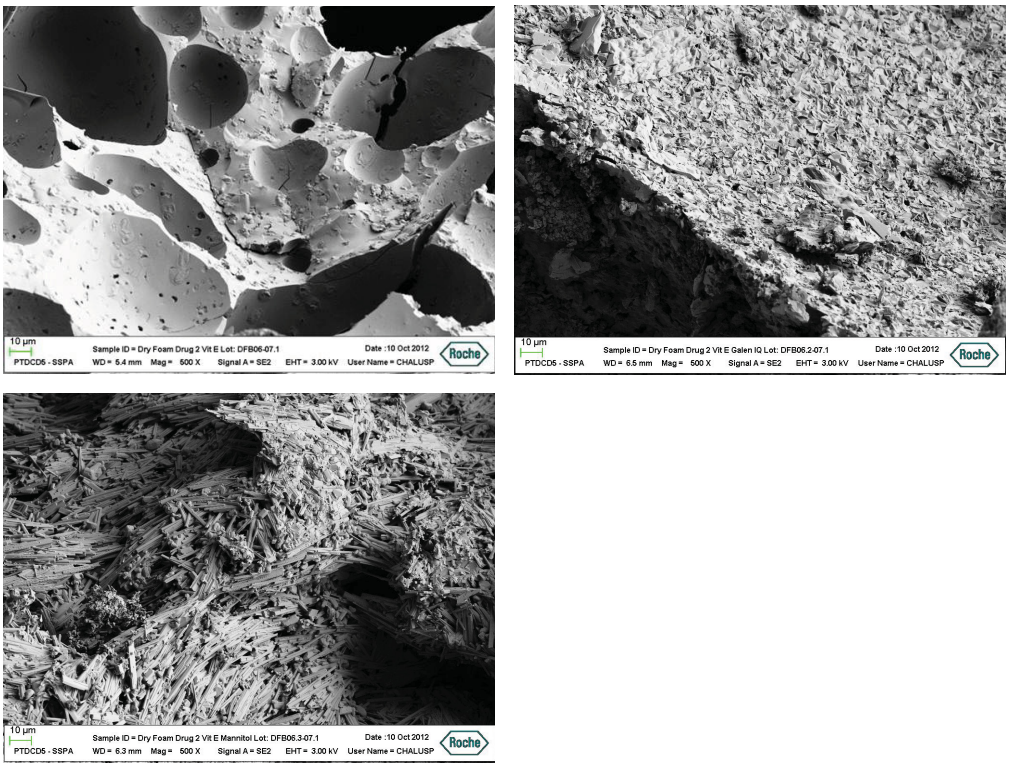

Figure 6.22: SEM images of DRX DFs using VitE as surfactant and M21D (top left), ISM (top right) or 50%MTL (bottom left) as filler.

6.6 Rheological measurements of paste

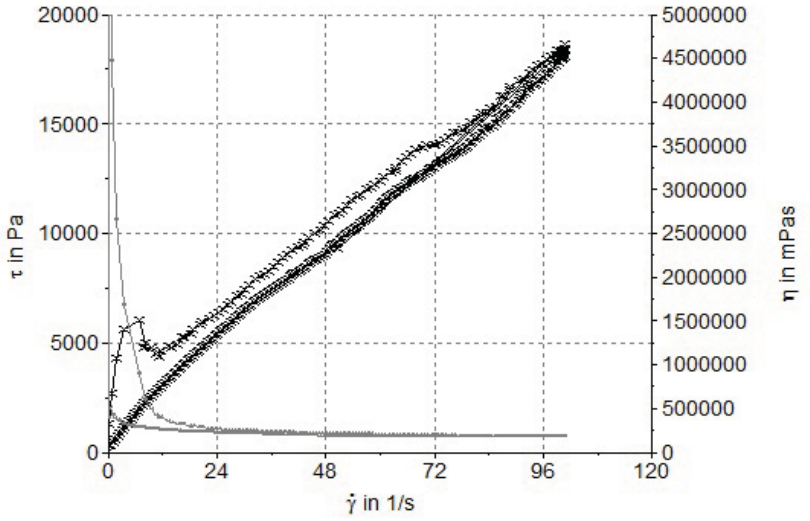

Figure 6.23: Exemplary rheological diagram, showing measured shear stress in black and apparent viscosity in grey, of DF M21D IDM VitE paste using a cone-plate geometry of 20 mm diameter up to a shear rate of 100 1/s.

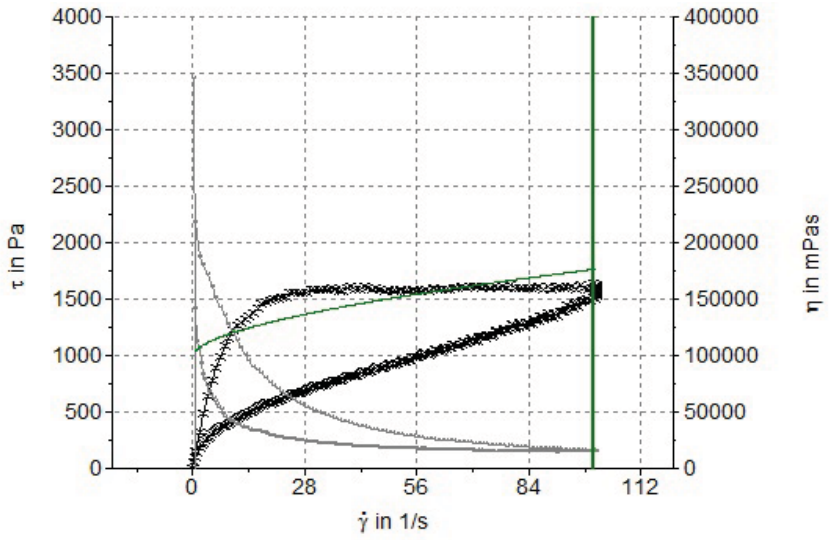

Figure 6.24: Exemplary rheological diagram, showing measured shear stress in black and apparent viscosity in grey, of DF ISM IDM VitE paste using a cone-plate geometry of 20 mm diameter up to a shear rate of 100 1/s.

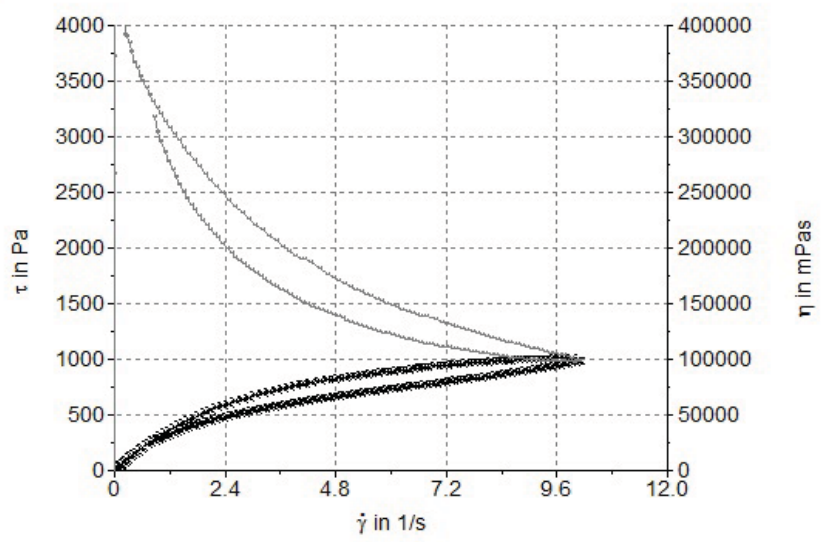

Figure 6.25: Exemplary rheological diagram, showing measured shear stress in black and apparent viscosity in grey, of DF ISM IDM VitE paste using a plate-plate geometry of 40 mm diameter up to a shear rate of 10 1/s.

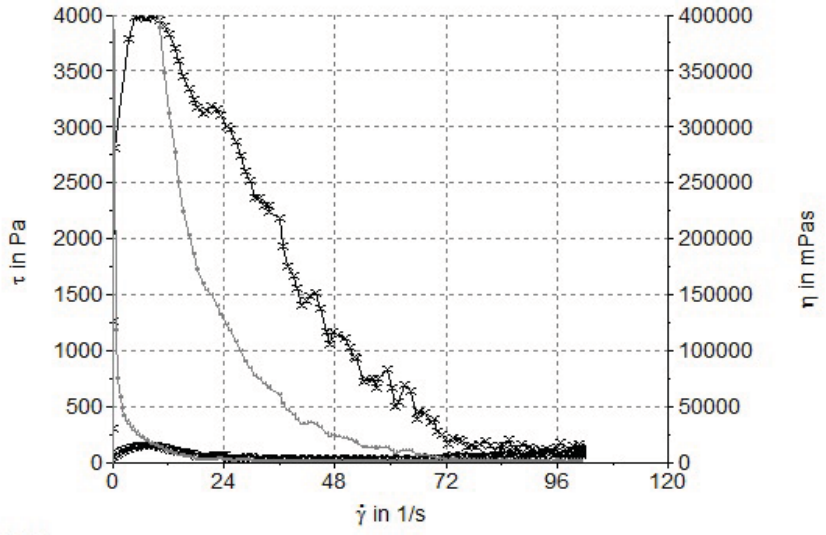

Figure 6.26: Exemplary rheological diagram, showing measured shear stress in black and apparent viscosity in grey, of DF 50%MTL IDM VitE paste using a cone-plate geometry of 20 mm diameter up to a shear rate of 100 1/s.

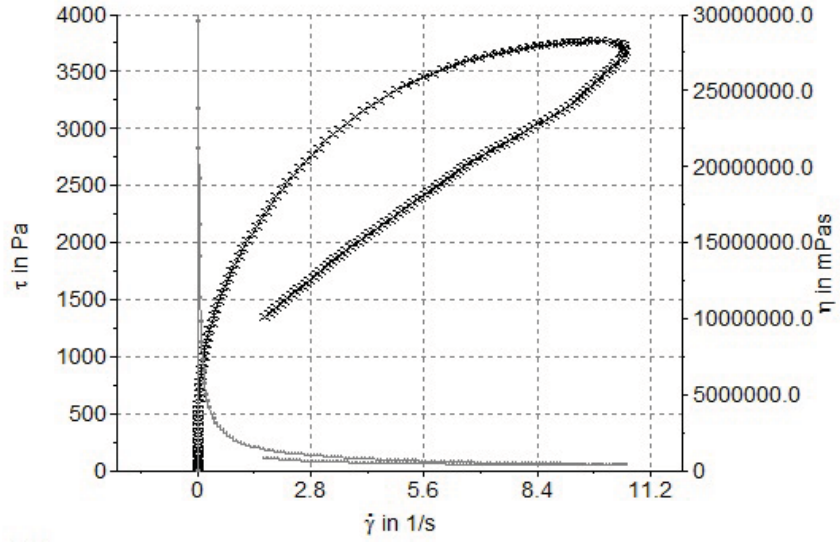

Figure 6.27: Exemplary rheological diagram, showing measured shear stress in black and apparent viscosity in grey, of DF 50%MTL IDM VitE paste using a plate-plate geometry of 40 mm diameter up to a shear rate of 10 1/s.

Table 6.3: Apparent viscosity [Pas] of dry foam paste at a shear rate of 10 1/s (η_{10}) or 100 1/s (η_{100}) respectively (part I).

API	filler	surfactant	η_{10}	η_{10}	η_{100}	η_{100}
IDM	M21D	DOSS	-	-	77.4	84.1
IDM	M21D	SDS	-	-	46.4	47.7
IDM	M21D	PS80	-	-	104.0	97.6
IDM	M21D	VitE	-	-	182.0	179.0
IDM	M21D	Myrj	-	-	132.0	135.0
IDM	M21D	PP103	-	-	144.0	149.0
IDM	ISM	DOSS	57.8	34.0	-	-
IDM	ISM	VitE	98.5	111.1	-	-
IDM	50%MTL	DOSS	86.1	88.0	-	-
IDM	50%MTL	VitE	364.9	267.1	-	-
FDP	M21D	DOSS	-	-	72.2	65.5
FDP	M21D	SDS	-	-	50.6	52.8
FDP	M21D	PS80	-	-	83.5	86.9
FDP	M21D	VitE	-	-	113.0	112.0
FDP	M21D	Myrj	-	-	111.0	108.0
FDP	M21D	PP103	-	-	131.0	134.0
FDP	ISM	DOSS	50.1	48.9	-	-
FDP	ISM	VitE	77.1	70.5	-	-
FDP	50%MTL	DOSS	116.0	128.0	-	-
FDP	50%MTL	VitE	350.0	361.0	-	-
FEN	M21D	DOSS	-	-	72.1	64.0
FEN	M21D	SDS	-	-	54.5	62.5
FEN	M21D	PS80	-	-	97.4	89.3
FEN	M21D	VitE	-	-	122.0	123.0
FEN	M21D	Myrj	-	-	113.0	116.0
FEN	M21D	PP103	-	-	119.0	117.0
FEN	ISM	DOSS	31.8	29.1	-	-
FEN	ISM	VitE	92.5	91.8	-	-
FEN	50%MTL	DOSS	170.0	167.0	-	-
FEN	50%MTL	VitE	345.0	497.0	-	-
THL	M21D	DOSS	-	-	117.0	95.6
THL	M21D	SDS	-	-	80.0	77.1
THL	M21D	PS80	-	-	80.7	81.2
THL	M21D	VitE	-	-	128.0	110.0
THL	M21D	Myrj	-	-	96.1	90.2
THL	M21D	PP103	-	-	128.0	132.0
THL	ISM	DOSS	65.9	63.0	-	-
THL	ISM	VitE	77.9	72.3	-	-
THL	50%MTL	DOSS	145.0	144.0	-	-
THL	50%MTL	VitE	251.0	258.0	-	-
NK1	M21D	DOSS	-	-	117.0	95.6
NK1	M21D	VitE	-	-	80.0	77.1
MAO	M21D	DOSS	-	-	80.7	81.2
MAO	M21D	VitE	-	-	128.0	110.0
CP2	M21D	DOSS	-	-	72.1	64.0
CP2	M21D	VitE	-	-	54.5	62.5
CP2	ISM	DOSS	-	-	97.4	89.3
CP2	ISM	VitE	-	-	122.0	123.0
CP2	50%MTL	DOSS	-	-	113.0	116.0
CP2	50%MTL	VitE	-	-	119.0	117.0

Table 6.4: Apparent viscosity [Pas] of dry foam paste at a shear rate of 10 1/s (η_{10}) or 100 1/s (η_{100}) respectively (part II).

API	filler	surfactant	η_{10}	η_{10}	η_{100}	η_{100}
DAL	M21D	DOSS	-	-	96.1	90.2
DAL	M21D	VitE	-	-	128.0	132.0
DAL	ISM	DOSS	65.9	63.0	-	-
DAL	ISM	VitE	77.9	72.3	-	-
DAL	50%MTL	DOSS	145.0	144.0	-	-
DAL	50%MTL	VitE	251.0	258.0	-	-
DRX	M21D	DOSS	31.8	29.1	-	-
DRX	M21D	VitE	92.5	91.8	-	-
DRX	ISM	DOSS	170.0	167.0	-	-
DRX	ISM	VitE	345.0	497.0	-	-
DRX	50%MTL	DOSS	-	-	72.2	65.5
DRX	50%MTL	VitE	-	-	50.6	52.8

6.7 Granule characteristics

6.7.1 Sieve analysis

Table 6.5: Amount [%] sieve analysis fractions [µm] of IDM granules.

batch	<90	90-125	125-180	180-250	250-355	355-500	500-710	710-1000	>1000
M21D DOSS	7.0	5.6	9.6	10.8	16.4	22.6	20.2	6.8	1.0
M21D SDS	34.7	15.3	16.4	10.5	9.5	7.6	4.2	1.6	0.3
M21D PS80	1.5	6.2	10.0	16.4	27.5	25.9	10.0	2.1	0.4
M21D VitE	9.2	9.1	18.7	21.4	23.1	12.5	4.6	1.3	0.1
M21D Myrj	4.1	5.6	9.9	15.3	27.0	25.5	10.0	2.3	0.4
M21D PP103	1.0	3.8	7.4	11.6	19.7	26.7	21.3	7.4	1.2
ISM DOSS	5.7	7.0	15.2	17.4	23.4	21.4	8.4	1.1	0.5
ISM VitE	2.1	13.0	9.7	12.5	17.1	18.0	16.0	9.0	2.6
50%MTL DOSS	3.1	2.6	5.3	7.5	13.4	22.4	26.0	17.2	2.6
50%MTL VitE	0.7	10.8	17.1	19.9	15.8	14.3	11.8	7.0	2.6
FBG DOSS	1.7	2.2	6.2	11.7	23.2	37.8	16.8	0.3	0.2
FBG SDS	2.4	3.6	13.6	24.7	32.6	19.6	3.0	0.3	0.2
FBG PS80	2.7	5.6	20.7	38.2	26.2	6.0	0.5	0.1	0.2
FBG VitE	5.5	6.2	21.6	26.4	25.9	12.1	2.3	0.0	0.0
FBG Myrj	3.8	5.5	25.5	43.1	19.3	2.4	0.2	0.1	0.1
FBG PP103	4.9	6.5	14.8	20.3	23.3	20.1	8.6	1.4	0.0

Table 6.6: Amount [%] sieve analysis fractions [µm] of FDP granules.

batch	<90	90-125	125-180	180-250	250-355	355-500	500-710	710-1000	>1000
M21D DOSS	7.8	6.4	9.9	11.2	16.2	22.4	18.5	6.7	1.0
M21D SDS	27.3	15.3	16.7	13.1	11.6	8.9	4.8	1.7	0.7
M21D PS80	2.2	3.7	8.1	14.3	25.9	30.6	12.7	2.1	0.4
M21D VitE	5.5	6.1	11.7	15.1	22.4	23.3	12.1	3.0	0.7
M21D Myrj	2.8	3.7	9.5	13.9	22.4	26.1	16.1	4.8	0.7
M21D PP103	1.5	4.9	8.3	12.0	19.4	25.3	19.1	7.7	1.8
ISM DOSS	7.3	7.7	16.0	18.8	22.0	19.4	7.3	1.4	0.2
ISM VitE	7.5	7.5	10.2	10.8	14.5	17.7	15.2	11.7	4.8
50%MTL DOSS	5.7	4.1	8.0	10.7	16.5	23.6	20.1	9.7	1.5
50%MTL VitE	7.5	10.3	18.9	10.3	12.3	13.7	11.8	9.5	5.7
FBG DOSS	1.6	2.7	6.7	12.9	24.1	30.2	20.2	1.3	0.3
FBG SDS	2.7	4.0	10.3	20.3	29.7	21.7	9.9	1.1	0.3
FBG PS80	0.7	4.9	11.1	25.3	32.5	16.4	7.1	1.5	0.4
FBG VitE	4.4	6.1	12.3	22.5	27.4	18.8	7.4	0.8	0.3
FBG Myrj	4.4	6.5	15.6	25.8	26.7	14.9	4.9	0.8	0.3
FBG PP103	2.9	6.5	13.6	23.9	26.3	17.5	7.5	1.5	0.3

Table 6.7: Amount [%] sieve analysis fractions [µm] of FEN granules.

batch	<90	90-125	125-180	180-250	250-355	355-500	500-710	710-1000	>1000
M21D DOSS	6.4	5.4	9.8	11.3	17.1	21.2	18.2	8.7	1.9
M21D SDS	13.0	9.8	11.0	13.4	18.9	18.3	12.5	2.4	0.6
M21D PS80	3.0	5.8	9.3	14.7	22.5	20.9	16.0	6.2	1.7
M21D VitE	6.2	6.3	11.4	18.0	29.9	19.1	7.3	1.4	0.4
M21D Myrj	4.2	4.6	8.7	17.8	31.7	22.5	8.8	1.3	0.3
M21D PP103	2.5	4.6	21.3	36.5	32.8	1.8	0.2	0.2	0.0
ISM DOSS	6.1	7.2	14.8	17.2	21.9	21.2	9.4	2.0	0.2
ISM VitE	8.3	6.4	8.6	10.6	15.5	16.8	18.5	11.1	4.2
50%MTL DOSS	3.0	3.7	8.2	11.9	17.0	22.3	28.0	5.2	0.6
50%MTL VitE	5.3	14.4	19.1	11.5	12.2	12.9	11.3	8.1	5.2
FBG DOSS	2.2	2.7	6.4	11.6	27.2	41.1	8.4	0.4	0.1
FBG SDS	5.9	7.2	22.2	20.0	21.8	15.9	5.1	1.4	0.3
FBG PS80	3.7	7.0	17.4	20.5	24.9	20.4	5.3	0.5	0.1
FBG VitE	6.7	8.2	18.3	20.9	21.7	16.5	6.1	1.4	0.2
FBG Myrj	6.9	9.6	25.1	25.4	20.6	9.2	2.3	0.6	0.2
FBG PP103	2.3	7.6	18.9	23.7	20.6	17.2	7.6	1.8	0.3

Table 6.8: Amount [%] of sieve analysis fractions [µm] of THL granules.

batch	<90	90-125	125-180	180-250	250-355	355-500	500-710	710-1000	>1000
M21D DOSS	1.6	4.0	12.1	16.7	23.1	21.8	15.3	4.5	0.8
M21D SDS	14.2	13.0	15.3	14.2	16.4	13.5	9.6	3.0	0.7
M21D PS80	2.6	4.4	7.4	10.3	20.7	27.9	21.7	4.4	0.7
M21D VitE	3.8	9.2	14.2	17.9	25.7	18.2	8.1	2.3	0.6
M21D Myrj	5.6	6.5	11.0	16.5	26.1	20.9	10.5	2.3	0.5
M21D PP103	3.4	5.2	9.0	14.5	22.0	23.1	17.5	4.8	0.6
ISM DOSS	5.2	5.9	12.4	14.9	20.5	22.2	14.5	3.9	0.4
ISM VitE	6.4	12.5	12.6	14.4	17.9	15.6	12.8	5.6	2.1
50%MTL DOSS	5.0	5.4	10.5	13.2	19.8	22.5	16.2	6.2	1.1
50%MTL VitE	8.5	12.8	10.4	10.6	12.9	12.5	14.6	10.3	7.2
FBG DOSS	2.3	3.3	8.1	16.7	32.5	29.0	7.8	0.3	0.0
FBG SDS	3.2	4.6	13.1	20.1	29.4	24.1	5.3	0.2	0.0
FBG PS80	1.7	3.7	16.8	20.7	24.6	20.4	10.3	1.7	0.0
FBG VitE	0.7	3.4	9.9	19.7	33.0	23.2	8.8	1.3	0.1
FBG Myrj	1.7	5.5	15.3	24.4	26.8	18.7	6.6	0.7	0.2
FBG PP103	1.2	4.7	11.0	22.0	32.6	20.6	7.1	0.8	0.0

Table 6.9: Amount [%] sieve analysis fractions [µm] of NK1 granules.

batch	<90	90-125	125-180	180-250	250-355	355-500	500-710	710-1000	>1000
M21D DOSS	5.7	5.1	7.6	11.1	18.0	21.1	21.7	8.3	1.3
M21D VitE	5.2	6.5	9.7	13.9	22.2	21.2	15.3	4.7	1.3
FBG DOSS	2.3	2.9	8.3	14.8	32.7	34.4	4.0	0.3	0.3
FBG VitE	5.5	6.0	21.6	33.0	26.1	7.1	0.4	0.1	0.2

Table 6.10: Amount [%] sieve analysis fractions [µm] of MAO granules.

batch	<90	90-125	125-180	180-250	250-355	355-500	500-710	710-1000	>1000
M21D DOSS	6.0	6.1	8.8	10.3	17.4	18.4	20.0	10.1	2.9
M21D VitE	16.4	11.8	13.4	14.6	17.7	13.9	8.6	2.7	0.8
FBG DOSS	2.8	3.9	9.8	20.2	31.2	21.9	8.9	1.1	0.1
FBG VitE	5.4	5.9	21.7	33.1	26.1	6.8	0.8	0.1	0.1

Table 6.11: Amount [%] sieve analysis fractions [µm] of CP2 granules.

batch	<90	90-125	125-180	180-250	250-355	355-500	500-710	710-1000	>1000
M21D DOSS	5.9	6.1	10.2	12.8	17.5	19.1	16.5	8.6	3.3
M21D VitE	10.2	10.8	14.1	17.5	20.5	14.1	7.5	3.4	1.9
ISM DOSS	10.0	8.0	14.0	14.4	17.8	16.7	11.5	5.4	2.2
ISM VitE	6.5	8.7	10.5	10.9	13.3	15.5	15.4	12.3	6.8
50%MTL DOSS	4.3	4.6	6.8	9.0	14.0	17.6	20.4	16.8	6.4
50%MTL VitE	2.9	7.4	13.9	17.2	14.6	14.2	13.2	10.3	6.2
FBG DOSS	3.4	3.5	4.3	9.1	21.3	38.7	16.7	1.9	1.0
FBG VitE	5.0	7.4	16.6	21.0	26.3	16.9	4.4	1.4	1.0

Table 6.12: Amount [%] sieve analysis fractions [µm] of DAL granules.

batch	<90	90-125	125-180	180-250	250-355	355-500	500-710	710-1000	>1000
M21D DOSS	8.5	4.3	7.7	10.1	18.7	27.6	19.8	5.7	0.6
M21D VitE	9.3	8.8	14.5	15.0	18.9	17.6	9.9	4.6	1.4
ISM DOSS	5.7	6.3	12.4	14.3	20.8	23.3	14.5	2.4	0.2
ISM VitE	9.1	7.1	10.5	11.4	15.6	18.3	17.2	4.6	6.4
50%MTL DOSS	3.4	4.5	9.8	12.3	18.8	22.9	20.8	6.9	0.6
50%MTL VitE	5.8	15.9	11.7	10.2	12.9	13.7	13.2	10.8	5.8
FBG DOSS	0.3	2.8	10.4	10.9	16.2	27.9	24.9	6.0	0.6
FBG VitE	4.3	5.9	15.7	21.5	29.4	20.1	2.8	0.2	0.1

Table 6.13: Amount [%] sieve analysis fractions [µm] of DRX granules.

batch	<90	90-125	125-180	180-250	250-355	355-500	500-710	710-1000	>1000
M21D DOSS	4.3	6.7	8.8	10.7	16.4	20.6	20.5	9.6	2.4
M21D VitE	3.0	14.2	20.0	23.0	22.1	11.8	4.4	1.2	0.3
ISM DOSS	3.0	5.1	11.4	18.0	24.7	24.5	10.7	2.0	0.5
ISM VitE	2.1	4.8	7.6	10.3	15.8	19.3	20.8	13.8	5.6
50%MTL DOSS	1.7	2.2	4.9	8.9	17.0	27.0	27.3	9.5	1.5
50%MTL VitE	5.9	5.9	9.2	10.0	12.8	14.7	17.2	14.8	9.6
FBG DOSS	3.0	3.4	7.8	12.1	24.6	35.5	13.0	0.6	0.0
FBG VitE	4.1	6.6	20.2	24.4	23.4	15.7	5.2	0.4	0.0

6.7.2 Bulk density, tapped density and loss on drying of granules

Table 6.14: Bulk density (ρ_{bulk} [g/ml]), tapped density (ρ_{tapped} [g/ml]), Hausner factor (HF) and loss on drying (LOD [m/m %]) of IDM granules.

batch	ρ_{bulk}	ρ_{tapped}	HF	LOD
M21D DOSS	0.6	0.7	1.3	3.6
M21D SDS	0.5	0.7	1.4	4.1
M21D PS80	0.5	0.6	1.3	2.9
M21D VitE	0.5	0.6	1.4	2.6
M21D Myrj	0.5	0.6	1.2	2.3
M21D PP103	0.5	0.7	1.3	3.2
ISM DOSS	0.4	0.5	1.3	1.1
ISM VitE	0.6	0.7	1.2	2.6
50%MTL DOSS	0.5	0.7	1.2	1.7
50%MTL VitE	0.5	0.7	1.3	0.9
FBG DOSS	0.4	0.5	1.2	1.1
FBG SDS	0.4	0.5	1.2	1.3
FBG PS80	0.4	0.6	1.2	1.3
FBG VitE	0.5	0.6	1.3	1.4
FBG Myrj	0.4	0.6	1.3	1.3
FBG PP103	0.5	0.6	1.3	1.3

Table 6.15: Bulk density (ρ_{bulk} [g/ml]), tapped density (ρ_{tapped} [g/ml]), Hausner factor (HF) and loss on drying (LOD [m/m %]) of FDP granules.

batch	ρ_{bulk}	ρ_{tapped}	HF	LOD
M21D DOSS	0.5	0.7	1.4	4.1
M21D SDS	0.5	0.7	1.4	3.9
M21D PS80	0.5	0.6	1.3	3.4
M21D VitE	0.4	0.6	1.3	4.0
M21D Myrj	0.5	0.7	1.3	3.4
M21D PP103	0.5	0.7	1.3	3.5
ISM DOSS	0.4	0.6	1.3	2.1
ISM VitE	0.6	0.8	1.3	1.3
50%MTL DOSS	0.5	0.7	1.3	2.3
50%MTL VitE	0.5	0.7	1.3	2.3
FBG DOSS	0.4	0.5	1.3	1.1
FBG SDS	0.4	0.5	1.2	1.1
FBG PS80	0.5	0.6	1.2	2.4
FBG VitE	0.5	0.6	1.2	0.8
FBG Myrj	0.5	0.6	1.3	1.2
FBG PP103	0.5	0.6	1.2	2.3

Table 6.16: Bulk density (ρ_{bulk} [g/ml]), tapped density (ρ_{tapped} [g/ml]), Hausner factor (HF) and loss on drying (LOD [m/m %]) of FEN granules.

batch	ρ_{bulk}	ρ_{tapped}	HF	LOD
M21D DOSS	0.6	0.7	1.3	6.1
M21D SDS	0.5	0.7	1.3	3.9
M21D PS80	0.5	0.7	1.3	5.0
M21D VitE	0.5	0.6	1.3	4.0
M21D Myrj	0.5	0.6	1.3	3.6
M21D PP103	0.5	0.7	1.3	5.0
ISM DOSS	0.5	0.6	1.3	2.1
ISM VitE	0.6	0.7	1.3	1.8
50%MTL DOSS	0.4	0.5	1.2	1.9
50%MTL VitE	0.5	0.7	1.3	1.5
FBG DOSS	0.5	0.5	1.2	1.2
FBG SDS	0.5	0.6	1.2	3.2
FBG PS80	0.5	0.6	1.2	1.2
FBG VitE	0.5	0.6	1.2	2.5
FBG Myrj	0.5	0.6	1.3	1.8
FBG PP103	0.5	0.6	1.2	2.3

Table 6.17: Bulk density (ρ_{bulk} [g/ml]), tapped density (ρ_{tapped} [g/ml]), Hausner factor (HF) and loss on drying (LOD [m/m %]) of THL granules.

batch	ρ_{bulk}	ρ_{tapped}	HF	LOD
M21D DOSS	0.5	0.6	1.3	4.9
M21D SDS	0.4	0.6	1.4	4.7
M21D PS80	0.5	0.6	1.2	3.7
M21D VitE	0.4	0.6	1.3	3.7
M21D Myrj	0.5	0.6	1.2	4.2
M21D PP103	0.5	0.6	1.3	4.4
ISM DOSS	0.4	0.5	1.3	2.0
ISM VitE	0.5	0.6	1.3	1.6
50%MTL DOSS	0.5	0.6	1.3	2.5
50%MTL VitE	0.5	0.6	1.2	1.6
FBG DOSS	0.4	0.5	1.2	2.5
FBG SDS	0.4	0.5	1.2	2.4
FBG PS80	0.4	0.5	1.2	2.8
FBG VitE	0.5	0.5	1.2	3.4
FBG Myrj	0.4	0.5	1.2	2.5
FBG PP103	0.5	0.5	1.2	2.8

Table 6.18: Bulk density (ρ_{bulk} [g/ml]), tapped density (ρ_{tapped} [g/ml]), Hausner factor (HF) and loss on drying (LOD [m/m %]) of NK1 granules.

batch	ρ_{bulk}	ρ_{tapped}	HF	LOD
M21D DOSS	0.5	0.7	1.3	3.4
M21D VitE	0.5	0.6	1.3	3.8
FBG DOSS	0.4	0.6	1.3	2.0
FBG VitE	0.4	0.6	1.3	1.0

Table 6.19: Bulk density (ρ_{bulk} [g/ml]), tapped density (ρ_{tapped} [g/ml]), Hausner factor (HF) and loss on drying (LOD [m/m %]) of MAO granules.

batch	ρ_{bulk}	ρ_{tapped}	HF	LOD
M21D DOSS	0.6	0.7	1.3	4.2
M21D VitE	0.4	0.6	1.3	2.3
FBG DOSS	0.4	0.5	1.3	1.3
FBG VitE	0.4	0.5	1.2	1.3

Table 6.20: Bulk density (ρ_{bulk} [g/ml]), tapped density (ρ_{tapped} [g/ml]), Hausner factor (HF) and loss on drying (LOD [m/m %]) of CP2 granules.

batch	ρ_{bulk}	ρ_{tapped}	HF	LOD
M21D DOSS	0.6	0.7	1.3	4.2
M21D VitE	0.5	0.6	1.3	3.2
ISM DOSS	0.5	0.6	1.3	2.3
ISM VitE	0.6	0.7	1.3	1.7
50%MTL DOSS	0.4	0.5	1.3	1.8
50%MTL VitE	0.5	0.7	1.4	1.2
FBG DOSS	0.5	0.6	1.3	1.9
FBG VitE	0.5	0.6	1.3	1.3

Table 6.21: Bulk density (ρ_{bulk} [g/ml]), tapped density (ρ_{tapped} [g/ml]), Hausner factor (HF) and loss on drying (LOD [m/m %]) of DAL granules.

batch	ρ_{bulk}	ρ_{tapped}	HF	LOD
M21D DOSS	0.5	0.7	1.2	4.6
M21D VitE	0.5	0.6	1.3	3.9
ISM DOSS	0.4	0.5	1.2	1.9
ISM VitE	0.5	0.8	1.5	1.5
50%MTL DOSS	0.4	0.5	1.2	0.7
50%MTL VitE	0.5	0.7	1.3	0.8
FBG DOSS	0.5	0.7	1.3	4.9
FBG VitE	0.5	0.6	1.2	1.3

Table 6.22: Bulk density (ρ_{bulk} [g/ml]), tapped density (ρ_{tapped} [g/ml]), Hausner factor (HF) and loss on drying (LOD [m/m %]) of DRX granules.

batch	ρ_{bulk}	ρ_{tapped}	HF	LOD
M21D DOSS	0.6	0.7	1.2	4.2
M21D VitE	0.4	0.6	1.3	3.0
ISM DOSS	0.4	0.5	1.3	2.0
ISM VitE	0.5	0.6	1.2	1.4
50%MTL DOSS	0.4	0.6	1.2	1.1
50%MTL VitE	0.5	0.6	1.3	1.3
FBG DOSS	0.4	0.5	1.2	1.9
FBG VitE	0.5	0.6	1.3	1.6

6.8 Dissolution analysis data

Table 6.23: Dissolved IDM [%] of applied dose (50 mg) in FaSSIF-V2 at time points [min].

batch	5	10	15	20	30	45	60	90	120	180	240
M21D DOSS	23.2	42.0	58.4	72.1	91.3	101.6	102.1	102.0	102.3	101.8	101.5
M21D DOSS	22.8	40.6	55.5	67.7	86.4	100.3	101.8	101.5	101.5	101.4	101.0
M21D DOSS	26.3	46.6	62.7	74.6	92.2	102.6	102.8	102.7	102.7	103.1	102.1
M21D SDS	39.0	63.1	80.2	91.5	99.6	99.5	99.3	99.3	99.4	99.4	99.0
M21D SDS	34.8	58.8	77.5	89.7	99.4	99.5	99.6	99.5	99.4	99.4	99.3
M21D SDS	36.0	60.5	77.5	88.6	98.8	99.8	99.8	99.9	99.2	99.3	99.1
M21D PS80	27.4	49.7	67.4	81.2	98.0	101.2	101.3	101.8	101.3	101.2	101.1
M21D PS80	29.6	51.6	69.2	82.1	97.4	101.9	101.9	101.4	101.1	101.6	101.4
M21D PS80	28.4	49.6	68.6	82.4	98.3	101.4	101.7	101.9	101.3	101.3	101.4
M21D VitE	29.6	52.2	70.7	85.8	99.6	105.0	104.9	105.0	104.6	104.3	104.0
M21D VitE	28.4	49.3	66.9	80.2	96.4	102.3	102.6	102.9	102.7	102.6	102.3
M21D VitE	29.8	52.4	69.8	83.1	98.3	104.1	104.4	104.3	104.6	104.0	103.8
M21D Myrj	25.3	46.2	62.9	75.3	91.7	99.7	100.0	100.3	100.4	100.2	99.8
M21D Myrj	26.0	46.1	62.8	76.5	92.5	100.2	100.6	101.1	100.6	101.0	100.4
M21D Myrj	25.9	46.6	63.0	75.7	91.4	99.2	99.9	100.2	100.6	100.4	99.9
M21D P103	23.1	41.5	56.4	68.8	85.2	98.6	99.0	98.9	98.7	98.7	98.4
M21D P103	24.4	46.5	64.3	77.9	94.8	97.9	98.0	98.8	97.5	98.4	97.6
M21D P103	22.8	40.4	56.0	68.2	85.1	98.0	98.9	99.1	99.3	98.7	99.0
ISM DOSS	41.9	73.3	92.7	100.0	102.3	102.9	102.8	102.8	103.2	102.9	103.4
ISM DOSS	44.4	72.7	93.4	102.2	102.0	103.2	103.2	103.1	103.4	103.2	103.3
ISM DOSS	49.8	80.3	97.2	100.8	101.0	101.9	101.8	101.8	101.9	102.1	101.6
ISM VitE	62.7	89.0	99.9	100.3	101.0	101.2	101.9	101.1	100.9	100.7	100.6
ISM VitE	66.7	96.4	101.3	101.8	102.3	102.5	102.7	102.5	102.9	101.9	101.9
ISM VitE	66.1	95.8	100.3	101.1	101.3	101.5	101.7	101.1	101.1	100.8	100.5
50%MTL DOSS	45.3	68.9	82.7	92.1	99.6	100.5	100.6	100.7	100.8	100.5	100.7
50%MTL DOSS	48.7	75.5	87.6	95.1	100.6	101.6	101.7	101.8	102.0	101.5	101.5
50%MTL DOSS	51.3	78.2	93.1	100.2	101.1	101.9	102.1	102.1	102.2	102.0	101.9
50%MTL VitE	52.9	83.8	100.2	103.5	103.7	103.6	103.7	103.3	103.3	103.2	103.1
50%MTL VitE	57.6	90.0	101.7	102.3	102.8	103.1	103.1	103.0	103.0	102.7	102.1
50%MTL VitE	55.6	87.2	101.3	102.4	102.6	103.0	102.4	102.2	102.4	102.2	101.8
FBG DOSS	85.9	97.8	98.2	98.4	98.5	98.3	98.4	98.2	99.0	98.0	98.1
FBG DOSS	66.0	99.1	99.2	99.4	101.1	99.4	99.5	99.3	99.5	99.2	99.2
FBG DOSS	55.6	95.3	96.7	96.9	96.8	96.6	96.7	96.6	97.4	96.5	96.5
FBG SDS	53.0	90.7	101.5	100.7	100.9	100.5	100.5	100.7	101.3	100.7	100.5
FBG SDS	65.8	98.3	99.8	99.7	99.6	99.6	99.6	99.5	99.5	99.4	99.0
FBG SDS	60.0	101.3	101.6	102.3	101.9	101.6	101.5	102.2	101.4	101.6	101.2
FBG PS80	57.9	102.1	103.5	103.5	103.4	103.9	103.6	103.8	103.4	103.4	103.3
FBG PS80	66.7	101.8	102.5	102.7	102.2	102.2	102.2	102.3	102.2	102.3	101.8
FBG PS80	72.5	99.5	102.8	103.0	102.9	103.0	103.1	103.2	103.1	103.3	103.1
FBG VitE	94.5	104.1	103.4	104.2	103.8	104.1	104.1	104.0	104.0	103.9	104.0
FBG VitE	82.7	103.9	103.8	104.2	104.2	104.3	104.5	104.5	104.4	104.3	104.0
FBG VitE	66.9	103.2	103.5	103.3	103.1	103.8	104.3	103.4	103.5	103.4	103.3
FBG Myrj	61.3	100.3	101.0	100.7	101.0	100.8	100.9	101.1	100.9	101.0	100.5
FBG Myrj	60.6	99.0	101.2	101.5	101.5	100.9	101.5	100.9	101.0	100.7	100.8
FBG Myrj	60.4	101.0	101.5	101.5	101.8	101.0	102.5	101.3	101.6	101.7	101.1
FBG PP103	28.5	53.2	84.5	91.6	98.5	97.9	97.5	97.3	97.4	98.0	98.5
FBG PP103	34.2	60.7	79.7	89.2	97.3	97.7	97.5	98.5	98.2	97.6	98.5
FBG PP103	35.9	75.5	90.8	96.8	98.2	98.3	98.1	98.0	97.4	98.3	98.0
RF	4.9	24.3	47.9	61.1	86.9	93.9	94.5	94.4	94.6	95.0	95.7
RF	12.2	40.4	52.3	59.9	77.8	86.0	91.2	94.7	94.8	95.0	94.8
RF	7.9	40.9	72.7	81.4	94.3	97.6	96.5	96.1	96.0	96.2	95.9

Table 6.24: Dissolved amount of FDP [mg/900 ml] in FaSSIF-V2 at time points [min].

batch	5	10	15	20	30	45	60	90	120	180	240
M21D DOSS	7.6	10.7	12.2	12.9	13.0	13.1	13.9	14.7	18.3	16.9	20.5
M21D DOSS	7.7	11.1	12.4	16.4	13.8	13.8	14.6	15.8	17.1	13.4	18.6
M21D DOSS	7.6	11.0	12.1	13.5	13.8	13.5	14.5	14.1	16.4	13.3	17.4
M21D SDS	6.6	9.9	11.6	12.4	12.5	12.3	12.2	13.6	13.3	15.3	13.9
M21D SDS	10.6	10.5	11.9	11.9	12.5	12.2	11.4	11.3	11.5	11.5	10.9
M21D SDS	7.6	10.2	11.8	12.0	12.3	12.4	12.1	12.1	12.1	12.6	12.3
M21D PS80	3.0	6.0	8.6	10.2	11.3	11.8	11.8	12.5	12.8	12.7	12.6
M21D PS80	2.5	4.8	7.5	9.5	10.4	10.8	10.8	10.8	10.8	10.5	10.6
M21D PS80	2.7	5.5	7.7	9.4	10.5	11.5	11.6	12.8	13.2	12.6	13.0
M21D VitE	6.4	9.4	10.3	10.7	11.3	11.5	11.5	11.8	11.6	11.8	11.8
M21D VitE	6.4	9.1	10.2	10.7	11.3	11.6	11.5	12.0	12.0	12.5	12.3
M21D VitE	3.3	6.4	8.8	10.3	11.3	11.7	11.6	11.8	11.7	11.7	11.9
M21D Myrj	2.9	5.3	7.5	9.0	10.6	11.5	11.9	12.0	12.1	12.4	12.0
M21D Myrj	3.0	9.1	10.4	11.0	11.4	11.4	11.5	11.8	12.1	11.8	11.9
M21D Myrj	2.2	4.3	8.6	9.7	10.1	10.6	10.9	11.5	11.1	11.3	11.5
M21D P103	1.8	4.3	7.0	8.2	9.2	10.1	10.1	11.2	11.5	10.8	11.1
M21D P103	1.8	4.3	6.8	8.0	9.8	10.5	10.9	11.0	10.9	10.7	10.3
M21D P103	2.1	4.7	7.5	8.8	10.6	11.2	12.1	11.9	11.4	11.3	11.3
ISM DOSS	7.9	12.9	14.0	12.9	11.6	10.5	10.3	10.2	10.1	9.9	9.8
ISM DOSS	8.0	11.3	11.6	11.7	12.2	12.5	13.5	10.6	10.4	10.4	10.2
ISM DOSS	8.5	11.4	15.4	11.8	10.9	10.4	10.5	10.2	10.0	9.9	9.8
ISM VitE	4.3	8.9	10.0	10.4	10.4	10.6	10.5	10.4	10.5	10.4	10.2
ISM VitE	4.4	8.3	10.0	10.1	10.5	10.8	11.0	10.9	11.0	10.1	10.1
ISM VitE	3.4	7.7	9.6	10.2	10.6	10.4	9.8	10.1	9.5	10.1	10.2
50%MTL DOSS	9.0	12.6	13.0	12.9	13.2	13.1	13.5	12.3	12.1	11.4	11.4
50%MTL DOSS	11.3	14.9	15.8	15.7	14.3	14.8	13.5	14.3	14.1	13.6	12.8
50%MTL DOSS	12.5	15.1	21.9	18.4	16.7	16.7	16.8	16.2	16.0	15.8	14.3
50%MTL VitE	10.0	14.8	16.5	16.0	16.1	16.5	16.4	16.4	13.0	13.8	12.1
50%MTL VitE	5.5	12.7	12.5	12.3	12.1	12.2	12.4	11.9	11.9	11.6	11.8
50%MTL VitE	5.1	10.3	12.9	12.9	12.6	11.9	12.3	12.0	12.3	11.7	11.9
FBG DOSS	11.6	16.0	16.1	14.9	16.6	16.1	17.5	17.7	18.2	24.7	22.4
FBG DOSS	9.5	14.3	14.9	14.4	15.2	14.8	16.4	18.9	19.1	17.7	19.4
FBG DOSS	9.7	13.7	14.9	14.2	14.2	15.4	16.3	16.1	16.2	15.3	17.0
FBG SDS	9.0	13.5	13.1	12.2	12.7	10.7	12.9	13.2	13.1	13.5	15.5
FBG SDS	10.2	13.8	13.9	12.6	12.7	13.2	12.3	13.8	14.2	13.4	12.3
FBG SDS	9.5	11.3	12.2	12.8	13.0	13.5	12.4	13.4	13.1	13.8	13.8
FBG PS80	7.0	10.2	11.1	12.0	12.4	13.7	14.7	16.0	15.8	14.4	14.0
FBG PS80	8.6	11.9	12.0	11.7	11.8	12.1	12.0	12.0	11.2	10.6	11.0
FBG PS80	9.1	10.9	12.2	14.2	11.8	12.7	12.4	13.1	12.0	12.6	13.2
FBG VitE	10.2	11.8	11.1	10.4	13.9	11.9	13.9	15.5	14.4	11.5	17.2
FBG VitE	9.7	11.2	11.5	11.4	11.7	11.7	11.4	10.6	10.6	10.4	10.4
FBG VitE	9.5	12.1	11.3	11.0	11.1	10.9	10.9	11.3	11.9	11.5	11.9
FBG Myrj	5.9	8.8	10.0	11.0	11.4	12.1	11.7	12.0	12.0	12.6	13.6
FBG Myrj	6.2	9.3	10.6	11.1	12.4	12.9	12.2	11.9	11.5	11.1	10.8
FBG Myrj	7.6	9.6	11.0	11.2	11.2	11.3	11.1	11.0	10.7	10.6	10.4
FBG PP103	8.9	11.0	12.7	12.1	12.2	12.6	12.4	13.2	12.6	12.2	18.2
FBG PP103	4.9	9.0	10.5	11.6	11.2	11.2	11.1	10.9	11.1	11.2	12.0
FBG PP103	7.0	10.3	11.6	11.7	11.7	11.4	11.8	11.6	11.6	11.7	11.1
RF	2.3	7.2	9.2	9.8	10.3	10.6	10.6	10.6	10.2	10.7	9.6
RF	1.5	6.5	9.5	10.2	10.7	10.8	10.9	11.1	11.2	11.3	10.6
RF	1.2	4.6	8.6	10.0	10.8	11.0	11.2	11.3	11.2	11.1	10.8

Table 6.25: Dissolved amount of FEN [mg/900 ml] in FaSSIF-V2 at time points [min].

batch	5	10	15	20	30	45	60	90	120	180	240
M21D DOSS	1.9	1.9	2.6	2.8	2.6	2.7	3.6	3.0	2.8	2.1	1.6
M21D DOSS	1.8	2.7	3.2	3.4	3.4	3.0	3.7	2.4	3.1	2.7	2.8
M21D DOSS	1.5	2.8	2.4	3.6	3.4	2.9	3.0	2.9	2.7	2.4	2.5
M21D SDS	0.4	1.2	1.9	2.3	2.6	2.8	2.8	2.8	2.5	2.8	2.7
M21D SDS	0.3	1.0	1.8	2.2	2.6	3.0	2.6	2.8	2.2	2.8	3.2
M21D SDS	0.3	1.1	1.9	2.3	2.3	2.5	2.5	2.6	2.6	2.7	2.8
M21D PS80	0.4	1.3	2.0	2.1	2.6	2.5	2.5	2.4	2.5	2.6	2.7
M21D PS80	0.6	1.4	2.2	2.6	2.8	3.1	2.9	2.4	3.0	2.7	2.9
M21D PS80	0.5	1.4	1.9	2.2	1.8	2.4	2.5	2.7	2.8	3.1	3.4
M21D VitE	0.5	1.2	1.7	2.2	2.7	3.0	2.6	3.0	3.2	3.2	3.2
M21D VitE	0.5	1.2	2.1	2.2	2.6	2.9	3.0	3.1	3.4	3.4	3.6
M21D VitE	0.4	1.1	1.6	2.0	2.5	2.6	2.7	2.1	2.8	3.1	3.4
M21D Myrj	0.5	1.3	1.9	2.5	2.8	2.9	3.1	3.0	3.4	3.2	3.1
M21D Myrj	0.6	1.3	2.0	2.5	2.6	2.8	2.8	2.8	2.6	2.9	3.2
M21D Myrj	0.5	1.2	2.0	2.5	2.4	2.5	2.5	2.6	2.9	2.7	3.0
M21D P103	0.5	1.1	2.1	2.1	2.4	2.6	2.5	2.6	2.5	3.1	3.3
M21D P103	0.4	1.0	1.8	2.1	2.4	2.5	2.4	2.1	2.6	3.0	3.2
M21D P103	0.4	1.1	1.8	2.2	2.3	2.4	2.1	2.5	2.6	2.8	2.8
ISM DOSS	1.0	2.3	3.1	2.9	2.9	3.1	3.0	3.2	3.1	3.3	3.2
ISM DOSS	1.1	2.4	2.7	2.8	3.0	3.1	3.2	3.3	3.2	3.4	3.5
ISM DOSS	1.0	2.4	3.1	2.9	2.9	3.0	3.2	3.2	3.0	3.2	2.9
ISM VitE	0.9	2.1	2.5	2.9	2.7	2.7	2.6	2.7	2.6	2.8	2.9
ISM VitE	1.0	2.3	2.7	2.9	2.7	2.7	2.8	3.0	3.0	3.3	3.3
ISM VitE	1.1	2.4	2.5	2.5	2.6	2.7	2.6	2.7	2.6	2.6	2.8
50%MTL DOSS	1.4	2.3	2.7	2.8	2.8	2.8	3.1	3.0	2.8	3.1	2.8
50%MTL DOSS	1.1	2.5	2.7	2.7	2.8	2.8	2.8	2.6	2.6	2.7	2.7
50%MTL DOSS	1.2	2.9	2.9	2.8	2.8	2.8	2.9	2.7	2.9	2.8	2.9
50%MTL VitE	1.5	3.0	3.2	3.1	3.0	2.9	3.1	3.0	2.9	3.0	3.1
50%MTL VitE	1.5	2.9	3.5	3.0	3.0	3.1	3.0	3.0	3.0	2.9	2.9
50%MTL VitE	1.6	3.2	3.2	3.0	3.1	3.0	3.0	3.0	3.1	3.0	3.0
FBG DOSS	1.8	2.8	2.9	3.1	3.4	3.7	3.1	3.0	2.8	2.8	2.8
FBG DOSS	2.0	2.6	2.8	3.0	3.0	3.5	3.3	3.9	4.1	4.7	3.9
FBG DOSS	1.8	3.0	3.0	2.9	2.7	3.0	3.3	3.2	2.7	3.3	3.2
FBG SDS	1.0	1.9	2.0	2.1	2.0	2.2	2.2	2.3	3.7	3.7	2.6
FBG SDS	1.3	1.8	1.9	2.0	2.2	2.2	2.2	2.4	2.6	3.1	3.4
FBG SDS	1.7	1.9	2.1	1.6	2.3	2.3	2.5	2.8	2.6	3.0	3.0
FBG PS80	1.9	2.6	2.8	2.5	2.6	2.6	2.3	2.7	3.3	3.3	2.2
FBG PS80	1.9	2.4	2.3	2.3	2.5	2.6	2.1	1.8	2.0	2.0	1.7
FBG PS80	2.0	2.9	2.8	2.7	2.5	2.5	2.5	2.6	2.0	2.5	2.4
FBG VitE	2.2	3.1	2.8	2.1	2.8	2.8	2.5	2.4	2.4	3.0	2.7
FBG VitE	2.2	2.6	2.6	2.6	2.7	2.5	2.3	2.4	2.4	2.6	2.3
FBG VitE	2.1	2.5	2.6	2.9	2.3	2.4	2.4	2.4	2.3	2.6	2.3
FBG Myrj	1.2	2.0	2.4	2.7	2.8	3.1	3.1	3.3	3.3	3.5	3.5
FBG Myrj	1.1	1.9	2.3	2.5	2.7	3.1	3.2	3.5	3.4	3.2	3.7
FBG Myrj	1.3	2.2	2.5	2.7	2.8	3.0	3.0	3.1	3.2	3.4	3.7
FBG PP103	0.5	1.2	2.2	2.7	2.6	3.0	3.1	3.0	3.0	3.5	3.5
FBG PP103	0.5	1.1	2.1	2.5	3.0	3.3	3.3	2.9	3.3	3.6	3.2
FBG PP103	0.8	1.6	2.3	3.6	3.2	3.4	3.2	2.6	3.0	2.9	3.0
RF	0.0	0.0	0.0	0.0	0.0	0.1	0.1	0.2	0.4	0.9	1.8
RF	0.0	0.0	0.0	0.0	0.4	0.1	0.3	0.3	0.4	0.7	1.1
RF	0.0	0.0	0.0	0.0	0.0	0.1	0.2	0.3	0.5	0.9	1.2

Table 6.26: Dissolved amount of THL [mg/900 ml] in FaSSIF-V2 at time points [min].

batch	5	10	15	20	30	45	60	90	120	180	240
M21D DOSS	0.0	0.0	0.0	0.0	1.3	1.2	1.1	1.3	1.9	2.0	1.9
M21D DOSS	0.0	0.0	0.0	0.0	0.9	1.0	1.9	1.9	1.9	1.9	2.2
M21D DOSS	0.0	0.0	0.0	0.0	0.0	0.0	0.8	1.1	0.9	1.6	1.2
M21D SDS	0.0	0.0	0.0	0.0	0.0	0.0	0.3	0.0	0.4	0.0	1.1
M21D SDS	0.0	0.0	0.0	0.0	0.0	1.2	0.8	1.8	1.7	1.8	1.9
M21D SDS	0.0	0.0	0.0	0.0	0.0	0.0	0.0	0.8	0.9	0.9	1.0
M21D PS80	0.0	1.5	1.8	1.9	1.9	2.0	1.8	1.9	1.9	2.1	2.2
M21D PS80	0.0	1.8	2.1	2.3	2.4	2.5	2.4	2.2	2.2	2.3	2.5
M21D PS80	0.0	1.6	1.8	1.9	2.1	2.6	3.2	2.5	2.2	2.2	2.3
M21D VitE	0.3	0.6	0.6	0.9	0.9	0.8	0.6	0.7	0.7	0.8	0.9
M21D VitE	0.0	0.3	0.3	0.7	1.0	0.6	0.5	0.6	0.6	0.7	0.9
M21D VitE	0.0	0.4	0.7	0.7	0.7	0.6	0.6	0.6	0.6	0.7	0.9
M21D Myrj	0.0	0.0	0.0	0.0	0.0	0.1	0.1	0.2	0.2	0.2	0.3
M21D Myrj	0.0	0.0	0.0	0.0	0.1	0.1	0.2	0.2	0.2	0.4	0.5
M21D Myrj	0.0	0.0	0.0	0.0	0.1	0.1	0.2	0.3	0.2	0.3	0.2
M21D P103	0.0	0.0	0.0	0.1	0.4	0.5	0.6	0.5	0.7	0.8	0.7
M21D P103	0.0	0.1	0.5	0.4	0.6	0.7	0.7	0.8	0.7	1.0	0.9
M21D P103	0.0	0.0	0.3	0.2	0.3	0.4	0.6	0.7	0.6	0.7	0.8
ISM DOSS	0.2	0.9	1.4	1.9	1.9	1.7	1.6	1.7	1.8	2.1	2.4
ISM DOSS	0.0	0.0	0.0	0.8	0.7	1.2	1.5	1.6	1.8	1.9	2.2
ISM DOSS	0.0	0.4	1.2	1.1	1.7	1.8	1.7	1.7	1.7	2.1	2.4
ISM VitE	2.8	2.6	-	-	2.9	3.3	2.0	0.8	2.0	2.5	2.4
ISM VitE	0.6	3.0	3.0	-	3.1	3.9	1.6	1.9	2.1	2.7	2.5
ISM VitE	2.9	2.6	2.5	-	3.3	2.9	2.5	1.6	2.3	2.5	2.5
50%MTL DOSS	0.0	0.0	0.5	0.7	0.9	1.0	1.2	1.2	1.3	1.5	1.8
50%MTL DOSS	0.0	0.0	0.0	0.4	0.7	0.9	1.1	1.2	1.3	1.7	1.7
50%MTL DOSS	0.0	0.0	0.0	0.3	0.4	0.8	0.7	1.1	1.3	1.6	1.8
50%MTL VitE	0.0	3.0	3.1	2.6	2.9	3.5	1.5	1.8	2.3	2.5	3.0
50%MTL VitE	0.4	1.7	0.0	0.0	3.6	2.8	2.2	2.2	2.6	2.6	2.8
50%MTL VitE	0.0	1.7	1.6	0.0	2.1	3.0	2.0	2.1	2.5	2.9	2.9
FBG DOSS	0.0	0.1	0.1	0.1	0.1	0.1	0.1	0.2	0.1	0.2	0.1
FBG DOSS	0.0	0.0	0.0	0.1	0.0	0.0	0.0	0.0	0.0	0.1	0.5
FBG DOSS	0.0	0.0	0.0	0.0	0.1	0.1	0.0	0.2	0.2	0.2	0.2
FBG SDS	0.0	0.0	0.0	0.0	0.6	0.7	0.0	0.0	0.6	0.6	0.8
FBG SDS	0.0	0.0	0.5	0.0	0.1	0.4	0.7	0.4	0.2	0.8	0.6
FBG SDS	0.0	0.0	0.0	0.0	0.0	0.0	0.4	0.9	0.3	0.3	0.4
FBG PS80	0.7	1.6	1.5	1.2	1.0	0.9	0.8	0.8	0.8	0.7	1.7
FBG PS80	0.8	2.4	0.5	0.9	0.7	0.8	1.0	0.7	0.7	1.2	1.5
FBG PS80	1.2	1.1	0.7	0.7	0.6	0.7	0.6	0.7	0.7	0.9	1.2
FBG VitE	0.0	0.0	0.0	0.0	0.5	0.6	0.6	0.6	0.7	0.6	0.8
FBG VitE	0.0	1.1	0.8	0.9	0.9	0.6	0.5	0.7	0.7	0.8	0.6
FBG VitE	0.0	0.3	0.3	0.7	0.7	0.7	0.7	0.7	0.7	0.9	0.8
FBG Myrj	0.0	0.0	0.0	0.0	0.0	0.1	0.0	0.0	0.2	0.0	0.1
FBG Myrj	0.0	0.5	0.0	0.0	0.0	0.0	0.0	0.0	0.0	0.0	0.1
FBG Myrj	0.0	0.0	0.0	0.0	0.0	0.0	0.0	0.0	0.0	0.1	0.1
FBG P103	0.0	0.0	0.0	0.9	1.6	0.7	0.2	0.0	0.2	0.1	0.0
FBG P103	0.0	0.0	0.3	0.1	0.0	0.1	0.0	0.1	0.0	0.0	0.2
FBG P103	0.0	1.5	1.4	0.8	0.1	0.0	0.1	0.0	0.0	0.2	0.2
Alli®	0.4	0.4	0.7	0.7	0.7	0.7	0.5	0.2	0.6	0.7	0.8
Alli®	0.0	0.0	0.0	0.0	0.0	0.5	0.5	0.6	0.6	0.8	0.9
Alli®	0.3	0.5	0.6	0.6	0.7	1.1	1.1	1.1	1.2	1.1	1.2

Table 6.27: Dissolved amount of THL [mg/900 ml] in USP 35 monography medium at time points [min].

batch	5	10	15	20	30	45	60	90	120	180	240
M21D DOSS	0.3	0.6	1.0	2.0	3.6	3.5	4.0	6.5	8.6	12.0	14.6
M21D DOSS	0.3	0.5	0.9	1.4	2.2	3.4	5.1	7.5	8.6	12.7	15.6
M21D DOSS	0.3	0.6	0.9	1.4	2.0	3.3	5.9	6.3	8.1	11.5	14.2
M21D SDS	0.0	0.3	0.6	0.9	1.7	2.9	4.9	8.2	9.2	12.8	15.9
M21D SDS	0.0	0.3	0.4	0.7	1.9	2.9	4.4	5.9	8.4	12.4	15.7
M21D SDS	0.0	0.3	0.5	0.8	1.7	3.2	4.9	7.6	8.7	12.5	15.6
M21D PS80	1.4	2.6	4.9	3.2	4.3	5.8	7.1	9.1	11.1	14.2	16.7
M21D PS80	0.7	1.4	3.0	4.1	6.6	7.6	7.4	9.0	11.0	13.9	16.5
M21D PS80	0.6	1.4	2.6	3.7	5.0	7.1	8.3	11.0	11.6	14.9	17.8
M21D VitE	0.8	2.5	4.7	3.6	4.8	6.8	10.1	8.1	10.0	13.2	15.7
M21D VitE	0.7	1.4	2.9	3.7	3.6	4.5	5.9	8.2	10.2	13.5	16.0
M21D VitE	0.7	1.7	4.6	4.0	3.5	4.5	5.8	8.1	10.2	13.4	16.0
M21D Myrj	0.2	0.4	0.8	1.2	2.3	4.1	5.2	6.9	8.4	11.7	14.3
M21D Myrj	0.2	0.2	0.4	0.6	1.3	2.5	4.1	6.3	8.9	11.3	13.9
M21D Myrj	0.2	0.4	0.9	1.6	2.4	2.5	3.7	6.0	8.1	11.7	14.5
M21D P103	0.7	1.1	1.7	2.4	3.5	4.9	6.0	7.8	9.3	12.1	14.6
M21D P103	0.6	1.0	1.6	2.2	3.7	5.0	7.5	8.4	8.9	11.6	14.0
M21D P103	0.6	1.1	1.8	2.4	3.6	5.1	6.2	7.9	10.3	12.5	13.8
ISM DOSS	1.1	2.3	4.4	4.8	3.8	5.8	7.7	11.1	14.0	18.8	22.6
ISM DOSS	1.2	2.3	3.6	6.9	5.2	6.6	8.6	12.2	15.4	20.2	24.0
ISM DOSS	1.1	2.4	3.9	5.1	8.7	6.6	8.5	12.0	15.1	20.0	23.7
ISM VitE	3.9	8.4	10.4	5.2	6.2	8.1	9.7	12.6	15.1	18.8	21.8
ISM VitE	3.8	6.9	9.1	9.2	12.3	7.9	9.5	12.3	14.7	18.2	21.0
ISM VitE	3.9	8.1	11.3	8.7	6.5	8.1	9.8	12.7	15.2	18.9	21.6
50%MTL DOSS	0.9	2.4	2.4	2.4	3.5	5.2	6.7	9.6	12.1	16.4	19.8
50%MTL DOSS	0.9	2.2	4.2	3.3	3.9	5.3	6.9	9.9	12.5	17.0	20.6
50%MTL DOSS	0.7	1.5	2.4	3.8	5.5	5.6	6.9	9.8	12.4	16.7	20.0
50%MTL VitE	4.0	7.0	10.8	5.9	6.9	7.9	9.4	11.8	14.0	17.4	19.7
50%MTL VitE	2.5	4.8	6.4	7.2	8.1	7.9	9.4	12.2	14.4	17.8	20.2
50%MTL VitE	2.3	12.0	5.6	4.6	5.5	7.5	9.3	12.1	14.5	17.8	20.2
FBG DOSS	1.5	5.2	5.9	4.2	3.3	4.5	5.7	7.5	9.2	12.2	14.6
FBG DOSS	1.1	1.5	2.1	3.3	4.9	8.4	5.6	7.5	9.1	12.1	14.6
FBG DOSS	0.9	1.5	2.3	3.9	6.1	4.7	5.5	7.4	9.1	12.1	14.7
FBG SDS	0.8	1.8	3.2	6.0	4.3	4.6	5.6	7.3	8.8	11.9	14.2
FBG SDS	2.0	3.2	6.8	4.5	4.1	5.3	6.5	9.5	9.8	12.8	16.2
FBG SDS	1.5	2.9	5.3	3.1	3.4	3.6	4.6	6.0	8.0	12.3	12.3
FBG PS80	4.2	7.2	4.3	4.5	5.2	6.4	7.4	9.3	11.1	14.0	16.4
FBG PS80	2.0	4.8	6.9	5.6	5.0	6.2	7.2	9.0	10.7	13.6	15.9
FBG PS80	3.6	4.6	5.9	8.1	4.9	6.2	7.3	9.2	10.9	13.9	16.3
FBG VitE	3.2	6.2	10.5	8.0	9.4	7.6	6.9	8.8	10.5	13.6	16.1
FBG VitE	1.5	3.7	5.6	6.7	4.6	5.6	6.8	8.7	10.4	13.4	15.8
FBG VitE	2.0	10.0	7.6	3.7	4.6	5.8	6.8	8.7	10.5	13.3	15.7
FBG Myrj	2.0	3.0	4.1	6.3	7.6	7.9	8.1	8.8	7.5	9.1	10.9
FBG Myrj	1.6	2.2	3.0	4.7	2.8	3.5	4.2	5.5	6.7	8.7	10.5
FBG Myrj	1.7	2.7	3.4	4.6	2.8	3.5	4.2	5.5	6.7	8.8	10.5
FBG P103	3.0	5.7	6.6	3.5	4.2	5.2	6.2	7.9	9.5	12.4	14.9
FBG P103	3.1	6.0	3.6	3.6	4.3	5.3	6.3	8.0	9.6	12.4	14.9
FBG P103	4.8	4.2	3.4	3.5	4.1	5.1	6.0	7.7	9.2	12.0	14.5
Alli®	1.0	2.0	3.8	3.3	3.2	4.2	5.2	7.1	8.9	12.2	15.2
Alli®	1.0	1.7	2.6	3.4	5.1	5.5	5.5	7.4	9.3	12.6	15.6
Alli®	0.9	1.7	2.4	4.2	5.3	4.1	4.9	6.7	8.4	11.4	14.2
RF	0.0	0.3	0.5	0.7	1.1	1.7	2.4	3.4	4.4	6.4	8.1
RF	0.0	0.2	0.4	0.7	0.7	1.2	1.3	1.6	2.0	2.9	3.7
RF	0.0	0.0	0.0	0.0	0.0	0.0	0.0	0.2	0.2	0.3	0.4

Table 6.28: Dissolved amount of NK1 [mg/900 ml] in FaSSIF-V2 at time points [min].

batch	5	10	15	20	30	45	60	90	120	180	240
M21D DOSS	0.4	1.1	1.7	1.9	1.9	1.3	1.1	1.3	1.2	1.0	0.8
M21D DOSS	0.3	0.9	1.4	1.6	1.5	1.3	1.1	1.0	0.8	0.7	0.7
M21D DOSS	0.5	1.1	1.3	1.2	1.1	1.0	0.8	0.7	0.8	1.0	0.3
M21D VitE	0.4	0.4	0.4	0.7	1.0	1.0	1.1	0.8	1.0	1.0	1.0
M21D VitE	0.4	0.4	0.6	0.7	1.0	0.9	1.0	1.0	1.1	1.0	0.9
M21D VitE	0.3	0.4	0.7	0.8	0.9	1.1	1.3	1.1	1.2	1.1	1.0
FBG DOSS	1.3	2.7	3.0	2.0	1.3	1.0	1.1	1.0	1.0	0.8	1.0
FBG DOSS	1.3	3.0	2.0	1.7	1.3	1.0	1.0	0.9	1.0	0.9	0.7
FBG DOSS	1.0	2.7	2.7	1.5	1.2	0.7	1.0	0.7	0.6	0.8	0.9
FBG VitE	0.8	1.0	1.0	1.0	0.8	0.6	1.1	1.8	1.1	1.0	1.7
FBG VitE	0.4	1.4	2.4	2.4	3.7	1.2	3.4	1.6	0.8	0.8	1.3
FBG VitE	0.9	1.4	1.4	1.2	1.4	1.3	1.0	1.7	1.0	0.9	1.0

Table 6.29: Dissolved amount of MAO [mg/900 ml] in FaSSIF-V2 at time points [min].

batch	5	10	15	20	30	45	60	90	120	180	240
M21D DOSS	4.6	5.1	5.1	5.0	5.0	5.1	5.0	5.5	5.8	3.9	3.5
M21D DOSS	3.9	4.5	4.6	4.5	4.6	5.2	5.5	3.3	3.8	3.9	3.8
M21D DOSS	3.7	4.6	4.8	4.7	7.7	4.1	3.8	3.4	3.6	3.2	3.6
M21D VitE	5.4	6.2	9.4	11.4	9.3	8.3	7.2	4.8	4.1	3.3	3.4
M21D VitE	4.7	5.7	6.1	6.0	14.1	10.3	7.2	7.8	4.8	4.6	3.7
M21D VitE	5.1	6.2	6.9	9.0	7.3	6.1	4.7	4.1	3.3	3.5	3.3
FBG DOSS	4.8	8.9	9.8	7.7	6.8	3.7	3.6	3.7	3.9	3.7	3.5
FBG DOSS	5.7	8.1	10.2	7.2	5.0	4.2	3.4	3.6	3.4	3.3	3.5
FBG DOSS	5.0	6.0	7.6	9.0	10.9	5.5	3.9	3.9	3.6	3.8	3.3
FBG VitE	6.3	8.7	14.0	10.7	7.5	4.6	3.8	3.5	3.5	3.5	3.6
FBG VitE	6.9	24.4	10.0	8.5	6.8	5.8	3.9	3.8	3.5	3.3	3.8
FBG VitE	6.0	15.8	13.3	9.8	7.0	4.7	3.8	3.3	3.6	3.5	3.5
RF	0.0	0.0	0.0	0.0	0.9	1.3	1.6	1.9	2.1	2.0	2.3
RF	0.0	0.0	0.0	0.0	0.3	1.1	1.3	1.7	1.9	2.3	2.5
RF	0.0	0.0	0.0	0.0	0.3	0.8	1.1	1.4	1.7	2.0	2.3

Table 6.30: Dissolved amount of CP2 [mg/900 ml] in FaSSIF-V2 at time points [min].

batch	5	10	15	20	30	45	60	90	120	180	240
M21D DOSS	0.5	0.8	1.9	1.4	0.7	0.4	0.4	0.4	0.4	0.3	0.3
M21D DOSS	0.4	0.7	1.5	1.1	0.8	0.4	0.4	0.3	0.4	0.3	0.3
M21D DOSS	0.5	0.7	1.1	0.8	0.4	0.4	0.3	0.3	0.3	0.4	0.3
M21D VitE	0.4	1.1	0.3	0.3	1.0	3.3	1.2	0.7	0.8	1.0	1.1
M21D VitE	0.4	1.1	1.0	0.3	0.8	6.0	1.6	0.9	0.4	0.3	1.0
M21D VitE	0.3	0.4	1.0	1.8	0.9	0.9	0.9	1.1	1.2	1.5	0.9
ISM DOSS	0.6	0.9	0.7	0.2	0.3	1.5	2.2	1.1	0.3	0.3	0.3
ISM DOSS	2.0	3.4	3.3	2.0	1.3	2.7	1.6	0.7	0.3	0.2	0.3
ISM DOSS	0.3	0.9	0.3	0.3	0.3	2.2	2.3	1.1	0.4	0.6	0.3
ISM VitE	0.2	0.5	0.8	0.3	0.2	1.8	1.0	1.1	1.1	1.0	0.4
ISM VitE	0.4	0.8	0.6	0.4	0.3	1.0	0.8	0.9	0.5	0.3	0.2
ISM VitE	0.4	1.2	0.6	0.3	0.2	1.0	0.7	0.4	0.4	0.3	0.2
50%MTL DOSS	0.3	0.5	0.1	0.2	0.2	0.8	0.6	0.4	0.3	0.3	0.2
50%MTL DOSS	0.2	0.3	0.3	0.1	0.2	1.0	0.7	0.4	0.3	0.2	0.1
50%MTL DOSS	0.3	0.3	0.4	1.8	0.3	1.8	1.0	0.4	1.1	0.3	0.4
50%MTL VitE	0.3	0.9	1.1	1.4	1.5	1.7	1.8	1.7	1.9	2.5	2.5
50%MTL VitE	0.4	1.1	1.0	1.4	1.2	1.5	2.3	2.1	1.7	1.5	1.1
50%MTL VitE	0.4	1.1	1.2	1.6	1.3	1.8	2.2	2.5	1.5	1.1	0.5
FBG DOSS	3.0	4.3	5.3	4.6	5.4	2.5	0.9	1.0	1.0	1.2	1.3
FBG DOSS	2.6	6.2	3.7	2.7	1.1	0.9	0.9	0.9	1.0	1.2	1.3
FBG DOSS	3.1	5.9	6.9	5.2	2.7	1.0	0.9	0.9	1.0	1.2	1.3
FBG VitE	2.3	1.8	1.4	1.2	1.3	1.3	1.1	1.4	1.4	1.8	1.6
FBG VitE	1.7	1.8	1.5	1.4	1.1	1.5	1.2	1.5	1.4	2.0	1.3
FBG VitE	2.9	2.6	1.9	2.0	1.4	1.2	1.0	1.1	1.5	1.6	1.3

Table 6.31: Dissolved amount of DRX [mg/900 ml] in FaSSIF-V2 at time points [min].

batch	5	10	15	20	30	45	60	90	120	180	240
M21D DOSS	2.1	2.3	2.3	2.3	2.4	2.3	2.4	2.3	2.4	2.4	2.5
M21D DOSS	2.3	2.3	2.3	2.3	2.3	2.3	2.2	2.4	2.3	2.5	2.6
M21D DOSS	2.1	2.2	2.3	2.3	2.2	2.2	2.2	2.2	2.3	2.6	2.7
M21D VitE	2.4	2.8	2.8	2.9	3.0	3.3	3.4	3.5	3.7	4.0	4.1
M21D VitE	1.6	1.9	2.2	2.6	2.6	3.0	2.9	2.9	3.0	3.0	2.9
M21D VitE	2.2	2.5	2.9	3.1	3.0	3.2	3.1	3.4	3.6	3.6	3.8
ISM DOSS	2.8	3.5	3.2	3.7	3.6	3.6	3.4	3.5	3.4	3.4	3.5
ISM DOSS	2.9	3.0	3.2	3.3	3.4	3.4	3.3	3.2	3.1	3.2	3.2
ISM DOSS	2.7	3.0	3.2	3.4	3.5	3.5	3.3	3.2	3.1	3.1	3.3
ISM VitE	3.5	4.0	5.0	5.7	6.1	5.9	6.3	6.0	5.8	5.5	5.4
ISM VitE	3.6	4.6	5.3	5.4	5.4	5.6	5.4	5.5	5.5	5.6	5.7
ISM VitE	3.6	4.4	5.0	5.6	5.8	5.9	5.6	5.6	5.6	5.5	5.5
50%MTL DOSS	3.4	4.0	5.2	4.3	4.3	4.2	4.0	3.9	3.7	3.8	3.9
50%MTL DOSS	3.3	3.6	4.0	4.4	4.4	4.0	3.9	3.8	3.7	3.7	3.8
50%MTL DOSS	3.4	3.8	4.3	4.1	4.0	3.8	3.7	3.7	3.7	3.7	3.8
50%MTL VitE	3.9	5.1	5.8	5.9	5.1	4.9	4.8	4.8	5.0	5.1	5.2
50%MTL VitE	4.0	4.9	5.7	6.2	5.2	4.8	4.7	4.8	5.0	5.3	5.3
50%MTL VitE	3.9	5.0	5.8	5.8	5.3	5.1	5.0	5.0	5.0	5.0	5.2
FBG DOSS	3.5	4.2	3.9	3.3	3.2	3.2	3.2	3.2	3.2	3.3	3.4
FBG DOSS	3.7	4.0	3.8	3.7	3.6	3.6	3.6	3.5	3.6	3.7	3.8
FBG DOSS	3.9	4.3	3.6	3.4	3.3	3.2	3.2	3.2	3.2	3.3	3.4
FBG VitE	4.5	5.3	4.9	4.7	4.4	3.8	3.7	3.7	3.7	3.8	3.9
FBG VitE	4.1	4.5	4.2	4.3	4.4	4.2	3.7	3.8	3.8	3.8	3.9
FBG VitE	3.6	3.6	4.3	3.7	3.6	3.6	3.6	3.6	3.8	3.8	3.8
RF	1.9	2.0	2.0	2.0	2.0	2.0	2.0	2.1	2.3	2.1	2.9
RF	2.5	2.3	2.5	2.4	2.4	2.3	2.4	2.4	2.4	2.4	2.4
RF	2.9	2.9	2.9	2.9	2.9	2.9	2.9	2.9	2.9	2.9	2.9

Table 6.32: Dissolved amount of DAL [mg/900 ml] in FaSSIF-V2 at time points [min]. M21D VitE amb was prepared at ambient pressure.

batch	5	10	15	20	30	45	60	90	120	180	240
M21D DOSS	1.5	1.8	2.1	2.8	4.1	5.3	6.2	7.4	8.0	8.7	9.0
M21D DOSS	1.6	1.5	2.0	2.7	4.0	5.3	6.2	7.3	7.9	8.7	9.1
M21D DOSS	0.7	1.5	2.4	3.1	4.3	5.6	6.4	7.5	8.1	8.9	9.5
M21D VitE	0.0	0.8	1.3	2.0	3.0	4.5	5.6	6.9	7.7	8.7	9.7
M21D VitE	1.8	2.5	2.4	2.9	3.6	4.9	6.0	7.6	8.6	9.8	11.4
M21D VitE	1.6	2.0	2.1	2.5	3.5	4.6	5.6	7.0	8.0	9.7	10.4
M21D VitE amb	0.9	1.3	1.6	1.9	2.5	3.3	3.7	4.4	4.9	5.6	5.9
M21D VitE amb	0.0	0.0	0.0	0.0	0.0	3.3	3.7	4.4	4.9	5.6	5.9
M21D VitE amb	0.9	1.2	1.9	1.8	2.3	3.0	3.5	4.2	4.7	5.4	5.7
ISM DOSS	1.4	2.5	3.8	4.0	4.7	5.7	6.4	7.2	7.7	8.9	9.3
ISM DOSS	1.1	2.3	3.7	3.7	4.5	5.5	6.3	7.1	7.8	9.0	9.2
ISM DOSS	1.3	2.4	3.3	4.0	5.0	5.8	6.5	7.8	8.6	9.4	9.5
ISM VitE	2.7	3.8	4.6	5.9	6.9	7.6	8.1	8.9	9.3	9.8	9.9
ISM VitE	1.7	3.4	4.9	5.2	5.7	5.7	7.6	8.0	8.4	8.7	9.1
ISM VitE	1.7	3.9	4.0	4.3	6.4	7.2	7.6	8.3	8.4	8.8	9.4
50%MTL DOSS	1.0	3.2	4.3	5.5	6.9	7.2	7.9	8.8	9.3	12.5	12.5
50%MTL DOSS	1.0	3.0	4.1	4.9	6.2	7.6	8.4	8.6	9.2	12.5	12.7
50%MTL DOSS	1.1	3.3	4.7	5.6	6.2	7.2	7.9	8.9	9.3	12.2	9.6
50%MTL VitE	1.5	3.2	4.5	5.8	7.6	7.8	8.5	9.4	9.9	12.9	13.0
50%MTL VitE	2.8	3.9	4.9	5.6	6.6	7.7	8.4	9.0	9.3	12.9	12.6
50%MTL VitE	1.3	3.4	4.7	6.3	7.4	7.7	8.3	9.1	9.2	12.6	12.3
FBG DOSS	2.1	4.2	5.3	5.8	6.4	6.8	6.7	7.0	8.5	9.1	8.5
FBG DOSS	1.8	4.2	5.6	6.0	6.5	6.6	6.7	6.8	6.9	7.6	7.3
FBG DOSS	2.8	4.4	5.4	5.7	5.9	6.6	6.5	5.8	6.2	5.1	5.0
FBG VitE	2.9	4.3	5.1	5.6	5.8	5.8	5.7	6.0	4.8	5.1	5.0
FBG VitE	2.1	3.4	4.3	4.6	5.1	5.0	4.9	5.1	5.4	5.4	5.9
FBG VitE	1.9	3.1	4.2	4.7	4.9	5.1	5.0	5.1	5.0	5.4	5.3
RF	0.0	0.0	0.0	0.0	0.0	0.4	0.5	0.8	1.2	2.7	3.5
RF	0.0	0.0	1.3	0.6	0.7	0.6	0.7	0.8	1.1	2.0	2.7
RF	0.1	0.1	0.1	0.1	0.1	0.2	0.2	0.4	0.5	0.7	0.9

6.9 X-ray μ-CT images of tablets

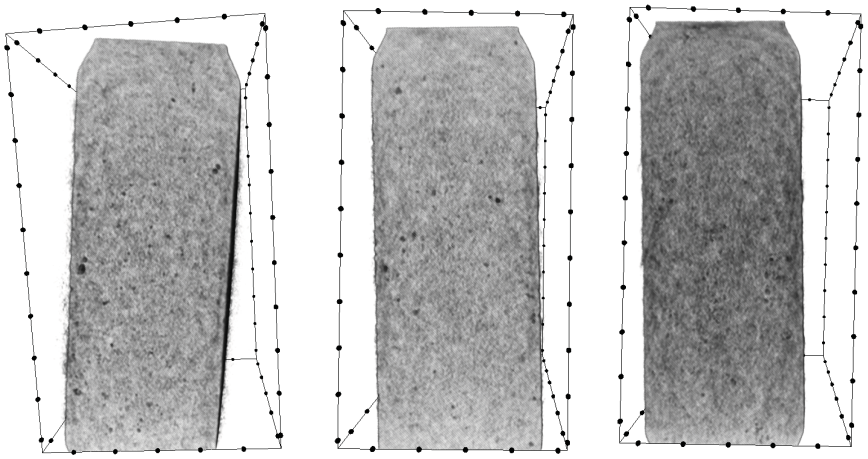

Figure 6.28: X-ray μ-CT images of DF THL VitE tablets prepared with M21D (left), ISM (middle) and 50%MTL (right) as filler.

Bibliography

G. L. Amidon, H. Lennernäs, V.P. Shah, and J.R. Crison. A theoretical basis for a biopharmaceutic drug classification: the correlation of in vitro drug product dissolution and in vivo biovailability. *Pharmaceutical Research*, 12:413–420, 1995.

F. Avaltroni, P. Bouquerand, and V. Normand. Maltodextrin molecular weight distribution influence on the glass transition temperature and viscosity in aqueous solutions. *Carbohydrate Polymers*, 58(3):323–334, 2004.

E. Basalious, W. El-Sebaie, and O. El-Hazayerly. Rapidly absorbed orodispersible tablet containing molecularly dispersed felodipine for management of hypertensive crisis: development, optimization and in vitro/in vivo studies. *Pharmaceutical Development and Technology*, 18(2):407–416, 2013.

L. Z. Benet, F. Broccatelli, and T. I. Oprea. BDDCS applied to over 900 drugs. *The AAPS Journal*, 13(4):519–47, 2011.

S. Brunauer, P.H. Emmet, and E.J. Teller. Adsorption of gases in multimolecular layers. *Journal of American Chemistry Society*, 60:309–319, 1938.

E. Brunner. Reaktionsgeschwindigkeit in heterogenen Systemen. *Zeitschrift für Physikalische Chemie*, 43:56–102, 1904.

P. Busson and M. Schröder. Process for preparing a pharmaceutical composition. F.Hoffmann-La Roche Ltd., PCT No. WO 2002/00201, 2006.

J. M. Butler and J. B. Dressman. The developability classification system: application of biopharmaceutics concepts to formulation development. *Journal of Pharmaceutical Sciences*, 99(12):4940–54, 2010.

D. E. Clark. Rapid calculation of polar molecular surface area and its application to the prediction of transport phenomena. 1. prediction of intestinal absorption. *Journal of Pharmaceutical Sciences*, 88:807–814, 1999.

G. Dalziel, E. Nauka, F. Zhang, S. Kothari, and M. Xie. Assessment of granulation technologies for an API with poor physical properties. *Drug Development and Industrial Pharmacy*, 39(7):985–95, 2013.

S. Eerikäinen and A.-S. Lindqvist. The behavior of various fillers in spheronized uncoated and film-coated granules containing slightly water-soluble indomethacin. *International Journal of Pharmaceutics*, 75:181–192, 1991.

European Medicines Agency. *Guideline on the Investigation of Bioequivalence*. Committee for Medicinal Products for Human Use, 2010.

Y. Fei, E. Kostewicz, and Dressman J. B. Sheu, M.-T. Analysis of the enhanced oral bioavailability of fenofibrate lipid formulations in fasted humans using an in vitro-in silico-in vivo approach. *European Journal of Pharmaceutics and Biopharmaceutics*, in press, 2013.

G. Gross, J. Tardio, and O. Kuhlmann. Solubility and stability of dalcetrapib in vehicles and biological media. *International Journal of Pharmaceutics*, 437:103–109, 2012.

A. A. Hajare, H. N. More, and S. S. Pisal. Stabilisation of doxorubicin hydrochloride using sugar-phosphate glass composites prepared by vacuum foam drying. *European Journal of Parenteral and Pharmaceutical Sciences*, 15(1):18–25, 2010.

J. B. Harp. Orlistat for the long-term treatment of obesity. *Drugs of Today, Prous science*, 35(2):139–145, 1999.

Q. He and J. Shi. Mesoporous silica nanoparticle based nano drug delivery systems: synthesis, controlled drug release and delivery, pharmacokinetics and biocompatibility. *Journal of Materials Chemistry*, 21:5845, 2011.

Y.-Y. Hsu, J. D. Gresser, D. J. Trantolo, C. M. Lyons, P. R. J. Gangadharam, and D. L. Wise. Effect of polymer foam morphology and density on kinetics of in vitro controlled release of isoniazid from compressed foam matrices. *Journal of Biomedical Materials Research*, 35:107–116, 1997.

E. Jantratid, N. Janssen, C. Reppas, and J. B. Dressman. Dissolution media simulating conditions in the proximal human gastrointestinal tract: An update. *Pharmaceutical Research*, 25(7):1663–1676, 2008.

Y. Kawabata, K. Wada, M. Nakatani, S. Yamada, and S. Onoue. Formulation design for poorly water-soluble drugs based on biopharmaceutics classification system: basic approaches and practical applications. *International Journal of Pharmaceutics*, 420(1):1–10, 2011.

G. M. Khan and J.-B. Zhu. Dissolution studies of ibuprofen powders: effect of particle size on dissolution rate and simulation of dissolution process of mixed binary systems. *Journal of Chinese Pharmaceutical Sciences*, 7(1):11–17, 1998.

M.S. Ku. Use of the biopharmaceutical classification system in early drug development. *The AAPS Journal*, 10(1):208–212, 2008.

M. Kuentz and G. Imanidis. In silico prediction of the solubility advantage for amorphous drugs are there property-based rules for drug discovery and early pharmaceutical development? *European Journal of Pharmaceutical Sciences*, 48: 554–562, 2013.

W. Kwapinski and E. Tsotsas. Determination of kinetics and equilibria for adsorption of water vapor on single zeolite particles by a magnetic suspension balance. *Chemical Engineering & Technology*, 27 (6):681–686, 2004.

R. Laakso and S. Eerikäinen. Effects of core components on indomethacin release from film-coated granules. *International Journal of Pharmaceutics*, 67:79–88, 1991.

E. Lenz. Einfluß verschiedener Füllstoffe auf die Freisetzung von Tabletten aus Trockenschäumen. Diploma thesis, Martin-Luther University Halle -Wittenberg, 2012.

E. Lenz, A. Sprunk, P. Kleinebudde, and S. Page. The influence of fillers on dry foam properties. In *Partec International Congress on Particle Technology, Nuremberg (Germany)*, 2013.

C. C. Mbah, C. O. Emosairue, P. F. Builders, C. Y. Isimi, and O. O. Kunle. Effect of process parameters on the properties of some metronidazole tablet and capsule formulations. *African Journal of Pharmacy and Pharmacology*, 6(24):1719–1725, 2012.

Arun S. Mujumdar. *Handbook of Industrial Drying, Third Edition*. CRC Press, 2006.

K. Nollenberger, A. Gryczke, C. Meier, J. Dressman, M. U. Schmidt, and S. Brühne. Pair distribution function of X-Ray analysis explains dissolution characteristics of felodipine melt extrusion products. *Journal of Pharmaceutical Sciences*, 98 (4): 1476–1486, 2009.

A. A. Noyes and W. R. Whitney. The rate of solution of solid substances in their own solutions. *Journal of American Chemistry Society*, 19:930–934, 1897.

T. Patel, L. D. Patel, T. Patel, S. Makwana, and T. Patel. Studies in formulation development of low dose content drug using fluid bed granulation technique. *Journal of Pharmaceutical Sciences and Research*, 2(4):264–271, 2010.

S. Pisal, G. Wawde, S. Salvankar, S. Lade, and S. Kadam. Vacuum foam drying for preservation of LaSota virus: effect of additives. *AAPS PharmSci Tech*, 7(3): article 60, 2006.

C. Rauner. Der Einfluß verschiedener Carrageenan-Typen auf die Herstellung von Trockenschäumen und der Weiterverarbeitung zu Tabletten. Diploma thesis, Eberhard Karls University, Tübingen, 2005.

A. Schoonman, G. Mayor, M.-L. Dillamnn, C. Bisperink, and J. Ubbink. The microstructure of foamed maltodextrin/sodium caseinate powders: a comparative study by microscopy and physical techniques. *Food Research International*, 34: 913–929, 2001.

M. Schröder. *Entwicklung von kompakten Darreichungsformen aus sprühgetrockneten Milcherzeugnissen zur spontanen Rekonstitution.* PhD thesis, Rheinische Friedrich-Wilhelms University, 1999.

M. Sjøqvist and P. Gatenholm. The effect of starch composition on structure of foams prepared by microwave treatment. *Journal of Polymers and the Environment*, 13 (1):29–37, 2005.

J. K. Spence, S. N. Bhattachar, J. A. Wesley, P. J. Martin, and S. R. Babu. Increased dissolution rate and bioavailability through comicronization with microcrystalline cellulose. *Pharmaceutical Development and Technology*, 10(4):451–60, 2005.

A. Sprunk, S. Page, and P. Kleinebudde. Dry foam technology - impact of water content and equipment used. In *8th World Meeting on Pharmaceutics, Biopharmaceutics and Pharmaceutical Technology, Istanbul*, 2012.

D. D. Sun, T. C. Ju, and P. I. Lee. Enhanced kinetic solubility profiles of indomethacin amorphous solid dispersions in poly(2-hydroxyethyl methacrylate) hydrogels. *European Journal of Pharmaceutics and Biopharmaceutics*, 81(1):149–58, 2012.

M. R. Thompson, S. Weatherley, R. N. Pukadyil, and P. J. Sheskey. Foam granulation: new developments in pharmaceutical solid oral dosage forms using twin screw extrusion machinery. *Drug Development and Industrial Pharmacy*, 38:771–84, 2012.

M.R. Thompson and P.J. Sheskey. Foam granulation: a new approach to continuous wet granulation using a twin-screw extruder. *Pharmaceutical Technology*, 37 (3): 36–40, 2013.

C. K. Tye, C. C. Sun, and G. E. Amidon. Evaluation of the effects of tableting speed on the relationships between compaction pressure, tablet tensile strength, and tablet solid fraction. *Journal of Pharmaceutical Sciences*, 94(3):465–72, 2005.

F. Ungaro, C. Giovino, C. Coletta, and R. Sorrentino. Engineering gas-foamed large porous particles for efficient local delivery of macromolecules to the lung. *European Jounal of Pharmaceutical Sciences*, 41:60–70, 2010.

M. van Speybroeck, R. Mellaerts, T. D. Thi, J. A. Martens, J. Van Humbeeck, P. Annaert, G. Van den Mooter, and P. Augustijns. Preventing release in the acidic environment of the stomach via occlusion in ordered mesoporous silica enhances the absorption of poorly soluble weakly acidic drugs. *Journal of Pharmaceutical Sciences*, 100(11):4864–76, 2011.

G. Verreck, A. Decorte, H. Li, D. Tomasko, A. Arien, J. Peeters, P. Rombaut, G. Van den Mooter, and M. E. Brewster. The effect of pressurized carbon dioxide as a plasticizer and foaming agent on the hot melt extrusion process and extrudate

properties of pharmaceutical polymers. *The Journal of Supercritical Fluids*, 38(3): 383–391, 2006.

M. Vialpando, J. A. Martens, and G. Van den Mooter. Potential of ordered mesoporous silica for oral delivery of poorly soluble drugs. *Therapeutic Delivery*, 2(8): 1079–1091, 2011.

M. Vogt, K. Kunath, and J. Dressman. Dissolution enhancement of fenofibrate by micronization, cogrinding and spray-drying: Comparison with commercial preparations. *European Journal of Pharmaceutics and Biopharmaceutics*, 68:283–288, 2008.

F. Wan, A. Bohr, M.J. Maltesen, S. Bjerregaard, C. Foged, J. Rantanen, and M. Yang. Critical solvent properties affecting the particle formation process and characteristics of celecoxib-loaded PLGA microparticles via spray drying. *Pharmaceutical Research*, 30:1065–1076, 2013.

E. W. Washburn. The dynamics of capillary flow. *Physical Review*, 17(3):273–283, 1921.

C. Wu, Z. Wang, Z. Zhi, T. Jiang, J. Zhang, and S. Wang. Development of biodegradable porous starch foam for improving oral delivery of poorly water soluble drugs. *International Journal of Pharmaceutics*, 403(1-2):162–9, 2011.

V.B. Yadav and A.V. Yadav. Improvement of solubility and dissolution of indomethacin by liquisolid and compaction granulation technique. *Journal of Pharmaceutical Sciences and Research*, 1(3):44–51, 2009.

H. Yano and P. Kleinebudde. Improvement of dissolution behavior for poorly water-soluble drug by application of cyclodextrin in extrusion process: comparison between melt extrusion and wet extrusion. *AAPS PharmSciTech*, 11(2):885–93, 2010.

Y. Zhang, Z. Zhi, T. Jiang, J. Zhang, Z. Wang, and S. Wang. Spherical mesoporous silica nanoparticles for loading and release of the poorly water-soluble drug telmisartan. *Journal of Controlled Release*, 145(3):257–63, 2010.

7 List of publications

A. Sprunk, S. Page, and P. Kleinebudde. Dry foam technology - impact of water content and equipment used. In *8th World Meeting on Pharmaceutics, Biopharmaceutics and Pharmaceutical Technology, Istanbul*, 2012.

A. Sprunk, S. Page, and P. Kleinebudde. Dry foam technology - improved dissolution of a poorly soluble model drug. In *8th World Meeting on Pharmaceutics, Biopharmaceutics and Pharmaceutical Technology, Istanbul*, 2012.

A. Sprunk, S. Page, and P. Kleinebudde. Screening study for poorly soluble APIs comparing dry foam technology and fluid bed granulation. In *AAPS annual meeting, Chicago (USA)*, 2012.

E. Lenz, A. Sprunk, P. Kleinebudde, and S. Page. The influence of fillers on dry foam properties. In *Partec International Congress on Particle Technology, Nuremberg (Germany)*, 2013.

A. Sprunk, S. Page, and P. Kleinebudde. Fast dissolving fillers in dry foam formulation. In *6th International Granulation Conference, University of Sheffield (England)*, 2013.

A. Sprunk, S. Page, and P. Kleinebudde. Influence of process parameters and equipment on dry foam formulation properties using indomethacin as model drug. *International Journal of Pharmaceutics*, 455(1-2):189–96, 2013.

E. Lenz, A. Sprunk, S. Page, and P. Kleinebudde. Impact of fillers on dissolution kinetic of fenofibrate dry foams. *Pharmaceutical Development and Technology (submitted)*, 2013.

A. Sprunk, S. Page, and P. Kleinebudde. Fast dissolving fillers in dry foam formulation. *Powder Technology (submitted)*, 2013.

8 Danksagung

Die vorliegende Arbeit entstand am Institut für Pharmazeutische Technologie und Biopharmazie der Heinrich-Heine-Universität Düsseldorf unter der Leitung von Prof. Dr. Peter Kleinebudde in Zusammenarbeit mit der Firma F. Hoffmann-La Roche Ltd, Basel. Ich bedanke mich bei meinem Doktorvater Prof. Dr. Peter Kleinebudde für die Aufnahme in seinen Arbeitskreis, für seine außergewöhnlich gute wissenschaftliche Betreuung sowie für seine stete Diskussionsbereitschaft. Insbesondere seine Anregungen und kritischen Einwände haben mir immer wieder neue Denkanstösse gegeben. Kein minderer Dank gilt Frau Dr. Susanne Page, die mir als Betreuerin bei der Firma F.Hoffmann-La Roche zur Seite stand. Ich bedanke mich für ihr immer offenes Ohr, die zahlreichen Diskussionen, ihren guten Rat und ihren unermüdlichen Einsatz. Durch die gute Zusammenarbeit meiner Betreuer und die Unterstützung der Firma F.Hoffmann-La Roche war es mir möglich, diverse Konferenzen und Kongresse zu besuchen, und so viele wertvolle neue Eindrücke und Erfahrungen zu sammeln. Herrn Prof. Dr. Breitkreutz danke ich für die Übernahme des Koreferates.

Ich möchte mich ganz herzlich bei der Gruppe Formulation Research and Development, F.Hoffmann-La Roche Ltd., Basel für die nette und freundschaftliche Aufnahme bedanken. Ich habe stets Unterstützung und Hilfsbereitschaft sowohl bei meinen Vorgesetzen, als auch bei meinen Kollegen erfahren dürfen, und wurde in die Gruppe als vollwertiges Mitglied eingebunden. Ich bedanke mich für die Offenheit gegenüber meinen Fragen und für die vielen, bereitwilligen kleinen und grösseren Handgriffe, die mir das Arbeiten erleichtert haben. Bei der Gruppe der Präformulierung möchte ich mich ebenso für die nette Aufnahme, die schönen Kaffeepausen und die Hilfsbereitschaft bei analytischen Fragen bedanken. Ebenso freundlich wurde ich von den Mitarbeitern der Pulvertechnologie, den Analytikern der Gruppe Dr. Siegfried Krimmer und der Gruppe von Dr. Günther Gross aufgenommen. Vielen Dank für eure Hilfsbereitschaft.

Ich möchte mich bei Patrick Busson für die praktische Einführung in die Schaumherstellung und die Wirbelschichtgranulation bedanken. Reto Maurer danke ich für die Einführung in die Bedienung des Vakuumbandtrockners, der HPLC-Anlage, sowie für eine tolle Büro- und Labornachbarschaft. Ausserdem danke ich Joe Tardio für die zahlreichen Diskussionen bei analytischen Fragen.

Elisabeth Lenz möchte ich für ihr Engagement und ihre Einsatzkraft im Rahmen ihrer Diplomarbeit und die gute Zusammenarbeit danken. Ich habe das von ihr hergestellte Fenofibrat-Isomaltschaumgranulat weiterverwendet. Ich wünsche ihr für ihre Doktorarbeit, ihren beruflichen Werdegang sowie für ihr Privatleben alles Gute.

Dr. Pascal Chalus möchte ich für die zahlreichen X-Ray µ-CT Aufnahmen und

Diskussionen danken. Katja Schulze danke ich für die vielen Elektronenmikroskopaufnahmen. Bei Dr. Marcello Bosco und Björn Vollmert möchte ich mich für die Einführung in die Bedienung der Magnetschwebewaage und die freundliche Unterstützung bedanken. Dr. Sylvie Fernandez und Silke Hohenberger danke ich für Einführung in die Bedienung der Freisetzungsanlage. Bei Dr. Regina Moog, Peter Egloff und Jean-Michel Clavey bedanke ich mich für die Einführung in die Benutzung des Rheometers sowie für die Ermöglichung der häufigen Nutzung. Bei Alf Willmann, Anton Flach, Daniel Rast und Rafael Flückiger möchte ich mich für die freundliche Einführung in die Pulvertechnologie bedanken. Ein besonderer Dank gilt auch den Handwerkern Patrik Henninger und Fernand Sarazin für ihre Hilfsbereitschaft und ihren schnellen, tatkräftigen Einsatz bei technischen Problemen. Ich möchte mich bei ihnen und der gesamten Werkstattgruppe für die freundliche Unterstützung, die Herstellung der Kartuschen sowie der Körbchen für die Magnetschwebewaageversuche bedanken.

Ich danke meinen Institutskollegen für ihre freundliche und offene Aufnahme bei meinen Arbeiten an der Universität. Dr. Klaus Knop und Dr. Markus Thommes danke ich für die flexible Unterstützung. Bei Dr. Cornelia Krüger und Julian Quodbach bedanke ich mich für die Einführung in die Benutzung des Quecksilberporosimeters.

Ein besonderer Dank geht an meine Eltern und meinen Bruder für ihre stete Unterstützung, ihr Verständnis und ihre Ermutigung. Meinem Bruder Christoph Sprunk danke ich für die Einführung in die Nutzung des Textsatzsystems LaTeX. Schliesslich möchte ich mich bei meinem Verlobten Felix Dischinger für seine endlose Geduld und Unterstützung bedanken. Danke für das Ertragen meiner schlechten Laune und deinen unermüdlichen Beistand.